Cyclic membrane gas separation processes

Lei Wang

UNIVERSITÉ DE LORRAINE

DOCTORAL SCHOOL RP2E N°410

P h D T H E S I S

In (Partial) Fulfillment of the Requirements for the Degree of

Doctor of Philosophy
Specialty : Chemical Engineering

Defended by

Lei WANG

Cyclic Membrane Gas Separation Processes

prepared at Reaction and Process Engineering Laboratory (LRGP)

defended on July 17th, 2012

Jury :

Advisors :	Eric FAVRE	-	LRGP (Nancy)
	Jean-Pierre CORRIOU	-	LRGP (Nancy)
President :	Daniel TONDEUR	-	LRGP (Nancy)
Reviewers :	Xuan MEYER	-	LGC (Toulouse)
	José SANCHEZ	-	IEM (Montpellier)
Examinators :	Hervé DUVAL	-	ECP (Paris)
Invited :	Christophe CASTEL	-	LRGP (Nancy)

ÉCOLE DOCTORALE RP2E N°410

T H È S E

présentée et soutenue publiquement le 17 juillet 2012

pour l'obtention du

Doctorat de l'Université de Lorraine
Spécialté : Génie des procédés et des produits

par

Lei WANG

Séparation Membranaire de Composés Gazeux en Régime Cyclique

préparée au Laboratoire Réactions et Génie des Procédés (LRGP)

Composition du jury :

Encadrants :	Eric FAVRE	-	LRGP (Nancy)
	Jean-Pierre CORRIOU	-	LRGP (Nancy)
Président :	Daniel TONDEUR	-	LRGP (Nancy)
Rapporteurs :	Xuan MEYER	-	LGC (Toulouse)
	José SANCHEZ	-	IEM (Montpellier)
Examinateurs :	Hervé DUVAL	-	ECP (Paris)
Invité :	Christophe CASTEL	-	LRGP (Nancy)

To my parents

Preface

This is the my third year in LRGP, sixth year in Nancy and eighth year in France! I remember very well that when I was 17 years old (2002), I suffered to finish a 'long thesis' of 800 characters in Chinese, but today, a thesis in English of more than 200 pages has been written by me! Moreover, I've made more than 600 pages manuscript during my study and the number is continuously increasing. What is more important is that all these works could be considered as 'valuable' since most of them are published already.

This thesis is not only a scientific research, but also an extremely enriching experience for me before going to industry.

In this preface, I give a brief account of how this thesis came about. It consists of a review of the research work I have done in the LRGP (Reactions and Chemical Engineering Laboratory) of Nancy over the last three years.

In October 2009, I joined the Membranes, Separation Processes Group (EPSM) of the LRGP and the Ph.D. study was officially launched. Initially, the objective was to find the optimized operation conditions of a cyclic membrane gas separation based on Paul [1971] initial idea and design an experimental pilot.

On July 20th 2009, almost one year after the beginning, I received an email from my supervisor, in which I felt his "slight dissatisfaction" about my progress in the study. Actually, I was not surprised, since I found that I did NOTHING during this year but only tried to be familiar with the membrane world and finished a 150-page report in French! However, I had to say that the French report serves nothing in the final thesis....

On August 2009, I went to Croatia for summer holiday, the most beautiful country in my opinion. When I came back, I found that I was inspired! I reviewed the existing cyclic processes in August and September 2010. Then the cyclic process simulation based on rubbery polymers was finished in October 2010. This latter with the bibliography research work led to my first publication in Journal of Membrane Science (Chapters 3 and 5). In this paper, we showed that the cyclic process based on Paul's idea is difficult to be cost effective in practice, while we began to think about other possibilities of cyclic operations. Fortunately, a novel cyclic process was proposed and tested successfully by means of numerical simulations. As a result, we applied to

patent our own cyclic process. After eight months, this process was registered successfully in November 2011 and formed the case study of Section 5.3.

When I tried to simulate the cyclic process with the Dual Mode Sorption theory in October 2010, a happy accident happened and led me to think about the transport mechanism in and through membrane. By studying works done in 1970s, I became dissatisfied with the time-lag prediction of the classical Dual Mode Sorption theory. I began to propose a 'new' transport mechanism in March 2011 within the frame of the famous theory. This reflection led to a paper in Industrial & Engineering Chemistry Research and resulted into the Chapter 4 in this thesis. The Dual Mode Sorption theory was later (April 2011) applied in a Mixed Matrix Membrane-based cyclic process investigation and led to another submitted paper in AIChE Journal.

Briefly, during the first six months of 2011, nearly all theoretical works in this thesis had been finished essentially. Then in July 2011, I gave my first talk in English in Auditorium of Amsterdam RAI, the biggest conference center of Holland. In October, I went to the USA and gave two talks in AIChE Annual Meeting. Finally, in November, I gave again a talk in Lille in SFGP Annual meeting. After this busy but amazing year of 2011, I went back to China to join my family for the Chinese new year.

The experimental works (Chapter 6) were done in the last year of my Ph.D. study as a support to our patented process. At the same time, since the patented process has been registered, we are writing another paper about this process but this part is not yet included in the thesis. Furthermore, a poster of this work will be presented during the Euromembrane congress in London in 2012. At the same time, the 'real' patented cyclic process representing exactly the patent design is being installed in our laboratory. More convincing results of this process will be reported later.

Acknowledgement

It is a great pleasure to thank the people who made this thesis possible. But the acknowledgement is always a compulsory and difficult task to compete for a Ph.D. thesis, because I risk to ignore someone.

First and foremost, I would like to express my sincere gratitude to my three supervisors Eric, Jean-Pierre and Christophe for their amazing proposal of the Ph.D. subject, for their patience, motivation, enthusiasm, immense knowledge and also chocolate eggs of Easter, wonderful meals in Christmas meal, original suggestions for traveling, beautiful stories everyday.... Their guidance helped me in all the time of research and writing of papers. I could not have imagined having better advisors and mentors for my Ph.D. study.

I am deeply grateful to my reviewers Xuan Meyer and José Sanchez for their detailed and constructive comments.

I want to thank all the mechanical department of LRGP, Pascal, Alain, Christian, Patrick and Yann. They did a remarkable work for my experimental research. Without them, I cannot imagine such a perfect apparatus. It is also difficult to overstate my gratitude to Mathieu and Hervé. I appreciate very much the friendly user interface made by Mathieu, which automated the whole process. The only thing that I needed to do was just to enter stage durations and press the "run" button.

I am indebted to all my colleagues in EMSP group for providing a stimulating and fun environment in which to learn and grow. I am grateful to all your helps on for my research. And also, there are so many things that I cannot forget: Minneapolis discovery with Fleur, Elodie and Bouchra, Mr. Dysson from Camel, Microsoft in a Mac from Bouchra, word puzzle with all group in Amsterdam : Denis, Haifa, Clément, Fleur, Elodie, Camel and Bouchra... and all days we spent together!

I am grateful also to the secretaries of LRGP, for helping all administrative affairs smoothly and for assisting me in many different ways. Annie, Nathalie, Véronique, Claudine, Nelly, Stéphanie, Josiane and Michèlle deserve special mention.

I wish to thank all my Chinese friends in Nancy: Minghai, Yuhai, Cheng, Zhou, Zhenghui, Junwei and all students of N+I for enjoying the life in Nancy. Without you, the Chinese traditional festivals would have faded and I would

have had to speak Chinese to air!

The financial support by the ICEEL (Carnot institutes Network) of France is gratefully acknowledged. The useful discussion with Prof. Koros about the Dual Mode Sorption theory during the AIChE Annual Meeting 2011 is appreciated too. I would like also express my acknowledgement to all anonymous reviewers who raised important remarks to our publications.

I think that I have to express special acknowledgements to all developers of LaTeX and other useful free software from the GNU project. Even if I know no one of them, their contributions to this thesis cannot be ignored.

Last but not least: my appreciation also goes to my parents for giving birth to me at the first place and their encouragement, love and support throughout my life. Thank you very much! To them I dedicate this thesis!

Lei WANG
June 2012

Summary

Membrane-based gas separation has attracted considerable interest over the past years because of its low energy consumption and cost effective separation. These processes are conventionally operated at steady-state: both feed pressure and permeate pressure are maintained at constant levels, and the permeation rate and permeate concentration do not depend on time, except at the initial start up stage. Although spectacular improvements in the case of operations under transient-state have been discovered in 1971 by means of a so-called cyclic membrane gas separation process, transient-state operations are rather unexplored compared to steady-state operations.

This study is devoted to a systematic investigation of the performance of cyclic membrane gas separation processes. First, a state of the art of membrane separation processes, including material challenges and mass transfer modeling issues is proposed. In a second step, a review of the different theoretical and experimental studies performed on cyclic processes is reported. With respect to the length of the high pressure stage and its fraction in one cycle, these operations are classified into short and long classes.

In a third step, a systematic analysis of the potential interest of short class of cyclic operation compared to steady-state performances has been achieved based on trade-off correlations applied on 2145 different gas pairs. Several different case studies, based on experimental solubility and diffusion data, have been investigated numerically and the pros and cons of short class processes compared to steady-state operations have been highlighted.

Using Mixed Matrix Membrane is known as a classical performance improvement for membrane processes. By means of numerical investigations of a novel design of short class processes dedicated to MMM, the unique advantages of cyclic processes are indeed enhanced while some unavoidable drawbacks are weakened by using MMM.

In parallel of the short class process study, a design of novel long class has been proposed in this thesis. This process possesses more degrees of freedom with regard to its operation. By means of simulation and optimizations, the competitiveness has been confirmed with regard to conventional steady-state operations. Last but not least, an experimental verification has been performed in order to provide a solid support to this novel long class process.

According to the RP2E doctoral school code, a long summary of this manuscript is given in Appendix E in French.

Nomenclature

A	Effective membrane area (m^2)
b	Hole affinity constant (atm^{-1})
C	Gas concentration (m^3 STP.m^{-3})
$C_H^{'}$	Hole-filling constant (m^3 STP.m^{-3})
$\mathcal{D}$	Diffusion coefficient ($m^2.s^{-1}$)
e	Relative error
F	Ratio of diffusion coefficients of two species
J	Gas flow rate through the membrane (cm^3 STP.$s^{-1}.m^{-2}$)
$\mathcal{K}$	Boltzmann constant ($J.K^{-1}$)
k_f	Forward rate constant (cm^{-3} STP.cm^3 polymer.s^{-1})
k_r	Reverse rate constant (s^{-1})
k_D	Henry sorption coefficient (cm^3 STP.cm^{-3} polymer.atm^{-1})
L	Membrane thickness (m)
l_t	Fiber length (m)
n	Number of moles (mol)
P	Pressure (Pa)
$\mathcal{P}$	Permeability (m^3 STP.$m^{-1}.Pa^{-1}.s^{-1}$)
R	Ideal gas constant ($J.K^{-1}.mol^{-1}$)
R_e	External radius (m)
R_i	Internal radius (m)
r	Radial position (m)
T	Temperature (K)
t	Time (s)
U	Coefficient used by Paul to define the short class process period
V	Volume (m^3)
v_d	Volume fraction of dispersed phase in membrane
v_p	Volume fraction of continuous phase in membrane
X	Upstream mole fraction
x	Opening duration of the valves in Paul's process (s)
Y	Mole fraction in the downstream side of the module
y	Mole fraction in tanks
z	Position in the membrane for a unidimensional model (m)

Subscripts

D	Ordinary dissolution
d	Downstream
$d, \mathcal{L}$	Downstream left tank
f	Feed
g	Transition point for an amorphous polymer
H	Hole-filling process
k	Index of component
m	Effective value
u	Upstream

Greek symbols

α	Permeability selectivity
$\alpha_{\mathcal{D}}$	Diffusion selectivity
α_{k_D}	Solubility ratio
γ	Volume ratio of Hollow Fiber module
$\epsilon/\mathcal{K}$	Lennard-Jones temperature (K)
ζ	Stage cut for a conventional steady-state membrane process
θ	Time-lag (s)
Θ	Exhaustion ratio in upstream
ρ	Molar density (mol/m^3)
τ	Period of pressure cycle for a cyclic process (s)
Ψ	Pressure ratio for a conventional steady-state membrane process
ψ	Relative error
ω	Fraction of period when the upstream pressure is high for a cycle

Publications resulting from the thesis research

The simulation/optimization part of this thesis is mainly presented in following scientific publications. The patent is included in the process design in Section 5.3.

Patents

(I) Procédé de Séparation Membranaire en Régime Discontinu. FR Patent 11 60587.

Articles

(I) Cyclic Gas Separation by Mixed Matrix Membranes (MMM). L. Wang, J.P. Corriou, C. Castel, E. Favre. *AIChE Journal*, (submitted in April 2012)

(II) Transport of Gases in Glassy Polymers under Transient Conditions: Limit Behavior Investigations of Dual Mode Sorption Theory. L. Wang, J.P. Corriou, C. Castel, E. Favre. *Industrial & Engineering Chemistry Research*, 2012, DOI: 10.1021/ie2027102

(III) A critical review of cyclic transient membrane gas separation processes: State of the art, opportunities and limitations. L. Wang, J.P. Corriou, C. Castel, E. Favre. *Journal of Membrane Science*, 383(2011), 170-188

Communications

(I) Novel Design of Cyclic Membrane Gas Separation Process (Poster). L. Wang, J.P. Corriou, C. Castel, E. Favre. *Euromembrane*, London, UK, 2012

(II) Séparation Membranaire de Mélanges Gazeux par Procédé Cyclique (Oral presentation). L. Wang, J.P. Corriou, C. Castel, E. Favre. *SFGP XIII^{ème}*, Lille, France, 2011

(III) Cyclic Membrane Gas Separation Process Assessment (Oral presentation). L. Wang, J.P. Corriou, C. Castel, E. Favre. *AIChE Annual Meeting*, Minneapolis, USA, 2011

(IV) Modeling transient diffusion of gases in glassy polymers by the Dual Mode Model: Is the local equilibrium hypothesis necessary? (Oral presentation) L. Wang, J.P. Corriou, C. Castel, E. Favre. *AIChE Annual Meeting*, Minneapolis, USA, 2011

(V) Cyclic membrane gas separation processes: Why? When? How? (Oral presentation) L. Wang, E. Favre, J.P. Corriou, C. Castel. *ICOM*, Amsterdam, Netherlands, 2011

(VI) Séparation membranaire des gaz par procédé cyclique (Poster). L. Wang, E. Favre, J.P. Corriou, C. Castel. *MemproIV*, Aix-en-Provence, France, 2010

(VII) Séparation membranaire des gaz par procédé cyclique (Poster). L. Wang, E. Favre, J.P. Corriou. *Séminaire RP2E*, Nancy, France, 2010

List of Tables

List of Figures

Contents

Chapter 1

Introduction

> The tailor who does not want to be a cook is not a good driver.
>
> Anonymous Chinese from the last decade

1.1 Background & Research objectives

A membrane is a layer of material which can be defined as a selective barrier between two phases and remains impermeable to specific particles, molecules, or substances when exposed to the action of a driving force [Bitter, 1991]. Some components are allowed to cross the membrane into a permeate stream, whereas others are accumulated in the retentate stream.

In living organisms, all the necessary separations are achieved by selective membranes, which explains why membranes first attracted the interest of natural scientists, especially biologists and physiologists. On a technical scale, however, membranes have been used in relatively few cases. About 40 years ago, industrial applications of membranes started to be developed rapidly, when scientists and engineers discovered the possibilities of reverse osmosis in their search for energy-saving sea water desalination processes and when all the industrially developed nations started major research programs for the development of high-performance membranes and modules [Rautenbach and Albrecht, 1989].

In recent years, membrane-based technology has found more use in industrial processes [Koros and Fleming, 1993]. It is widely applied in purification, concentration and fractionation of fluid mixtures with evident advantages of

energy saving, compactness, ease of operation and maintenance, continuous operation, and environmental friendliness. Membranes have found applications in areas that were previously dominated by more traditional processes, such as distillation, absorption, adsorption, extraction and filtration. Even if in many cases membranes could not completely replace these technologies, hybrid systems combining membranes with one of the traditional techniques are accepted as attractive options [Spillman, 1989]. The membrane process development is summarized in Tab. 1.1.

Category	Process	Status
Developed	Microfiltration Ultrafiltration Reverse osmosis Electrodialysis	Well-established unit operations. No major breakthroughs seem imminent.
Developing	Gas separation Pervaporation	A number of plants have been installed. Market and applications served are expanding.
To be developed	Carrier facilitated transport membranes Piezodialysis	Major problems exist before large scale systems will be installed.

Table 1.1: Development status of membrane processes [Ravanchi et al., 2009]

Although extensive research and development have been carried out in the past two decades, membrane-based gas separation is still in a far less advanced state compared with other more mature membrane processes such as dialysis, reverse osmosis, microfiltration, and ultrafiltration (Tab. 1.1). The development of new membrane materials are required to improve the process efficiency for industrial applications. Besides the new material investigation, attention has also been payed on the improvements of membrane processes in order to optimize the efficiency of membrane based operations.

The objectives of this research on the improvements of membrane processes have been derived in the light of the aforementioned discussions and are presented below:

- To review the existing cyclic membrane gas separation processes in the literature then classify them according to well defined criteria.
- To perform a general inventory in order to identify potentially interesting binary gas mixtures for cyclic operations.

- To develop a complete benchmark between cyclic processes and conventional operations by means of numerical simulations.
- To explore a novel design of cyclic membrane processes for gas separation and prove it in a pilot experiment.

1.2 Framework of the thesis study

In order to have an overview of the research in the thesis, the framework of the thesis is briefly illustrated in Fig. 1.1. In general, the research of this thesis was conducted in three stages in its core part.

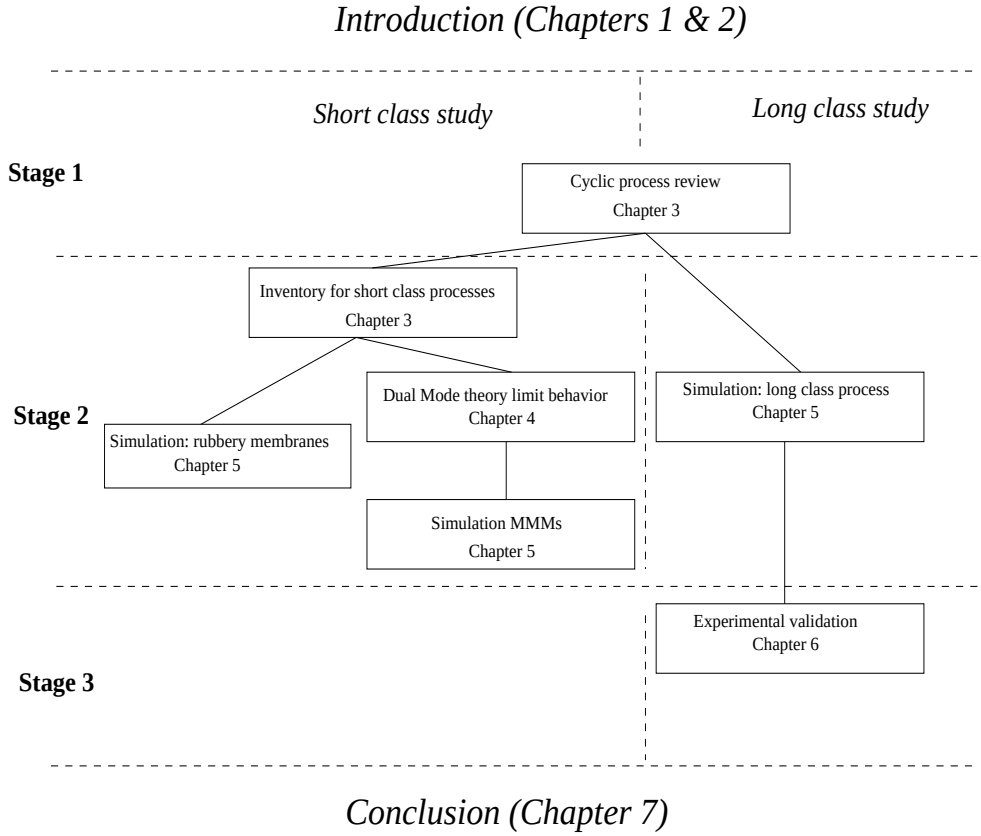

Figure 1.1: Framework of the thesis study

It is shown in Fig. 1.1 that the current chapter (Chapter 1) presents the background and the objectives of the thesis study. Chapter 2 contains an overview of membrane-based gas separation concerning membrane materials, membrane formations, membrane modules and performance improvement

methods. Basic notations of a membrane-based gas separation process are given in this chapter.

In Chapter 3, a critical review focused on the existing cyclic membrane processes is carried out. According to the fraction of high pressure duration with respect to the total duration of cycle, the cyclic operations were classified into two classes: the short class refers to a low ($< 10\%$ in general) fraction of high pressure duration in one cycle while the long class refers to a high fraction ($> 90\%$ in general). Then, an inventory for short class processes was performed in order to identify interesting gas pairs of industrial interests. All these discussions are covered in Chapter 3.

Chapter 4 deals in particular with the transport mechanism in and through polymeric membranes. In this chapter, a classical modeling named as Dual Mode Sorption theory is first reviewed and completed by a limit behavior investigation. Then, in the same chapter, the modeling tools, solving algorithms and optimization tools used in this thesis are presented briefly.

Based on well defined binary gas mixtures, three cyclic process case studies are performed in Chapter 5: short class processes based on rubbery membranes and Mixed Matrix Membranes, as well as a patented long class process. For each case study, systematical comparisons to conventional steady-state operations are given in order to highlight the pros & cons of the corresponding cyclic processes.

An experimental proof is given in Chapter 6 as a support to the patented long class process. The simulation results for the patented process in Chapter 5 are confirmed experimentally in LRGP (Reactions and Chemical Engineering Laboratory).

Finally, the general conclusions drawn from the study, along with the major contribution to research and recommendations for future work, are summarized in Chapter 7.

Moreover, fives chapters are given as appendix. The Appendix A and B provide some theoretical supports to the limit behavior investigations performed in Chapter 4. A study about the fiber filling is performed in Appendix C in order to validate the assumption about the filling duration in Chapter 5. Then, the numerical method used in our simulation study is detailed in Appendix D. Finally, a long summary of this thesis is given in French as Appendix E.

Chapter 2

Membrane-based gas separation: bibliography study

> A journey of a thousand miles
> starts with a single step.
>
> Laozi

In the present chapter, a general description of membrane gas separations is given. Basic notions of such a process are defined. This chapter attempts to provide a review of the current literature concerning in particular polymeric membrane gas separations and to address some issues that need to be solved; a more specific literature review about cyclic operations will be presented in Chapter 3.

2.1 Introduction

Membrane-based gas separations make use of the difference on gas permeation rates of a gaseous mixture through membranes. As shown in Fig. 2.1, the feed flow at a high pressure get contact to the membrane in a membrane module. Then the more permeable gaseous components go across the membrane because of a driving force and are preferentially accumulated in a so-called permeate flow. On the other hand, the so-called retentate flow is enriched in the less permeable gaseous components. A separation is thus achieved. The driving force of the transport through a membrane can be a chemical or electrical potential. In the case of gas separations, it is usually the chemical

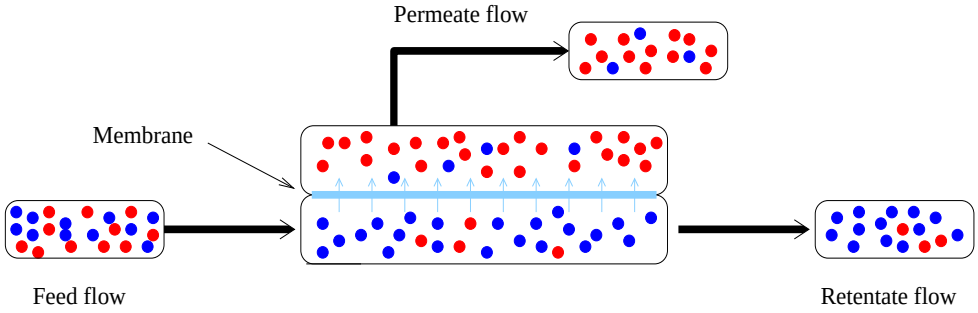

Figure 2.1: Schematic membrane-based gas separation process

potential (represented by a concentration or pressure gradient) which drives the gas diffusion.

In general, one conventional process of membrane-based gas separation runs in steady-state and can be characterized by the following factors (Fig. 2.2):

- For each stream (feed, retentate and permeate), three parameters are attributed: flow rates Q, mole fraction X or Y and pressure P.
- The membrane is characterized by its effective area A, effective thickness L and permeability for each gaseous component which measures the ability of a gaseous fluid to flow through the membrane under steady state conditions. This latter will be detailed and defined mathematically later according to gas transport mechanisms in and through membranes.
- The separation efficiency is also influenced by two dimensionless parameters:

  Pressure ratio Ψ

  $$\Psi = \frac{P_d}{P_u} \tag{2.1}$$

  Stage cut ζ

  $$\zeta = \frac{Q_d}{Q_f} = 1 - \frac{Q_u}{Q_f} \tag{2.2}$$

- Hydrodynamic conditions: stirred model, countercurrent flow or cross flow. This feature will be discussed in Chapter 4.

By providing all previous parameters, a process of membrane-based separation is well defined. Furthermore, if the transport mechanisms of gaseous components are well known, the process performance can be obtained by theoretical studies, such as simulations. For example, **M3Pro** developed in the EMSP

(Membranes, separation processes) team of the LRGP (Reactions and Chemical Engineering Laboratory) is able to carry out this task within some seconds (http://www.lrgp.ensic.inpl-nancy.fr/en/research/axe-2-intensification-et-architecture-des-procedes/membranes-separations-procedes/msps-breaking-news.html).

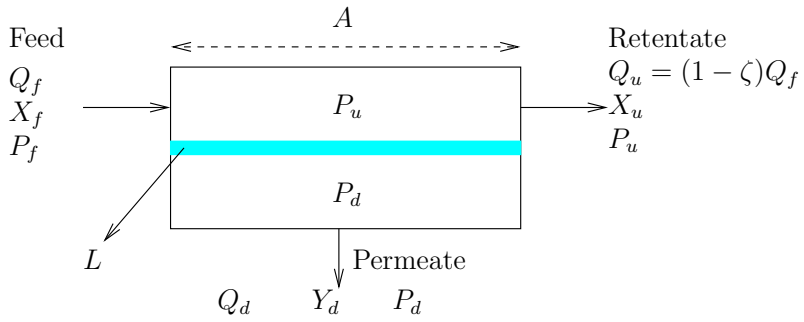

Figure 2.2: Notations of a conventional membrane-based gas separation process

2.2 Characteristics of membrane-based gas separation

Nowadays, there are four important methods applied to the separations of gaseous components in industry: absorption, adsorption, cryogenics and membranes. These technologies except membranes are compared in Table 2.1.

Compared to other well-developed gas separation processes mentioned in Tab. 2.1, membrane-based gas separation has the following features:

- Membrane-based gas separation does not involve phase change.
- Membranes are typically promoted as simple passive devices. Operations are under steady-state.
- Membrane-based gas separation is efficient for bulk separation. The driving force for gas permeation is the partial pressure difference across the membrane. In general, it is not significantly economical to obtain products with very high purities due to the quite low driving force available under these conditions [Spillman, 1989].
- The membranes are modular in design and easy to scale up. They can be used in either a large or small processing capacity without significant economy of scale. At small to medium scales, membranes are

Technology	Pros	Cons
Cryogenic (without distillation)	High recovery of products Low cost Low pressure loss of light product	Low purity of light products
Cryogenic (with distillation)	High recovery of products High purity of light products Can operate at high pressures Good purity of heavy products Low pressure loss of light product	High cost High energy consumption
Absorption	Simple process Low pressure loss of light product	Low purity of light ends or low recovery of heavy ends
Adsorption (pressure swing)	Very high purity of light product Simple process	Low recovery Operates most favorably at lower pressures (20-30 bar)
Adsorption (thermal swing)	Can remove minor components virtually completely	Expensive for bulk removal of impurities

Table 2.1: Comparison between gas separation technologies except membranes [Ravanchi et al., 2009]

in general more competitive than traditional separation technologies [Rautenbach and Albrecht, 1989].

- Membrane-based gas separation is environmentally friendly [Spillman, 1989]. It does not require additional mass agent for separation and thus does not generate secondary waste (e.g. vapor, solvents or solid particles).
- Membranes are relatively compact and light, easy to operate and maintain [Chenar et al., 2006, Spillman, 1989].

Koros and Fleming [1993] describe a successful membrane-based gas separation with three criteria: productivity, selectivity and membrane stability.

- Membrane productivity is concerned with the permeation rate, determined by the intrinsic permeability of the material, the effective membrane thickness, and also the membrane packing density, i.e., the amount of effective membrane area per unit module volume. A high permeation flux can be achieved by using thin membranes, and using properly designed membrane modules, such as hollow fibers (which will be detailed in following section) for a large effective membrane area.
- Membrane selectivity depends not only on the intrinsic selectivity of the polymer and the integrity of the selective layer but also on the process conditions (such as the pressure ratio Ψ and the stage cut ζ), which affect the driving force of the transport and the transport resistance of

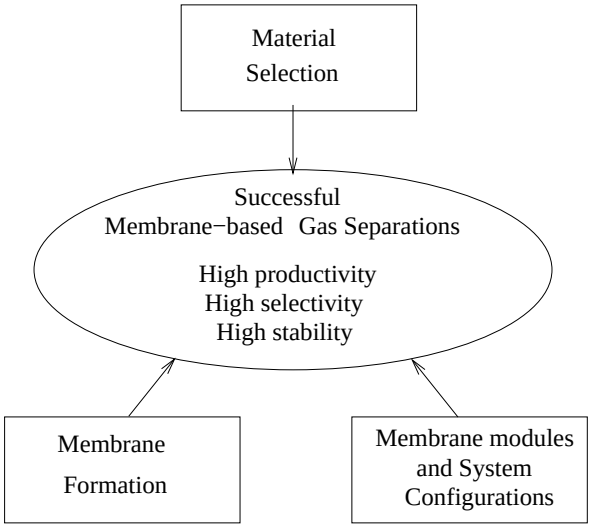

Figure 2.3: Critical issues controlling successful membrane-based gas separation [Koros and Fleming, 1993]

the layer. It can be noticed that, in most cases, the productivity and the selectivity cannot be optimized at the same time in a given process, a trade-off in forms of a Pareto zone is usually used to represent their relationship [Robeson, 2008].

- Lastly, membrane stability is the ability to maintain membrane permeability and selectivity for a long period of time. For the applications of condensible gas separation, membranes with good chemical resistance, and thermal and mechanical stabilities are required.

Therefore, a successful membrane gas separation process satisfying the previous criteria can be determined by three factors, including membrane material selection, membrane formation, membrane modules as indicated in Fig. 2.3. These three factors will be detailed in this order in the following sections. In this thesis, most considered gases in case study are non condensible, therefore the membrane stability is not developed in detail. Only the productivity and selectivity are taken into account as two major issues of separation efficiency and their mathematical definitions will be given later in case study chapters (Chapter 5).

2.3 Material selection

The material selection of the membrane is almost the top issue for such a process since this selection determines the transport mechanism in and through

the membrane. In the material selection, two consecutive procedures are considered: membrane material selection and membrane preparation. The selection of membrane material allows also controlling the nature and magnitude of the gas-membrane physicochemical interactions. On the other hand, the choice of membrane determines the packing density [Lloyd, 1985]. The membrane preparation determine membrane morphology and the extent to which physical considerations, such as the influence on the permeation rate. Together, material selection and membrane preparation influence the transport mechanism in membranes. This latter is the key issue of the discussion of this section.

The transport mechanism in membranes depends on whether the membrane is porous or nonporous (dense). In general, nonporous polymeric membranes are used as selective gas permeation barriers while porous membranes are used as substrates for mechanical support in industry [Koros and Fleming, 1993]. In Fig. 2.4, three mechanisms of gas permeations are drawn: in general, the solution-diffusion mechanism describes well the gas permeation in dense nonporous membranes, while in porous membranes the gas permeation follows viscous flow (convective flow), Knudsen flow, molecular sieving or a combination of them [Koros and Fleming, 1993], depending on the relative size of the penetrant molecules and the pores in the membrane.

- Knudsen-diffusion. In this case, diffusion occurs in a long pore with a narrow diameter (2-50 nm) in which molecules frequently collide with the pore wall. If the pore diameter is smaller than the mean free path of the diffusing gas molecules and the density of the gas is low, the gas molecules collide with the pore walls more frequently than with each other. For an equimolar feed, such a "Knudsen" diffusion process gives relative permeation rates equal to the inverse square root ratio of the molecular weights of the gaseous components. For standard applications, such membranes are not commercially attractive in general due to their low selectivities. To our knowledge, the only large-scale application of Knudsen diffusion was the separation of uranium isotopes, as a part of the Manhattan Project. This separation will be detailed in Section 5.1.

- Molecular sieving. Ultramicroporous molecular sieving separation is based primarily on the much higher diffusion rates of the smallest molecule, but sorption level differences may be important factors for similarly sized penetrants. This kind of membrane has received attention due to reported higher productivities and selectivities than solution-diffusion membranes.

- Solution-diffusion. Membranes based on solution-diffusion are nearly exclusively available commercially for gas separations. This mechanism

will be detailed in following sections and further discussed in Chapter 4.

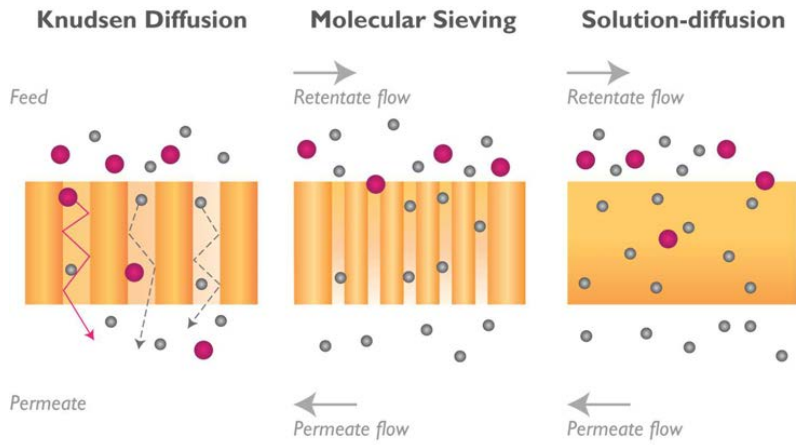

Figure 2.4: Schematic representation of main mechanisms of gas permeations through membrane [Koros and Fleming, 1993]

Nevertheless, Koros and Fleming [1993] noticed two important exceptions to this generalization:

- Ultra-pure hydrogen. Membranes made from palladium-silver have extremely high hydrogen selectivities relative to other gaseous components, since this kind of membranes operates by a catalytic dissociation of hydrogen and recombination on the downstream side.
- In some microporous membranes, if surface diffusion or capillary-condensation allow a much more condensible component A to effectively exclude much of the second component B from the porous network, high selectivities can be observed.

It should be noticed that of the three mechanisms in Fig. 2.4, the solution-diffusion mechanism is used exclusively in current commercial devices and will be essentially discussed in this thesis.

2.3.1 Solution-diffusion mechanism

The so-called solution-diffusion mechanism dates back to the work of investigators made by Barrer [1937]. Even more, the fundamental equations of diffusion were derived by Fick [1855], who perceived the analogy applying between mass transfer and heat transfer.

The mechanism is described by Vieth [1991] as: when a gas permeates through a polymer membrane, several processes are involved (Fig. 2.5): the gas is sorbed at the entering face, dissolving there, with equilibrium being established rapidly between the two phases. The dissolved penetrating molecules then diffuse through the membrane, via a random walk hopping mechanism, desorbing at the exit face. The mechanism of permeation, thus, involves both solution and diffusion. A gas mixture is thus separated because of the differences in the solubility and mobility of the gaseous components in the membrane matrix.

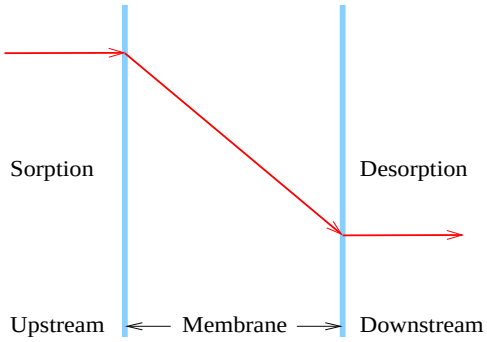

Figure 2.5: Schematic diagram of the solution-diffusion mechanism

It can be noticed that gas fugacities rather than simple partial pressures are appropriate when high pressures lead to non-ideal gas phase behavior [Koros et al., 1981]. However, in most cases, the correction is not significant [Koros et al., 1977, Paul and Koros, 1976]. Thus, in this thesis, partial pressures are used everywhere as an approximation. The equilibrium concentration C on the surface of membrane is related to the partial gas pressure P,

$$C = k_D P \tag{2.3}$$

where C is the gas concentration in the membrane, P the partial pressure of penetrant at the interface and k_D the sorption coefficient. Assuming that the concentration gradient is the only driving force of transfer in an isothermal condition, the penetrant flux or the permeance J in and through membrane can be given by Fick's first law,

$$J = -\mathcal{D}\nabla C \tag{2.4}$$

where ∇C is the concentration gradient in the membrane and $\mathcal{D}$ the molecular diffusion coefficient. The negative sign indicates that diffusion occurs spontaneously in the direction of concentration decrease.

Fick's second law is then obtained by evaluating the net change in flux

with an elemental control volume,

$$\nabla J = \nabla \cdot [\mathcal{D}\nabla C] = \mathcal{D}\nabla^2 C + \nabla \mathcal{D} \nabla C = \frac{\partial C}{\partial t} \tag{2.5}$$

During the early development of the theory, the diffusion coefficient $\mathcal{D}$ is considered as constant under isothermal conditions,

$$\mathcal{D}\nabla^2 C = \frac{\partial C}{\partial t} \tag{2.6}$$

In one-dimensional Cartesian coordinates,

$$\frac{\partial C}{\partial t} = \mathcal{D}\frac{\partial^2 C}{\partial x^2} \tag{2.7}$$

Eq. (2.7) is the linear form of Fick's law of the solution-diffusion mechanism for one component in one-dimensional planar coordinates.

In practice, the situation might be more complex, for example, $\mathcal{D}$ can depend on the gas concentration C and the geometry of the membrane can be complex. In these conditions, the solution-diffusion mechanism is still applicable but the mathematical treatment has to be modified. More complex cases will be further discussed in Chapter 4.

Assuming that the polymeric membrane is used under constant upstream/downstream pressures, the time-dependent term in Eq. (2.7) is eliminated. As a result, the permeance J is given as

$$J = \mathcal{D}k_D \frac{\Delta P}{L} \tag{2.8}$$

where L is the effective membrane thickness and ΔP is the pressure difference between upstream and downstream sides. Since the permeability $\mathcal{P}$ is defined as $\frac{J}{\Delta P/L}$, in this simple case, the permeability $\mathcal{P}$ can be written as the product of the diffusion coefficient $\mathcal{D}$ and the sorption coefficient k_D.

Furthermore, the permeability (or permeance) ratio of two gas species (i, j and $\mathcal{P}_i > \mathcal{P}_j$) is defined as the ideal selectivity (or permselectivity) α,

$$\alpha = \frac{\mathcal{P}_i}{\mathcal{P}_j} = \frac{J_i}{J_j} = \frac{\mathcal{D}_i k_{Di}}{\mathcal{D}_j k_{Dj}} \tag{2.9}$$

Conventionally, the permselectivity is always larger than 1. As a result, the gaseous component with larger permeability is always in the numerator in Eq. (2.9). Both performance factors permeability and permselectivity will be further discussed in following chapters. It can be noticed that the ratio of the diffusion coefficients is also defined as diffusion selectivity $\alpha_{\mathcal{D}} = \frac{\mathcal{D}_i}{\mathcal{D}_j}$ and the ratio of the sorption coefficients as solution selectivity $\alpha_{k_D} = \frac{k_{Di}}{k_{Dj}}$. These notions will be used later in Chapter 3.

2.3.2 Solution-diffusion mechanism in amorphous polymers

As an amorphous material, a polymeric membrane can exist in two states which are split by a called transition temperature T_g. Above this transition temperature, the situation is rather simple. The distribution and heat motions of the chain segments in polymers at temperatures well above the glass transition look like those in a normal liquid. Simple gaseous components are not very soluble in such polymers. Thus the simple approach (Eq. (2.3)) is largely used as a good approximation in qualitative or semiquantitative descriptions for a large number of membranes. However, the situation is much more complicated when the polymer membrane is below its transition temperature. The linear relation of Eq. (2.3) is not quantitatively observed for the same polymer below its transition temperature [Koros and Paul, 1978, Meares, 1954] (Fig. 2.6).

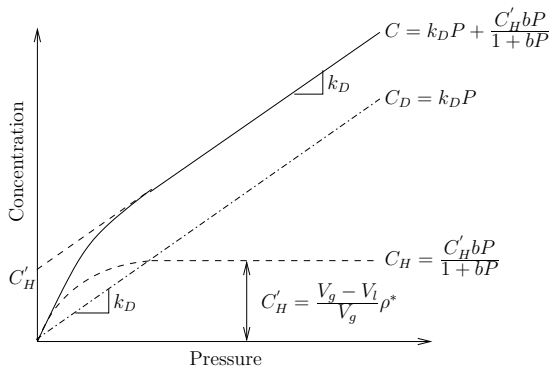

Figure 2.6: Schematic representation of a Dual Mode Sorption theory in a glassy polymer

In order to explain the non-linear isothermal sorption for glassy polymers, [Barrer et al., 1957] suggested that the polymer in a glassy state contains a distribution of frozen microvoids (Fig. 2.7) in the structure as the polymer is cooled when crossing its glass transition temperature. Thus, free segmental rotations of the polymer molecular chains are restricted in a glassy state, resulting in fixed microvoids throughout the polymer membrane. These microvoids in the glassy polymer network act in order to partially or totally immobilize a portion of the penetrated molecules by entrapment or by binding at high energy sites at their molecular peripheries, in a way similar to an adsorption phenomena. Based on this concept of microvoids in glassy polymers and experimental observation, Meares [1954] originally postulated two concurrent sorption mechanisms, ordinary Dissolution described by Henry's law concentration C_D and a Hole-filling process described by Langmuir ad-

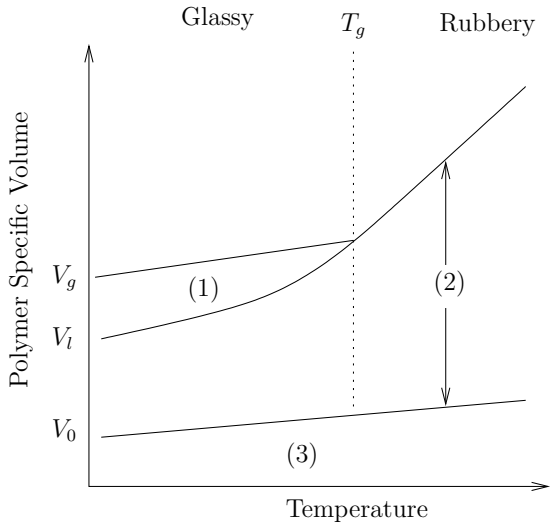

Figure 2.7: Schematic representation of the relationship between the polymer specific volume and temperature in amorphous polymers. Zone (1) refers to the unrelaxed volume in polymers: adsorption obeys Langmuir law in microvoids. Zone (2) refers to the overall free volume in polymers. Zone (3) refers to the occupied volume by the polymers.

sorption concentration C_H (Fig. 2.6)

$$\begin{aligned} C_D &= k_D P \\ C_H &= \frac{C_H^{'} b P}{1 + bP} \end{aligned} \tag{2.10}$$

where $C_H^{'}$ is the hole-filling constant, b is the hole affinity constant and P is the partial pressure of the concerned component. Then

$$C = C_D + C_H = k_D P + \frac{C_H^{'} b P}{1 + bP} \tag{2.11}$$

According to the explication of [Meares, 1954], the k_D parameter represents the penetrant dissolved in the polymer matrix at equilibrium and b characterizes the sorption affinity for a particular gas-polymer system. $C_H^{'}$ is often used to measure the amount of the non-equilibrium excess free volume in the glassy state. Eq. (2.11) forms the basis of the Dual Mode Sorption theory [Koros et al., 1977, Vieth and Sladek, 1965, Vieth et al., 1976], whose application in gas transport modeling in polymeric membranes will be further discussed in Chapter 4.

A physical interpretation of the Langmuir capacity $C_H^{'}$ in glassy polymers for condensible penetrants was given by Koros and Paul [1978] in the following

terms:

$$C'_H = \frac{V_g - V_l}{V_g}\rho^* \tag{2.12}$$

where $\frac{V_g - V_l}{V_g}$ is the unrelaxed volume fraction in the polymer shown in Fig. 2.7, and ρ^* is the molar density of penetrant sorbed in this volume. In addition, Fig. 2.7 presents the conventional relationship between polymer specific volume and temperature. When the operating temperature goes close to the transition temperature T_g, the unrelaxed volume fraction $\frac{V_g - V_l}{V_g}$ decreases until zero as well as the presence of the Langmuir population. On the other hand, as the polymer glass transition temperature T_g increases, the non-equilibrium unrelaxed volume (zone (1) in Fig. 2.7) increases at a given temperature T.

2.4 Membrane formation

Dense homogeneous membranes are frequently used in laboratory research to characterize the intrinsic permeation properties. They are normally prepared by the solvent casting or melt extrusion techniques. For the solvent casting technique, the polymer solution with a certain viscosity is cast on a flat plate followed by solvent evaporation at a given temperature. For polymers such as polyethylene, polypropylene and polyamide that are difficult to dissolve in solvents, the membranes can be produced by the melt extrusion technique. The membranes are formed by compressing the polymers between two heated plates at a temperature just below the melt point of the polymers [Lloyd, 1985].

Most of the membranes for gas separations in industry are asymmetric or composite membranes [Koros and Fleming, 1993]. These membranes have a very thin selective layer, formed by solvent casting or dipcoating, supported on a porous substrate in order to achieve a high permeation flux. According to the solution-diffusion mechanism and the definition of the permeance (Eq. (2.8), a thin membrane effective thickness favors the permeation rate, as well as the productivity of the whole process.

- **Asymmetric membranes**. Asymmetric membranes (Fig. 2.8, left) are layered structures in which the porosity, pore size or the membrane composition changes gradually from one side to the other side of the membrane. The membranes are normally prepared by a phase inversion process, in which a polymer solution is separated into two phases: a solid, polymer-rich phase that forms the matrix of the membrane, and a liquid,

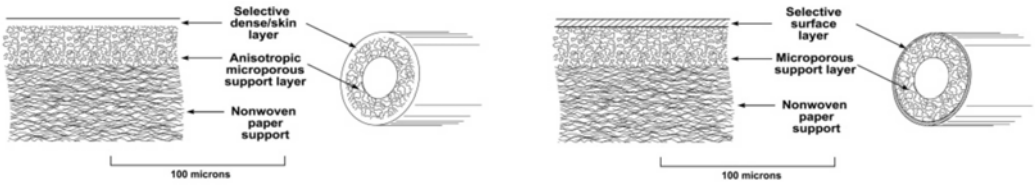

Figure 2.8: Structure of membranes used in membrane-based gas separation [Baker and Lokhandwala, 2008]. Left: Asymmetric membranes (Anisotropic Loeb-Sourirajan Membranes [Spillman, 1989]). Right: Composite membranes.

polymer-poor phase that forms the pore of the membrane [Kesting, 1985]. It can be noticed that the membrane used in experimental developments of this thesis (Chapter 6) is a kind of asymmetric membrane with a thin selective layer of poly(phenylene oxide) for $\{N_2/O_2\}$ separation.

- **Composite membranes**. Composite membranes (Fig. 2.8, right) are formed primarily for two reasons: to seal the defects on the surface of an asymmetric membrane ("resistance model" composite membrane), or to form a dense selective layer on the top of a porous substrate (thin-film composite membrane). Several methods have been developed to prepare composite membranes: solution coating, interfacial polymerization, thin-film lamination and plasma polymerization.

The membrane formation is not the key issue of discussion within the frame of the thesis study. For sake of convenience, the membranes used in simulation of this thesis are all assumed to be homogeneous in thickness, in other words, the effective membrane thickness is considered as equal to the real fiber's thickness and the permeation parameters are independent on the membrane thickness.

2.5 Membrane modules for gas separation

The core part of any membrane plant is the module, i.e. the technical arrangement of the membranes. Three major types of modules can be distinguished (Fig. 2.9):

- **Plate and frame.** The plate and frame modules are one of the earliest types of membrane modules. Simply, a planar membrane separates the permeate and the retantate flows. It results in relatively high cost and low packing density. Nevertheless, the cleaning work is relatively easy to perform. Consequently, plate and frame modules are now used only in

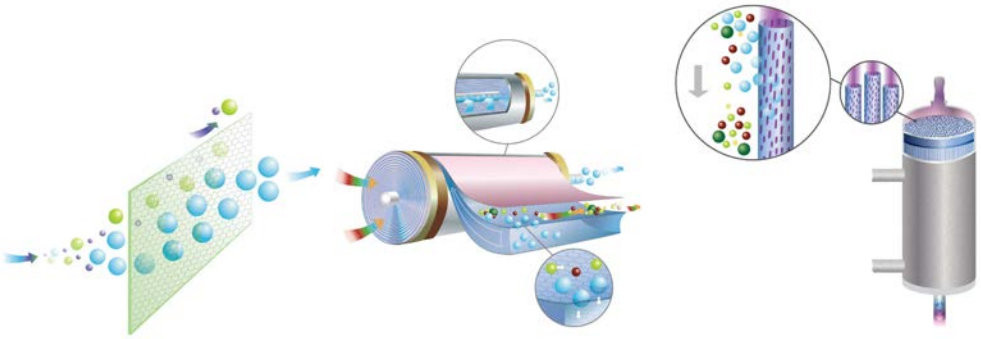

Figure 2.9: Schematic membrane modules. Left: Plate and frame module. Middle: Spiral-wound module. Right: Hollow fiber module (http://www.co2crc.com.au/)

some electrodialysis and pervaporation systems and in a limited number of reverse osmosis and ultrafiltration applications with highly fouling conditions.

- **Spiral-wound.** The spiral-wound module is characterized by a relative high packing density (>900 $m^2.m^{-3}$) and a simple design. Essentially, two or more 'membrane pockets' are wound around a permeate collecting tube with a special mesh being used as spacers. The membrane 'pocket' consists of two membrane sheets, with a highly porous support material (permeate-side spacer) in between, which are glued together along three edges. The fourth edge of the pocket is attached to the collecting tube. Several such pockets are spirally wound around the collecting tube with a feed-side spacer placed between the pockets forming a so-called 'element'. Usually, several elements are assembled in one pressure vessel. The feed-side flow is strictly axial in most designs (UOP, Abocor, Film Tec) or enters at the cylindrical surface of the element and exits axially. In any case, the permeate flows through the porous support inside the 'pocket' along the spiral to the collecting tube. Like the hollow fiber module, the spiral wound module cannot be cleaned mechanically. The classic spiral wound module is characterized by cross-flow and accurate modeling must, therefore, take into account the two-dimensional nature of velocity, pressure and concentration distribution for both feed and permeate channels. All models considering distributions only on one side (permeate or feed chamber) and assuming constant values on the other side are of limited use.

- **Hollow fiber.** Essentially the hollow fiber module consists of a pressure vessel containing a bundle of individual fibers [Rautenbach and Albrecht,

1989]. The open ends of the usually hairpin-like bent fibers are 'potted' into a head plate (an exception to this design is a gas permeation module manufactured by Dow Chemical with straight hollow fibers potted into a head plate at both ends). The feed solution may flow radially or in parallel with respect to the hollow fibers. Since the permeate is collected at the open ends of the fibers, the parallel flow may be either cocurrent or countercurrent, depending on whether the permeate in the fibers flows in the direction of the feed flow or against it. The distinction is important since the high friction losses in the fibers affect the local trans-membrane pressure difference.

It can be noticed that the two last modules combining a high packing density and reasonable manufacturing costs are by far the most successful designs. As a result, most of today's membrane-based gas separations are performed in hollow fiber modules, with perhaps fewer than 20% being performed in spiral-wound modules [Baker, 2002]. Baker and Lokhandwala [2008] indicate that one trend of the development of the membrane module is a move to larger ones in order to reduce the whole cost of the separation. Fig. 2.10 highlights

Figure 2.10: Photograph showing the development of hollow fiber modules at Cynara [Baker and Lokhandwala, 2008], from the first 5-in. modules of the 1980s to the 30-in. diameter behemoths currently being introduced. Photo courtesy of Cynara Company (now part of NATCO Group, Inc).

the size evolution of hollow fiber modules during the last 30 years.

Consequently, the most applied module-hollow fiber module is chosen as the only membrane module in our simulation studies of this thesis.

2.6 Processes and applications

Membrane-based gas separations can be applied for both non-condensible gas separation and condensible gas and vapor separation. Non-condensible gases (called also permanent gases) are those gases with a critical temperature lower than the room temperature, and they do not condense even when a very high pressure is applied at room temperature (e.g. H_2, N_2, O_2 and He). In contrast, condensible gases are the gases or vapors that could be condensed at the room temperature. Most membrane processes for non-condensible gas separation (such as hydrogen separation and air separation) have been well established, while processes for condensible gas separation, including CO_2 separation, organic vapor separation and gas dehydration, are being developed or to be developed. In the past decade, a few review papers were published adressing the development, perspective, and strategies of the applications of membrane-based gas separation [Adhikari and Fernando, 2006, Baker, 2002, Baker and Lokhandwala, 2008, Freeman and Pinnau, 2004, Koros and Fleming, 1993].

2.6.1 Non-condensible gas separation

2.6.1.1 H_2 separation

Hydrogen separation from N_2 in ammonia synthesis purge gas streams is the first large-scale commercial application of membrane gas separation. Hydrogen is a small, non-condensible gas, which is highly permeable compared to other gases in glassy polymers. Polysulfone and cellulose acetate are the membrane materials used for hydrogen separation in the early days, and now a variety of membrane materials are being used, including polyimides (Ube, Praxair), polyaramide (Medal) or brominated polysulfone (Permea) [Baker, 2004].

Recently, large scale applications of hydrogen recovery have been extended to waste gases (refinery fuel gas stream, PSA vent gas and hydrocracker/hydrotreater off-gas) in refinery plants because of the increase in hydrogen demand in refineries with ever increasingly stringent environmental regulations and heavier crude feed stocks. The problems that affect this application are the membrane reliability, caused by fouling, plasticization and condensation of hydrocarbon vapors on the membrane surface. These problems may be solved by either developing more robust membranes or using better pre-treatment techniques to reduce the dew point of the hydrocarbon in the feed gas streams to be treated by membranes.

In Chapter 5, several H_2 separations are taken into account in case studies.

2.6.1.2 O_2/N_2 separation

The production of nitrogen from air is by far the largest membrane gas separation process. The current membranes have O_2/N_2 selectivities up to 8, and can generate a 99% nitrogen product at an overall nitrogen recovery of 50% at an operating pressure of 0.8-1.0 MPa [Baker, 2002].

It is much more difficult to produce high-purity oxygen from air than high-purity nitrogen because of the low concentration of oxygen in feed (air in most cases) than nitrogen and the oxygen product is in the permeate side of the membrane where some N_2 always permeates with O_2. As a result, a permeate containing 30-60% O_2 can be produced by a one-step membrane process with an O_2/N_2 selectivity of 8. At this purity, the oxygen-enriched air can be used in number of processes, for example, in Claus plants and FCC catalyst regeneration in refineries or in improving the efficiency of high temperature furnaces or cement kilns [Baker, 2002]. However, most users require purer O_2. To be competitive with current cryogenic technology, membranes with both a high selectivity and a high flux are required. Facilitated transport membranes (Tab. 1.1) are one of approaches to improve the membrane permselectivity. In these membranes, an oxygen-complexing carrier compound acts as a "shuttle" to selectively transport oxygen across the membrane [Baker, 2002, Ravanchi et al., 2009]. One example of facilitated transport membrane for O_2 permeation is given in Fig. 2.11. A reversible complexation between O_2 and a cobalt carrier enhance largely O_2 sorption in the membrane as well as its permeation rate with respect to other gaseous components in a mixture. As a result, the membrane becomes extremely selective and permeable with regard to O_2. These spectacular permeability and selectivity of this type of membrane have maintained interest in facilitated transport despite many problems, mostly related to the poor chemical stability of the carriers and the evaporation, degradation, and other problems of the immobilized liquid membrane. Baker [2002] indicates that the membrane example shown in Fig. 2.11 never functioned for more that a month. Nevertheless, this is an area of research where a breakthrough could lead to a significant commercial result.

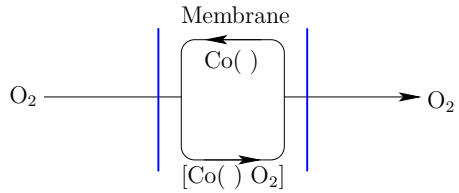

Figure 2.11: Schema of a facilitated transport membrane using the cobalt carrier Co(3-MeOsaltmen) [Co()] to transport oxygen across an immobilized liquid membrane according to Baker [2002].

In Chapter 6, a commercially available hollow fiber module is applied for O_2/N_2 separation in a pilot apparatus.

2.6.2 Condensible gas and vapor separation

2.6.2.1 CO_2 separation

Both glassy polymers and rubbery polymers can be used for CO_2 separation, taking advantage of their mobility selectivity and solubility selectivity, respectively. In practice, glassy polymer membranes are usually used for the separation of CO_2 from natural gas [Baker, 2002]. In spite of the simple flow configuration and low maintenance, only small scale membrane systems can compete with traditional amine absorption systems mainly because of the limited selectivity and flux of current membranes. Membrane swelling caused by carbon dioxide and hydrocarbons will significantly lower the membrane selectivity. Currently, cellulose acetate membranes only have a selectivity of 12-15 for CO_2/CH_4 under normal operating conditions [Brandrup and Immergut, 1989]. These membranes are now slowly replaced by the more selective polyimide and polyamide membranes whose selectivities are in the range of 20-25.

Another application of increasing interest is the separation of CO_2 from flue gases. The emission of CO_2 from combustion flue gas is a major contributor to global warming, and the capture/separation of CO_2 from flue gas is an important step for greenhouse gas emission control. Membrane process is very efficient for bulk separation where a very high purity is not required, which makes membrane process particularly attractive for flue gas separation. Membrane-based gas separation is a pressure driven process, where a pressure difference across the membrane should be maintained to provide the driving force necessary for permeation. For this process, a critical issue is the energy used to power the compressors or vacuum pumps for the separation. The quantity of flue gas to be treated is very large with relatively low source pressure. Increasing the operating pressure will increase the membrane productivity, but this is at the expense of increased compressing costs. Considering the cost of gas compression, membranes with a high permeance and reasonable selectivity are needed in order to make the separation process cost effective. In Sections 5.2 and 5.3, two case studies for cyclic membrane processes about the CO_2 recovery from flue gas are given with systematical comparisons to conventional operations.

2.6.2.2 Other separations

Membrane technology is also applied in the separation of vapor/gas mixtures. In principle, either rubbery polymers (such as silicone rubbers, which can

selectively permeate the more condensible vapor) or glassy polymers (which can permeate the smaller gas preferentially) can be used. In most industrial applications, vapor permeable rubbery membranes are used because of their both high permeation flux and selectivity. To achieve a target product concentration and recovery, either multi-stage membrane systems or hybrid systems combining vapor permeation with condensation or sorption are often used.

Membranes provide also a promising technology for the separation of light olefin from their associated paraffins because the currently used low temperature distillation is capital- and energy-intensive due to the close volatilities of the components in the mixtures. Some work has been done using the traditional polymeric membranes. The selectivities are, however, low due to the membrane plasticization. Therefore, there is a substantial loss in the selectivity under the plant operating conditions. Facilitated transport membranes have received much attention as a potential technology for future olefin/paraffin separation. They are based on selective and reversible reaction of unsaturated hydrocarbons with certain metal ions by π complexation. The metal ions act as a carrier for the olefin transport, thereby facilitating the permeation of olefin through the membrane. Membranes made from polymer electrolytes of poly(ethylene oxide) and $AgBF_4$ have shown a very high permeability and selectivity for olefin/ paraffin separation. However, this type of membranes suffers from problems associated with the membrane stability. Further efforts are needed to improve the membrane stability before they can be used for commercial applications.

2.7 Membrane process improvement

Considering three performance criteria indicated in Fig. 2.3 and the comparison in Tab. 1.1, membrane-based gas separation is far from perfect. Membrane process should be enhanced essentially in two ways: material investigations and process operation optimizations.

2.7.1 Material investigations: Mixed Matrix Membranes

As discussed previously, most conventional membrane processes of gas separations are performed by means of dense polymeric materials at steady state. The relatively poor permeability/permselectivity is the key issue according to which the membrane-based process is not competitive with respect to other technologies such as cryogenics and adsorption. Thus, the seek of efficient polymeric membranes with both high permeability and permselectivity is one of the top issue investigations of membrane process enhancement.

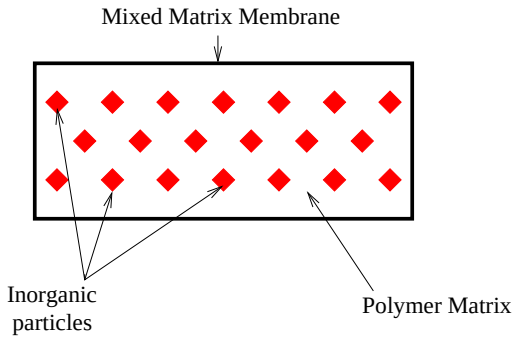

Figure 2.12: Schematic representation of a typical MMM [Aroon et al., 2010].

Despite concentrated efforts to tailor polymer structure to affect separation properties, pure polymeric membrane materials have seemingly reached a limit in the trade-off (called Robeson's upper bound) between permeability and permselectivity [Freeman, 1999, Robeson, 2008]. On the other hand, zeolite membranes and carbon molecular sieves, classified as inorganic membranes or nonporous membranes [Rautenbach and Albrecht, 1989], offer in general both higher permeability and permselectivity than classical polymeric membranes [Caro et al., 2000]. Nevertheless, processing challenges and high costs hinder their industrial application. For example, a zeolite membrane module costs around US$ 3000/m^2 of effective membrane area while it is only US$ 20/m^2 for existing polymeric hollow fiber membrane modules. In addition, the manufacture of zeolite and carbon molecular sieve membrane involves high-temperature processes [Vu et al., 1996, 2003]. Mixed Matrix Membranes

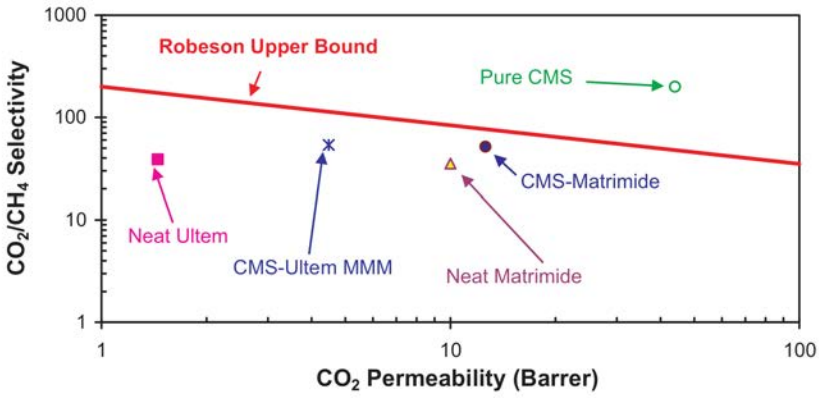

Figure 2.13: Effect of CMS on the performance of polymeric Matrimide and Ultem membranes [Aroon et al., 2010].

(MMMs) [Aroon et al., 2010] have been thus proposed as an intermediate approach between polymeric and inorganic membranes in order to reach the best trade-off (Fig. 2.12): highly selective but expensive adsorptive fillers (usually inorganic particles) are incorporated into a processable polymeric matrix. This heterogeneous membrane concept combines the advantages of each medium: high separation ability, desirable mechanical properties and economical processing capabilities [Paul and Kemp, 1973, Vu et al., 2003]. By doing so, the classical trade-off can thus be exceeded. For example, Singh and Koros [1996] showed that the performance of carbon molecular sieve (CMS) membranes was beyond Robeson's upper bound and showed also that CMS membranes had good potential for use in gas separation. Another example is given in Fig. 2.13 according to Aroon et al. [2010], CMS as a porous dispersed phase can increase separation properties of both polymeric Ultem and Matrimide polymeric membranes close to the known Robeson upper bound.

2.7.2 Operation optimizations

As explained previously, all industrialized membrane processes are performed under steady state where numerous advantages can be achieved. Besides the material development, another possibility to enhance the membrane process efficiency is to perform the separation under transient state by abandoning some other clear advantages. To our knowledge, Paul [1971] performed the first theoretical investigations of a membrane separation process working under cyclic transient operations. The essential idea was to use the difference of diffusion rates during the transient state, which is usually much more important than that under steady state, in order to perform an efficient separation. This idea and the corresponding processes are critically reviewed in Chapter 3.

In this thesis, process enhancements by cyclic operations are essentially investigated and systematically compared to those of conventional operations. Novel opportunities are exhibited through some examples. In addition, a combination of material improvement and cyclic operations is also considered in one case study (Section 5.2). By simulation and optimization studies, this combination is shown as a synergistic strategy.

Chapter 3

Cyclic membrane process review

> Science... never solves a problem without creating ten more.
>
> George Bernard Shaw

In this chapter, various theoretical and experimental cyclic membrane gas separation process studies are reviewed. With respect to the cycle duration, these processes are classified into short and long classes. In a second step, a systematic analysis of potential interests of the short class of cyclic processes compared to steady-state performances has been performed based on trade-off correlations. Finely, both short and long class processes are compared. These review works constituted the first part of a publication in *Journal of Membrane Science* [Wang et al., 2011a].

3.1 Gas transfer through membranes under transient state

The solution-diffusion mechanism [Bitter, 1991] which is mentioned in Chapter 2 and will be detailed in Section 2.3 is a simple but efficient description of gas transfer phenomena in rubbery membranes [Barrer, 1937]. In the case of glassy membranes, it is also well adapted for an approximative qualitative description. For a binary gas mixture (gas 1 and 2), the permselectivity α is characterized by

$$\alpha = \frac{\mathcal{D}_1 k_{D1}}{\mathcal{D}_2 k_{D2}} \tag{3.1}$$

where $\mathcal{D}$ is the diffusion coefficient, a kinetic term, and k_D is the sorption coefficient, a thermodynamic term. For most polymer membranes with few exceptions, k_D is favored while $\mathcal{D}$ is disfavored in case of a large molecular size [Corriou et al., 2008]. Thus, for a steady-state operation, these two ratios often have opposite behaviors resulting in a decreased overall selectivity α, although $\frac{\mathcal{D}_1}{\mathcal{D}_2}$ or $\frac{k_{D1}}{k_{D2}}$ can be rather large individually.

Assuming a binary gas mixture with diffusion coefficients $\mathcal{D}_1 = 2\mathcal{D}_2 = 0.1\ 10^{-10}\ \mathrm{m^2.s^{-1}}$, permeabilities $\mathcal{P}_1 = \mathcal{P}_2 = 0.05\ 10^{-16}\ \mathrm{m^3\ STP.m^{-1}.Pa^{-1}.s^{-1}}$ and identical initial mole fractions, the behavior in the transient state through a membrane of 20 μm after an upstream pressure step leading to the permeation time lag is simulated by means of a simple solution-diffusion model. This experiment is called time-lag measurement and will be detailed in Chapter 4. According to Fig. 3.1, Gas 1 is for a 'short' duration accumulated more rapidly in the permeate. When the permeation duration becomes long, on the other hand, the pressure profiles for both gases tend to be parallel. For long times, the composition in downstream volume tends toward the initial composition of the binary gas mixture.

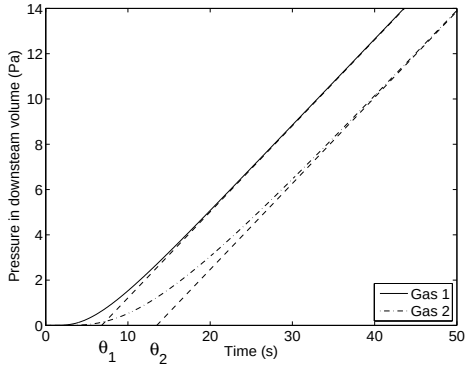

Figure 3.1: Simulation results of the time lag behavior of gases 1 and 2 with diffusion coefficients $\mathcal{D}_1 = 2\mathcal{D}_2$ and permeabilities $\mathcal{P}_1 = \mathcal{P}_2$.

The permeation rate of the same binary gas mixture is shown in Fig. 3.2 for the same permeation time lag simulation. The permeation rates are normalized with respect to the permeation rate at steady state, at which, both gases in Fig. 3.2 have the same permeating rate since their permeabilities are identical ($\mathcal{P}_1 = \mathcal{P}_2$). After some time (50 s in Fig. 3.2), an asymptotic regime is reached where the fluxes are constant, therefore the downstream pressure increases linearly with time, which corresponds to a steady state.

This time duration, called time lag θ, differs for each gas, and is governed

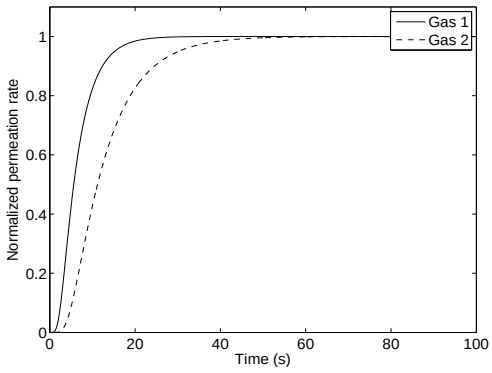

Figure 3.2: Permeation rate for gases 1 and 2 with diffusion coefficients $\mathcal{D}_1 = 2\mathcal{D}_2$ and permeabilities $\mathcal{P}_1 = \mathcal{P}_2$. Results are obtained by simulation of the time lag behavior.

by its diffusion coefficient $\mathcal{D}$, according to

$$\theta_k = \frac{L^2}{6\mathcal{D}_k} \tag{3.2}$$

where L is the membrane thickness. Consequently, in transient mode, gas 1 will respond twice faster through the same membrane since $\mathcal{D}_1 = 2\mathcal{D}_2$. Fig. 3.3 reveals that the ratio of the permeation fluxes is extremely important during the transient state, and a significant separation can be expected in the same time domain.

3.2 First study of cyclic transient operation

Inspired by this permeation time lag simulation (Section 3.1), Paul [1971] discovered some potential advantages of cyclic transient operation. Paul proposes to collect the permeate cyclically for a duration lower than the time lag θ_2 and larger than the time lag θ_1; consequently the permeate is mainly composed by gas 1 (Fig. 3.1). In another way, the thermodynamic effect related to solubility k_D is minor and the cyclic period is comparable to the time lag of the gas with the lower diffusion coefficient.

Based on this idea, Paul developed a cyclic process (Fig. 3.4), in which two tanks are disposed upstream and two tanks downstream. Paul studied the possibility of separation when the valves are operated in a cyclic manner consisting of stages of alternatively high and low upstream pressures (Fig. 3.5). The valves are considered to be synchronous which means that the duration of

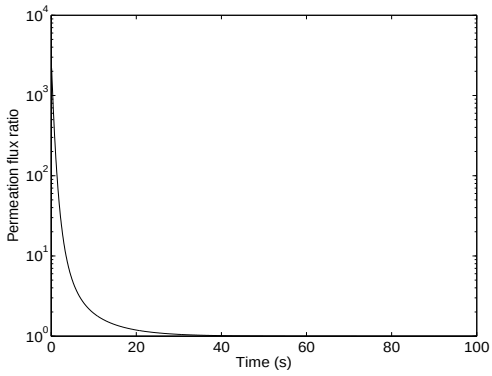

Figure 3.3: Permeation flux ratio of gases 1 and 2 with diffusion coefficients $\mathcal{D}_1 = 2\mathcal{D}_2$ and permeabilities $\mathcal{P}_1 = \mathcal{P}_2$. Results are obtained by simulation of the time lag behavior.

the stages is the same for an upstream high pressure and downstream receiving tank on the left. The permeate collected in the receiving tank on the left in Fig. 3.4 will always be more enriched in the component with the higher diffusion coefficient while the one on the right will contain a permeate more enriched in the component with the lower diffusion coefficient. Thus, an improvement in selectivity is expected in the downstream receiving tank on the left.

In order to obtain a simulation result of this process, a series of of simplifying assumptions are made by Paul:

- The permeate quantity is neglected with respect to the feed. This means that the upstream composition is assumed to be constant.
- The downstream volume is small and thus there occurs virtually no mixing of the cuts when the downstream valves are reversed.
- The plasticization of the membrane and the flux coupling between gases are totally neglected.
- The mass transfer mechanism is considered to be solution-diffusion.
- Once the membrane material and the operating temperature are fixed, $\mathcal{D}_k$ and $\mathcal{P}_k$ are constant and equal to the values of steady-state operation.

The problem is solved by an analogy to a classical heat-transfer problem [Carslaw and Jaeger, 1959]. An analytical solution for the concentration profile is obtained by an appropriate change of variables; the permeate flow rate is then obtained from the profile by appropriate differentiations and integrations.

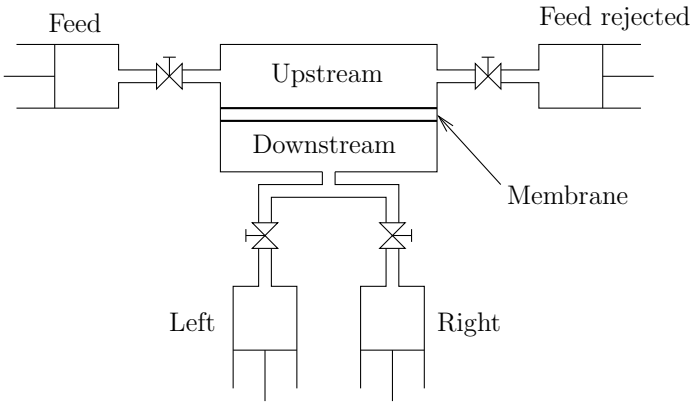

Figure 3.4: Membrane process of cyclic transient operation according to Paul [1971].

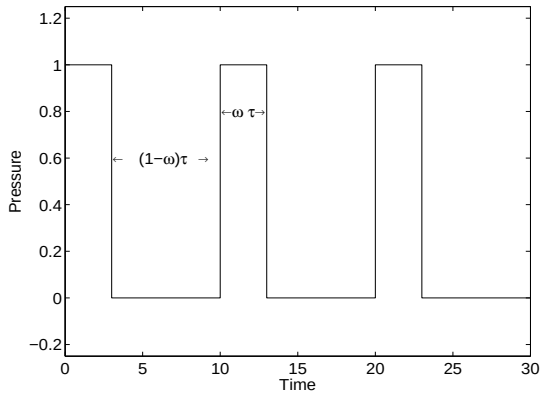

Figure 3.5: Upstream pressure pulse shape, according to Paul [1971], τ period of pressure cycle and ω fraction of period where the pressure is high.

By studying this analytical solution, Paul defines an optimized operation of his cyclic transient process. In order to maximize the selectivity, the duration of a cycle τ should be

$$\tau = U\theta_k \tag{3.3}$$

where θ_k is the time lag of the gas with the lower diffusion coefficient and U is a coefficient depending only on ω, the fraction of period during which the upstream pressure is high. Paul suggests that ω should be minimized in order to optimize the selectivity, even though the productivity decreases when ω is low. For example, in order to maximize the selectivity, U is equal to 3 whereas $\omega = 10\%$. Thus, one characteristic of Paul's cyclic transient operations is highlighted, i.e., the duration of one cycle τ should be wisely

chosen and is usually comparable to the time lag of the gas with the lower diffusion coefficient.

The simulation results show that the selectivity of Paul's process is significantly improved with recovery of helium from natural gas as a real example. The following conclusions are given by Paul:

- Spectacular enhancements in selectivity in the receiving tank on the left occur at small values of ω. The improvement is not clear if $\omega > 0.8$.
- For a given ω, the enhancement increases as the diffusion selectivity equal to the ratio of diffusion coefficients $\frac{\mathcal{D}_1}{\mathcal{D}_2}$ becomes larger but a finite limit is reached.

It can be noticed that Paul's process has some similar points with Pressure Swing Adsorption (PSA) processes:

- The notion of cycle exists in the PSA process as well as in Paul's process.
- The separation is performed in the transient state, for which reason a regeneration step is necessary in order to render the unit usable for a next cycle.

Consequently, a possible reason for little activity after Paul's article is that membranes are typically promoted as simple passive devices, which serves as a selling argument with regard to PSA processes. The latter require multiple vessels and many valves which are often switched and in need of maintenance. However, the cyclic transient membrane processes can no longer be considered as simple and will require a complex environment structure in some ways similar to a PSA process.

In conclusion, Paul's process minimizes the influence of the solubility k_D in membrane separation processes, which is generally negative. Consequently, this operation enables an enhancement of the process selectivity. The study carried out by Paul gives a global view of a typical example of cyclic transient operations and offers an interesting perspective of membrane gas separation. However, Paul's study remains mainly qualitative and describes more a principle than the actual conditions of operation. First, his simulation is based on an unrealistic condition. For example, the feed composition is considered to be constant which means that the productivity of the process is null, i.e., a vanishing stage cut is required. Second, in order to simplify the solution of the problem, several parameters are considered to be constant. For example, only a synchronous operation and a simple mass transfer mechanism are taken into account. Moreover, the results remain theoretical, the process complexity is not discussed and the process is not verified experimentally.

3.3 Classification of cyclic transient operations

Paul develops the notion of cyclic transient processes and demonstrates the relevance of his cyclic transient process. It can be noticed that his process is characterized by a short duration of high pressure and a relatively long duration of low pressure. These characteristics of Paul's process are also confirmed and highlighted by other researchers, which will be discussed later in this paper. Thus, these processes are classified in the short class, with reference to the short duration of high pressure. In contrast, processes where this duration is larger than the time lag will belong to the long class. Even if Paul does not mention it, the membrane thickness is of importance in order for his process to be controllable in reality. This is another essential characteristic of Paul's process, which will be also discussed later. Consequently, with respect to Paul's notions, the cyclic transient operations can be classified into two main families shown in Table 3.1.

	Short class: class of Paul's process	Long class: class of longer cyclic transient operations
Stage duration	$\approx$ time lag	$\gg$ time lag
Regeneration stage	Necessarily long	Not necessarily long
Membrane thickness	Thick	Not necessarily thick
	Short cycle	Long cycle

Table 3.1: Classification of cyclic transient operations

More fundamentally, in the short class processes, the transient behavior in the selective layer of the membrane is utilized, whereas in the long class processes, the transient behaviors occur in the system outside the membrane. This paper first reviews the processes similar to Paul's, i.e., those of the short class, after which some cyclic transient operations belonging to the long class are discussed. All these cyclic transient operations are summarized in Table 3.2.

3.4 Short class studies

3.4.1 Higuchi study

Following Paul's study, Higuchi and Nakagawa [1989] simulate a separation of $\{N_2,O_2\}$, using a real polydimethyl siloxane membrane of 0.01cm.

Higuchi considers similar assumptions to those of Paul, but proposes a different analytical solution of the problem. From this analytical solution,

Researchers	Class	Year	Investigation	Mixture
Paul [1971]	Short	1971	Simulation	{CH_4 , He}
Higuchi and Nakagawa [1989]	Short	1989	Simulation	{O_2 , N_2}
Beckman et al. [1991]	Short	1991	Simulation & Experiments	{He , CO_2}
LaPack and Dupuis [1994]	Short	1994	Experiments	Organic gases
Corriou et al. [2008]	Short	2008	Simulation	{H_2 , CO_2}
Ueda et al. [1990]	Long	1990	Experiment	{O_2 , N_2}
Feng et al. [2000]	Long	2000	Simulation & Experiments	{H_2 , N_2}
Nemser [2005]	Long	2005	Experiment	{Air , VOC}

Table 3.2: Summary of cyclic transient operations studied by different researchers

Higuchi draws the following conclusions:

- The conclusion obtained by Paul is confirmed by another solution: a cyclic transient process presents an improvement in selectivity over steady-state operation.
- Some real operation conditions are considered: Higuchi indicates that a thick membrane is required in order to achieve a practical time interval of the upstream pressure pulse. In Paul's study, this practical aspect is totally neglected.
- The importance of the membrane regeneration for a transient process is emphasized, which is not clearly mentioned in Paul's study. Due to this compulsory regeneration duration, which is rather long compared to the high pressure duration, Higuchi indicates that the cyclic transient process productivity is greatly reduced compared to a steady-state operation. However, no quantitative comparison between transient and steady-state operating modes is performed.

Higuchi also uses his analytical solution to simulate the process of concentration of uranium 235 from natural uranium, however in this case by means of inorganic microporous membranes working in the Knudsen regime. As the cyclic transient process is more selective, Higuchi indicates that the membrane device for the concentration of the uranium 235 will be 1/31 in size compared to the conventional device and will lead to the curtailment of operating costs if the upstream pressure is regulated and the permeation occurs at the transient state.

Nevertheless, this conclusion is given by considering only the selectivity. If the productivity is taken into account, the transient operation device would need to be huge in order to reach the productivity of a conventional device. It thus follows that the capital costs may not be advantageous. This separation will be discussed further in this paper.

3.4.2 Beckman process

Beckman et al. [1991] also investigate the separation of gas mixtures in unsteady state conditions. His process is of the same nature as Paul's. Assuming two types of cyclic inlet sources taken as sinusoidal and square pulsed inlets, Beckman independently obtains his analytical solution which again confirms the advantage of cyclic transient operation. Beckman also ignores the productivity and recommends his process as separating membranes covering sensors which require very high selectivity factors whereas a decrease in productivity is of less importance, since the sensor sensitivity is quite high.

After this theoretical study, an experimental verification [Beckman et al., 1991] of his proposal is carried out with the use of a polyvinyltrimethylsilane (PVTMS) film with a thickness of 147 μm as a membrane. It can be noticed that the thickness of the membrane is critical as predicted by Higuchi. The investigation is performed on a {He,CO_2} gas mixture composed of 47% He and 53% CO_2. The mass transport parameters of He and CO_2 in PVTMS are given in Table 3.3. One can see that the permeability of both gases is approximately equal, whereas their diffusion coefficients differ greatly. As a result, a steady-state operation of the membrane process cannot separate this mixture, although theoretically the transient operation is expected to give a significant separation.

Through this proposal, Beckman experimentally confirms that his transient cyclic operation can efficiently separate the gas mixture. Surprisingly, Beckman claims that his application of unsteady-state boundary conditions allows a significant increase of the selectivity of the gas separation process with only a small decrease in productivity.

Property	He	CO_2
Diffusion coefficient $\times 10^{-10}$	37	0.5
Sorption coefficient $\times 10^{-6}$	0.37	28.89
Permeability $\times 10^{-16}$	13.68	14.44

Table 3.3: Transport parameters of He and CO_2 in PVTMS according to Beckman et al. [1991]. (S.I. units)

3.4.3 LaPack process

LaPack and Dupuis [1994] describe another unsteady-state process to improve the permeation selectivity by operating the membrane permeation system dynamically. This is also a cyclic transient operation similar to Paul's.

The apparatus (Fig. 3.6) comprises a membrane module with a permeable membrane which separates the main module into 2 compartments: upstream and downstream volumes. The former can be fed by a gas mixture to be separated or purged by an inert flow or totally emptied by a vacuum pump (not represented in Fig. 3.6). The downstream volume can be emptied by a vacuum pump after which its contents can be transported to a collector or diverted to another container. LaPack indicates that his process is not only applicable for gas separation but also usable for liquid separation. We notice that for liquid mass transport through a membrane, the solution-diffusion mechanism might be critical.

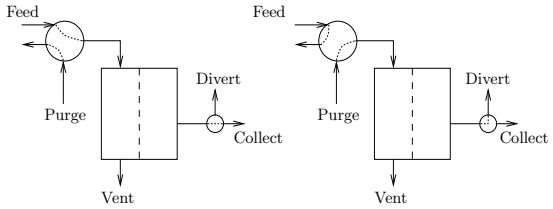

Figure 3.6: Cyclic transient process proposed by LaPack and Dupuis [1994]: Stage of high pressure in upstream volume (left) and stage of low pressure in upstream volume (right)

Similarly to Paul's process, one cycle is separated into two stages by LaPack:

- Stage 1 (Fig. 3.6, left): The desired component is collected during this stage. A feeding flow is introduced and maintained in the upstream volume. The downstream volume is held at low pressure by a vacuum pump and its contents are transfered to the collector.
- Stage 2 (Fig. 3.6, right): By switching the valves, the feeding flow is cut off while the downstream volume is still emptied by the vacuum pump but its contents are diverted during stage 2. LaPack subsequently proposes three ways to regenerate the membrane during this stage:
    1. An inert flow, called purge in Fig. 3.6, is sent through the upstream volume. This flow can be gas or liquid.
    2. The upstream volume is also emptied by a vacuum pump.

3. A solid inert barrier, such as a piston, is used to cut contact between membrane and the upstream volume.

Once the membrane is considered to be regenerated, the next cycle starts.

With regard to the duration of each stage, LaPack proposes to perform experiments, as opposed to Paul's simulation. Through some time lag experiments, the duration of each stage can be defined. Normally, both methods give identical results. But it is important to notice that the experimental method is more direct and involves no risk of inappropriate assumptions, regarding for example, the mass transfer mechanism. However, compared to the simulation method, the experimental approach is both time and money consuming.

An experimental verification of LaPack's design confirmed again that cyclic transient operations can improve the selectivity of membrane processes compared to steady-state operations and LaPack indicates qualitatively a productivity decrease. Furthermore, LaPack suggests that his process is particularly beneficial and useful for producing a permeate for chemical analysis operation requiring a high purity, e.g., mass spectrometry.

This design and Paul's process are very similar. Although using two separate ways, simulation vs. experiments, both show the advantages of cyclic transient operations. At the same time, both emphasize the optimal operating conditions, i.e., that the high pressure duration should be lower than the time lag of the component with the lower diffusion coefficient and that membrane regeneration is necessary. However, productivity loss is only quantitatively mentioned by Paul and LaPack. LaPack indicates that this process is particularly useful for an analytical instrument, for which the concentration is not a very sensible issue.

3.4.4 Corriou study

Corriou et al. [2008] perform a systematic evaluation of Paul's idea. A preliminary study is carried out; the illustrative gas mixture and the corresponding membrane are wisely selected according to the following arguments:

- Industrial application needs.
- Availability of the material.
- Quasi constant transport parameters in order to maintain the assumption.
- Absence of flux coupling in the mass transfer situation.

Under these conditions, the diffusion of a gas component k in a plane membrane is governed by Fick's second law. In the case of a single membrane of thickness L submitted to an upstream partial pressure P_k^0, when vacuum is initially created upstream and downstream, Corriou models this transport for a plane membrane with the following initial and boundary conditions,

$$\begin{aligned} &\frac{\partial C_k(z,t)}{\partial t} = \frac{\partial}{\partial z}\mathcal{D}_k\frac{\partial C_k(z,t)}{\partial z} \\ &C_k(z,0) = 0 \qquad \forall 0 \leq z \leq L \\ &C_k(0,t) = k_{Dk}P_k^0 \qquad \forall t \\ &C_k(L,t) = k_{Dk}P_k^d \qquad \forall t \end{aligned} \tag{3.4}$$

where $\mathcal{D}_k$ is the diffusion coefficient of component k which eventually can depend on its concentration $C_k(z,t)$, k_{Dk} is the sorption coefficient and P_k^d is the downstream partial pressure of component k.

By taking into account these factors, a $\{CO_2,H_2\}$ equimolar gas mixture separation through an elastomeric polyisoprene-co-acrylonitrile membrane is selected to illustrate the process performance. Paul's approach is simulated by a rigorous numerical study, the finite volume method, instead of an analytical solution. The gas transport parameters of $\{CO_2,H_2\}$ are given in Table 3.4. According to their permeabilities, this gas mixture is difficult to separate with the used polymer, while an important difference on the diffusion coefficients suggests that the short class process should be efficient. It can be noticed that the transport parameters used in Corriou's original short class simulations differ from the reference to the Polymer Handbook [Brandrup and Immergut, 1989] (Table 3.4). With Corriou's parameters, the short class process performance is slightly overestimated since the difference between the diffusion coefficients are more important than the data from the Polymer Handbook [Brandrup and Immergut, 1989]. However, in Corriou's simulation of the reference conventional process performances, the permeability values from the Polymer Handbook [Brandrup and Immergut, 1989] is used. In a general manner, the principle underlined by Corriou et al. [2008] remains valid.

Property	H_2	CO_2
Diffusion coefficient $\times 10^{-10}$	2.47	0.031 *(0.0031)*
Sorption coefficient $\times 10^{-6}$	0.227 *(0.277)*	10.6
Permeability $\times 10^{-16}$	0.558	0.326

Table 3.4: Transport parameters of H_2 and CO_2 in polyisoprene-co-acrylonitrile according to Brandrup and Immergut [1989]. The data used by Corriou et al. [2008] is given in italic. (S.I. units)

It is important to notice two points of Corriou's solution that differ from that of other researchers:

- The operation is not necessarily synchronous. Note respectively x_1, x_2, x_3, x_4, the opening durations of the upstream left, upstream right, downstream left and downstream right of the valves of the process (Fig. 3.4). Four valves can be opened or closed independently with the following constraint: $x_1 + x_2 = x_3 + x_4$.
- The upstream side is still considered to be constant (P_k^0 is constant), while accumulation in the downstream side is taken into account by

$$\frac{dP_k^d}{dt} = \frac{dn_k^{\text{in}}}{dt}\frac{RT}{V^d} \tag{3.5}$$

with the molar flow rate entering into the downstream side

$$\frac{dn_k^{\text{in}}}{dt} = -\mathcal{D}\left.\frac{\partial C_k}{\partial z}\right|_L A \tag{3.6}$$

where A is the surface area of the membrane. It can be seen that as the diffusions of both components are totally independent, Eqs. (3.5-3.6) are independently applicable to both components.

A separation factor is defined by Corriou as

$$\text{separation factor} = \frac{y_1^{d,\mathcal{L}}}{1 - y_1^{d,\mathcal{L}}}\frac{1 - y_1^u}{y_1^u} \tag{3.7}$$

where $y_1^{d,\mathcal{L}}$ is the mole fraction of component 1 in the downstream receiving tank and y_1^u is the upstream mole fraction of component 1. The productivity is defined as the number of moles of component 1 that are obtained in the downstream left tank divided by the total duration of operation.

First, instead of using Paul's analytical resolution, the numerical solution is systematically employed by Corriou and the selectivity of the cyclic process is optimized by two methods, nonlinear programming by means of NLPQL code for single objective optimization and genetic algorithm for multiobjective optimization. Both methods show that the optimized selectivity is found when the high pressure fraction of a cycle is minimized and the operation of the valves is quasi-synchronous. This is consistent with Paul's conclusion.

The numerical study does not only show again the advantage with regard to selectivity of the transient operation, it also indicates that the product composition becomes nearly constant after the third cycle. This observation

suggests that the start-up of short class processes is rather rapid, as it may take only 3 cycles.

The reduction of productivity is qualitatively self evident as the average pressure in a cyclic process is always lower than the feed pressure whereas a steady-state process runs at the feed pressure at all times. Secondly, even if no production is performed during the regeneration step, this stage is compulsory in order to ensure an enhanced separation factor. Such an observation has been confirmed by the simulation studies. After this single objective optimization study, the productivity is considered together with separation factor in a multiobjective optimization performed by a genetic algorithm (Fig. 3.7).

This key feature of Paul's process cannot be circumvented. Then, by comparing the performance of steady-state operation, cyclic synchronous operation and cyclic asynchronous operation, it is clearly shown that the cyclic operation offers the opportunity to largely expand the separation factor/productivity domain, compared to steady-state operation, while in the optimized separation factor situation, the cyclic operation productivity is probably too low to be used in reality.

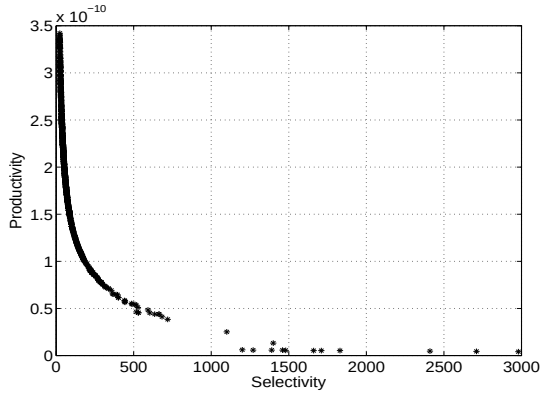

Figure 3.7: One example of Pareto's zone for the multiobjective genetic optimization (10^{th} generation) with respect to separation factor and productivity, according to Corriou et al. [2008]

As the upstream exhaustion is not taken into account, an exhaustion ratio of the upstream feed flux cannot be directly defined. Nevertheless, this exhaustion ratio should not be important since the productivity is very low compared to the feed flow rate.

One result of multiobjective optimization is shown in Fig. 3.8. All points of the last generation (10^{th} generation) of optimization are gathered along the bisecting line corresponding to equality of opening durations for the left

upstream and left downstream valves. This result is consistent with that of the single objective optimization (separation factor) where x_1 and x_3 are almost equal and both are close to zero.

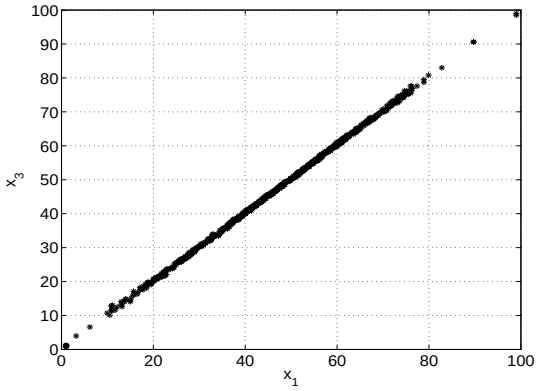

Figure 3.8: One example of Pareto's zone for the multiobjective genetic optimization (10^{th} generation) with respect to the opening durations of left upstream and downstream valves, according to Corriou et al. [2008]

This study performed by Corriou reports a systematic theoretical evaluation of cyclic transient operation of a membrane separation process, which is based on a description by Paul. It gives the following conclusions:

- The performance of cyclic transient process is again confirmed by a rigorous numerical simulation. Its best functioning is found by a numerical optimization.
- The compromise between separation factor and productivity of cyclic transient operation is highlighted and quantified. The loss of productivity can sometimes be too important to make the whole process cost effective.
- The effect of the membrane thickness is not studied; only a value of 10 μm is used in the study. Nevertheless, this choice is physically acceptable. According to Paul's analytical solution, the membrane thickness influences the cycle duration, as well as the opening of valves. According to Eq. (3.3), the optimal cycle duration should be 54 s for this gas mixture and membrane thickness in order to maximize the separation factor. In this simulation and optimization, it is arbitrarily assumed that each valve is constrained in the interval [1, 100]s corresponding to a fast opening operation for valves and a large time limit for a cycle. The optimized conditions are thus just included in the interval.

3.5 Inventory for short class processes

It is shown that short class processes allow an improvement of the selectivity by minimizing the effect of the thermodynamical term, i.e., the solubility (Eq. (3.1)). Nevertheless, a necessary condition for short class processes is that one component diffuses faster than the other one during the high pressure stage. As the high-pressure stage of short class processes is comparable to the time lag of the gas with lower diffusion coefficient, the diffusion selectivity $\alpha_{\mathcal{D}}$, i.e., ratio of diffusion coefficients, should be significantly larger than the steady-state selectivity α (Eq. (3.1)) in order to expect an improvement compared to steady-state operations. Thus, an inventory of common gaseous components is performed in order to identify potentially interesting gas mixtures based on this behavior. In this inventory, the gas mixture is assumed to be binary.

Nowadays, several correlations are available to estimate a theoretical upper bound of mass transfer parameters $(\mathcal{P}, \mathcal{D}, k_D)$ from physical data of a considered gas. A good consistency is proved by numerous investigations [Freeman, 1999, Robeson, 2008]. Thus, it is possible to estimate and compare the theoretical upper bound of the diffusion selectivity $\alpha_{\mathcal{D}}$ and the steady-state permeability selectivity α by using these correlations. As the solution-diffusion mechanism is admitted for most gas mass transfers in dense polymers, the diffusion selectivity and the steady-state selectivity in dense polymers can be related by

$$\frac{\alpha_{\mathcal{D}}}{\alpha} = \alpha_{k_D}^{-1} \tag{3.8}$$

As a result, the solubility ratio α_{k_D} is a key criterion to determine whether or not short class processes are potentially interesting to separate a binary gas mixture. In order to estimate the gas solubility in a solution, Hildebrand [1962] investigated an empirical correlation. Later, Michaels and Bixler [1951] applied this idea in the case of the gas solubility in polymers. This latter is used here in order to estimate k_{Dk} for the gaseous components of a binary gas mixture $\{1, 2\}$

$$\begin{aligned} \ln\left(k_{D1}\right) &= M + N\left(\epsilon/\mathcal{K}\right)_1 \\ \ln\left(k_{D2}\right) &= M + N\left(\epsilon/\mathcal{K}\right)_2 \end{aligned} \tag{3.9}$$

where $\mathcal{K}$ is Boltzmann's constant, $\epsilon/\mathcal{K}$ is the Lennard-Jones temperature, M and N are two empirical parameters. M is sensitive to polymer-penetrant interactions and, consequently, varies somewhat from polymer to polymer. However, as the key issue is the solubility ratio α_{k_D} for a given membrane, M can be eliminated by combining Eqs. (3.9)

$$\ln\left(\alpha_{k_D}\right) = N\left[\left(\epsilon/\mathcal{K}\right)_1 - \left(\epsilon/\mathcal{K}\right)_2\right] \tag{3.10}$$

As for a variety of liquids, rubbery and glassy polymers have N as 0.023 K^{-1}. This prediction should be accurate for most materials used in membrane separation processes.

α is conventionally defined to be larger or equal to 1. Furthermore, α_{k_D} is always defined as $\alpha_{k_{D1/2}}$. Consequently, two cases are possible

$$\begin{cases} \mathcal{P}_1 > \mathcal{P}_2 \Rightarrow \alpha_{1/2} > 1 \Rightarrow \frac{\alpha_{\mathcal{D}}}{\alpha} = \frac{\alpha_{\mathcal{D}}}{\alpha_{1/2}} = \alpha_{k_D}^{-1} \\ \mathcal{P}_1 < \mathcal{P}_2 \Rightarrow \alpha_{1/2} < 1 \Rightarrow \frac{\alpha_{\mathcal{D}}}{\alpha} = \frac{\alpha_{\mathcal{D}}}{\alpha_{2/1}} = \alpha_{k_D} \end{cases} \tag{3.11}$$

It is thus necessary to first test which component has the larger permeability, before a correct ratio can be estimated. To do so, Freeman [1999] gives the following correlation

$$\ln\alpha_{1/2} = \left(d_2^2 - d_1^2\right)\left(\frac{1-a}{RT}\right)c + \ln\alpha_{k_D} \tag{3.12}$$

where a is a constant parameter equal to 0.64, c is a parameter depending on the polymer material, d_1 and d_2 are the penetrant diameters.

Krevelen [1990] reports c values from 250 for extremely flexible elastomeric poly(dimethylsiloxane) to approximately 1100 cal/(mol.Å^2) for stiff-chain, glassy poly(vinyl chloride). During our inventory, both bounds of c are taken into account in order to highlight the impact of the polymer type.

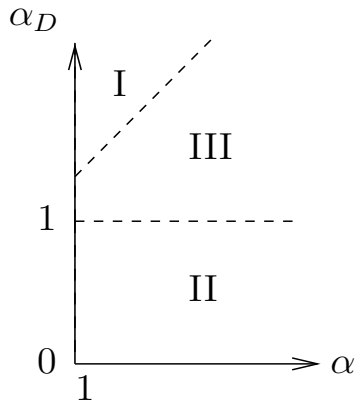

Figure 3.9: Classification of inventory results, the boundaries are drawn qualitatively. Conventionally, the selectivity ratio α is larger than 1, thus the x-axis starts at 1.

According to Fig. 3.9, three domains can be distinguished for the ratio $\frac{\alpha_{\mathcal{D}}}{\alpha}$.

- Domain I: $\frac{\alpha_{\mathcal{D}}}{\alpha} \gg 1$, short class processes are potentially interesting to yield an **improved selectivity** compared to steady-state operation.
- Domain II: $\frac{\alpha_{\mathcal{D}}}{\alpha} \ll 1$, the rapid gas in steady state with the higher permeability becomes the slow one with the lower diffusion coefficient during the time lag. This suggests that short class processes can potentially provide a **reverse selectivity**, which means that another component can be enriched in permeate compared to a steady-state operation.
- Domain III: $\frac{\alpha_{\mathcal{D}}}{\alpha} \approx 1$, the interest of short class processes is highly questionable. Short class processes might provide a slightly improved selectivity compared to a steady-state operation while the productivity loss and process complexity should be carefully taken into account. This type of gas mixture should be studied case by case.

It can be noticed that Fig. 3.9 is a qualitative representation where the slope of the dividing line between Domains I and III can be considered as any value larger than 1. The dividing line between Domains II and III is also qualitative and its y-intercept can be any value lower than 1.

Based on Eqs. (3.10) and (3.12) and two limit values of c, 66 gaseous components [Sherwood et al., 1975] are considered. This results in a large number of gas pairs (complete tables are available on request to the corresponding author). Freeman [1999] indicates that for light gaseous components, the kinetic diameter characterizing the smallest zeolite window through which a penetrant molecule can fit, is the most appropriate measure of penetrant size for transport property correlations. Thus, in this inventory, kinetic diameters are used to assess the interests of short class processes for light gaseous components: He, H_2, O_2, CO, CH_4, N_2, CO_2 and C_3H_8 [Dal-Cin et al., 2008], while Lennard-Jones diameters are in general utilized for other heavy gaseous components. It can be noticed that the choice of literature diameters is to be discussed for some gaseous components and it can induce inaccuracies with respect to the evaluation of the upper bounds of membrane performances [Dal-Cin et al., 2008].

The value of the selectivity ratio α and the ratio of diffusion coefficients $\alpha_{\mathcal{D}}$ are also individually estimated in Fig. 3.10 by using Eqs. (3.9), (3.10), (3.11) and (3.12). In the left part of Fig. 3.10, the potentially interesting gas mixture for short class processes is identified with a small α and a large $\alpha_{\mathcal{D}}$. In the right part, a zoom is made in order to highlight the reverse selectivity: in the case of a small α, short class processes do not only provide a reverse selectivity, but also lead to a more efficient separation.

It can be noticed that for the example He/CH_4 used by Paul, a significant improvement of selectivity is expected for $c = 1100$ cal.mol^{-1}.Å^{-2} (Fig. 3.10,

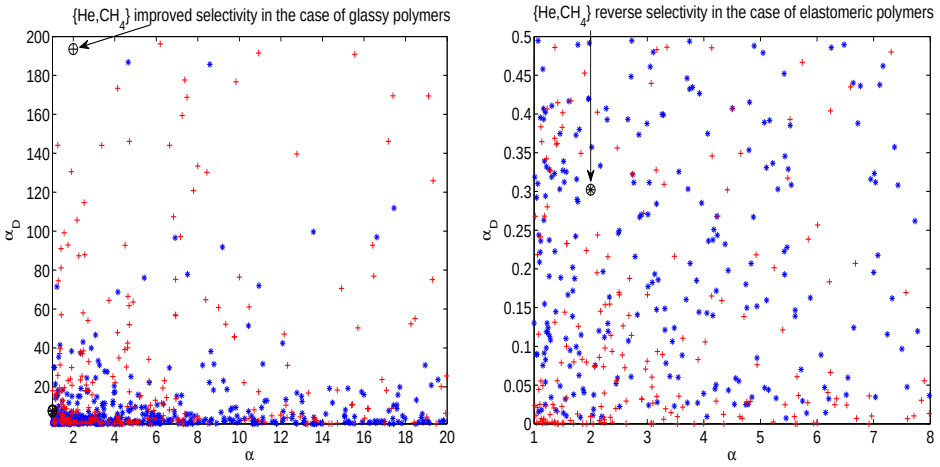

Figure 3.10: Inventory results: comparison between the selectivity ratio α and the ratio of diffusion coefficients $\alpha_{\mathcal{D}}$. '$*$' represents estimated parameters for $c = 250$ cal.mol^{-1}.Å^{-2} (elastomeric polymers) and '+' represents estimated parameters for $c = 1100$ cal.mol^{-1}.Å^{-2} (glassy polymers). The right part is the zoom of the Domain III of the left part in order to highlight the reverse selectivity.

left), whereas for $c = 250$ cal.mol^{-1}.Å^{-2}, a reverse selectivity is expected (Fig. 3.10, right).

Assuming that the boundaries of the three domains are arbitrarily taken as 0.2 and 2 (Fig. 3.11), more inventory results for existing applications of gas separations processes on an industrial scale and some potential applications are evaluated in Table 3.5. These applications are partially summarized by Koros and Fleming [1993] as well as by Baker [2002]. It can be noted that the value for air drying (H_2O/N_2) is surprisingly small. Similarly, all results of combinations with H_2O take the same order of magnitude, around 10^{-8}. This can be explained by two points:

- H_2O possesses an extremely important Lennard-Jones temperature which leads to a huge solubility in the polymer. Because of this large solubility, the difference between the permeability and the diffusion coefficient of H_2O is remarkable.
- H_2O is a relatively small gas and its kinetic diameter is not available. The Lennard-Jones diameter might not be appropriate to correctly describe its mass transfer parameters with our correlations.

A summary of the domain distribution for two extreme cases with regard

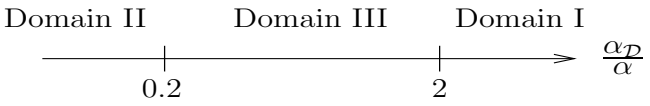

Figure 3.11: Distribution of domains of inventory.

to polymer type is given in Table 3.6. As a large number of results (2145 combinations of binary gas mixtures) are summarized, three points with respect to the influence of the polymer type can be noticed for short class processes:

- Our inventory gives no clear conclusion for about 20% of combinations for both polymer types (domain III).
- In the case of an elastomeric polymer, only 5.4% (domain I) of binary gas mixtures possess an improved selectivity with respect to conventional processes as opposed to 73.8% (domain II) for a reverse selectivity.
- In the case of a glassy polymer, 31.4% (domain I) of binary gas mixtures present an improved selectivity with respect to conventional processes, whereas 50.7% (domain II) display a reverse selectivity.

Nevertheless, empirical and theoretical correlations cannot exclude exceptions, thus it is important to notice that these correlations yield a theoretical maximum membrane performance. However, this does not mean that the upper bound can be reached by available polymers. On the other hand, two types of diameters are used during the inventory, and the boundary between light and heavy gaseous components is not strictly defined. As mentioned by Dal-Cin et al. [2008], some inaccuracy with regard to the evaluation of membrane performance can be due to the choice of diameters, so that the comparison between two gaseous components, neither strictly light nor heavy, might be critical.

Consequently, once a potentially interesting binary gas mixture is chosen through the inventory, the second stage is to verify in a polymer data bank [Brandrup and Immergut, 1989] whether a current polymer can deliver this performance. Nevertheless, it is also important to notice that this inventory takes into account only the selectivity. Other important factors such as productivity, process complexity and operating cost, are not considered. Thus, a deeper investigation is needed to identify a competitive utilization.

Gas pair	Application	Domain		
		I	II	III
{N_2, O_2}	Air separation			0.44
{H_2, C_3H_8}	Hydrogen purification	*58.8*	0.017	
{H_2, CO}	Syngas ratio adjustment	2.07		
{H_2, C_2H_4}	Ethylene cracking	*44.17*	0.023	
{CO_2, CH_4}	Natural gas treatment			0.35
{H_2O, N_2}	Air drying		$4\ 10^{-8}$	
{iso-C_4H_{10}, N_2}	VOC recovery	*387*	0.003	
{He, CH_4}	Helium recovery	*24.3*	0.04	
{N_2, CH_4}	Natural gas treatment		0.17	
{H_2S, CH_4}	Natural sweetening		0.03	
{Kr, Xe}	Rare gas separation in nuclear industry			0.53(*1.9*)
{H_2, O_2}	Hydrogen production by water electrolysis	*2.95*		0.34
{O_2, CO_2}	Gas recycling on bioreactors		0.13	
{CO_2, N_2}	Postcombustion CO_2 capture		0.06	
{H_2, CO_2}	Coal gasification (hydrogen production)		0.045	
{O_2, CH_4}	Biogas purification	*2.63*		0.38
{C_2H_4, C_2H_6}	C2 splitter			0.81

Table 3.5: Ratio $\alpha_{\mathcal{D}}/\alpha$ for existing (top Table) gas separations and potential (bottom Table) applications for short class processes. In case of identical results for $c = 250$ cal.mol^{-1}.Å^{-2} (elastomeric polymers) and $c = 1100$ cal.mol^{-1}.Å^{-2} (glassy polymers), a unique value is given in the table. Otherwise, the result for glassy polymers is given in italic in order to show the difference.

3.6 Long class studies

As explained previously in the classification of cyclic transient operations, cyclic transient operations can be handled in other ways than short class process. The operating time during which the mass transfer occurs is no longer limited to the time lag. The upstream/downstream pressure is still controlled periodically, thus the cyclic period can be very long compared to the time lag of the gas whose diffusion coefficient is lower. This type of cyclic transient operations is radically different from short class processes. As the mass transfer duration is much longer than the time lag and the regeneration stage is not necessarily long, the productivity and the exhaustion ratio of the feed mixture

Polymer type	Domain		
	I	II	III
$c = 250$ (elastomeric)	115 (5.4%)	1583 (73.8%)	447 (20.8%)
$c = 1100$ (glassy)	673 (31.4%)	1088 (50.7%)	384 (17.9%)

Table 3.6: Summary of the ratio $\alpha_{\mathcal{D}}/\alpha$ for inventory of 66 gaseous components, 2145 possible combinations. c in cal.mol^{-1}.Å^{-2}.

can be held at a relatively high level. Moreover, any complex valve control such as high frequency switching is no longer required. Does this type of cyclic transient operations present any advantages compared to a steady-state operation? Different operations have been investigated both theoretically and experimentally by several authors.

3.6.1 Feng process

A process called pressure swing permeation is studied by Feng et al. [2000]. This process is analogous to pressure swing adsorption and has the potential to be synergistically integrated with the pressure swing adsorption process for an enhanced separation of gaseous components.

According to Feng, two or more membrane modules are needed for pressure swing permeation. Each of them is operated cyclically in the following sequence:

1. Collection of the low pressure permeate from another module.
2. Pressurization of the permeate by the high pressure feed gas.
3. Release of permeate product at an elevated pressure.
4. Admission of feed to carry on permeation.
5. Withdrawal of residue stream.

Feng mentions that multimodule arrangements can also be used for large processing capacities with relatively steady and continuous flows of feed and purified product.

As an illustration example, Feng gives a design of two membrane modules (Fig. 3.12). A brief description of the cycle stages is shown in Table 3.7.

Considering the permeation system of Fig. 3.12, Feng performs a simulation of a binary gas mixture separation. In order to formulate mathematical equations, the following assumptions are made:

Stage	Module A	Module B
1	Admission of feed gas and permeation	Reception of permeate from module A
2	Withdrawal of residue from module	Pressurization with feed gas and product release
3	Removal of residue remaining in gas line	Gas feed stopped
4	Reception of permeate from module B	Admission of feed gas permeation
5	Pressurization with feed gas and product release	Withdrawal of residue from module
6	Gas feeding stopped	Removal of residue remaining in gas line

Table 3.7: Cycle stages in a two-module pressure swing permeation process according to Feng et al. [2000]

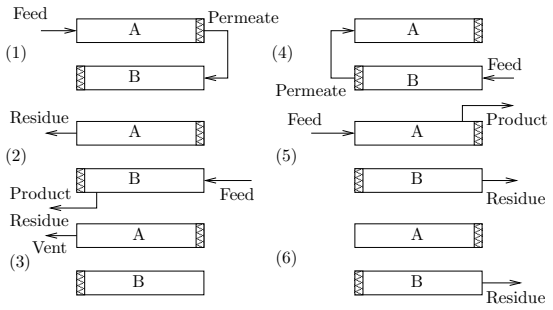

Figure 3.12: Cycle sequence of a two-permeator pressure swing permeation process, according to Feng et al. [2000]

1. The time lag of permeation due to transmission of gas molecules through the membrane is negligible. The permeate is thus assumed to be received in the reception vessel as soon as the permeation takes place.

2. The permselectivity of the membrane is independent of gas composition and pressure.

3. The membrane permeability during unsteady-state operation is the same as that at steady state.

4. These is no concentration polarization on the feed side, i.e., the concentration on the membrane surface is the same as the bulk concentration of the feed.

5. On the permeate side, these is no back diffusion from the bulk permeate to the membrane surface.

6. During permeation, the feed gas is maintained at a constant pressure, and the pressure on the permeate side gradually increases with time due to the fixed volume of permeate gas.

It is important to notice that the first assumption constitutes a radical difference with regard to short class processes: as in short class processes, the permeation occurs mainly during the time lag, while this part is totally neglected in Feng's process because of the duration. Two conclusions result:

1. The permeation of the component k is not dominated by diffusion coefficient $\mathcal{D}$ (Eq. (5.4)), but by permeability $\mathcal{P}$ as

$$\dot{n}_k = \mathcal{P}_k \frac{\Delta P_k}{L} A \tag{3.13}$$

   where $\dot{n}_k$ is the permeation flow rate, ΔP_k partial pressure drop of the component k between upstream and downstream. Thus the benefits of short class processes cannot be obtained for Feng's process.

2. Since the main permeation quantity of short class processes is neglected in Feng's process, this latter is expected to provide a relatively large productivity compared to short class processes.

Subject to the previous assumptions, Feng gives the following permeation rate for one component k of a binary mixture at a given instant

$$\frac{dQ_k}{dt} = J_k A(P^u X_k - P^d Y_k) \tag{3.14}$$

where J_k is the membrane permeance equal to $\frac{\mathcal{P}_k}{L}$, Q_k is the quantity of permeate, and P_u and P^d are the upstream pressure and downstream pressure, respectively. Moreover, X_k is the upstream mole fraction of the component k and Y_k the downstream mole fraction of the same component.

On the basis of a mass balance and assuming an ideal gas behavior, the residue mole fraction X_k on the upstream side of the membrane is related to the mole fraction of the feed X_k^f by

$$X_k = \frac{(PV^f/RT)X_k^f + \left(\sum_{i=1}^{2} Q_i\right) X_k^f - Q_k}{PV^f/RT} \tag{3.15}$$

Then, Feng proposes to use the value of the local mole fraction Y_k of permeate leaving the membrane

$$Y_k = \frac{\left(\frac{dQ_k}{dt}\right)}{\sum_{i=1}^{2}\left(\frac{dQ_i}{dt}\right)} \tag{3.16}$$

The pressure variation on the permeate side of membrane is related to the permeation rate as

$$\frac{dP^d}{dt} = \left(\sum_{i=1}^{2}\left(\frac{dQ_i}{dt}\right)\right)\frac{RT}{V^d} \tag{3.17}$$

where V^d is the volume of the permeate receiver. Feng solves the previous set of equations with initial conditions by a trial and error method.

Feng's modeling suggests that the permeated gas is transported instantly into a permeate receiver. Consequently, the local pressure on the permeate side of the membrane is constant during all operations whereas the permeate is accumulated in a permeate receiver. However, the pressure variation on the permeate side of the membrane is not considered constant by Feng, but rather related to the permeation rate (Eq. (3.17)).

Consequently, for the permeate side of the membrane, Eq. (3.16) does not take into account the accumulation term while Eq. (3.17) does. However, both terms P^d and Y_k are used at the same time in Eq. (3.14). This could be a slight error of modeling. If the accumulation in downstream volume is indeed taken into account, Y_k should be written as

$$Y_k = \frac{\int_0^{t_f}\left(\frac{dQ_k}{dt}\right)dt}{\sum_{i=1}^{2}\left[\int_0^{t_f}\left(\frac{dQ_i}{dt}\right)dt\right]} \tag{3.18}$$

Nevertheless, Feng recommends to operate the pressure swing permeation at a relatively high frequency to keep the permeation time reasonably short. This is done in order to retain the advantage of his process. It can be noticed that in case of a short cycle duration, both expressions of Y by Eqs. ((3.16) and (3.18)) give a similar result, as both permeation rates are nearly linear close to the initial time. Fig. 3.13 compares the simulation results of Feng's model and the refined model with expression of Y_k by Eq. (3.18). This comparison confirms that during the first fractions of a second of permeation, the difference between both models is not significant. Therefore, Feng's calculation of Y_k can

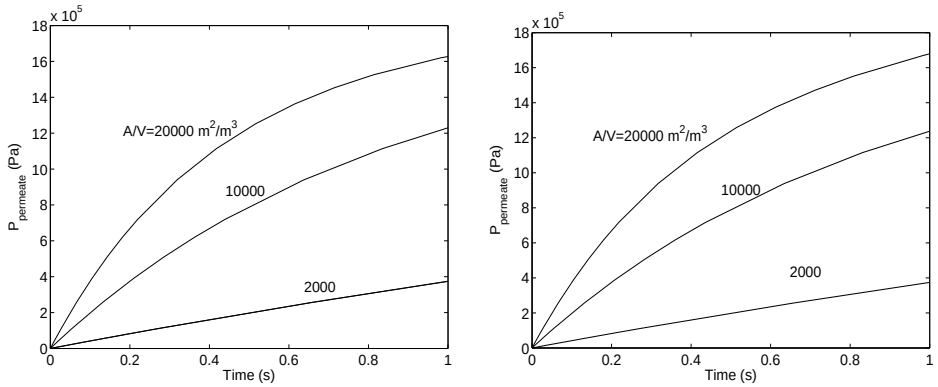

Figure 3.13: Comparison of Feng's modeling result (right, Eq. (3.16)) and the refined modeling (left, Eq. (3.18))

also be considered as an approximation to simplify modeling and simulation. Thus, in the case of a short cycle duration, Feng's simulation is close to reality.

Feng observes that, as the permeation goes on, the residue is depleted in the fast-permeating species, and the permeate pressure builds up. Therefore, the transmembrane driving force for permeation is gradually decreased. Consequently, the permeation rate is initially fast and gradually slows down. As permeation continues, the reduction in the driving force for the fast gas permeation is more significant compared to the slow permeating gas. Thus, the mole fraction of the fast permeating component in the permeate leaving the membrane surface gradually decreases, resulting in a reduction of the bulk permeate mole fraction of that component.

In addition to analyzing the permeation behavior, Feng performs an experimental demonstration of his process, not mentioning the polymer type. The demonstration unit comprises two identical hollow-fiber membrane modules (Fig. 3.12). The membrane has an asymmetric structure with a thin outer skin layer on a microporous support. A hydrogen/nitrogen mixture is used in this demonstration. The characteristics are given in Table 3.8.

Some of his results are presented in Table 3.9. Feng compares these results to a conventional steady-state process taken as a shell-side feed and countercurrent flow configuration. Feng indicates that, at a residue concentration of 42.9% H_2, which is equivalent to the overall residual concentration in Table 3.9, the permeate concentration and permeate flow rate are 54.9% H_2 and 0.28 cm^3(STP)/min, respectively. Both values are substantially lower than those shown in Table 3.9. Two advantages of pressure swing permeation are indicated by:

Selectivity (hydrogen/nitrogen)	55
Outside diameter	165 μm
Packing density	8600 m^2/m^3
Temperature	300 K
Fiber length	22.5 cm
Number of fibers per module	300

Table 3.8: Experimental characteristics of the demonstration of the 'Swing Pressure Process' by Feng.

1. Higher selectivity compared to that of steady-state operations.
2. Higher permeate pressure compared to classic operations.

	Pressure kPa Gauge	Concentration H_2 vol %	Flow Rate cm^3(STP)/min
Feed	1590	49.4	386.6
Residue product	∼94	41.3	300.0
Residue vent	94	71.4	16.6
Permeate	1321	78.8	70.0

Table 3.9: Pressure Swing Permeation Test for Hydrogen/Nitrogen separation, according to Feng

Feng also indicates that the maximum permeate hydrogen concentration that can be obtained at zero stage cut corresponding to zero permeate flow for a classic counter-current flow process is calculated to be 58.3% whereas a conventional steady-state process can only provide a permeate concentration of 54.9% H_2 under the conditions of Table 3.9. Thus, Feng concludes that the results of Table 3.9 are not achievable with the conventional process.

However, this conclusion of Feng can be criticized since Feng assumes that the ratio of permeate pressure/feed pressure is 1321/1590 for the corresponding steady-state operation (experimental values in Table 3.9). It can be noticed that a conventional steady-state process is practically never operated under conditions where the permeate pressure is very close to that of the feed. Assuming that the ratio of permeate pressure over feed pressure is 0.1, a counter-current flow model with characteristics of Table 3.8 is simulated and its performance is presented in Fig. 3.14. One can see that the hydrogen concentration can reach 97.7% at zero stage cut. The experimental result of Feng (Table 3.9) represents a stage cut of 0.18. At the same stage cut, the hydrogen concentration in the permeate can exceed 95% under the conditions

of a counter-current flow model at steady state. Thus, in normal industrial conditions, a classic counter-current flow process can provide a better selectivity than Feng's process. Nevertheless, the permeate pressure is clearly lower than that of the feed flow. Thus, the second advantage of Feng's process, i.e., a permeate at high pressure, remains valid as opposed to the first claimed advantage of higher selectivity.

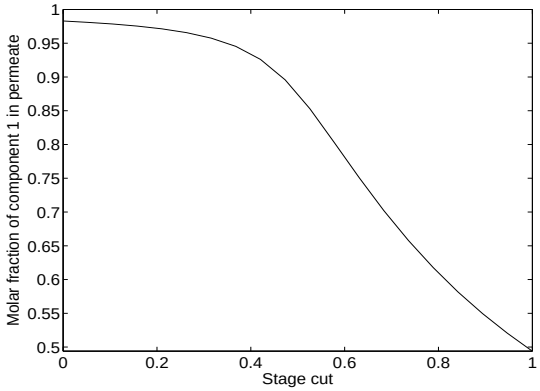

Figure 3.14: Performance of a counter-current flow model at steady state, operation conditions of Table 3.8, with $\frac{P^d}{P^u} = 0.1$

However, ignoring the energy cost, the advantage of producing a permeate at high pressure is negated by producing a residue at low pressure. In this respect, the comparison with steady state should be done by using a turbine to reduce the pressure of the residue from 1590 to 94 kPa Gauge and use the turbine to drive a compressor which raises the pressure of the permeate from a low pressure to be determined to 1321 kPa Gauge. Consequently, the permeate flow rate is much smaller than that of the residue, and the achievable effective permeate pressure will thus be quite low.

In conclusion, a novel cyclic permeation process for gas separation, which is different from short class processes, is developed by Feng. If the only considered criterion is selectivity, Feng's process does not prove to be more advantageous than a real steady-state operation. Feng's process can indeed produce a permeate at a high pressure, while the effective flow rate will be quite low. Another potential advantage that has not been discussed might be the saving of permeate compression costs.

This process can be interesting for an efficient membrane material, which provides a very high selectivity coefficient. In that case, a permeate with an acceptable purity can be produced at high pressure. Whereas no optimization is used in Feng's process, an improvement of performance could be expected with

less energy consumption after optimization. On the other hand, as explained by Feng, 'Pressure Swing Permeation' can be integrated to pressure swing adsorption, in order to enhance the overall separation performance without the need for an interstage compressor. This is rather interesting for industry, since no great investment is required for an already existing process. Consequently, the most important advantage of Feng's process might be energy saving; however, this point is not discussed in detail.

3.6.2 Ueda process

Ueda et al. [1990] designed a cyclic membrane process to enrich and separate a specific component from air. Concerning the membrane, a non-porous thin layer (5 to 50 μm) on a porous support (50 to 500 μm) is recommended according to various methods. This process is adapted to all types of modules, plate-and-frame types, spiral types and also hollow fibers types.

The process is described in Fig. 3.15. The main interest of the design is that only one pump is used to feed the membrane module and to transport the permeate. Nevertheless, Ueda suggests installing several modules in parallel and placing one pump for each flow in order to obtain the following benefits for industry:

1. Improve the productivity and obtain a continuous production.
2. Make the total process easy to control and more stable.

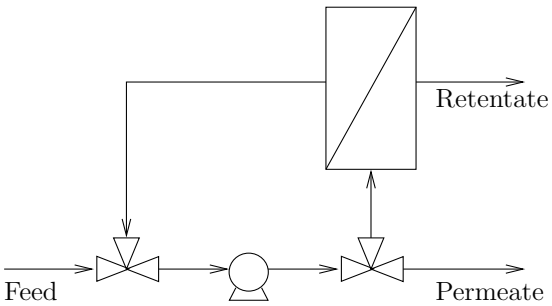

Figure 3.15: Cyclic process for separating gas of Ueda et al. [1990]

The process functioning is cyclic and each cycle can be separated into 2 stages (Fig. 3.16):

- Stage 1: The upstream volume of the membrane module is pressurized and fed with air. In parallel, the permeation through the membrane

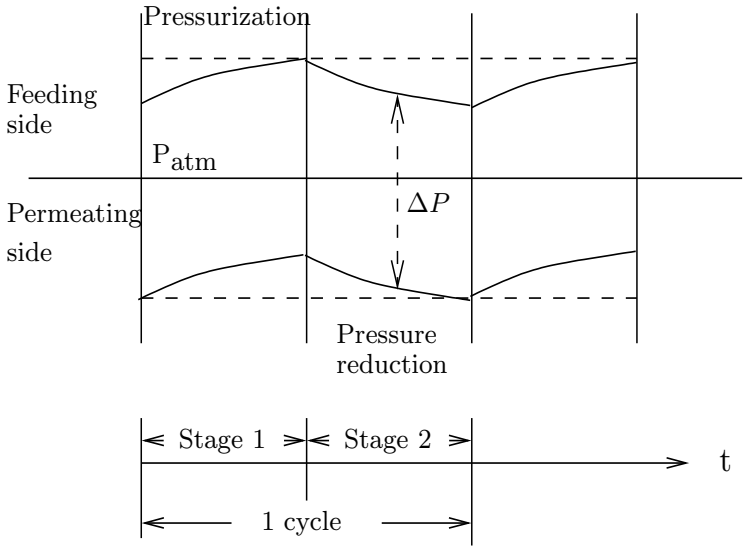

Figure 3.16: Cyclic functioning of Ueda's process

makes the downstream volume pressure increase. The feed flow rate can be regulated to ensure a constant pressure drop ΔP between the upstream and downstream volumes in order to obtain a stable production. If it is the retentate that contains more of the desired gas, the retentate is transported to a gas receiver during this stage. Here, the pump is used to pressurize the upstream side (Fig. 3.17, up).

- Stage 2: Feeding of the upstream volume is stopped. The downstream volume is partially evacuated by one pump (which could be the same for feeding upstream or another one reserved to do so) and its contents are transported to a gas receiver if the permeate contains a majority of the desired gas. Otherwise, the evacuated part is vented. The evacuating flow rate can also be regulated. In this stage, the pump is used to evacuate the downstream side as a vacuum pump (Fig. 3.17, down).

According to this description, when the feed of gases and suction under vacuum from the downstream side are repeatedly and alternately carried out, a residual pressure is generated at both the upstream and downstream sides. These residual pressures easily provide a larger pressure drop between the two sides compared to that occurring by a steady-state operation. Ueda indicates that to ensure such a pressure drop, more energy is needed in the case of steady-state operations. The functioning is not optimized mathematically, while Ueda proposes a symmetrical cycle scenario. Since the mass transport mechanism is not sufficiently investigated, Ueda suggests to determine the stage duration

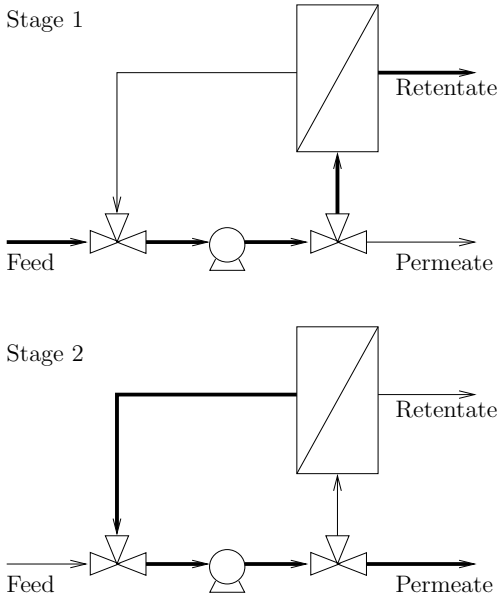

Figure 3.17: Functioning of Ueda's cyclic process [Ueda et al., 1990]. Functioning flows are shown by thicker lines

experimentally for different membranes and different gases. He believes that the duration of one stage should be approximately between 2 s and 5 min and 5 - 20 s might be the best choice. Oxygen and nitrogen are both rapid gaseous components in terms of mass transport through a membrane. As the membrane is assumed to be thin, the time lags for both gaseous components are very short (<0.1 s), and the mass transport during the time lag can thus be neglected logically. Obviously, this cyclic process belongs to the long class.

The process is not advantageous compared to steady-state operations if the stage duration is too long or too short, because in this case, the process tends towards a steady state. Ueda also indicates that his process allows it possible to effectively use the entire area of a membrane.

Ueda performs some experimental demonstration using a hollow fiber type module to separate oxygen and nitrogen from air. He indicates that his process does not only save energy to maintain a high pressure gap, but also results in a better selectivity. However, Ueda does not explain the mechanism of the selectivity increase. Furthermore, Ueda indicates that for some cases, a better productivity compared to steady-state operations is achieved. This is rather exceptional for a cyclic process.

However, it is important to notice that the process start-up can be very delicate and a long time may be required to reach a steady functioning state.

This also means that the products coming from the very first cycles provide a composition that differs with regard to the steady-state operation.

3.6.3 Nemser process

Nemser [2005] develops a cyclic process related to a membrane separation process useful for recovery of volatile organic components (VOC) emitted from storage tanks. This is done using a membrane including a selectively gas permeable membrane polymer. The process involves repetitively cycling operations through the membrane.

The membrane of PDD (Perfluoro-2,2-dimethyl-1,3-dioxole) is used to separate air, considered as a binary mixture of oxygen and nitrogen, and VOC. The mass transport mechanism is complex for this membrane and associated gaseous components. For air, the permeability is quasi-constant in concentration, 990 Barrer for oxygen and 490 Barrer for nitrogen. However, for various VOCs, the permeability depends on the VOC concentration in the membrane. Even though the exact mass transport mechanism is not yet clear, the example of experimental results given in Table 3.10 shows the complexity of this relationship between the pressure and the permeability of VOC.

Pressure (kPa)	Permeability (Barrer)
124	14
207	75
469	250

Table 3.10: Permeability of CFC-12 (dichlorodifluoromethane) through membrane PDD (perfluoro-2,2-dimethyl-1,3-dioxole) for different pressures on the membrane [Nemser and Roman, 1991]

Table 3.10 shows the permeability of a typical VOC, CFC-12, through PDD. For a low partial pressure of VOC, VOC is poorly permeable, and thus the membrane is very selective for the {air, VOC} mixture. However, when the membrane is charged with VOC, the permeability of VOC will approach that of air, and thus the separation through the membrane becomes much less significant. Consequently, in order to ensure a good separation, it is necessary to maintain a low partial pressure of VOC.

For this purpose, Nemser develops a dedicated cyclic process. The apparatus is installed on top of a fuel tank (Fig. 3.18). Two stages per cycle are defined by Nemser:

- Stage 1: A pressure sensor is installed on the fuel tank. Once the pressure of the fuel tank exceeds the high pressure set point, stage 1 is launched.

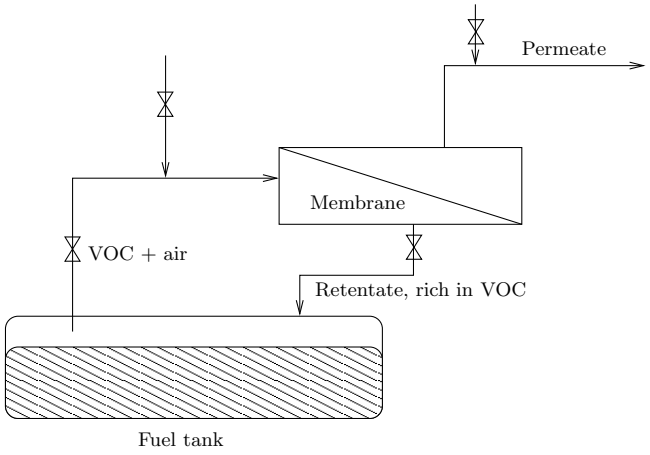

Figure 3.18: Cyclic process design by Nemser [2005]

The membrane module is fed by a gas mixture (VOC + air) from the fuel tank by opening the associated valves. The selective membrane lets air pass as the permeate which is later escaped to the atmosphere, while the retentate, rich in VOC, is sent back to the fuel tank. Consequently, the pressure in the fuel tank decreases. Nemser indicates that the duration of stage 1 can last from 15 s to several minutes.

- Stage 2: Once the fuel tank pressure becomes lower than the set point of low pressure, stage 2 is launched. The connection between the membrane module and the fuel tank is cut off by closing the associated valves. At the same time, the membrane module is connected to a vacuum system. By creating vacuum in the membrane module, the VOC in the membrane is evacuated. Nemser also proposes an alternative choice to clean the membrane, by sending an inert gas through the membrane module. Once the pressure sensor detects again a pressure larger than the high pressure set point, the next cycle is launched. Generally, stage 2 lasts 15 minutes to 3 hours according to Nemser.

For this problem of VOC recovery, the flow rate of VOC plus air mixture is unsteady, and a steady-state operation is thus not possible. Consequently, this operation is run as a cyclic process because of the nature of the separation application.

Nemser's process is a special case of cyclic transient operations. Contrary to most other cyclic operations, the stage duration is not predefined, but determined by process control. As the mass transport mechanism is complex, the definition of time lag is not clear. Therefore, this cyclic process is not

classified as belonging to the short class.

Stage 2 is the stage of regeneration of the membrane, and is characteristic of cyclic operations. This step makes it possible to keep the VOC concentration in the membrane at a low level for each cycle. Due to this regeneration, the separation is so efficient that stage 1 does not take more than a few minutes.

Nemser's process gives a novel perspective of cyclic transient operations. By combining it with a process control system, the cyclic nature enables this type of process to treat unsteady flow rates, which is very difficult in a steady-state operation.

3.7 Comparison of short and long class processes

Since Paul [1971], ideas of cyclic transient operations have been investigated by several authors through experiments or theoretical modeling.

The process described by Paul belongs to the short class which uses the large difference of the diffusion rates in transient states of different gas components. For long class processes, a general relationship, also common for steady-state operations, can be applied

$$\dot{n}_k = f(\mathcal{P}_k, \Delta P_k, L, A) \tag{3.19}$$

For steady-state operations, once the process is launched, all these parameters are fixed. On the opposite, the long class processes allow some parameters to be varied, in particular the permeability $\mathcal{P}_k$ [Nemser, 2005] and the instantaneous pressure drop ΔP_k [Feng et al., 2000, Ueda et al., 1990] in order to achieve some performance improvements.

To carry out a comparison between cyclic processes and steady-state operations, pressure references must first be chosen. For short class processes, since the exhaustion ratio and the accumulation rate are very low during the high pressure stage, the pressures in the upstream and downstream sides of the membrane can be considered as constant. Consequently, the pressures during the high-pressure stage are used conventionally as the common reference for comparison. It is confirmed that the short class processes can indeed offer clear advantages with respect to selectivity at the expense of an important loss in productivity. Nevertheless, if thin membranes are used for steady-state operations, the productivity lag between the two types of operations becomes much more significant. On the other hand, the very low exhaustion ratio limits also its application.

Furthermore, a comparison difficulty resides in a common reference for steady-state operations and long class processes since the operating pressures of the latter are variable in a large range (Fig. 3.19).

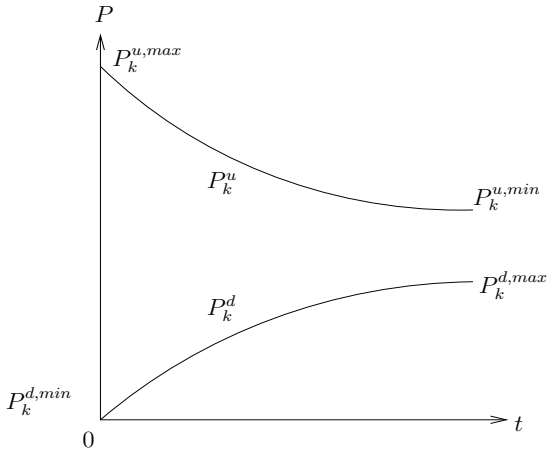

Figure 3.19: Typical behavior of upstream and downstream pressures for a long class process. P_k^u is the operating upstream partial pressure of a component k and P_k^d is the downstream counterpart of the same component.

The permeation rate expressions are common for long class processes and steady-state operations (Eq. (3.13)). Thus, in the case where the minimum downstream pressure $P_k^{d,min}$ and the maximum upstream pressure $P_k^{u,max}$ of Fig. 3.19 are used as the common references, the average pressure drop ΔP_k of the long class process is lower than that in steady state, as well as the average pressure drop ratios $\Delta P_1/\Delta P_2$, considering that component 1 is desired. Consequently, the productivity and the selectivity are both lower in the case of the long class process compared to a steady-state operation.

However, if the $P_k^{d,max}$ and $P_k^{u,min}$ of Fig. 3.19 are used as the common references, it is obvious that the average pressure drop and the average pressure ratio can be larger in the case of the long class process. An improvement of performances can thus be observed.

For example, Feng considers that the upstream pressure is maintained constant by a continuous pressurization while the final downstream pressure corresponding to $P_k^{d,max}$ is used as the common downstream pressure reference. In the case of Ueda's process, although the authors do not give a clear description of the functioning, one can suspect that the maximum downstream pressure $P_k^{d,max}$ is used as the reference since an improvement in selectivity (and even in productivity) is indicated by Ueda.

Nevertheless, pressure control requires an important energy supply. A more convincing assessment of the long class processes with respect to steady-state operations can only be obtained by taking into account the energy consumption. Consequently, a performance comparison of short class and long class

processes (Table 3.1) is completed in Table 3.11.

	Short class	Long class
Stage duration	$\approx$ time lag	$\gg$ time lag
Regeneration stage	Necessarily long	Not necessarily long
Membrane thickness	Thick	Not necessarily thick
Selectivity improvement	Very high	Low
Productivity loss	High	Low
Other interests	Few	Certain

Table 3.11: Classification of cyclic transient operations and performance comparison

3.8 Conclusion

A general overview of cyclic membrane gas separation processes is given in this chapter. To our knowledge, cyclic transient operations are not yet performed in industry. The most important advantage of cyclic transient operations compared to steady-state operations is an improvement in selectivity, which can only be obtained at the expense of productivity. A reasonable selectivity improvement goes with a moderate productivity loss, such as for long class processes, while a great selectivity improvement goes with a significant productivity loss, such as for short class processes, and so does the process complexity. Although Ueda indicates an increase in productivity for his process compared to steady-state operations, one can suspect that a more significant energy consumption is unavoidable.

Consequently, it is important to find the best trade-off between selectivity and other factors of separation. Cyclic transient operations of the short class, such as Paul's processes, are studied in detail by different authors. The optimized operation can be analyzed by analytical and numerical simulations. The same operating mode is also confirmed by some experiments. Another key issue of cyclic transient operations is the identification of the most appropriate gas mixtures for separation. A theoretical inventory taking into account only the selectivity improvement has been reported in this paper. For short class processes, some potentially interesting gas mixture separations have been performed within the framework of this study. However, as the productivity loss is too important and the exhaustion ratio is too low, short class processes might only be interesting for separation of specific gaseous components. Some case studies will be given in Section 5.1.

Cyclic transient operations of the long class have more degrees of freedom

with regard to their operation and their productivity is comparable to steady-state operations. They could thus have larger perspectives compared to their short class counterparts. However, experimental proofs of concept are needed in this domain. It can be noticed that in the previous investigations, long class processes were rarely optimized by means of a rigorous numerical model. During this thesis, a novel design classified as a long class process is simulated then optimized and finally patented. This process is explained in Section 5.3. Furthermore, an experimental validation has also been performed and will be exhibited in chapter 6.

Chapter 4

Modeling and optimization

> Science is a differential equation.
> Religion is a boundary
> condition.
>
> Alan Turing

The investigation of cyclic process has been performed essentially by means of simulation and optimization. Thus the first thing to do is to define an adequate model of the transport phenomena: the model should be simple but efficient. For this purpose, the Dual Mode Sorption theory has been chosen. In this chapter, the existing gas transfer models within the frame of Dual Mode Sorption theory in and through different membranes are compared. In particular, a limit behavior study of gas transfer in glassy polymers has been performed. Furthermore, the novel limit behavior investigation led to a submitted publication in *Industrial & Engineering Chemistry Research* [Wang et al., 2012 (DOI: 10.1021/ie2027102]. Hence, the mathematical treatments to solve corresponding equations are also detailed. Finally, in order to determine the best performance of a given process, an optimization tool, i.e., genetic algorithm is incorporated in the simulation.

4.1 Gas transport in and through polymeric membranes

In this thesis, the study covers essentially only the polymeric membranes in isothermal conditions. According to Chapter 2, the latter is in general based on the solution-diffusion mechanism. As an amorphous material, the polymeric

membrane can exist in two states which are split by a called transition temperature T_g. In order to provide a general description of transport phenomena in both states, the Dual Mode Sorption theory is applied in this thesis.

4.1.1 Dual Mode Sorption theory - Sorption modeling

4.1.1.1 Pure gas sorption

As explained in Chapter 2, the sorption isotherm for a pure gas in a glassy polymer is usually given by the Dual Mode Sorption theory as Eq. (2.11), which can be transformed into linear forms in certain conditions [Vieth et al., 1976]:

- Low partial pressure, $bp \ll 1$, the sorption isotherm is reduced to a linear expression

$$C = (k_D + C_H^{'} b)P \tag{4.1}$$

- Sufficiently high partial pressure, $bp \gg 1$, the microvoids become saturated and the Langmuir adsorption reaches its saturation limit $C_H^{'}$, again, the sorption isotherm is reduced to a linear expression

$$C = k_D P + C_H^{'} \tag{4.2}$$

Consequently, it is possible to quantitatively separate the two contributions to the sorption isotherm by approaching the two asymptotes. k_D can be obtained from the slope of Eq. (4.2) and $C_H^{'}$ can be obtained from the y-intercept of the same equation. By subtracting the ordinary dissolution part C_D from the total concentration C, the Langmuir adsorption concentration C_H is isolated at any pressure

$$C_H = C - k_D P = \frac{C_H^{'} bP}{1 + bP} \tag{4.3}$$

Eq. (4.3) can be rearranged as

$$\frac{P}{C_H} = \frac{1}{C_H^{'} b} + \frac{P}{C_H^{'}} \tag{4.4}$$

Therefore, the hole affinity constant b can be determined from the y-intercept of Eq. (4.4). $C_H^{'}$ can again be determined from the slope of 4.4. In parallel, the sorption modeling can be validated by the linearity of experimental data of Eq. (4.4). Then the sorption modeling can be validated by fitting the experimental

data to Eq. (2.11). This type of experimental confirmation has been carried out by numerous researchers for different gaseous components covering a large pressure range in different polymers [Assink, 1975, Vieth et al., 1966, 1976]. En parallel, the transport parameters $C_H^{'}$, b and k_D can be determined by the same experiments.

Besides this classical model of sorption (Eq. (2.11)), some other investigations of sorption expression within the frame of dual mode sorption theory were also performed. For example, Bhatia and Vieth [1980] attempted to consider the mobile species as Langmuirian, in the same way as the immobile species.

It is also reported that the model applicability is not absolutely general insofar. Eq. (2.11) is inadequate to describe some exceptional isotherms, even qualitatively. For example, Doghieri et al. [1996], Nakanishi et al. [1987] indicated that for ethanol vapors in poly[- (trimethylsilyl)-1-propyne] (PTMSP), an S-shaped isotherm cannot be explained by Eq. (2.11). Similar observations have also been reported for alcohols in poly(trimethyl silyl norbornene) (PTMSN) [Galizia et al., 2011]. On the other hand, the underlying physical picture of dual mode sorption theory is clearly oversimplified. The three parameters ($C_H^{'}$, b and k_D) of the model can only be obtained from a data-fitting procedure based on experimental data for each given gas-polymer couple, so that the model lacks a predictive basis; moreover, the parameter values were also found to depend on the pressure range used for the fitting procedure [Sarti and Doghieri, 1998]. Consequently, more elaborate models based on a more fundamental background have been developed in order to compensate this drawback (e.g. Non-Equilibrium Lattice Fluids [Angelis et al., 2007, Doghieri and Sarti, 1996, 1998, Minelli et al., 2011, Sanchez and Lacombe, 1978, Sarti and Doghieri, 1998]). Due to their complexity, the discussion of these models will not be considered in this thesis. Based on these isotherms, more complicated transport models have been proposed [Doghieri et al., 1996, Galizia et al., 2011].

Nevertheless, since the Dual Mode Sorption theory is indeed very easy to apply and quite useful from an engineering point of view [Doghieri and Sarti, 1996, 1998], the isotherm has found extensive and successful applications over years [Koros et al., 1976, Vieth et al., 1976]. Eq. (2.11) is considered as a good and simple enough description of reality and will be used in this thesis as the only sorption model.

4.1.1.2 Mixed gas sorption

In the case of a binary gas mixture, Eq. (2.11) deviates from the reality [Koros, 1980, Sanders and Koros, 1986]. Thus, the dual mode sorption theory has been

later extended for binary mixtures {A,B} by Koros [1980]. It is assumed that there is a finite amount of nonequilibrium excess volume in glassy polymers and, in mixture situations, the components of the mixture must compete for the available volume. Thus the ordinary dissolution is essentially independent of the second component while competition by both penetrants for the hole-filling process occurs in glassy polymers

$$C_A = C_{DA} + C_{HA} = k_{DA}P_A + \frac{C'_{HA}b_AP_A}{1 + b_AP_A + b_BP_B} \tag{4.5}$$

where all parameters (k_D, b and C'_H) for each gas can be obtained from pure gas sorption measurements or from mixed gas sorption measurements. Thus Eq. (2.11) is considered as a special case of Eq. (4.5).

Sanders and Koros [1986] show that the sorption measurements for pure or mixed gases lead to consistent sorption parameters. It is remarkable that this point is an important advantage of this Dual Mode Sorption theory, as once the sorption parameters for single gaseous components are known, the sorption behavior of a gas mixture can be predicted accurately by the model. According to Story and Koros [1989], Eq. (4.5) predicts the sorption of tested binary mixtures within 2%. From these data, it appears that Eq. (4.5) provides an accurate description of the sorption phenomenon. Thus, any important inaccuracy in transport modeling should be directly attributed to assumptions/simplifications of transport, but not to those of sorption.

4.1.2 Immobilization Model

The Dual Mode Sorption theory first explains successfully the non-linear isothermal sorption for glassy polymers. It has been later extended to explain the second part of the solution-diffusion mechanism: diffusion in glassy polymers. It should be noticed in the first place that all discussions about the diffusion are based on pure gas but should be able to expend to mixed gas.

With regard to the diffusion modeling, many tentative investigations have been performed. Paul and Koros [1976] proposed to describe the transport based on the gradients of gas concentrations. Petropoulos [1970] presented a theory similar to that of Paul and Koros [1976] but based on chemical potential gradients. Later, Islam and Buschatz [2002] tried also to model the same phenomena by an expression of chemical potential taking into account a pressure gradient inside the membrane. This assumption is however in contradiction with the solution-diffusion theory, as noticed by Koros and Madden [2003].

Among these investigations, Paul and Koros [1976] description is considered as the basic frame in our study. In order to achieve a simple enough but

also efficient model, assumptions have been taken which simplify the mathematical description while correctly respecting the physical behavior, although all of them are questionable and have been discussed by different authors. Removing some simplifying assumptions could indeed improve the model at the expense of a useless increasing complexity. Thus the following basic assumptions are applied to the transport model without further discussion.

- All diffusion phenomena through glassy polymers can be described by Fick's law, the driving force for gas transport is based on the gradients of gas concentrations [Paul and Koros, 1976].
- The plasticization effect is neglected, although this effect is sometimes reported as significant for high solubility gaseous components [Chiou and Paul, 1989].
- Coupling terms in the flux expression are neglected. This latter was theoretically studied by Barrer [1984] and Fredrickson and Helfand [1985].
- The diffusion coefficients for given gas states depend only on temperature, thus they are constant for an isothermal model. The concentration dependence of the diffusion coefficients was studied by Sefcik and Schaefer [1983] through a ^{13}C NMR experiment.

In the early development of dual mode theory, the assumption of Immobilization was taken into account for pure gas diffusion in glassy polymers.

• **Immobilization**: The molecules obeying Langmuir's law are considered as totally immobilized along the direction of diffusion.

The Langmuir and Henry populations are thus related by a so-called Local Equilibrium in the polymers.

• **Local Equilibrium**: The local equilibrium between two types of molecules is maintained simultaneously everywhere throughout the membrane [Paul, 1969, Vieth and Sladek, 1965].

Consequently, it is possible to establish a relation between C_D and C_H by replacing the partial pressure P of the considered pure gas in the Langmuir sorption (Eq. (2.10)) by C_D,

$$C_H = \frac{\frac{C_H' b}{k_D} C_D}{1 + \frac{b}{k_D} C_D} \tag{4.6}$$

Since the assumption of Immobilization is admitted, the Langmuir species are totally immobile. Thus the model is denoted as Immobilization Model

(IM). The transport phenomenon is described by Fick's second law on one-dimensional radial coordinates

$$\frac{\partial(C_D + C_H)}{\partial t} = \frac{\partial}{\partial r}\left(\mathcal{D}\frac{\partial C_D}{\partial r}\right) \tag{4.7}$$

where $\mathcal{D}$ is the constant diffusion coefficient and r the position in the membrane.

Insertion of Eqs. (4.6) into (4.7) eliminates C_H and gives

$$\left[1 + \frac{K}{(1 + aC_D)^2}\right]\frac{\partial C_D}{\partial t} = \mathcal{D}\frac{\partial^2 C_D}{\partial r^2} \tag{4.8}$$

where $K = \frac{C_H^{'} b}{k_D}$ and $a = \frac{b}{k_D}$ are used in order to simplify this equation. This formulation was initially given by Vieth and Sladek [1965].

4.1.3 Immobilization Model in heterogeneous membranes (MMM)

Although the IM was shown to be not quantitatively accurate for glassy polymers, Paul and Kemp [1973] propose to use the Dual Mode Sorption theory, especially the IM, to explain the transport phenomena in a polymer membrane containing adsorptive fillers. The latter is obtained by adding adsorptive materials under the form of a dispersed phase in a rubbery polymer membrane in order to modify the membrane transport property [Aroon et al., 2010]. It is also well known as Mixed Matrix Membranes (MMM). The adsorptive materials can adsorb a part of penetrant molecules and keep them totally immobile in the membrane. This adsorption is in agreement with a Langmuir's isotherm. The rubbery polymer membrane, which is the continuous phase dissolves penetrant molecules according to Henry's law and these molecules can diffuse according to Fick's law. Thus, the heterogeneous membrane is decomposed by two well defined phases and possesses properties similar to glassy polymers as it possesses two types of sorption and molecules adsorbed by Langmuir's law are totally immobile.

Assuming that a rubbery membrane is composed of a dispersed phase of an adsorptive filler which occupies a volume fraction v_d, thus the volume fraction of the polymeric continuous phase is $v_p = 1 - v_d$. Paul and Kemp [1973] describe this situation by adapting Eq. (2.11) as

$$C = \underbrace{v_p k_D P}_{\text{Term 1}} + \underbrace{v_d \frac{C_A^{'} b P}{1 + bP}}_{\text{Term 2}} \tag{4.9}$$

where Term 1 represents the rubbery polymer characteristics and Term 2 represents those of the adsorptive fillers. Consequently, Eq. (4.8) is redefined by adding v_p and v_d as

$$\left[1 + \frac{K\frac{v_d}{v_p}}{(1 + \frac{a}{v_p}C_D)^2}\right] \frac{\partial C_D}{\partial t} = \mathcal{D}_m \frac{\partial^2 C_D}{\partial r^2} \tag{4.10}$$

where $\mathcal{D}_m$ is the effective diffusion coefficient which can be determined experimentally or by some correlations [Paul and Kemp, 1973] from the diffusion coefficient of the original rubbery polymer.

With these changes, the prediction of the time-lag of this heterogeneous membrane is written as

$$\theta = \frac{l^2}{6\mathcal{D}_m}[1 + \left(\frac{v_d}{v_p}\right) K f(P)] \tag{4.11}$$

with

$$f(P) = 6(bP)^{-3}\left[\frac{1}{2}(bP)^2 + bP - (1 + bP)\ln(1 + bP)\right] \tag{4.12}$$

Eq. (4.11) was validated experimentally by Paul and Kemp [1973]. The validation proceeds in a way similar to the case for a glassy polymer. Paul concluded that the time-lag in such an heterogeneous membrane can be predicted accurately by the IM. In other words, the transient permeation of gas in a heterogeneous membrane is well described by this model. As the added adsorptive fillers do not have much effect on the transport at steady-state, the consistency of time-lag behaviors can be considered as sufficient to validate this model for a heterogeneous membrane. Besides the validation of Paul and Kemp [1973], a similar work is performed by Kemp and Paul [1974] also, which gives a strong support to the model.

Consequently, the Immobilization Model is used in this thesis as the description of gas transport in a Mixed Matrix Membrane (Section 5.2).

4.1.4 Partial Immobilization models

As discussed previously, Eq. (4.8) cannot describe satisfyingly pure gas permeation through glassy polymeric membranes and the permeability at steady-state is upstream pressure depending. Some researchers propose to replace the assumption of Immobilization by the assumption of Partial Immobilization in order to improve the model performance.

• **Partial Immobilization**: The molecules obeying Langmuir's law are considered as partially immobilized along the direction of diffusion.

In this improved model, different mobilities are assigned to the two gas species present in glassy polymers. Thus the model is named as Partial Immobilization Model.

As the molecules obeying Langmuir's law are also mobile, the transport phenomenon is described by the unidimensional Fick's second law as

$$\frac{\partial(C_D + C_H)}{\partial t} = \frac{\partial}{\partial r}\left(\mathcal{D}_D \frac{\partial C_D}{\partial r} + \mathcal{D}_H \frac{\partial C_H}{\partial r}\right) \tag{4.13}$$

where $\mathcal{D}_D$ is the diffusion coefficient of Henry population and $\mathcal{D}_H$ the diffusion coefficient of Langmuir population. The Local Equilibrium assumption (Eq. (4.6)) is always considered, Eq. (4.13) thus can be rearranged to a more convenient form by eliminating C_H

$$\left[1 + \frac{K}{(1 + aC_D)^2}\right] \frac{\partial C_D}{\partial t} = \frac{\partial}{\partial r}\left[\mathcal{D}_D \left(1 + F\frac{dC_H}{dC_D}\right) \frac{\partial C_D}{\partial r}\right] \tag{4.14}$$

where $F = \frac{D_H}{D_D}$. The ratio $\frac{\partial C_H}{\partial C_D}$ can be determined analytically from the Local Equilibrium (Eq. (4.6))

$$\frac{dC_H}{dC_D} = \frac{K}{(1 + aC_D)^2} \tag{4.15}$$

Thus, the transport model is formulated by combining Eqs. (4.14) and (4.15) as

$$\left[1 + \frac{K}{(1 + aC_D)^2}\right] \frac{\partial C_D}{\partial t} = \frac{\partial}{\partial r}\left[\mathcal{D}_D \left(1 + \frac{FK}{(1 + aC_D)^2}\right) \frac{\partial C_D}{\partial r}\right] \tag{4.16}$$

The only unknown in Eq. (4.16) is C_D. It can be noticed that the case $F = 0$ means that the molecules adsorbed are immobile, Eq. (4.16) is reduced to Eq. (4.8). The PIM is reduced to the IM.

4.1.5 Dual Diffusion model

As described previously, the IM can be considered as on limit behavior of the Dual Mode Sorption theory by assuming the diffusion coefficients for two populations are very different ($\mathcal{D}_D \gg \mathcal{D}_H$. The Dual Mode Sorption theory can be proposed in a more general form by removing this equilibrium. The relationship between free gas molecule, the adsorption site and the adsorbed molecule (complex) is considered in that case as a reversible chemical reaction [Tshudy and Frankenberg, 1973]. For sake of simplicity, each adsorption site is assumed to immobilize only one gas molecule

$$\text{site } (C_H' - C_H) + \text{dissolved gas molecule } (C_D) \underset{k_r}{\overset{k_f}{\rightleftharpoons}} \text{complex } (C_H)$$

Thus the time rate of change of concentration of gas molecules is

$$\begin{aligned} \frac{\partial C_D}{\partial t} &= \frac{\partial}{\partial r}(\mathcal{D}_D \frac{\partial C_D}{\partial r}) - \Big[k_f C_D (C_H' - C_H) - k_r C_H\Big] \\ \frac{\partial C_H}{\partial t} &= \frac{\partial}{\partial r}(\mathcal{D}_H \frac{\partial C_H}{\partial r}) + \Big[k_f C_D (C_H' - C_H) - k_r C_H\Big] \end{aligned} \tag{4.17}$$

where k_f and k_r are the forward and reverse rate constants of the respective reaction. The underlying mechanism which is described postulates a rapid exchange between the sorbed molecules and the dissolved molecules through a one to one exchange process, without necessarily reaching equilibrium. Consequently, the two populations interact and sorbed molecules become part of the dissolved population when a successful diffusion jump occurs (and vice versa). The only hypothesis that is required in that case is the existence of a continuous phase and a dispersed phase (microcavities), so that the local mass balances fit the mathematical set of equations. This set of equations has been already proposed by several investigators for the Dual Mode model [Tshudy and Frankenberg, 1973]. Similar situations can be found in two-phase systems governed by a dual diffusion mechanism, such as in controlled release matrix [Papadokostaki et al., 2008] or for pollutants transport in soils. Two limit behaviors can be considered:

- In the case of a rapid exchange, k_f and k_r tend toward infinity, the equilibrium Eq. (4.6) is established instantaneously [Tshudy and Frankenberg, 1973]. In other words, the Local Equilibrium is admitted. This limit behavior corresponds to the PIM.

- In the case of a low exchange, k_f and k_r tend toward zero. The two populations approach steady-state at their own characteristic rates. Eq. (4.17) are reduced to

$$\begin{aligned} \frac{\partial C_D}{\partial t} &= \frac{\partial}{\partial r}\left(\mathcal{D}_D \frac{\partial C_D}{\partial x}\right) \\ \frac{\partial C_H}{\partial t} &= \frac{\partial}{\partial r}\left(\mathcal{D}_H \frac{\partial C_H}{\partial x}\right) \end{aligned} \tag{4.18}$$

  This second limit case of Dual Mode Sorption theory is named as the Dual Diffusion Model in order to make a difference with the Partial Immobilization Model. Instead of a non linear partial differential equation, the gas transport behavior is modeled by a combination of two linear partial differential equations. To our knowledge, this second limit case has never been studied before and will be further discussed by comparison to the PIM in this thesis.

4.1.6 Discussions of the Dual Mode Sorption theory limit behaviors

The DDM will be compared to the PIM essentially with respect to the time-lag method. The time-lag method is a popular method to determine the transport parameters for a given membrane-gas couple. In a time-lag method experiment, the upstream and downstream faces of a polymer membrane are maintained at constant partial pressures, respectively P_u and P_d, where $P_u \gg P_d$, and the increase of pressure of the gas is followed in downstream side of membrane. By proper design of the experimental apparatus, this increase of pressure can be maintained at a small value compared to the upstream pressure. Thus, the driving force for diffusion can be considered for a short duration as nearly constant ($P_u - P_d \approx P_u$).

The data of downstream pressure *versus* time in conjunction with the known downstream volume can be used to determine the cumulative amount Q_t of the penetrant gas having permeated the membrane at time t. A plot of Q_t with respect to time t (4.1) illustrates the transient period and the achievement of the steady-state permeation. By extrapolating the steady-state portion of the curve, the time-lag θ is defined as the intercept of this extrapolation line and the time axis, whereas the slope of the linear portion of the curve gives the permeability $\mathcal{P}$ at steady-state

$$\mathcal{P} = \frac{\text{slope}}{(P_u - P_d)A/L} \tag{4.19}$$

where L is the membrane thickness.

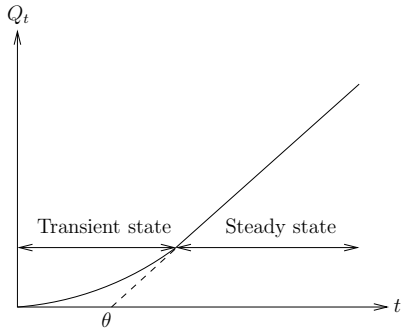

Figure 4.1: Qualitative plot of the quantity of permeate, Q_t with respect to time.

It can be deduced that the permeability at steady-state in the conditions of a time-lag measurement is written in the same way as the PIM

$$\mathcal{P} = k_D \mathcal{D}_D \left[1 + \frac{FK}{1 + bP_u}\right] \tag{4.20}$$

This similarity can be extended readily to a more general case: for any fixed pressure conditions at upstream or downstream sides, both PIM and DDM predict the same permeability at steady-state (see Appendix A). Thus both limit behaviors are equivalent for steady-state simulation. Furthermore, if one sums the two equations of Eqs. (4.17), the "reaction" terms are eliminated (Eq. (4.13)), independently of any assumption with regard to the magnitude of the rates (k_f and k_r). That is why it is not surprising that the steady-state expression of the flux is the same for both limit behaviors. Thus it would be the same for the infinite number of assumptions possible for exchange rates between the two populations.

The time-lag can be predicted by the PIM as [Paul and Koros, 1976]

$$\theta = \frac{L^2}{6\mathcal{D}_D} \frac{1 + K(f_0 + FKf_1 + (FK)^2 f_2) + FKf_3 + (FK)^2 f_4}{\left(1 + \frac{FK}{1+y}\right)^3} \tag{4.21}$$

with

$$\begin{aligned}
f_0 &= \frac{6}{y^3}\left(\frac{y^2}{2} + y - (1+y)\ln(1+y)\right) \\
f_1 &= \frac{6}{y^3}\left(\frac{y}{2} + \frac{3y}{2(1+y)} - \frac{\ln(1+y)}{1+y}\right) \\
f_2 &= \frac{6}{y^3}\left(\frac{1}{6} - \frac{1}{2(1+y)} + \frac{1}{2(1+y)^2} - \frac{1}{6(1+y)^3}\right) \\
f_3 &= \frac{6}{y^3}\left(-\frac{3}{2}y + \frac{y}{2(1+y)} + (1+y)\ln(1+y)\right) \\
f_4 &= \frac{6}{y^3}\left(\frac{1}{2} - \frac{1}{2(1+y)^2} - \frac{\ln(1+y)}{1+y}\right) \\
y &= bP_u
\end{aligned} \tag{4.22}$$

Eq. (4.21) can be reduced to two special cases:

- $K = 0$, which means that the Langmuir adsorption is supposed to be null, the time-lag is independent of the upstream pressure. This is the time-lag prediction in a rubbery polymeric membrane [Barrer, 1939].
- $F = 0$, which means that the adsorbed molecules are immobile with respect to dissolved molecules ($\mathcal{D}_D \gg \mathcal{D}_H$). This is the time-lag prediction of the IM [Paul, 1969].

For the second limit behavior, the time-lag can also be predicted analytically by the DDM

$$\theta = \frac{l^2}{6\mathcal{D}_D} \frac{1 + K + bP_u}{1 + FK + bP_u} \tag{4.23}$$

The way how to determine Eq. (4.23) is detailed in Appendix B. It should be noticed that all parameters in Eq. (4.23) are obtained by the solubility isotherm (K and b) and by steady-state permeability (F and $\mathcal{D}_D$) measurements, which is the same as for the time-lag prediction of the PIM (4.21).

It can be first noticed that Eq. (4.23) is much simpler but consistent with Eq. (4.21) with regard to the asymptotic behaviors at low and high pressures in an ordinary case where $0 < F < 1$ and $K > 0$

$$\begin{aligned} \lim_{P_u \to 0} \theta &= \frac{l^2}{6\mathcal{D}_D} \frac{1+K}{1+FK} \\ \lim_{P_u \to +\infty} \theta &= \frac{l^2}{6\mathcal{D}_D} \end{aligned} \tag{4.24}$$

In the case of a low pressure, the time-lag tends to a maximum value, the impact of the Langmuir population reaches its maximum. In the case of a high pressure, the Langmuir adsorption sites are saturated, but the Henry population can increase without limitation. The time-lag is only governed by the Henry population thus is independent of the upstream pressure. These asymptotic behaviors at low and high pressures will be referred in the following as the two limit cases.

It can be noticed that in Fig. 4.2 both predictions constitute a closed time-lag zone: the PIM represents the time-lag upper bound while the lower bound is given by the DDM.

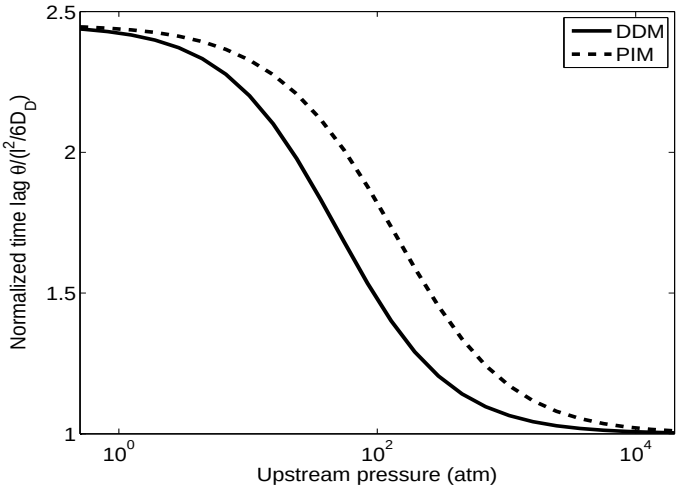

Figure 4.2: Predicted time-lags by two limit behaviors for a general case with $K = 5$ and $b = 0.05$ atm^{-1}. (DDM = Dual Diffusion Model, PIM = Partial Immobilization Model).

With respect to both limit behaviors, the steady-state permeability is independent of the exchange rates of Eq. (4.17). However, time-lag predictions depend on exchange rates.

Assuming that the time-lag experiment is extended to a long duration (much longer than the time-lag), the upstream exhaustion and the downstream accumulation become significant, thus a pressure equilibrium between upstream and downstream will be reached. This experiment is here denoted as "Free diffusion to pressure equilibrium". Since these two limit behaviors can provide different time-lag predictions, some difference is expected in "Free diffusion to pressure equilibrium" experiment. Based on the transport of CO_2 through a glassy polyimide [Thundyil et al., 1999], such an experiment is simulated numerically by both DDM and PIM. Nevertheless, Fig. 4.3 shows that no relative significant difference is achieved (Dashed lines are not visible on the Figure since they are perfectly superimposed by continued lines.). This observation confirms that even if the time-lag predictions differ, both models are equivalent for a long time scale (compared to the time-lag).

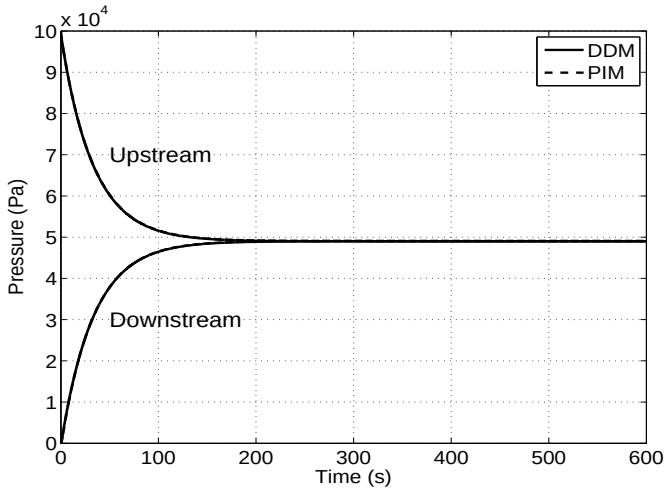

Figure 4.3: Comparison of simulated "Free diffusion to pressure equilibrium" of different models.(DDM = Dual Diffusion Model, PIM = Partial Immobilization Model.)

Consequently, it can be concluded that the only difference between exchange rates appears in the quantitative time-lag prediction. This latter will be discussed by comparing to experimental data in the following sections.

Comparison with experimental time-lag data

This comparison is performed with data from four different papers.

Experimental data of Koros et al. [1977] are first used as a reference in

the comparison. In order to validate the PIM, Koros et al. [1977] determined the transport parameters of five gaseous components for a bisphenol-A polycarbonate at 35℃ using only sorption and steady-state permeation results. These determined parameters are listed in Tab. 4.1. As discussed previously, these data can be used in the DDM and in the PIM. Then, a comparison between his experimental results with the PIM prediction of time-lag is performed and Koros concluded to an acceptable agreement, while a tendency for the experimental time-lags to lie below the predicted lines is noted.

Koros noticed that the measurements for CO_2, CH_4 and N_2 were made on 3 mil film, while the argon data were measured with a 4.2 mil film and the helium data were obtained from a 63.5 mil membrane since their time-lags for a 3 mil film were too short to be accurately measured. In the comparison, all measured time-lags for other thickness have been scaled to a 3 mil basis.

	Unit	CO_2	CH_4	Ar	N_2	He
k_D	$cm^3(STP)/cm^3atm$	0.6852	0.1473	0.1534	0.0909	0.0145
C'_H	$cm^3(STP)/cm^3$	18.805	8.382	3.093	2.109	0.313
b	atm^{-1}	0.2618	0.0841	0.063	0.0564	0.0121
$\mathcal{D}_D$	$\times 10^{-9}$ cm^2/s	62.2	10.9	33.0	17.6	5500
$\mathcal{D}_H$	$\times 10^{-9}$ cm^2/s	4.85	1.258	5.94	5.09	7440
F		0.078	0.115	0.180	0.289	1.33

Table 4.1: Dual mode sorption parameters for bisphenol-A polycarbonate at 35℃, reported by Koros et al. [1977]

All predictions of the three available models and the reference data for four gaseous components are represented in Fig. 4.4, except for He whose case will be discussed later. Some points can be highlighted:

- For all gaseous components, the IM presents the most important deviation with respect to the experimental results, which confirms that it is not an adequate model for glassy polymers.
- Even if no model can give a perfect quantitative time-lag prediction, the agreement with the DDM predictions are closer to the experimental data than to the PIM ones.
- Koros noticed that a trend exists for the experimental time-lags to lie below the predicted lines of the PIM. This behavior is less significant for the DDM and almost not observed in the case of CO_2.

As Koros et al. [1977] noticed that the determination of transport parameters of He is different from others and might be less accurate, its comparison is

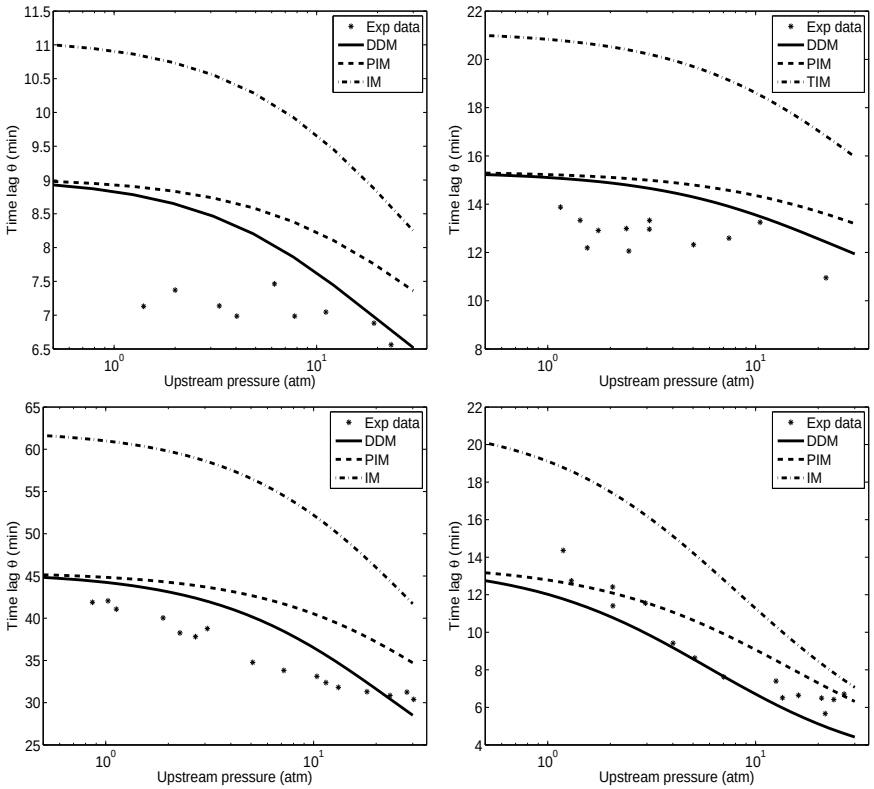

Figure 4.4: Comparison of experimental [Koros et al., 1977] and predicted time-lags by different models for various gaseous components in polycarbonate at 35℃. Ar: top left, N_2: top right, CH_4: bottom left, CO_2: bottom right. (DDM = Dual Diffusion Model, PIM = Partial Immobilization Model, IM = Immobilization Model).

performed separately in Fig. 4.5. Since the measured diffusion coefficient for adsorbed molecules $\mathcal{D}_H$ is greater than the diffusion coefficient for dissolved species $\mathcal{D}_D$, a special Partial Immobilization Model with $F = 1$ is also inserted to help the comparison. The assumption $F = 1$ means that the two species have the same mobility, which is a 'total mobile' model for helium. As shown in Fig. 4.5, similar agreements can be obtained. The predictions of the DDM and of the PIM are nearly superimposed. Thus, the agreement with experimental results gives a strong support to the DDM.

In another paper, Koros and Paul [1978] performed the sorption measurements and the time-lag method measurement for different systems. They measured the sorption and transport coefficients and the time-lags for CO_2 in a semicrystalline poly(ethylene terephthalate) for temperatures ranging from 25℃ to 115℃ over the pressure range from 0.1 to 30 atm. A part of their

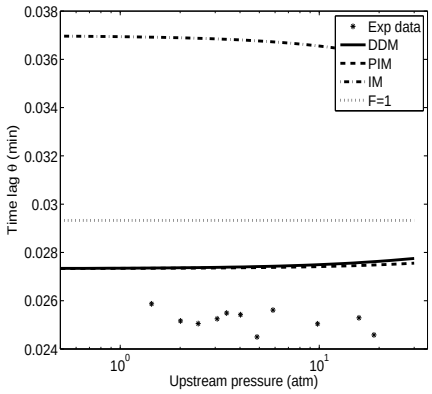

Figure 4.5: Comparison of experimental [Koros et al., 1977] and predicted time-lags by different models for He in polycarbonate at 35℃. (DDM = Dual Diffusion Model, PIM = Partial Immobilization Model, IM = Immobilization Model, $'F = 1'$ = no immobilization model).

measurements are given in Tab. 4.2 at which temperature the polymer is glassy. Based on these data, the time-lags are predicted by three models and compared to the experimental data in Figs. 4.6 and 4.7.

In this case, the DDM predicts correctly and even better the time-lags in the temperature range from 25℃ to 65℃. The only exception is observed in the case of 75℃. Koros and Paul [1978] indicated that the glass transition temperature T_g of tested polymer is approximately 85℃. Once the experiment temperature goes close to the transition temperature, the glassy characteristics become less significant, none of dual mode models provides a satisfying prediction. Again the DDM is validated and predicts better the time-lag than any other model.

	Unit	25℃	35℃	45℃	55℃	65℃	75℃
k_D	$\mathrm{cm^3(STP)/cm^3\ atm}$	0.362	0.330	0.260	0.234	0.214	0.210
$C_H^{'}$	$\mathrm{cm^3(STP)/cm^3}$	7.913	5.760	4.960	3.753	2.735	1.814
b	$\mathrm{atm^{-1}}$	0.351	0.322	0.282	0.252	0.197	0.165
$\mathcal{D}_D$	$\times 10^{-9}\ \mathrm{cm^2/s}$	2.002	3.146	5.260	8.330	11.65	16.79
$\mathcal{D}_H$	$\times 10^{-9}\ \mathrm{cm^2/s}$	0.0956	0.221	0.410	0.490	1.10	1.326
F		0.048	0.0712	0.078	0.059	0.095	0.079

Table 4.2: Dual mode sorption parameters for CO_2 in PET at different temperatures, reported by Koros and Paul [1978]

Koros et al. [1976] performed another CO_2 time-lag measurement with determinations of gas transport parameters (Tab. 4.3). The comparison between

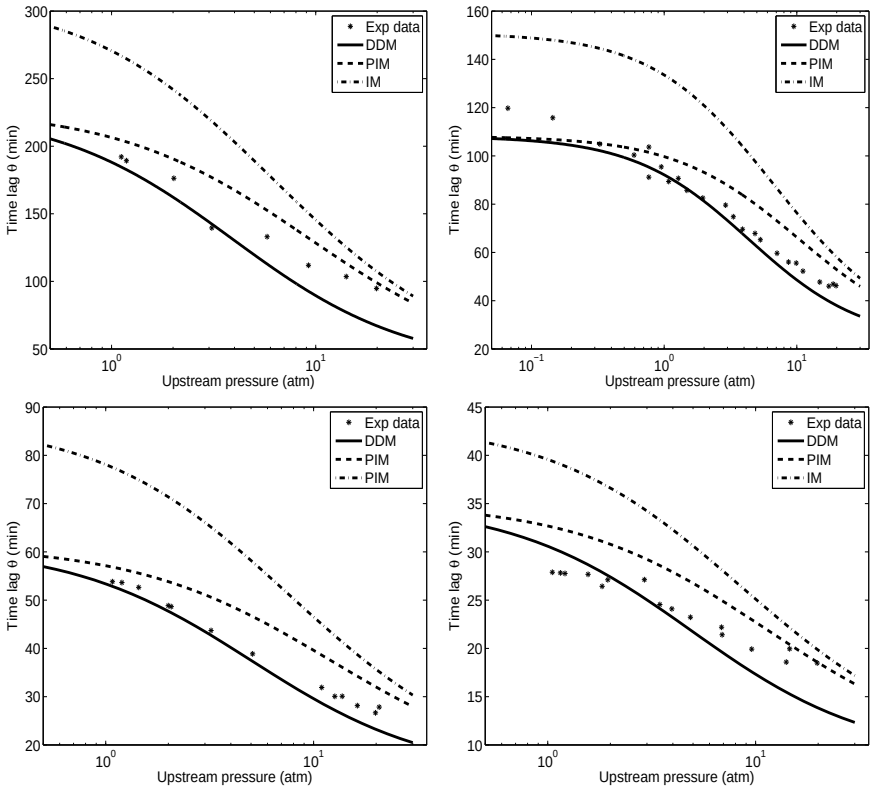

Figure 4.6: Comparison of experimental [Koros and Paul, 1978] and predicted time-lags by different models for CO_2 in PET at different temperatures below T_g. 25℃: top left, 35℃: top right, 45℃: bottom left, 55℃: bottom right. (DDM = Dual Diffusion Model, PIM = Partial Immobilization Model, IM = Immobilization Model).

predictions and experimental data is given in Fig. 4.8. Similar to Figs. 4.6 and 4.7, the DDM shows again its efficiency, presenting the best agreement to the experimental data compared to all other models.

More recently, Garrido et al. [2008] performed also some time-lag tests for CO_2 in poly[bisphenol A carbonate-*co*-4,4'-(3,3,5-trimethylcyclohexyliden) diphenol carbonate] film at 303K. First, they determined the gas transport parameters (Tab. 4.4) according to Koros suggestion. The predictions of three models and the experimental data are represented together in Fig. 4.9. Opposite to previously discussed cases, the prediction of the PIM represents the best agreement with the experiments although the prediction of the DDM is not far from the experimental data. However, the tendency of the time-lag overestimation indicated by Koros et al. [1977], which is regularly observed in all other measurements, surprisingly is not observed here.

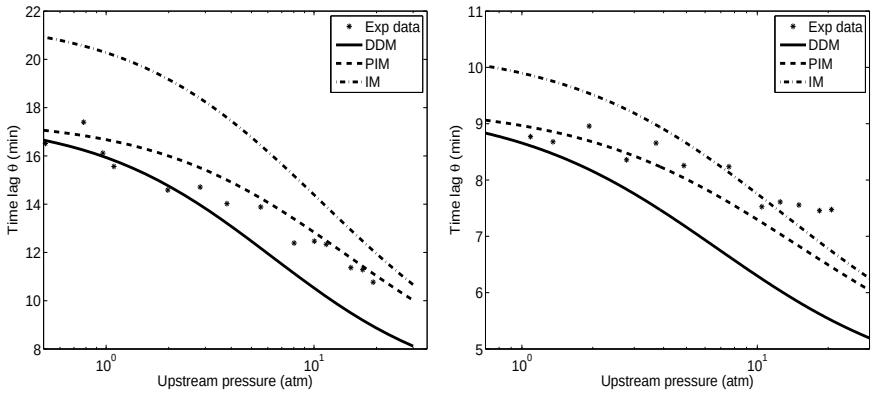

Figure 4.7: Comparison of experimental [Koros and Paul, 1978] and predicted time-lags by different models for CO_2 in PET at different temperatures below T_g. 65℃ (left) and 75℃ (right). (DDM = Dual Diffusion Model, PIM = Partial Immobilization Model, IM = Immobilization Model).

k_D	$cm^3(STP)/cm^3$ atm	0.866
C'_H	$cm^3(STP)/cm^3$	16.7
b	atm^{-1}	0.309
$\mathcal{D}_D$	$\times 10^{-9}$ cm^2/s	46.7
$\mathcal{D}_H$	$\times 10^{-9}$ cm^2/s	4.717
F		0.101

Table 4.3: Dual mode sorption parameters for CO_2 in polycarbonate at 35℃, reported by Koros et al. [1976]

Secondly, the experimental data given by Garrido et al. [2008] are much more regular than those from Koros, therefore a smooth decreasing curve over the tested pressure range can be readily produced. It can be noticed that the DDM correctly predicts this decreasing behavior: the slopes of the experimental decreasing curve and the DDM prediction curve are rather close for all points. Nevertheless, although the PIM better predicts the absolute time-lag value, the decreasing tendency of time-lags is not correctly simulated. Thus it can be suspected that the deviation between the PIM prediction and the real value will be probably increased when the upstream pressure is high. Therefore, in this way, the DDM prediction still presents an advantage compared to the PIM.

Chiou and Paul [1989] reported some rare exceptions, the isothermal permeabilities at steady-state for N_2, Ar and CH_4 in poly(ethyl methacrylate) (PEMA) below its T_g are independent of pressure, while the time-lags de-

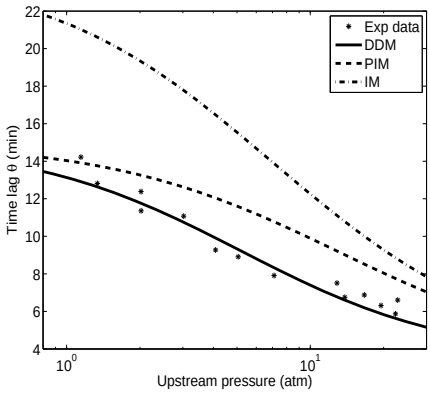

Figure 4.8: Comparison of experimental [Koros et al., 1976] and predicted time-lags by different models for CO_2 in polycarbonate at 35℃. (DDM = Dual Diffusion Model, PIM = Partial Immobilization Model, IM = Immobilization Model).

k_D	$cm^3(STP)/cm^3$ atm	1.0868
C'_H	$cm^3(STP)/cm^3$	20.6
b	atm^{-1}	0.2584
$\mathcal{D}_D$	$\times 10^{-9}$ cm^2/s	79.0
$\mathcal{D}_H$	$\times 10^{-9}$ cm^2/s	14.2
F		0.18

Table 4.4: Dual mode sorption parameters for CO_2 - poly[bisphenol A carbonate-*co*-4,4'-(3,3,5-trimethylcyclohexyliden) diphenol carbonate] at 303K, reported by Garrido et al. [2008]

crease with pressure. Since their time-lag predictions according to the IM are consistent with the experimental data, Chiou and Paul [1989] concluded that the transport of these gaseous components in this polymer follows the IM. The transport parameters (Tab. 4.5) are obtained by sorption and permeation experiments through a film of 3.95 mil. Nevertheless, Chiou and Paul [1989] pointed out that the sorption parameters of N_2 cannot be obtained using the same methodology since the concentration of N_2 is so low that the scatter of the data does not allow the fitting of the isotherm to Eq. (2.11). Using these measured coefficients, Chiou and Paul [1989] estimate correctly the time-lag with the IM. It can be noticed that the DDM can also be suitable to describe this case by making F tend towards zero.

In a similar way, the predictions of two models and the experimental data are represented together in Fig. 4.10. Again, the DDM predictions show a

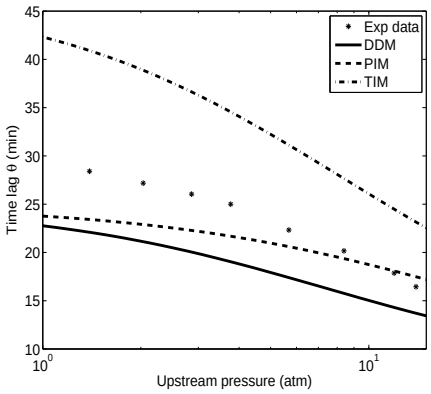

Figure 4.9: Comparison of experimental [Garrido et al., 2008] and predicted time-lags by different models for CO_2 in poly[bisphenol A carbonate-*co*-4,4'-(3,3,5-trimethylcyclohexyliden) diphenol carbonate] film at 303K. (DDM = Dual Diffusion Model, PIM = Partial Immobilization Model, IM = Immobilization Model).

	Unit	Ar	CH_4
k_D	$cm^3(STP)/cm^3$ atm	0.0902	0.165
C'_H	$cm^3(STP)/cm^3$	1.20	2.24
b	atm^{-1}	0.0405	0.0536
$\mathcal{D}_D$	$\times 10^{-8}$ cm^2/s	7.78	1.60
F		0	0

Table 4.5: Dual mode sorption parameters for Ar and CH_4 in PEMA at 35℃, reported by Chiou and Paul [1989]

better agreement with the experimental data.

It can be concluded that in most cases, the two limits of Dual Mode Sorption theory represent correctly the experimental time-lag zones, while the lower bound which is given by the DDM provides somehow a better agreement with respect to experimental data. It is interesting to note that in all four cited time-lag behaviors, the lower bound given by the DDM provides good time-lag predictions in particular for CO_2 through different membranes.

As explained, the only difference between the PIM and the DDM is the time-lag prediction. Consequently, it is reasonable to conclude that the DDM is validated, even a better choice for modeling the transport behavior in glassy membranes, at least for these gaseous components through the concerned polycarbonate polymer under the tested pressure range. The DDM can be considered as a simpler but more efficient description of gas transport in glassy

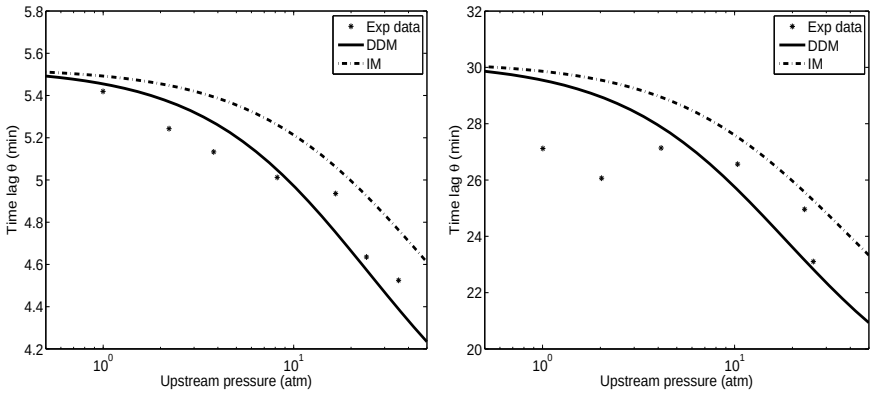

Figure 4.10: Comparison of experimental [Chiou and Paul, 1989] and predicted time-lags by different models for Ar (left) and CH_4 (right) in PEMA film at 35℃. (DDM = Dual Diffusion Model, IM = Immobilization Model).

polymers.

Comparisons are also performed in Figs. 4.11, 4.12 and 4.13, for CO_2 in PET membranes, 4 gaseous components in polycarbonate membranes, CH_4 and Ar in PEMA membrane respectively. In these figures, the experimental time-lag and the theoretical prediction are compared on the same plot for all conditions for a given material. It can be noticed that the lower bound given by the DDM is shown as the best approach in time-lag predictions. However, it can be noticed that in Fig. 4.11, the points above about 100 minutes which present a deviation with respect to the bisector are those obtained at 25℃ in Fig. 4.6.

In order to quantify the predicting ability in three conditions, the relative error e for each material is defined as

$$e = \frac{|\theta_{exp} - \theta_i|}{\theta_{exp}} \qquad i = \text{DDM, PIM and IM} \tag{4.25}$$

According to Tab. 4.6, for all three membrane materials, the prediction lower bounds provide the best agreement to the experiment data. The prediction relative error is in general lower than 11%.

It is very important to notice that both PIM and DDM are limit behaviors of the Dual Mode Sorption theory. In reality, neither of them can be reached, the effective exchange rate k_f and k_r in Eq. (4.17) could not be assumed to be infinity neither be null. That explains the fact that most experimental time-lag data are found inside the time-lag interval. Assink [1975] confirmed by a NMR study that the local equilibrium can be considered as instantaneous in the case of ammonia sorbed by polystyrene. Nevertheless, it should be noticed that as

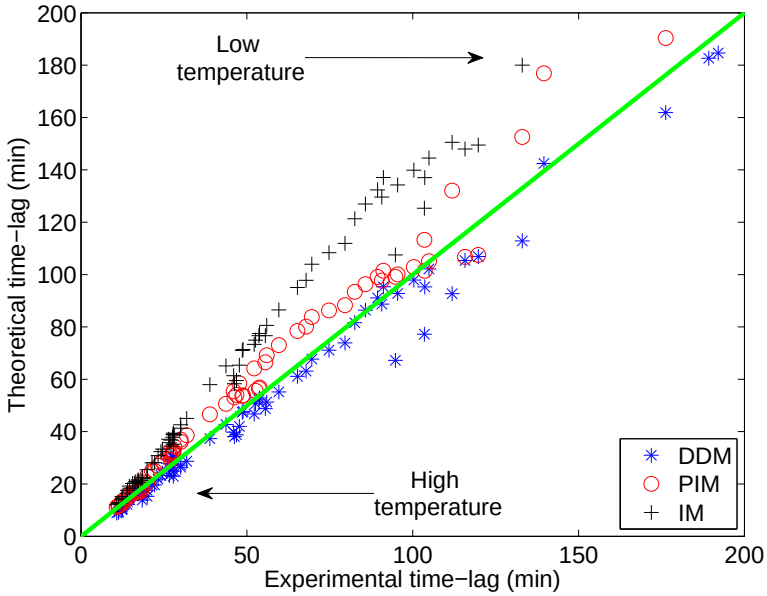

Figure 4.11: Comparison of experimental [Koros and Paul, 1978] and predicted time-lags by different models for CO_2 from 25℃ to 65℃ in PET film. (DDM = Dual Diffusion Model, PIM = Partial Immobilization Model, IM = Immobilization Model).

a highly polar molecule, the ammonia might represent exceptional sorption ability with respect to less polar gases such as CO_2, CH_4 and O_2 discussed in this paper. Consequently, the conclusion of Assink might not be considered as a general conclusion.

However, it is important to notice that the determination of time-lags is subject to relatively large errors. The history dependence of diffusion in glassy polymers can create problems. How the films are conditioned (pressure gradient versus uniform high pressure exposure), how long each measurement is taken (a measurement at steady-state for a prolonged period can affect the

Membrane material	e_{DDM}	e_{PIM}	e_{IM}
PET	8.43%	11.46%	33.46%
Polycarbonate	10.42%	17.08%	50.03%
PEMA	3.79%	-	5.77%

Table 4.6: Average relative error e for PET, Polycarbonate and PEMA membranes

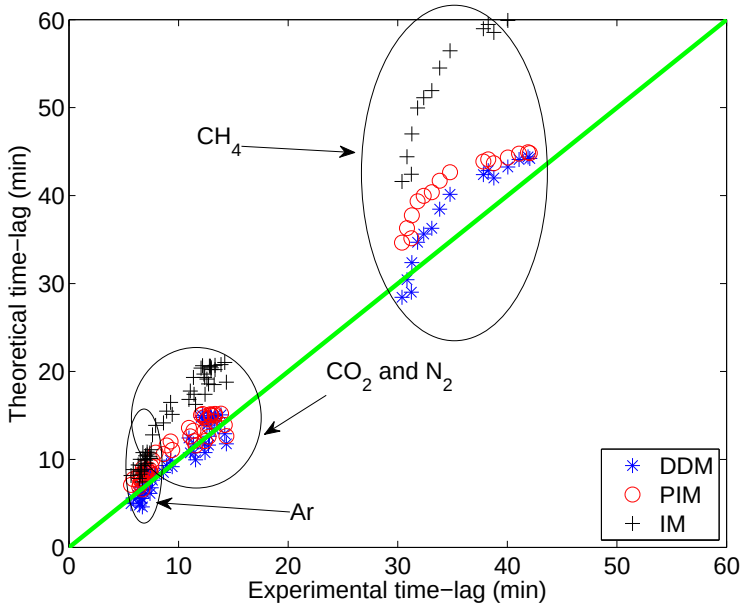

Figure 4.12: Comparison of experimental [Koros et al., 1976, 1977] and predicted time-lags by different models for CO_2, CH_4, N_2 and Ar in polycarbonate film. (DDM = Dual Diffusion Model, PIM = Partial Immobilization Model, IM = Immobilization Model).

next result), and how the film is depressurized prior to the next transient measurement, all these experimental conditions lead to the scatter shown in figures of comparison like Fig. 4.6. Furthermore, the thickness changes with pressure and the time-lag dependence on membrane thickness as L^2 can introduce a supplementary error. Lastly, diffusion coefficients $\mathcal{D}_D$ and $\mathcal{D}_H$ are fitting parameters and the scatter in steady-state permeabilities with pressure is sufficient to reveal that the time-lag results can be difficult to reproduce in some systems.

4.1.7 Time-lag prediction in membrane processes

As explained in Chapter 2, membrane processes for gas separations are conventionally operated by means of dense polymeric materials at steady-state, both feed pressure and permeate pressure are maintained at constant levels, thus the permeation rate and permeate concentration are dominated only by the permeabilities, except at the initial start-up stage. According to Appendix A, both limit models (DDM and PIM) provide the same permeability prediction at steady-state. Consequently, both limit models are identical in steady-state

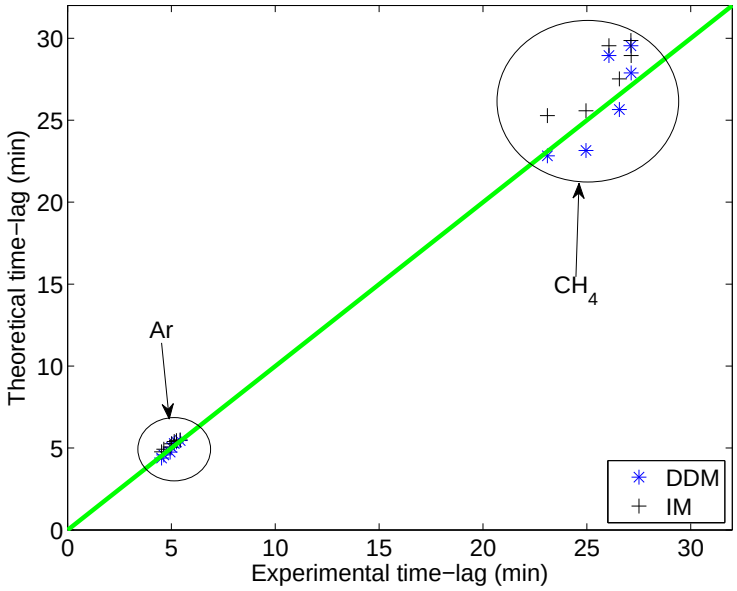

Figure 4.13: Comparison of experimental [Chiou and Paul, 1989] and predicted time-lags by different models for Ar and CH_4 in PEMA film at 35°C. (DDM = Dual Diffusion Model, IM = Immobilization Model).

membrane process simulation.

According to some simulations and experimental investigations reviewed in Chapter 3, the cyclic membrane processes, in particular the short class processes, are able to provide some exclusive advantages [Wang et al., 2011a] with respect to conventional operations, such as important selectivity improvement. It is highlighted in Chapter 3 that the key issue of short class cyclic processes is the time-lag, which distinguishes the steady-state and the transient-state permeations. As a result, an efficient time-lag prediction method should be used in order to accurately simulate a cyclic process simulation. In this respect, the lower bound prediction (DDM) providing in general a better agreement with experiments will be a better choice than the upper bound prediction (PIM).

Besides the short class cyclic processes, the description of the transient mass transfer of gaseous species in glassy polymers is also of major interest for other industrial applications, such as packaging, adhesives and controlled release, etc. For example, Higuchi and Higuchi [1960] were interested in developing protective ointments or creams (polymers) which could be applied to the skin for the purpose of providing the treated area with protection from toxic agents that could be absorbed through the skin. In this respect, at least one of the two following specifications is required for these protective polymers:

1. The steady-state rate of transport of the agent through the polymers should be low.

2. The permeation rate should be much lower before reaching the steady-state, thus the time-lag for the toxic agent should be large.

The second point is more appropriate when any measurable steady-state rate would produce a lethal effect. As a result, the time-lag prediction is especially important for this purpose. On the other hand, it is better to under estimate the time-lag than to over estimate it for reason of security in this kind of applications. Consequently, the time-lag lower bound provider - the DDM should be a better choice to estimate the boundary between the transient-state and the steady-state.

4.1.8 Conclusion for transport mechanisms

Since 1950s, the Dual Mode Sorption theory has been developed then extended. The first mathematical description of this transport phenomena, the Immobilization Model cannot accurately describe the transport behavior in most glassy polymers, except one case mentioned by Chiou and Paul [1989]. Nevertheless, the IM is found adequate to describe the transport phenomena in Mixed Matrix Membranes. By better understanding the transport mechanism in glassy polymers and performing experimental verifications, the Langmuir population is no more considered as totally immobilized. Using numerous measurements according to the time-lag method, the Partial Immobilization Model is closer to the reality, thus it is nowadays considered as a good approach to this phenomenon.

By considering the adsorption process as a reversible chemical reaction in the framework of the dual mode theory, two limit cases will be distinguished according to the influence of the forward and reverse reaction rates. In that case, the Partial Immobilization Model becomes one limit case of the dual mode theory as both forward and reverse reactions rates are considered as rapid. Another limit condition of the Dual Mode Sorption theory named as Dual Diffusion Model where both reaction rates are considered as slow is essentially investigated in this paper and compared to the PIM. First, in a steady-state simulation, these two models are equivalent as well as all intermediate conditions. Secondly, with respect to the time-lag values, in general, experimental data lie between two bounds provided by the PIM and the DDM. Furthermore, the lower bound provided by the DDM seems to be closer to experimental data, especially in the case of CO_2 in glassy polymers. Consequently, the time-lag lower bound (DDM) completes the dual mode sorption theory and can be considered as an efficient and easy-to-use approach of the

theory with respect to conventional models, especially in time-lag prediction applications.

As a result, within the frame of the thesis, the transport equations given by the Dual Mode Sorption theory are solved in the general case with $K \neq 0$ and $F \neq 0$. The solving program is given in Appendix D. Nevertheless, the transport parameters are given in the literature in forms of only k_D and $\mathcal{D}$ as an approximation in most cases [Brandrup and Immergut, 1989]. Consequently, the simplified transport model for rubbery membranes using only k_D and $\mathcal{D}$ (linear Fick's law with $K = 0$ and $F = 0$) is primarily used in our simulation study (Sections 5.1 and 5.3). As a Mixed Matrix Membrane is studied in detail by Paul [1969], Paul and Kemp [1973], full Dual Mode Sorption parameters are available for the considered gas-MMM couple, the processes based on this MMM (Section 5.2) is simulated using the IM.

4.2 Process modeling

A membrane gas separation process is composed of a membrane module and its accessories: basically several valves and receiving tanks. As explained previously, the gas transport in and through the membrane is modeled by the Dual Mode Sorption theory. Then the module geometry and all the accessories should be incorporated in the process model.

In this section, the hollow fiber geometry is first modeled with its accessories based on the general Partial Immobilization Model. Then numerical methods used to solve the corresponding problem are exhibited. Finally, the process optimization method is detailed.

4.2.1 Effect of flow pattern

In reality, the permeate pressure is never null thus a back pressure effect reduces the separation efficiency of a membrane process [Ruthven et al., 1993]. The flow pattern has a pronounced effect on the back pressure profile (Figs. 4.14, 4.15 and 4.16). In any mass transfer process, the worst case from the point of view of process efficiency is the stirred model (Fig. 4.14 (perfect mixing on both sides of the membrane) for any steady-state operations. This provides a useful limiting case for assessing the effect of flow pattern on performance, but in general one would try to avoid this condition in an operating system.

The countercurrent (Fig. 4.15) flow maximizes the average driving force and therefore provides the most efficient arrangement in theory. Nevertheless, in practice, it is relatively easy to achieve a reasonable approximation to plug

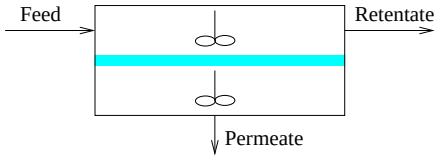

Figure 4.14: Schematic flow pattern: Stirred pattern.

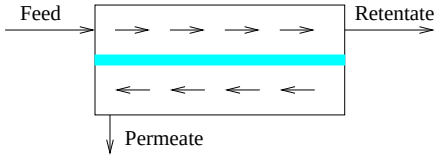

Figure 4.15: Schematic flow pattern : Countercurrent flow pattern.

flow on the high pressure side (retentate), whereas the same operation is much more difficult on the low pressure side (permeate) because of the wide variation in the gas velocity (from close to zero at the closed end to a significant value at the permeate exit). If the pressure ratio is large, deviations from the ideal plug flow on the low pressure side have a relatively minor effect on performance, provided that plug flow is maintained on the high pressure side. The operation of many membrane modules, in particular those of the hollow fiber type, is therefore well represented by the "cross flow" model (Fig. 4.16, which assumes plug flow on the high pressure side with perfect mixing on the low pressure side. Consequently, the "cross flow" model is in general used in this thesis to represent the performance of steady-state operations. Nevertheless, in the case

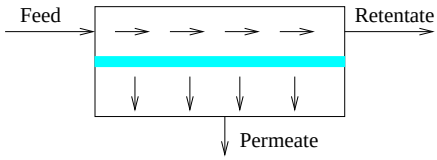

Figure 4.16: Schematic flow pattern: Cross flow pattern

of Paul [1971] process (which will be detailed later), the perfect mixing model is the only possible case since there are no convective flux in both upstream and downstream during the diffusion. Consequently, the perfect mixing model is considered as the general case for all kinds of cyclic processes in this thesis.

4.2.2 Hollow fiber geometry modeling

As explained in Chapter 2, the hollow fiber module is chosen as the standard module of the thesis due to its high specific surface. One hollow fiber module

is modeled as a set of identical fibers. Thus each fiber and its environment are first modeled individually (Fig. 4.17). Then the whole performance of the module is obtained by summing the set. Gas flows into the hollow fibers which represent the upstream volume so that the total free space between fibers corresponds to the downstream volume (Fig. 4.18). The following assumptions are considered for the membrane:

- The resistance to mass transfer is only located in the effective membrane, the mechanical support part of the fibers does not have any resistance.
- The active (selective) membrane film is situated at the outside of the membrane, thus the effective membrane surface is calculated with respect to the external radius of the fiber.
- All operations are isothermal.
- Dual Mode mass transfer parameters (k_D, $\mathcal{D}_D$, C'_H, b and F) are all constant.

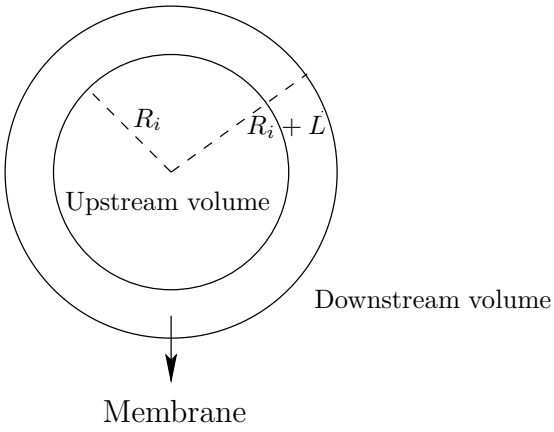

Figure 4.17: One fiber of a hollow fiber module

Consequently, the total upstream volume is obtained by multiplying individual internal volume of a fiber by the number of fibers, as well as the total active surface. On the other hand, the total downstream volume is adjustable by modifying the whole volume of the module.

As explained in Section 4.1.8, for a mixture of n components, the behavior of the membrane can be modeled by the one-dimensional Fick's law for component k in a radial coordinate system assuming that Dual Mode Sorption

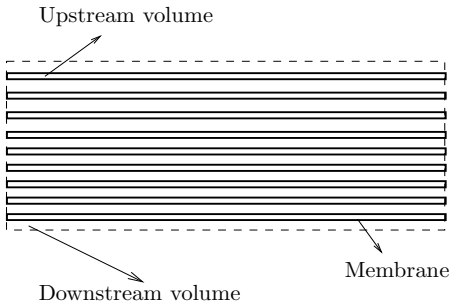

Figure 4.18: Modeling of a hollow fiber module

theory is applicable

$$\left[1+\frac{K_k}{(1+\sum_{i=1}^{n}a_iC_i)^2}\right]\frac{\partial C_k}{\partial t}=\frac{1}{r}\frac{\partial}{\partial r}\left[r\mathcal{D}_k\left(1+\frac{F_kK_k}{(1+\sum_{i=1}^{n}a_iC_i)^2}\right)\frac{\partial C_k}{\partial r}\right] \tag{4.26}$$

where Henry population concentration C_D is replaced by C and Henry diffusion coefficient $\mathcal{D}_D$ is replaced by a simple symbol $\mathcal{D}$ for sake of convenience. Eq. (4.26) is consistent with two case studies of the thesis:

- In the case where the Langmuir population is immobile with $F_k = 0$, Eq. (4.26) is reduced to

$$\left[1+\frac{K_k}{(1+\sum_{i=1}^{n}a_iC_i)^2}\right]\frac{\partial C_k}{\partial t}=\frac{1}{r}\frac{\partial}{\partial r}\left(r\mathcal{D}_k\frac{\partial C_k}{\partial r}\right) \tag{4.27}$$

- In the case of rubbery membranes with $K_k = 0$ and $a_k = 0$, Eq. (4.26) is reduced to a linear Fick's law

$$\frac{\partial C_k}{\partial t}=\frac{1}{r}\frac{\partial}{\partial r}\left[r\mathcal{D}_k\frac{\partial C_k}{\partial r}\right] \tag{4.28}$$

Thus, the Partial Immobilization Model (Eq. (4.26)) can be considered as a general description of gas behavior. Consequently, in following process modeling of the thesis, the general Partial Immobilization Model (Eq. (4.26)) is

used to describe the transport phenomena. Transport behaviors of special cases such as Mixed Matrix Membranes and rubbery membranes are derived according to their proper assumptions (Sections 4.1.8).

Since a single membrane of thickness L is submitted to a partial upstream pressure P_k^0 and vacuum is initially created in the upstream and downstream, the initial and boundary conditions for Eq. (4.26) are

$$\begin{aligned} &C_k(r,0) = 0 \qquad \forall R_i \leq r \leq R_i + L \\ &C_k(R_i,t) = k_{Dk} P_k^u \qquad \forall t \\ &C_k(R_i + L,t) = k_{Dk} P_k^d \qquad \forall t \end{aligned} \tag{4.29}$$

According to valve opening conditions, two major situations of boundary conditions are considered:

- By opening corresponding valves, upstream and/or downstream volume pressures are maintained at constant values (high pressure in the case of feeding, low pressure in the case of exerting a vacuum), the boundary conditions for Eq. (4.26) are

$$\begin{aligned} C_k(R_i,t) = k_{Dk} P_k^0 = \text{constant} \qquad \forall t \\ \text{and/or} \quad C_k(R_i + L,t) = 0 = \text{constant} \qquad \forall t \end{aligned} \tag{4.30}$$

- By closing the corresponding valves, upstream and/or downstream volume are isolated from outside, thus pressures evolve with the diffusion phenomena. Consequently, for upstream volume, assuming perfect gas law and the perfect mixing in the volume, the mass balance results in the following equation to estimate the exhaustion in upstream

$$\frac{dP_k^u}{dt} = \frac{dn_k^{\text{out}}}{dt} \frac{RT}{V^u} \tag{4.31}$$

with the molar flow rate leaving upstream

$$\frac{dn_k^{\text{out}}}{dt} = -\left[\mathcal{D}_{Dk} \frac{\partial C_{Dk}}{\partial r} + \mathcal{D}_{Hk} \frac{\partial C_{Hk}}{\partial r}\right]\Bigg|_{R_i} A \tag{4.32}$$

where A is the membrane surface. For the downstream volume, the accumulation is estimated in a similar way

$$\frac{dP_k^d}{dt} = \frac{dn_k^{\text{in}}}{dt} \frac{RT}{V^d} \tag{4.33}$$

with the molar flow rate entering into downstream

$$\frac{dn_k^{\text{in}}}{dt} = -\left[\mathcal{D}_{Dk} \frac{\partial C_{Dk}}{\partial r} + \mathcal{D}_{Hk} \frac{\partial C_{Hk}}{\partial r}\right]\Bigg|_{R_i+L} A \tag{4.34}$$

4.2.3 Applied numerical solution algorithms

As explained in previous sections, the process simulation consists of determining gas behaviors under different operating conditions. In the case of one-dimensional coordinates, the gas concentration is a function of the position in the polymer (r for radial coordinates) and the time t under transient-state. Consequently, from a point of view of mathematics, the problem is to solve partial differential equations (PDE) with different initial and boundary conditions.

Simple PDEs, especially the linear ones, can be solved analytically with simple boundary conditions [Carslaw and Jaeger, 1959]. Nevertheless, for most cases of our simulation, there is no available analytical solution for the corresponding PDEs due to the complexity of equations and boundary conditions. Consequently, numerical methods are in general applied to obtain approximative solutions.

Solving such a diffusion problem is a typical application of Computational Fluid Dynamics (CFD). To our knowledge, there are four distinct streams of numerical solution techniques: finite differences, finite elements, spectral and finite volumes. In outline, the numerical methods that form the basis of the solver perform the following steps:

- Approximation of the unknown flow variables by means of simple functions.
- Discretization by substitution of the approximations into the governing flow equations and subsequent mathematical manipulations.
- Solution of the algebraic equations.

The main differences between the separate streams are associated with the way in which the flow variables are approximated [Versteeg and Malalasekera, 1995].

- **Finite difference methods.** Finite difference methods describe the unknowns ϕ of the flow problem at the node points of a grid of coordinate lines. Truncated Taylor series expansions are often used to generate finite difference approximations of deviation of ϕ at each grid point and its immediate neighbors. These derivatives appearing in the governing equations are replaced by finite differences yielding an algebraic equation for the values of ϕ at each grid point. It can be noticed that the function *pdepe* available in Matlab is a typical solver of diffusion problems based on the finite difference method, in which only the spatial derivations are discretized resulting in a set of ordinary differential equations.

- **Finite element methods.** Finite element methods use simple piecewise functions (e.g. linear or quadratic) valid on elements to describe the local variations of unknown flow variables ϕ. The governing equation is precisely satisfied by the exact solution ϕ. If the piecewise approximating functions for ϕ are substituted into the equation, it will not hold exactly and a residual is defined to measure the errors. Next, the residuals (and hence the errors) are minimized in some sense by multiplying them by a set of weighting functions and integrating. A set of algebraic equation results for the unknown coefficients of the approximating functions. The theory of finite elements has been developed initially for structural stress analysis. This method is widely used in commercially available CFD codes, such as COMSOL.

- **Spectral methods.** Spectral methods approximate the unknowns by means of truncated Fourier series or series of Chebyshev polynomials. Unlike the finite difference or finite element approach, the approximations are not local but valid throughout the entire computational domain. Again the unknowns are replaced in the governing equation by the truncated series. The constraint that leads to the algebraic equations for the coefficients of the Fourier or Chebyshev series is provided by a weighted residuals concept similar to the finite element method or by making the approximate function coincide with the exact solution at a number of grid points.

In this thesis, the most employed method is named as **Finite Volume Method**. This method was originally developed as a special finite difference formulation, whose algorithm consists of the following steps:

- Formal integration of the governing equations of fluid flow over all the (finite) control volumes of the solution domain. It is this first step, the control volume integration, that distinguishes the finite volume method from all other numerical techniques. The resulting statements express the exact conservation of relevant properties for each finite volume. This clear relationship between the numerical algorithm and the underlying physical conservation principle forms one of the main attractive aspects of the finite volume method and makes its concepts much simpler to understand than finite element and spectral methods.

- Discretization involves the substitution of a variety of finite-difference-type approximations for the terms in the integrated equation representing flow processes such as convection, diffusion and sources. This converts the integral equations into a system of algebraic equations.

- Solution of the algebraic equations by an iterative method.

Three mathematical concepts are useful in determining the success or otherwise of one algorithm [Versteeg and Malalasekera, 1995]:

- **Convergence**. The property of a numerical method to produce a solution which approaches the exact solution as the grid spacing, control volume size or element size is reduced to zero.

- **Consistency**. Consistent numerical schema produce systems of algebraic equations which can be demonstrated to be equivalent to the original governing equation as the grid spacing tends to zero.

- **Stability**. If a method is not stable, even roundoff errors in the initial data can cause wild oscillations or divergence.

Once a numerical problem is posed, one important thing to do is to check whether the method applied satisfies the previous criteria. The convergence of the solution is ordinarily difficult to establish. However, the consistency is straight-forward to verify and the stability is typically much easier to check. The Lax equivalence theorem [Lax and Richtmyer, 1956] states that for linear problems a necessary and sufficient condition for convergence is that the method is both consistent and stable. Hence, the convergence is usually shown via this Lax equivalence theorem.

Consequently, the general Partial Immobilization Model (Eq. (4.26)) together with initial and boundary conditions is solved in FORTRAN by the finite volume method [Patankar, 1980] for each set of valve opening. To do so, the membrane is discretized spatially uniformly into 51 points [Corriou et al., 2008] while the time step is precisely chosen according to cases. The discretization and its mathematical transformation are detailed in Appendix D. The FORTRAN code was validated by Corriou et al. [2008]. In this thesis, before any complex process simulation, the finite volume method solutions are validated by comparing to analytical solutions provided by Paul [1971] (Section 5.1.3). Furthermore, this code of finite volume method is validated again by comparing to solutions obtained from *pdepe* (Matlab) and also solutions from COMSOL in some non linear cases.

It can be noticed that according to our simulation, the spatial discretization has much a lower influence on solution convergence than the temporal discretization. For example, in order to solve correctly some stiff cases (glassy membranes or heterogeneous membranes) where the total duration is around ten seconds, 10^{-3} s is used as the time step while the membrane is always spatially discretized into 51 points in order to ensure the convergence. As a result, the small time step makes the calculation time rather long in stiff cases.

4.3 Process optimization

In order to perform comparisons to conventional processes, cyclic process performances are optimized by modifying valve opening durations. In our study, the process performance is in general represented by two or more criteria. Mathematically, this kind of multicriteria optimization problem is described by

$$\max_{x_i, i=1..k} \begin{pmatrix} \text{Criterion 1} \\ .... \\ \text{Criterion n} \end{pmatrix}$$

submitted to

$$g_j(\boldsymbol{x}) \leq 0 \qquad j = 1, m$$

Thus the process possesses k controllable valves whose openings are submitted to m constraints and n criteria are considered in optimization. To solve these multicriteria optimization problems, a genetic algorithm written in FORTRAN code is applied in our study.

Genetic algorithms belong to the larger class of Evolutionary Algorithms (EA), which generate solutions to optimization problems using techniques inspired by natural evolution, such as inheritance, mutation, selection, and crossover. Genetic algorithms are qualified as quasi-global, i.e., whole variable range is sufficiently scanned so that the global optimum can be in general expected. This latter makes the genetic algorithm an adequate tool to perform our process optimization.

The optimization problem is first arranged in the genetic proper presentation. Then the genetic algorithm proceeds by following steps:

- Initialization. 1000 variable combinations (valve opening durations, in most of our cases) are randomly generated according to a uniform distribution [Press et al., 2007] in their respective ranges in order to form an initial population.
- Selection. During each successive generation, a proportion of the existing population is selected to breed a new generation.
- Reproduction. The population of the next generation is generated from those selected in last step: such as crossover (or recombination), mutation, regrouping, colonization-extinction, or migration. In our study, only crossover (or recombination) and/or mutation are applied. These

processes ultimately result in the population of the next generation that is different from the previous generation. In general, the average fitness will have increased by reproduction, since only the best individuals from the first generation are selected for breeding, along with a small proportion of less fit solutions, for reasons such as mutation. The mutation ratio is fixed to 10% in our study.

- Termination. The generational process is repeated until a termination condition has been reached. In our study, the optimization process is terminated at the end of the 10^{th} generation. Corriou et al. [2008] confirm that the optimum can be well reached with this number of generations.

On the other hand, the uniform random value generator [Press et al., 2007] incorporated in initialization step is also applied in Sections 5.2 and 5.3 in order to obtain an overview of process performances by generating random values in a given range.

Chapter 5

Case studies

> In science, one tries to tell people, in such a way as to be understood by everyone, something that no one ever knew before. But in poetry, it's the exact opposite.
>
> Paul Dirac

In this chapter, three different cases within the frame of cyclic transient membrane gas separation processes have been investigated in detail by simulation and optimization: short class processes based on rubbery membranes and heterogeneous membranes and a long class process. Each case study is systematically followed by a comparison to conventional processes under similar operation conditions. First, based on some gas pairs with industrial interests through rubbery polymers, a process of Paul's type but more realistic is analyzed. In this way, the short class processes are reassessed, their pros & cons have been highlighted and compared to those indicated in literature. This latter constituted the second part of the publication in *Journal of Membrane Science* [Wang et al., 2011a]. Then, a novel cyclic process, designed to improve the short class process performance by means of Mixed Matrix Membranes, is investigated based on experimental data. This study led to a submitted publication in *AIChE Journal* [Wang et al., 2012 (Submitted]. Moreover, another novel cyclic process design [Wang et al., 2011b] classified as a long class process is introduced as an example of long class cyclic process. By way of optimizations according to different criteria, its great advantages with respect to conventional steady-state operations have been highlighted. Finally, it should be noticed that for the three case studies, the membrane module is always the same: a hollow fiber module.

5.1 Short class processes based on rubbery polymers

Through the inventory in Section 3.5 and a verification in Polymer Handbook [Brandrup and Immergut, 1989], three different binary gas mixtures are selected and verified (Tabs. 5.1, 5.2 and 5.3) as interesting gas mixtures for short class processes. These gas mixtures present the following properties:

Usage: Helium recovery $\alpha = 1.03$			
Gas	$\mathcal{P}\times 10^{15}$	$\mathcal{D}\times 10^{10}$	$k_D\times 10^{6}$
He	175	41	0.424
N_2	170	8.5	2.0

Table 5.1: Mass transport parameters from Polymer Handbook [Brandrup and Immergut, 1989]. Poly(oxydimethylsilylene) with 10% filler Scantocel CS, vulcanized silicon rubber. (S.I. units)

Usage: Rare gas separation $\alpha = 109.22$			
Gas	$\mathcal{P}\times 10^{15}$	$\mathcal{D}\times 10^{10}$	$k_D\times 10^{6}$
He	2.37	3.1	0.077
Ar	0.0217	0.0024	0.79

Table 5.2: Mass transport parameters from Polymer Handbook [Brandrup and Immergut, 1989]. Poly(oxyethyleneoxytenephthaloyl), amorphous (VI/443). (S.I. units) It can be noticed that the permeability value of Ar (0.0217 10^{-15}) given by Polymer Handbook [Brandrup and Immergut, 1989] is not the same as the product (0.0189 10^{-15}) of the diffusion coefficient and the sorption coefficient. In following simulation study, the value (0.0217 10^{-15}) is used as the permeability of Ar in order to determine the performance of steady-state operations.

- Tab. 5.1 shows a very interesting case demonstrating the advantage of cyclic transient operations. The two gaseous components are difficult to separate by a steady-state operation. However, according to conclusions obtained from Chapter 3, a significant separation is expected for this process. It can be noticed that the gas mixtures {He,N_2} can also be efficiently separated with glassy membranes. For example, the selectivity for {He,N_2} is reported as 330 in the case of a poly(vinylidene chloride) (Saran) membrane [Brandrup and Immergut, 1989].
- Rare gaseous components are usually used with a rather high purity.

Usage: Hydrogen purification $\alpha = 1.90$			
Gas	$\mathcal{P}\times\ 10^{15}$	$\mathcal{D}\times\ 10^{10}$	$k_D\times\ 10^{6}$
H_2	5.43	1.52	0.355
C_3H_8	10.3	0.0224	46.4

Table 5.3: Mass transport parameters from Polymer Handbook [Brandrup and Immergut, 1989]. Poly(ethylene-co-propylene-co-diene),Poly(isobutene-co-isoprene) 98/2 (Butyl rubber). (S.I. units)

The gaseous components of Tab. 5.2 can be well separated by a steady-state operation, while a better selectivity is expected in case of short class processes.

- Separation of the gaseous components from Tab. 5.3 is not significant according to their permeabilities $\mathcal{P}$. However, with short class processes, these gaseous components are not only easy to separate, but a reverse selectivity is also expected.

5.1.1 Process description

A design (Fig. 5.1) similar to Paul's one is simulated and then numerically optimized in this thesis. The apparatus is globally the same as Paul's one, whereas it is important to notice three different points between the studied process and Paul's process.

1. Instead of the plate sheets module proposed by Paul, a hollow fiber module is considered (Fig. 5.1).

2. Instead of imposing upstream/downstream composition and pressure, both exhaustion in upstream and accumulation in downstream are taken into account. The permeate accumulated in the downstream part of the module will be transported to the downstream tanks by opening the valves C1 or C2. The exhausted upstream gases will be transported to the upstream tank by opening the valve B.

3. All valves are independent instead of synchronous operations. As a result, the component with larger diffusion coefficient is preferentially accumulated in the downstream tank 1 (Fig. 5.1) corresponding to the left receiver tank of Paul's process (Fig. 3.4). The downstream tank 2, in which the separation is less significant [Paul, 1971] could also have been considered. Nevertheless, this possibility has not been taken into account for sake of simplicity. The enrichment in the component with the

larger diffusion coefficient will thus be the only target of the simulation and optimization study.

The length of the hollow fiber module is 1 m and the internal fiber diameter is fixed to 50 μm. The gas mixture flows into the hollow fibers which thus represent the upstream volume so that the total free space between fibers corresponds to the downstream volume. This membrane geometry enables a large specific interfacial area (Chapter 2). This value can reach some thousands of m^{-1} [Baker, 2002], and a relative high production is thus expected.

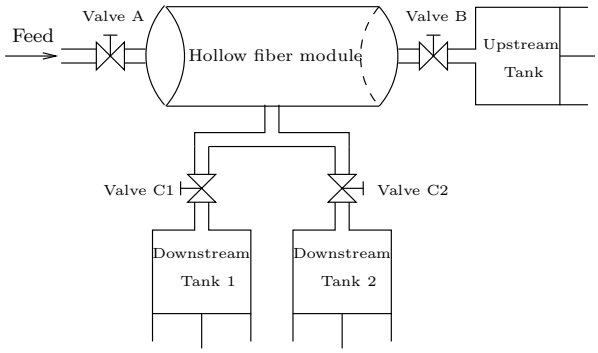

Figure 5.1: Design of the model of a short class process

5.1.2 Mathematical descriptions

The transfer phenomena in rubbery membranes is modeled by the Dual Mode Sorption theory with $K = 0$ (Section 4.2.2). Necessary assumptions (Section 4.2.2) are considered for the transport model. The operation of the valves is asynchronous, like in Corriou's simulation [Corriou et al., 2008]; the opening durations of the upstream left, upstream right, downstream left and downstream right of the valves of the process (Fig. 3.4) are noted respectively as x_1, x_2, x_3 and x_4. These are variables of an optimization problem and submitted to two constraints: $x_1 + x_2 = x_3 + x_4$ and $x_1 + x_2 \leq 100s$, the latter value representing a large bound for a cycle.

The performance of a separation process is represented by two factors, separation factor and productivity. Assuming that component 1 is the desired component, the separation factor is defined as

$$\text{separation factor} = \frac{y_1^{d,\mathcal{L}}}{1 - y_1^{d,\mathcal{L}}} \frac{1 - y_1^f}{y_1^f} \tag{5.1}$$

where $y_1^{d,\mathcal{L}}$ is the mole fraction of component 1 in the downstream tank 1 (Fig. 5.1) in which the desired component is expected to be enriched [Paul, 1971], and y_1^f the mole fraction of the same component in the feed flow. The productivity is defined as the number of moles of the desired component 1 that are collected in the downstream tank 1 divided by the total duration of operation and by the surface area of the membrane offered to transfer

$$\text{productivity (mol/m}^2\text{.s)} = \frac{n_1^{d,\mathcal{L}}}{A\Delta t} \tag{5.2}$$

For the simulation, an equimolar binary mixture is considered for separation and the objective is to obtain one gaseous component with a good separation factor and productivity by means of short class processes.

Consequently, the optimization problem with respect to separation factor and productivity in the gas receiver is set as follows

$$\max_{x_1,x_2,x_3} \begin{pmatrix} \text{separation factor} \\ \text{productivity} \end{pmatrix}$$

submitted to

$$\begin{gathered} x_1 + x_2 = x_3 + x_4 \\ x_1 + x_2 \leq 100\text{s} \end{gathered}$$

To solve this multicriteria optimization problem of two objective functions and three variables, the model together with the initial and boundary conditions is solved by the finite volume method (Section 4.2.3) for each set of values $(x_i,\ i = 1, ..., 4)$. With respect to membrane thickness, Paul's conclusion [Paul, 1971] is used here: the total cycle duration τ can be expressed as a function of the membrane thickness L and the lowest diffusion coefficient $\mathcal{D}_k$ of the gas mixture

$$\tau = U\frac{L^2}{6\mathcal{D}_k} \tag{5.3}$$

According to Paul [1971], the optimum separation effect is observed at $U = 3$ assuming that the fraction of period ω when the upstream pressure is high is fixed to 10%.

According to a tube filling modeling, the fibers can be filled from vacuum to 1 atm in less than 0.22 second (Appendix C). Thus, the upstream side of the module can be considered as instantaneously uniform at a given pressure once the valve A is opened. It is important to stress at this stage that care should be taken to select realistic operating conditions [Corriou et al., 2008].

This point applies particularly to the minimum opening or closing time of the valves, which will remain systematically larger than 1 second [Feng et al., 2000]. It can be noticed that this minimum operating duration is considered as a global constraint in all our realistic process simulations.

Thus the membrane thickness L is judiciously chosen according to Eq. (5.3) in order to ensure that the total cycle duration τ is included in the interval [1, 100]s and that the high pressure duration is longer than 1 s.

It can be noticed that for some binary gas mixtures and a given membrane, the thickness used for short class processes is very important compared to an industrial use for gas separations; otherwise, the opening and closing of valves cannot be mastered in reality. This peculiarity could be a decisive penalty for short class processes and will be discussed.

The conditions of simulation are the same for three binary gas mixtures except the membrane material and its thickness (Tab. 5.4). The performance of the steady-state operations is estimated by considering a cross flow model.

Membrane surface	10^3	m^2
Temperature	297.15	K
High upstream pressure	$1.013\ 10^5$	Pa
Initial downstream pressure	0	Pa
Upstream and downstream volume	0.0125	m^3
Left downstream tank volume	0.0125	m^3
Right downstream tank volume	0.0125	m^3

Table 5.4: Simulation conditions of a short class process.

5.1.3 Numerical solution validation

As mentioned in Section 4.2.3, all process models are in general solved by the finite volume method which is numerical. Thus in the first step, its solution in simple conditions is compared to well-known analytical solutions in order to validate the solution algorithm.

Paul [1971] solved analytically synchronous operations by assuming no accumulation in downstream and no exhaustion in upstream. By providing valve operations, mole fractions of each gas in each tank can be obtained. The same scenarios can be solved by the finite volume method. Gas transport parameters for the test pair $\{O_2, CO_2\}$ are given in Tab. 5.5. Synchronous valve operations are defined by Eq. (5.3): the fraction of period ω when the upstream pressure is high is fixed to 10%, then the total cycle duration τ is obtained by assigning U.

$\alpha = 5.81$			
Gas	$\mathcal{P}\times\ 10^{18}$	$\mathcal{D}\times\ 10^{10}$	$k_D\times\ 10^{6}$
O_2	7.189	0.079	0.91
CO_2	41.8	0.02	20.9

Table 5.5: Mass transport parameters from Polymer Handbook [Brandrup and Immergut, 1989]. Poly(vinyl-benzoate). (S.I. units)

In Tab. 5.6, the simulated O_2 mole fractions in downstream tank 1 (Fig. 3.4) with different valve opening conditions U are compared where the relative error is defined by the absolute value of the difference divided by the solution obtained analytically. The low value of relative error allows to validate our finite volume method and it will be used further in more complex models. It can also be noticed that the maximum mole fraction of O_2 among tested scenarios is indeed obtained at $U = 3$, Paul's conclusion is roughly confirmed.

	U=2	U=3	U=4	U=5
Analytical	0.4895	0.7941	0.7608	0.6554
Finite volume method	0.5003	0.7831	0.7616	0.6559
Relative error	2.2%	1.4%	0.1%	<0.1%

Table 5.6: Comparison of O_2 mole fraction in downstream tank 1 between analytical solutions provided by Paul [1971] and numerical solutions obtained according to finite volume method. O_2 feed mole fraction : 0.5.

5.1.4 Results & discussions

It should be first noticed that all performances for steady operations are obtained based on a pressure ratio Ψ permeate/retentate = 0.01 (retentate pressure = 1.013 10^5 Pa) and the cross flow pattern. The stage cut ζ varies in order to obtained a performance curve. Other design factors which do not influence the productivity and the separation factor are not taken into account, such as the package density.

The comparison of the separation performances on the gas mixture {He,N_2} is shown in Fig. 5.2. The separation factor and the productivity are calculated with respect to He. A mixture of nearly inseparable gaseous components is successfully separated by steady-state operation, thus showing a spectacular improvement in separation factor. In this way, the advantage of short class processes is again confirmed. However, in the case of a high separation factor, the productivity loss is also remarkable. This is consistent

with conclusions in literature (Chapter 3).

The comparison of the separation performances on the gas mixture {He,Ar} is shown in Fig. 5.3. The separation factor and the productivity are calculated with respect to He. Fig. 5.3 shows that when the ratio $\frac{\alpha_{\mathcal{P}}}{\alpha}$ is much larger than 1, the separation performance can be enhanced with respect to a steady-state operation even if the steady-state operation can already provide a good separation factor. This can be especially useful for purification of rare gaseous components. A very high separation factor improvement is again observed.

The productivity defined by Eq. (5.2) is a production per effective membrane surface. In the case of the cyclic processes, the gas composition along the fibers is uniform and only permeation occurs, thus a uniform productivity defined by Eq. (5.2) is observed along the fibers (Fig. 5.4). Therefore, it is logical that the selectivity decreases with the productivity increase. This trade-off is observed consistently in Fig. 5.3.

The situation is complicated for the cross flow operation at steady-state, in which the gas flux is directed along the fibers (Fig. 5.4) whereas the permeation direction is perpendicular to the gas flux direction. As a result, the productivity is a non linear decreasing function of the fiber length from the input feed point to the output feed point, so is the selectivity. Thus the maximum productivity per effective membrane surface and the maximum selectivity are obtained under the same conditions (Fig. 5.4). However, it is important to notice that these maximum performances can only be obtained for an effective membrane surface tending to zero. It results that the global maximum productivity cannot be achieved with the global maximum selectivity.

As a result, the productivity comparison between steady-state operations and cyclic processes is delicate. Nevertheless, in Fig. 5.3, productivities of steady-state operations are in general larger than those of cyclic processes. Consequently, despite comparison difficulties, a low productivity is still highlighted as the major drawback of cyclic processes.

A comparison of the separation performances of the gas mixture $\{H_2,C_3H_8\}$ is shown in Fig. 5.5. The separation factor and the productivity are calculated with respect to H_2. With regard to the values of $\mathcal{P}$, the steady-state operation is poorly selective, even more, the separation factor with respect to H_2 is lower than 1. In Fig. 5.5, the performance of the steady-state operation is not observed as the figure starts from a separation factor equal to 1. However, a reversed and enhanced separation factor of the gas pair $\{H_2,C_3H_8\}$ is observed in case of a short class process, which is predicted by the inventory.

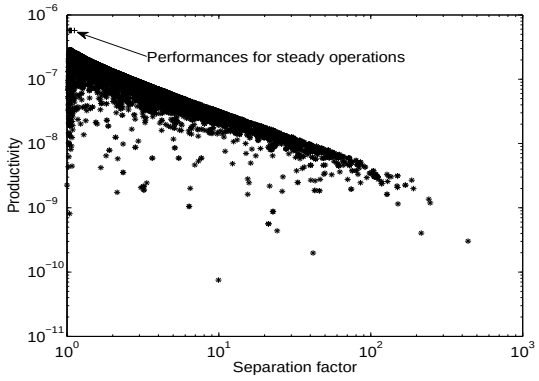

Figure 5.2: Comparison of separation performances for steady-state operations(+) and a short class process (*), with a {He,N_2} mixture. Test conditions in Tab. 5.4 and transport parameters in Tab. 5.1 for a membrane of 300 μm.

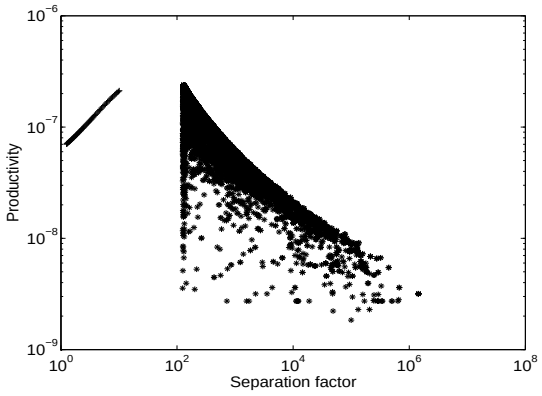

Figure 5.3: Comparison of separation performances for steady-state operations(+) and a short class process (*), with a {He,Ar} mixture. Test conditions in Tab. 5.4 and transport parameters in Tab. 5.2 for a membrane of 5 μm.

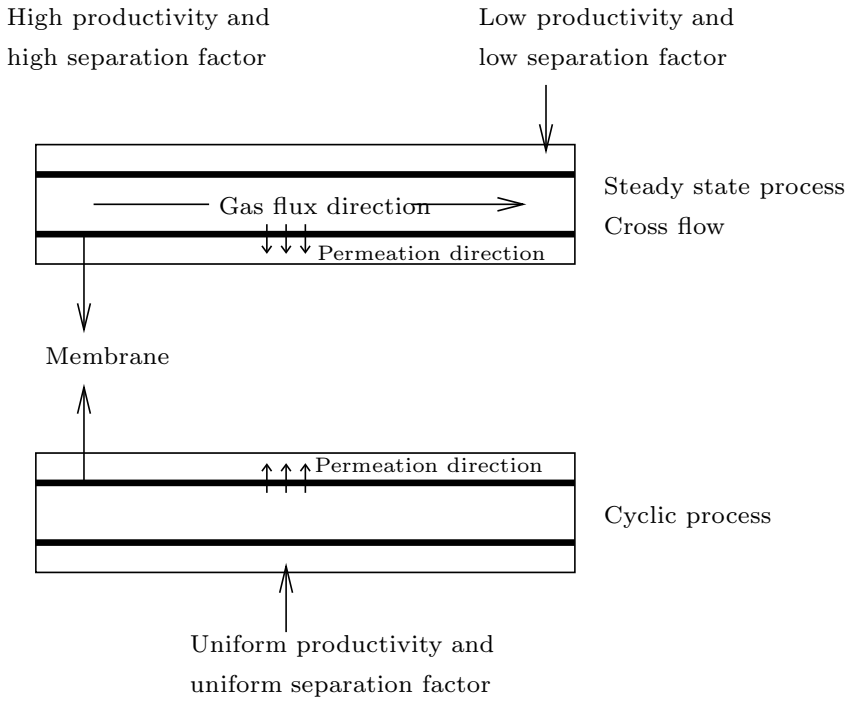

Figure 5.4: The performances of the steady-state operation in cross flow are not uniform along the fibers, whereas those of the cyclic process are.

5.1.5 Purification of uranium

Higuchi and Nakagawa [1989] mention that short class processes can provide an improved selectivity in the field of concentration of uranium 235 from natural uranium compared to a steady-state operation. Uranium gas mixtures are an expensive resource. Consequently, a recycling is necessary and the selectivity gain might make it possible to decrease recycling times to reach the same purity set point. However, this application is not selected as a potentially interesting binary gas mixture through our inventory since their ratio $\frac{\alpha_{\mathcal{D}}}{\alpha}$ is equal to 1. Nevertheless, this special case is also simulated here. The mass transport parameters of uranium 235 hexafluoride and uranium 238 hexafluoride are given in Tab. 5.7. The comparison of the separation performances on the gas mixture $\{^{235}UF_6, ^{238}UF_6\}$ is shown in Fig. 5.6; the separation factor and the productivity are calculated with respect to $^{235}UF_6$. Although the separation factor is still rather low, an enhancement compared to steady-state operation is observed. However, the productivity loss should be seriously taken into account.

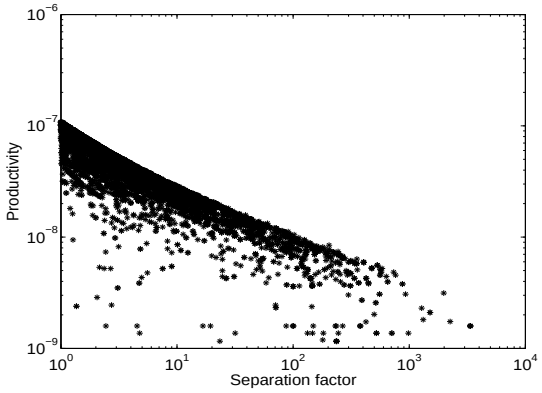

Figure 5.5: Separation performances for a short class process (*), with a $\{H_2,C_3H_8\}$ mixture. Test conditions in Tab. 5.4 and transport parameters in Tab. 5.3 for a membrane of 15 μm. In this case, the steady-state separation factor is always lower than 1 and the corresponding points are not represented in this figure.

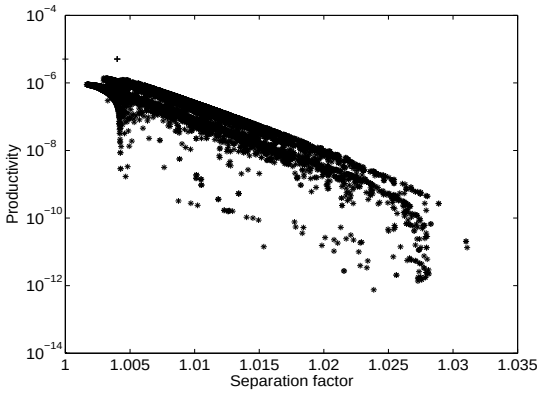

Figure 5.6: Comparison of separation performances for steady-state operations(+) and a short class process (*) with a UF_6 mixture. Test conditions in Tab. 5.7 for a membrane of 2 mm.

Usage: Uranium 235 concentration			
Gas	$\mathcal{P}\times 10^{15}$	$\mathcal{D}\times 10^{10}$	$\mathcal{S}\times 10^{6}$
$^{235}UF_6$	1.00429	10.0429	1.0
$^{238}UF_6$	1.0	10.0	1.0

Table 5.7: Mass transport parameters from Higuchi and Nakagawa [1989]. (S.I. units)

5.1.6 Upstream exhaustion study for short class processes

Even if the upstream exhaustion is taken into in our simulation, it is not significantly observed under our simulation conditions. It should be noticed that low upstream exhaustion highly limits industrial applications of cyclic processes.

Consider a plane membrane of thickness L, initial upstream pressure P^0 and downstream pressure 0. The mass transfer is assumed to be one dimensional. Presuming that the permeate is enriched in the component k by a short class process, the exhaustion of component k in the upstream side will symmetrically be larger than for the other component. For a duration lower than the time-lag, the molar flow rate entering downstream volume of the component k is given by

$$\frac{dn_k^{\text{in}}}{dt} = -\mathcal{D}_k \left.\frac{\partial C_k}{\partial z}\right|_L A \tag{5.4}$$

where $\mathcal{D}_k$ is the diffusion coefficient, C_k is the gas concentration in the membrane and z is the position in the membrane. As the behavior of the membrane can be modeled by Fick's law for each component, the following inequality is always valid

$$-\left.\frac{\partial C_k}{\partial z}\right|_L \leq \frac{C_k^0}{L} \tag{5.5}$$

Here, C_k^0 is the initial upstream boundary concentration of the membrane which is determined by Henry's law

$$C_k^0 = \mathcal{S}_k P_k^0 \tag{5.6}$$

where $\mathcal{S}_k$ is the sorption coefficient. Thus

$$\frac{dn_k^{\text{in}}}{dt} \leq \mathcal{D}_k \frac{C_k^0}{L} A = \mathcal{P}_k \frac{P_k^0}{L} A \tag{5.7}$$

where $\mathcal{P}_k$ is the permeability equal to $\mathcal{D}_k\mathcal{S}_k$ according to the solution-diffusion mechanism.

As the duration of the high-pressure stage of a cycle should be lower than the time-lag of the gas with lower diffusion coefficient, the time-lag can be considered as an upper bound of the duration of the high-pressure stage

$$\Delta t_{HP\max} = \frac{L^2}{6\mathcal{D}_{\text{slow}}} \tag{5.8}$$

It should be noticed that the diffusion coefficient $\mathcal{D}_{\text{slow}}$ is lower than the diffusion coefficient $\mathcal{D}_k$ of the component k. The initial gas quantity n_k^0 in the upstream volume is given by the ideal gas law

$$n_k^0 = \frac{P_k^0 V}{RT_K} \tag{5.9}$$

The upper bound of the gas concentration in the membrane is $C_k^0 = \mathcal{S}_k P_k^0$ and the occupied membrane volume is $V^{\text{membrane}} = A\,L$. During permeation, part of the gas stays in the membrane, this gas quantity can be upper bounded as

$$n_k^{\text{membrane}} < C_k^0 V^{\text{membrane}} = \mathcal{S}_k P_k^0 A\,L \tag{5.10}$$

Thus, the exhaustion ratio Θ_k of the component k can be defined as the ratio of the quantity of exiting gas from the upstream volume dn_k^{out} over the initial gas quantity in the upstream volume for a cycle

$$\Theta_k = \frac{\displaystyle\int_0^{t\text{end}} \left(\frac{dn_k^{\text{out}}}{dt}\right) dt}{n_k^0} \tag{5.11}$$

By combining Eqs. (5.7 - 5.11), an upper bound of the exhaustion ratio Θ_k is obtained

$$\begin{aligned}\Theta_k &= \frac{\displaystyle\int_0^{t\text{end}} \left(\frac{dn_k^{\text{in}}}{dt}\right) dt + n_k^{\text{membrane}}}{n_k^0} \\ &< \frac{\left(\mathcal{P}_k \dfrac{P_k^0}{L} A\right) \dfrac{L^2}{6\mathcal{D}_{\text{slow}}} + \mathcal{S}^l P_k^0 AL}{\dfrac{P_k^0 V}{RT_K}} = \frac{ALRT}{V}\left(\frac{\mathcal{P}_k}{6\mathcal{D}_{\text{slow}}} + \mathcal{S}_k\right)\end{aligned} \tag{5.12}$$

With the exception of some cases, the magnitudes of previous parameters are given in Tab. 5.8.

A	L	$\mathcal{P}_k$	$\mathcal{D}_{\text{slow}}$	$\mathcal{S}_k$
10^3 - 10^4	10^{-5}	10^{-20} - 10^{-16}	10^{-12}	10^{-6}

Table 5.8: Magnitudes of parameters for membrane gas separation processes (S.I. units)

V is assumed to be 1 m^3 as a reference. The numerical application of Eq. (5.12) is performed by taking into account the boundary values yielding the following upper bound of Θ_k

$$\Theta_k < 0.1\% \tag{5.13}$$

It is remarkable that this value is obtained by taking into account all "extreme" values leading to an exhaustion, thus the real exhaustion would be definitely lower than 0.1%. This result suggests that the short class process cannot really separate a mixture, but only extract some of the rapid component with a high purity from the gas mixture compared to a steady-state operation. In other words, the stage cut defined as the ratio of the permeate flow over the feed flow is necessarily very low. This point is interesting because it validates a constant upstream composition corresponding to a boundary condition in Paul's analysis. Unfortunately, this particularity indicates that the effective productivity of this process is necessarily very low, i.e., the ratio of the feed mixture which is effectively separated by the membrane.

5.1.7 Conclusion for short class processes based on rubbery membranes

In general, for the tested gas mixture and the corresponding membrane, the productivity is less sensitive than the separation factor with respect to valve operations. However the productivity is generally rather low, lower than 10^{-6} $mol.m^{-2}.s^{-1}$. Although the hollow fiber modules which provide the largest specific surface compared to other modules are used, it is still very difficult to reach a commonly acceptable productivity in industry where a usual production of gas separation by membrane makes use of hundreds of modules [Baker, 2002]. To achieve this value, the contact membrane surface should be larger than 10^8 m^2 according to our simulation.

On the other hand, the upstream exhaustion study suggests that first there is no composition change in retentate which is an important drawback with respect to conventional processes. Secondly, such cyclic processes are probably not suitable for a large production requirement, the low exhaustion ratio clearly limits the use of short class processes.

It is also important to notice that the process performance is calculated based on a predefined membrane thickness. Consequently, the productivity is estimated for the same membrane thickness for both processes. As previously explained, for short class processes, the membrane thickness is usually rather important in order to make the valves opening controllable with respect to frequency. On the other hand, for steady-state operations, the productivity is inversely proportional to the membrane thickness, thus this latter is usually minimized in order to increase the productivity [Koros and Fleming, 1993]. Consequently, for an appreciable steady-state operation, the industrial production is a hundred or even a thousand times larger than our estimations with the proposed process. For example, according to our simulation/optimization, for the concentration of uranium 235, the membrane thickness should be around 2 mm to perform a realizable valve operation (opening time included in [1, 100]s). For a steady-state operation, the applied membrane thickness should be only about one thousandth of this value.

Nevertheless, with respect to the rare gases concentration, both gaseous components are valuable and a recycling operation is usually needed. In that case, short class processes might still be an interesting choice.

5.2 Short class processes based on Mixed Matrix Membranes

As a process enhancement, two important drawbacks of classical short class process (designed by Paul) using rubbery membranes have been highlighted in our review (Chapter 3) and confirmed by some numerical case studies in Section 5.1: no composition change in retentate and very low permeate flux. Furthermore, both drawbacks can be explained by the low difference between time-lags of gas mixture. If this difference can be some orders of magnitudes, the drawbacks might be lowered even eliminated.

As mentioned in chapter 4, Paul [1969] reported that in a rubbery membrane containing adsorptive fillers, the time-lag of the more adsorbable gas in this Mixed Matrix Membrane is largely increased with respect to that of the same gas in the ordinary pure rubbery membrane. At the same time, the time-lag of the less adsorbable one can be kept at a low value. Consequently, in this section, the short class process is performed on a Mixed Matrix Membrane in order to reduce these classical drawbacks.

5.2.1 Diffusion model

As mentioned in Section 4.1.2, in the case of a gas mixture, a competitive term will appear in the Langmuir population. Nevertheless, it is particularly interesting to investigate the case where only one gas in a binary mixture can be adsorbed significantly, while the adsorption of the other gas can be neglected. It results that the time-lag of one gas is largely increased while the other one does not change. In other terms, the difference of permeation rates at transient stage is amplified so that the interest of the short class process is also expected to be increased [Wang et al., 2011a]. Therefore, a binary gas mixture in which only one component is strongly influenced by the adsorption is studied in this thesis. Thus Eq. (4.9) is sufficient to correctly describe the sorption behavior for one gas of a binary mixture as the competitive term is neglected. For the other gas whole adsorption effect is neglected, the sorption is given by Henry's law taking into account the fraction of the dispersed phase

$$C = v_p k_D P \tag{5.14}$$

Consequently, considering assumptions discussed in Section 4.1.2, it results that the behavior of a hollow fiber membrane can be modeled by one dimensional Fick's law in a radial coordinate system, for the gas whose adsorption is significant

$$\frac{\partial (C_D + C_H)}{\partial t} = \frac{1}{r} \mathcal{D}_m \frac{\partial}{\partial r} \left(r \frac{\partial C_D}{\partial r} \right) \tag{5.15}$$

and for the gas whose adsorption is neglected

$$\frac{\partial C}{\partial t} = \frac{1}{r}\mathcal{D}_m \frac{\partial}{\partial r}\left(r\frac{\partial C}{\partial r}\right) \tag{5.16}$$

where $\mathcal{D}_m$ is the effective diffusion coefficient due to the phase mixture and r the radial position in the membrane. The effective diffusion coefficient $\mathcal{D}_m$ can be measured directly or determined from the diffusion coefficient of the homogeneous rubbery polymer by some correlations. Paul suggests that Higuchi [1958] correlation gives the best agreement to his experimental results

$$\begin{aligned} &\frac{1}{\kappa} = \frac{2(2+v_d) - K_H(1-v_d)}{2+K_H} \quad \text{with} \quad K_H = 0.78 \\ &\mathcal{D}_m = \kappa\mathcal{D} \end{aligned} \tag{5.17}$$

where κ is a structural factor that accounts for the geometric obstruction by the impermeable filler.

Paul and Kemp [1973] indicate that through their experiments, the time-lag increase is obviously observed for CO_2, but not for He. The adsorptive fillers only influence the diffusion of CO_2. Consequently, since the adsorption coefficient of He is considered as null in our simulation, its diffusion behavior is described by Eq. (5.16). On the other hand, as there is no competitive term related to He for the second gas CO_2, the latter's diffusion behavior is governed by Eq. (5.15).

	C'_H	b	$k_D \times 10^3$	$\mathcal{D} \times 10^9$
	$cm^3(STP)/cm^3$	$(cmHg)^{-1}$	$cm^3(STP)/cm^3.cmHg$	m^2/s
CO_2	102.6	0.0928	14.5	2.14
He	-	-	0.582	7.86

Table 5.9: Transport parameters in RTV-602 Silicone Rubber with 21.6 vol.% of zeolites according to Paul and Kemp [1973].

All transport parameters of measured gaseous components are listed in Tab. 5.9. It can be noticed that for conventional processes, CO_2 is the rapid gas, and will be enriched in permeate while the slow gas He will be enriched in retentate. The steady-state selectivity α is thus calculated as

$$\alpha = \frac{(k_D\mathcal{D}_m)_{CO_2}}{(k_D\mathcal{D}_m)_{He}} = \frac{(k_D\mathcal{D})_{CO_2}}{(k_D\mathcal{D})_{He}} = 6.78 \tag{5.18}$$

This ratio value of 6.78 suggests that the chosen rubbery membrane cannot provide an efficient separation for the binary gas mixture CO_2/He using a conventional process under steady-state conditions.

5.2.2 Process description

Based on the idea of short class process, a realistic process based on Mixed Matrix Membranes is proposed and studied in this thesis (Fig. 5.7). The membrane is installed in a hollow fiber module which is connected to three tanks via several valves. The valve A is connected to the feed reserve. Each tank has its own vacuum pump which allows to transport the contents in the module to the given tank or empty the corresponding volume of the module by opening or closing respective valves. All valves are initially closed. The hollow fiber module is initially emptied as well as all tanks. Then the process is performed by 4 stages (Tab. 5.10).

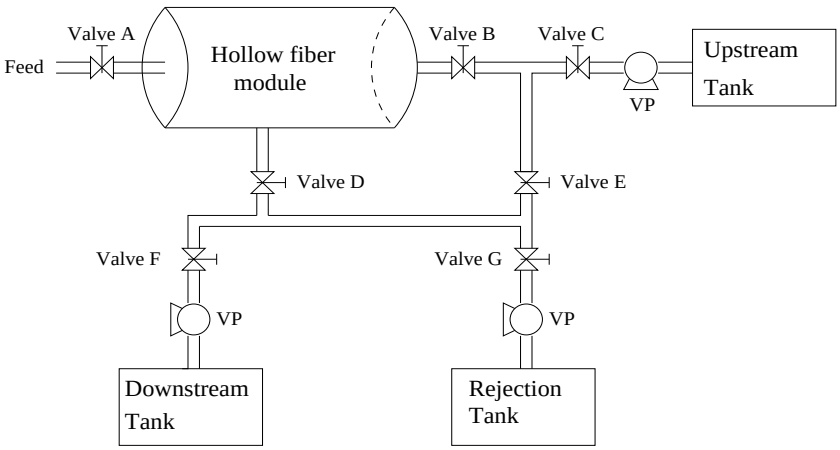

Figure 5.7: Simplified design of the short class cyclic process dedicated to Mixed Matrix Membranes. (VP = Vacuum Pump)

1. Feed stage. By opening the valve A, the internal volume of the fibers which is denoted as the upstream volume is fed up to a given pressure by the feed flux of gas mixture. In this stage, the gas diffuses towards the external volume of the fibers which is denoted as downstream.

2. Free diffusion stage. All valves are closed. The gas in upstream volume diffuses freely towards the downstream due to the pressure difference.

3. Reception stage. Valves B, C, D and F are opened whereas A, E and G are closed, thus the permeate in the downstream volume of the module is transported to the downstream tank while the upstream volume of the module is transported to the upstream tank.

4. Regeneration stage. Valves B, D, E and G are opened whereas A, C and F are closed. The whole module is thus emptied. All residual upstream

and downstream contents are transported to the reject tank. Once this step is finished, all valves are closed again and a new cycle will start by repeating Feed stage.

Valve	A	B	C	D	E	F	G
Feed stage	o	-	-	-	-	-	-
Free diffusion stage	-	-	-	-	-	-	-
Reception stage	-	o	o	o	-	o	-
Regeneration stage	-	o	-	o	o	-	o

Table 5.10: Cyclic operations of process design of Fig. 5.7. ('o' for open and '-' for closed.)

By an analogy to short class cyclic process concept (Fig. 5.1) , for the gas pair {He, CH_4} a purified gas enriched in He whose diffusion coefficient $\mathcal{D}$ is larger is expected to be collected in the downstream tank. However, in this thesis, the gas compositions in upstream tank and rejection tank are also discussed.

The length of the hollow fiber module is 1 m and the fiber internal diameter R_i is fixed to 200 μm and the operation is considered as isothermal. Therefore, Eqs. (5.15) and (5.16) with boundary conditions (defined by valve operations, Tab. 5.10) are solved by the finite volume method explained in Section 4.2.3.

5.2.3 Numerical method validation

The numerical procedure is validated first by a comparison to the numerical solutions from Comsol using the finite element method and from Matlab using the method of lines where only the spatial derivations are discretized resulting in a set of ordinary differential equations.

In this validation, CO_2 transport in a polyimide membrane is considered [Thundyil et al., 1999]. Using each numerical method, the concentration evolution of CO_2 in a polyimide membrane of 1 μm in a time-lag measurement experiment is calculated. The transport parameters of CO_2 in the polyimide membrane are given in Tab. 5.11. Fig. 5.8 shows that the difference between three methods are somehow visible at a short time. While $t > 0.2$s, the difference becomes invisible.

In order to quantify the deviance, a called normalized error δ is defined as

$$\delta = \left| \frac{C(x,t)_{M1} - C(x,t)_{M2}}{C(0,t)} \right| /100 \tag{5.19}$$

k_D $\mathrm{cm^3(STP)/cm^3\ psia}$	b $\mathrm{psia^{-1}}$	C_H' $\mathrm{cm^3(STP)/cm^3}$	$\mathcal{D}$ $\times 10^{-9}\ \mathrm{cm^2/s}$
0.1343	0.0732	33.4	22.90

Table 5.11: CO_2 transport parameters for a polyimide membrane at 35°C, according to Thundyil et al. [1999]

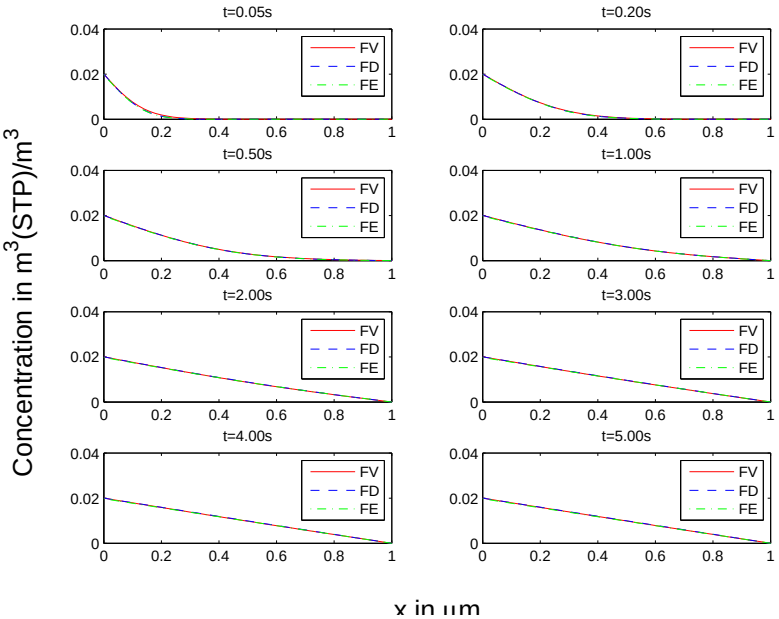

Figure 5.8: Comparison between solved results from three numerical methods. FV : finite volume method. FD: finite difference method. FE: finite element method

where M indicates the used method. Consequently, the method deviance at $t = 0.20$s is quantified in Fig. 5.9.

In Fig. 5.9, it shows that even in the case of the maximum deviance ($t = 0.20$s), the normalized error between the finite volume method and two other classical methods are less than 3.5%. The excellent agreement of the solutions of the three methods validates our numerical solution. Secondly, numerical time-lag predictions are validated by an available analytical prediction proposed by Paul and Kemp [1973]. When the integration time step is decreased to less than 0.001s, the deviation variation is negligible (relative error < 0.0001) while the calculation time increases significantly as mentioned in Section 4.2.3. On the other hand, the spatial discretization in the membrane has less influence on the solution. Consequently, the integration time

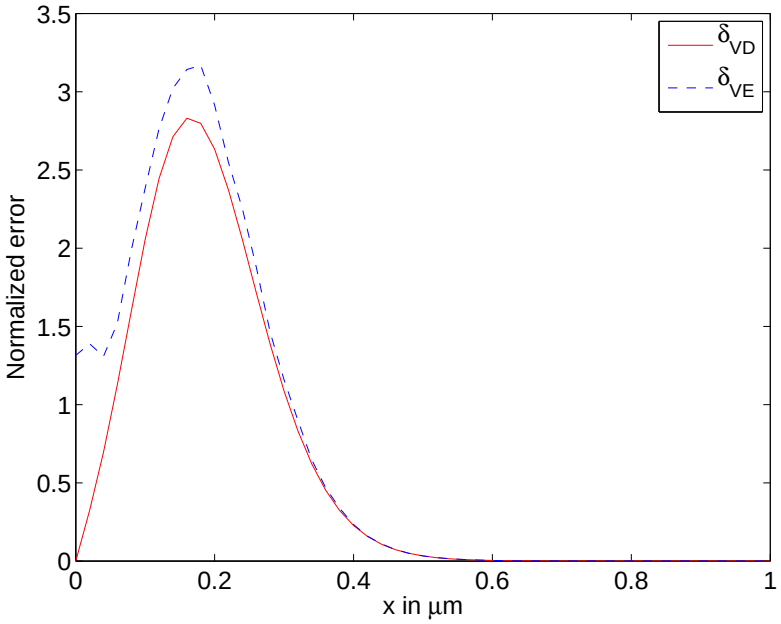

Figure 5.9: Normalized error for three numerical methods. δ_{VD} refers to the normalized error between the finite volume method and the finite difference method. δ_{VE} refers to the normalized error between the finite volume method and the finite element method.

step is chosen as 0.01s and 51 points are chosen for spatial discretization in the membrane.

The operating conditions are given in Tab. 5.12. It can be noticed that the feed flow pressure and the membrane thickness are not mentioned in Tab. 5.12 and will be discussed later.

5.2.4 Operating conditions

Before simulating the whole process, a preliminary study of the feed flow pressure and the membrane thickness is performed, in order to identify the adequate operating conditions.

5.2.4.1 Feed flow pressure

In reality, it is convenient to perform the gas separation at a sufficiently high pressure in order to avoid operating problems such as sealing and to improve the global productivity. However, Paul and Kemp [1973] indicate that the

Number of modules	1	
Length of the module	1	m
Membrane specific surface	10^3	m^2/m^2
Temperature	303.15	K
Gas composition in the feed flow	1:1	
Initial downstream pressure	0	Pa
Upstream and downstream volume in the module	0.0125	m^3
Upstream tank volume	1	m^3
Downstream tank volume	1	m^3
Reject tank volume	1	m^3
Integration time step	0.01	s
Number of discretization points in the membrane	51	

Table 5.12: Simulation conditions of the cyclic process dedicated to MMM.

increase of the time-lag becomes less important when the upstream pressure becomes high. Thus, a trade-off pressure should be judiciously chosen.

The dependence of the classical time-lag [Vieth et al., 1976] θ on upstream pressure is simulated by solving the corresponding equations (Eq. (4.8)) with the initial and boundary conditions of Paul and Kemp [1973]) based on transport parameters of CO_2 (Tab. 5.9) and is shown in Fig. 5.10. The dimensionless time-lag represented in Fig. 5.10 is defined as θ/θ_0 where θ_0 is the time-lag in the heterogeneous membrane at infinitely high pressure.

Fig. 5.10 highlights the fact that the time-lag of the same gas in the heterogeneous membrane can be largely increased compared to that in the ordinary rubbery membrane. At a low upstream pressure, the dimensionless time-lag can reach 185. Nevertheless, it decreases when the upstream pressure becomes large. Thus it results that the operating high pressure of the cyclic process should be low enough to obtain sufficiently long time-lags. For the concerned gas, the maximum time-lag can only be obtained at very low upstream pressure ($\approx$ 100 - 1000 Pa) which cannot be performed in reality. Consequently, taking into account the practical operation difficulties and the conclusion deduced from Fig.5.10, the total upstream pressure is fixed at 1 bar for all simulations as a trade-off value, so that the initial partial pressure of CO_2 is 0.5 bar and in those conditions, the time-lag in the heterogeneous membrane can be deduced

$$\frac{\theta}{\theta_0} = 73 \tag{5.20}$$

thus a significantly increased time-lag of CO_2 can be expected. On the other hand, the time-lag of He does not depend on its upstream pressure.

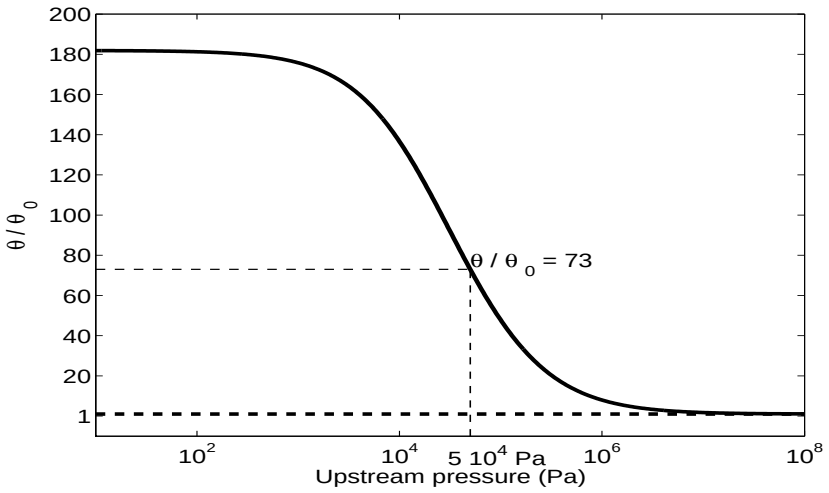

Figure 5.10: Dimensionless time-lag of CO_2 in the heterogeneous membrane Dimensionless time-lag of CO_2 as a pure gas in the heterogeneous membrane with respect to its upstream pressure.

5.2.4.2 Feed step duration

Similar to the short class process studied previously (Section 5.1), the Feed step duration should be minimized. Theoretically, the stage stops once the upstream pressure reaches its setpoint. This latter needs only 0.022 s according to Appendix C. As the minimum operating duration [Feng et al., 2000] is considered as a global constraint in a realistic process simulation, the Feed step duration is fixed at 1 second.

5.2.4.3 Membrane thickness

According to the cyclic functioning, during a part of a cycle, the upstream side of the module is under a high pressure close to that of the feed flow (fixed at 1 atm for reasons explained previously) and during the other part of the cycle under a low pressure considered as vacuum.

The operating step durations are strongly related to the lower time-lag values (Chapter 3 and Section 5.1), while the membrane thickness is one of the determining factors of the time-lag. Thus, the membrane thickness should be deliberately chosen in order to make the time-lag compatible with the characteristic diffusion time in the membrane and to satisfy the valves opening and closing time constraints. As the Feed stage is fixed to be 1 second, the Free diffusion stage should also last more than 1 second due to the valve constraint,

the total duration of high pressure of one cycle should be equal to or longer than 2 seconds, and the total duration of low pressure should be also longer than 2 seconds (Reception stage and Regeneration stage).

In the case of infinitely high pressure, the membrane thickness L is the unique parameter influencing the value θ_0

$$\theta_0 = \frac{L^2}{6\mathcal{D}_m} \tag{5.21}$$

As explained previously, the diffusion coefficient is reduced in an heterogeneous membrane, thus, the effective diffusion coefficient $\mathcal{D}_m$ is used instead of the ordinary one $\mathcal{D}$. For a MMM with 21.6 vol.% of adsorptive fillers, the structural factor κ is estimated to be 0.728 according to Eq. (5.17) [Paul and Kemp, 1973], thus the effective diffusion coefficient $\mathcal{D}_m$ is estimated as

$$\mathcal{D}_{m,i} = 0.728\mathcal{D}_i \qquad \forall i = \mathrm{CO_2}, \mathrm{He} \tag{5.22}$$

Combining Eqs. (5.20), (5.21) and (5.22) gives the expression of the effective time-lag of CO_2 in the MMM as a function of the membrane thickness

$$\theta_{\mathrm{CO_2}} = 16.72\frac{L^2}{\mathcal{D}_{\mathrm{CO_2}}} \tag{5.23}$$

The time-lag of He in the same heterogeneous membrane is given by Eq. (5.21) as He is not adsorbed

$$\theta_{\mathrm{He}} = \frac{L^2}{6\mathcal{D}_{m,\mathrm{He}}} \tag{5.24}$$

Thus

$$\frac{\theta_{\mathrm{CO_2}}}{\theta_{\mathrm{He}}} = 73\frac{\mathcal{D}_{m,\mathrm{He}}}{\mathcal{D}_{m,\mathrm{CO_2}}} = 73\frac{\mathcal{D}_{\mathrm{He}}}{\mathcal{D}_{\mathrm{CO_2}}} = 268 \gg 1 \tag{5.25}$$

Consequently, CO_2 needs much more time to reach the steady-state than He in MMM, so that He can rapidly pass through the membrane and be accumulated in the permeate and a significant separation can be expected due to the large difference of the time-lags [Paul, 1971].

According to Paul's conclusion, the duration τ of a cycle of the cyclic process optimized with respect to selectivity is determined by the time-lag of the slow gas in transient-state, in our case, CO_2

$$\tau = 3\theta_{\mathrm{CO_2}} = 50\frac{L^2}{\mathcal{D}_{\mathrm{CO_2}}} \tag{5.26}$$

in the case that the fraction of period where the upstream pressure is high for a cycle is equal to 10%. Wang et al. [2011a] confirm that Paul's conclusion gives a correct order of magnitude for a highly selective cyclic process, which is one conclusion obtained in Section 5.1. Consequently, the value given by Eq. (5.26) is considered as an approximative estimation of the cycle duration of our process.

Taking into account all these discussed factors, a rather large membrane thickness 50 μm has been chosen. In that situation, the optimized cyclic duration τ is estimated to be about 60 s, and during the first eight seconds of a cycle, the upstream is under high pressure. These characteristics satisfy the valve constraints.

Thus, Tab. 5.13 gives the complements to simulation conditions of Tab. 5.12.

Total feed flow pressure	10^5	Pa
Feed stage duration	1	s
Membrane thickness	$50\ 10^{-6}$	m

Table 5.13: Complements of simulation conditions of the cyclic process.

5.2.5 Preliminary study of the process

In a first step, following scenario is studied: the Free diffusion duration is assumed to be 60 s in order to have a rough understanding of the gas behaviors through the membrane and to get the possible compositions in different tanks. Based on this qualitative consideration, a more detailed study can be performed.

Using the previously discussed simulation conditions (Tabs. 5.12 and 5.13), the diffusion behavior of the gas mixture He/CO_2 is simulated. In parallel, a simulation under the same conditions is performed based on the homogeneous rubbery membrane, i.e., the adsorption coefficients for both gaseous components are assumed to be null, as well as the fraction of dispersed phase.

5.2.5.1 Downstream

In Fig. 5.11, the accumulations of permeate in the downstream part of the module are compared. First, it can be noticed that He, with the larger diffusion coefficient, is the rapid gas at transient-state, while at steady-state, CO_2, with the larger permeability, is the rapid one. Thus the pressure profiles of both gaseous components should cross themselves in the case of a startup operation.

However, this intersection is not visible in the homogeneous membrane (Fig. 5.11 (top right)), as the transient-state which is characterized by time-lag is too short for both gaseous components compared to the total simulation time 60 s. In homogeneous membrane, the time-lags of CO_2 and He are respectively 0.195 s and 0.053 s at the given membrane thickness, thus they can be neglected.

As the additive fillers increase considerably the time-lag of CO_2, the crossing phenomenon of the profiles should be clearly observed in the heterogeneous membrane. Nevertheless, according to our simulation, this phenomenon is no more observed in the heterogeneous membrane (Fig. 5.11 (top left)). This observation can be explained in the following way: during the adsorption, the adsorptive fillers capture a great amount of CO_2, thus its driving force of permeation, i.e., the concentration gradient, increases strongly. Even if CO_2 permeability is higher than that of He, the permeation rate $\frac{\mathcal{P}}{L\Delta P}$ becomes lower than that of He. It results in the disappearance of the crossing of the profiles.

It is also important to notice that at about 10 seconds, i.e., close to the profitability threshold of high selectivity, about 4 500 Pa of He is accumulated in the downstream side. Knowing that the total quantity of He injected in the module for one cycle is 50 000 Pa for the same volume, it corresponds to an exhaustion ratio of about 9%. It is shown in Section 5.1 that this exhaustion ratio for a typical rubbery membrane cannot exceed 0.1%, which is thus largely exceeded by use of MMM.

Fig. 5.11 (right) shows that the homogeneous membrane allows separating the binary gas mixture, whereas the mole fraction of the enriched gas cannot reach 85%. Contrarily, the interest of the heterogeneous membrane is highlighted in Fig. 5.11 (left). It allows the separation of a binary gas mixture efficiently. For a duration less than the break-even point (10 seconds), a permeate of nearly 100% of He can be collected in the downstream side (Fig. 5.11 (left)). Thus once the Reception stage is launched, the permeate enriched in He is expected to be collected in the downstream tank.

5.2.5.2 Upstream

The upstream exhaustions in two types of membrane are compared in Fig. 5.12. Due to the important force of adsorption, CO_2 through the heterogeneous membrane is exhausted more rapidly in the upstream side than through the homogeneous membrane. A better separation is observed for the heterogeneous membrane compared to the homogeneous membrane in this upstream side. However, this selectivity is favored in the case of a long duration of high pressure, which is in contradiction with the good selectivity in the downstream side. As the best selectivity in upstream side is always less important than

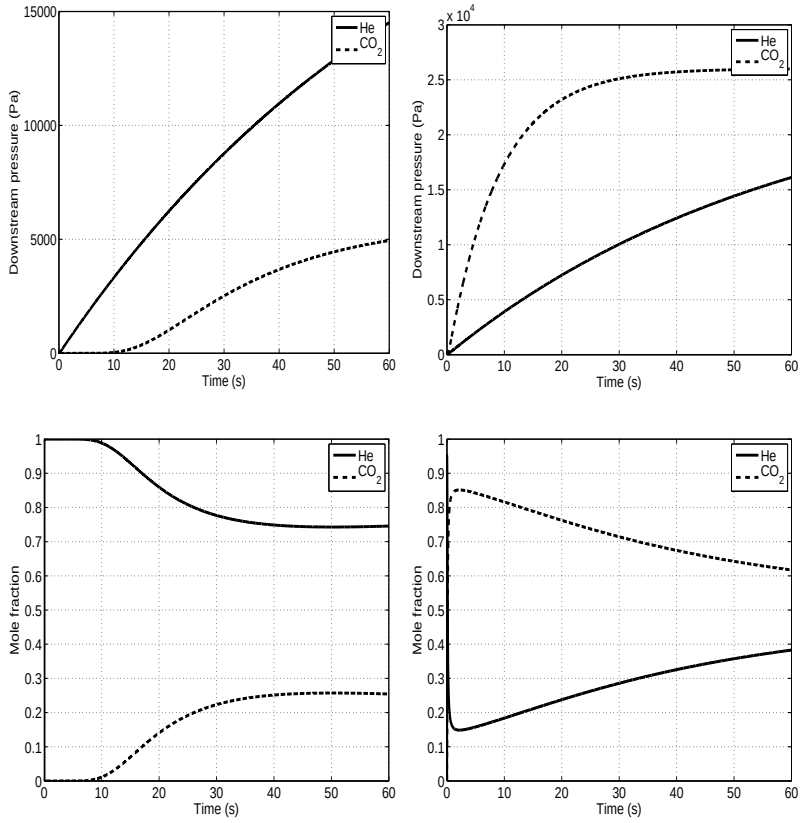

Figure 5.11: Permeate accumulations and mole fractions of each component in the downstream part of the hollow fiber module. Left: heterogeneous membrane; Right: homogeneous membrane. Top: Pressure profiles. Down: Mole fraction profiles.

that in the downstream side, the selectivity in upstream side might not be considered as the top priority in the case of high purity standard production. It should be noticed that during Reception stage, the residual upstream gases will be polluted by the residual gases in the membrane then transported to the upstream tank. If the gas mixture in the upstream tank is still enriched in one gas, a second interest of the cyclic process will be highlighted.

5.2.5.3 Membrane

As Fig. 5.12 shows that an important quantity of CO_2 is adsorbed in the membrane, it is also interesting to check the average concentrations in the membrane (Fig. 5.13). As predicted by Fig. 5.12, in the case of MMM, the

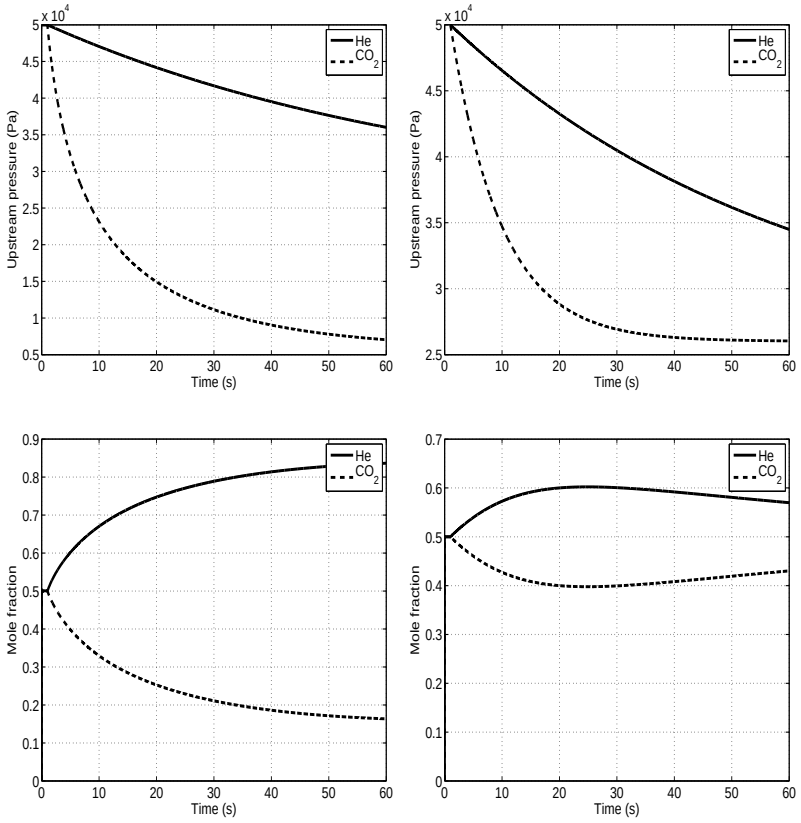

Figure 5.12: Upstream exhaustions and mole fractions of each component in the upstream part of the hollow fiber module. Left: heterogeneous membrane; Right: homogeneous membrane. Top: Pressure profiles. Down: Mole fraction profiles.

concentration of CO_2 in the membrane is multiplied by a factor of about 30 with respect to the homogeneous membrane. On the other hand, the concentration of He in both membranes remains the same. Thus a better separation is obviously observed in MMM.

According to the process design, the gaseous components in the membrane will be transported to its proper tank - rejection tank during Regeneration stage. However, it is important to notice that during the previous step, i.e., Reception stage, both upstream and downstream sides of membrane are already emptied. Once upstream/downstream are de-pressurized, residual gases in membrane cannot be prevented to release into low pressure zone. According to Figs. 5.11, 5.12 and 5.13, membrane and upstream/downstream sides of module are not enriched in the same gas. Consequently, the gases collected

in upstream and downstream tanks will be polluted by the gas released from membrane during this step. Thus, the Reception stage should be minimized in order to reduce this negative effect. Taking into account the valve constraint, the Reception stage is thus fixed to 1 s.

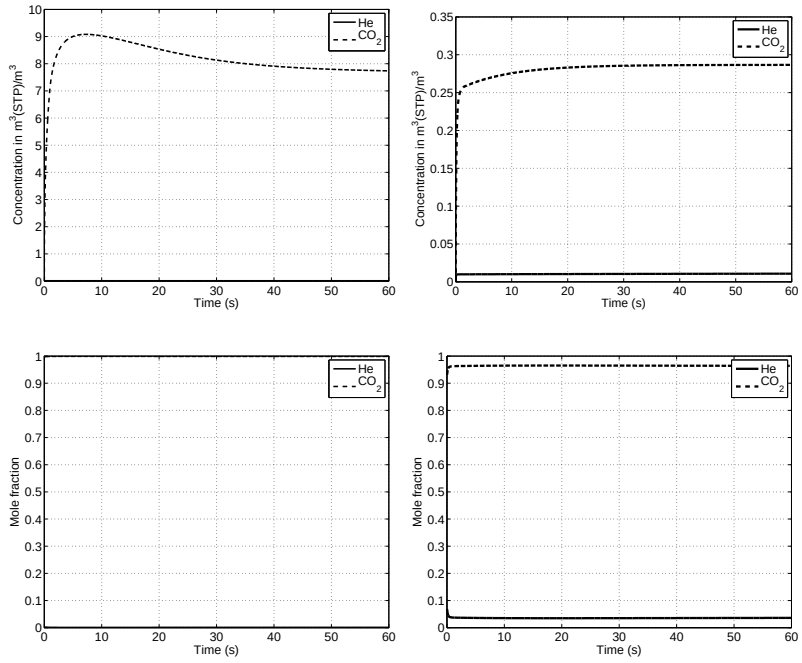

Figure 5.13: Average concentrations in the membrane of the hollow fiber module. Left: heterogeneous membrane; Right: homogeneous membrane. Top: Concentration profiles. Down: Mole fraction profiles.

5.2.6 Pseudo steady-state

Although the studied process uses the difference of permeation rates in transient-state, an industrial process should be performed in a steady cyclic way. Furthermore, the startup duration of cyclic processes can be neglected. It is shown in Section 5.1 that a cyclic process based on a rubbery membrane reaches its 'pseudo steady-state' after the third cycle, which means that the product composition becomes nearly constant in tanks. In order to evaluate the startup duration necessary to establish the 'pseudo steady-state' for the new design, two simulations of different step times (which are chosen arbitrarily) are performed for the eight first consecutive cycles in Figs. 5.14 and 5.15. Compared to the cyclic process based on a rubbery membrane, the cyclic process based on an heterogeneous membrane needs more cycles to reach the

'pseudo steady-state'. Visibly, almost four cycles are required to establish it.

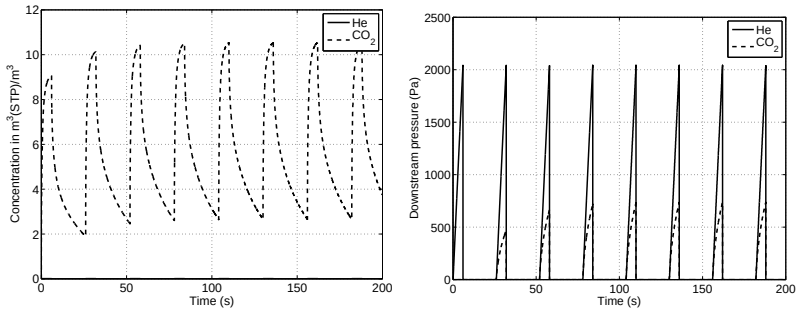

Figure 5.14: Evaluation of average concentrations in the membrane and the partial pressures in the downstream side of the module for the eight first consecutive cycles. Free diffusion stage duration = 5s; Regeneration stage duration = 20s. Left: Average concentrations in the membrane; Right: Partial pressures in the downstream side of the module.

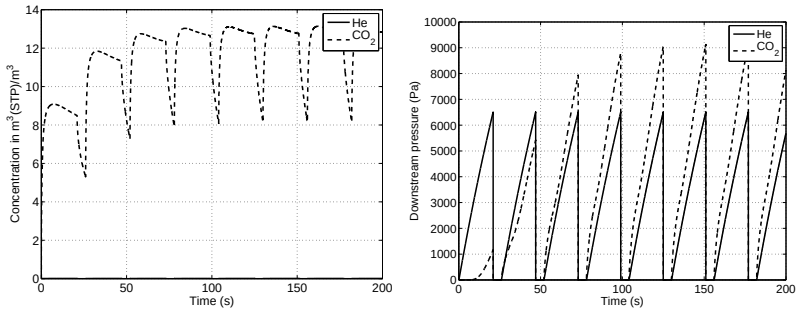

Figure 5.15: Evaluation of average concentrations in the membrane and the partial pressures in the downstream side of the module for the eight first consecutive cycles. Free diffusion stage duration = 20s; Regeneration stage duration = 5s. Left: Average concentrations in the membrane; Right: Partial pressures in the downstream side of the module.

For a long term production, it is logical that the performance of the startup is neglected. The performance of the cyclic process should be observed at pseudo steady-state, thus the contents of upstream and downstream sides resulting from the first 6 cycles in the three tanks are assumed to be rejected in our simulation in order to obtain the performances of the cyclic process at the pseudo steady-state.

Based on this idea, the evaluation of the composition in the downstream tank is simulated in Fig. 5.16 for a 'roughly optimized' operating condition

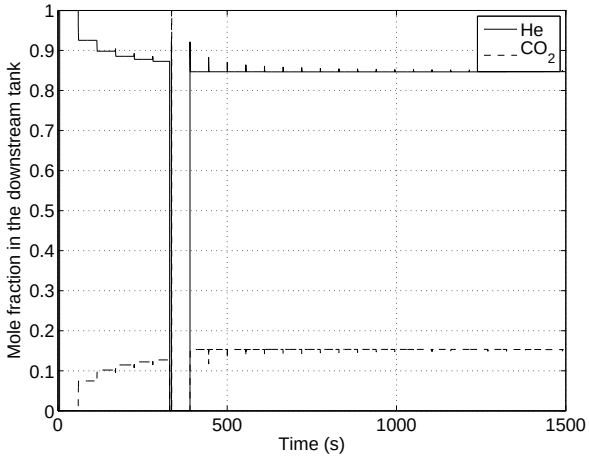

Figure 5.16: Evaluation of mole fractions in the downstream tank. Free diffusion stage duration = 4s; Regeneration stage duration = 50s.

according to Paul [1971]: the total high pressure duration is lower than 8 s and the low pressure duration is 10 times larger than the high pressure one.

Fig. 5.16 shows that the gas composition becomes stable after the rejection at the end of the 6^{th} cycle. In other words, the startup effect is neglected due to this rejection operation. Consequently, for the rest of the study, it was decided to perform simulations of 10 cycles. At the end of the 6^{th} cycle for a given simulation, all three tanks are emptied in order to establish the pseudo steady-state. As a result, the process performance is determined based on the period from 7^{th} to 10^{th} cycles.

5.2.7 Comparison of short processes based on rubbery membranes and MMM

In order to better illustrate the advantages of using adsorptive fillers, complete cyclic processes using unfilled rubbery membranes and MMM are simulated under the same conditions. The practical constraints are respected in order to simulate a feasible process. As a result, the durations of Feed stage and Reception stage are fixed to 1 s for each one. Furthermore, the durations of Free diffusion stage and Regeneration stage are variable in our simulation study (Tab. 5.14).

By considering any combination of the durations of Free diffusion stage and Regeneration stage, the gas properties in the three tanks can be obtained in the simulation study. Therefore, 10 000 combinations have been generated

Stage	Durations
Feed stage	1 s
Free diffusion stage	1-100 s
Reception stage	1 s
Regeneration stage	1-200 s

Table 5.14: Durations of different stages in comparison study.

randomly by the random value generator explained in Section 4.3 in their respective ranges in order to evaluate the cyclic process ability. Furthermore, the pseudo steady-state simulation results are obtained at the end of a series of 10 cycles after elimination of the first 6 cycles as previously explained.

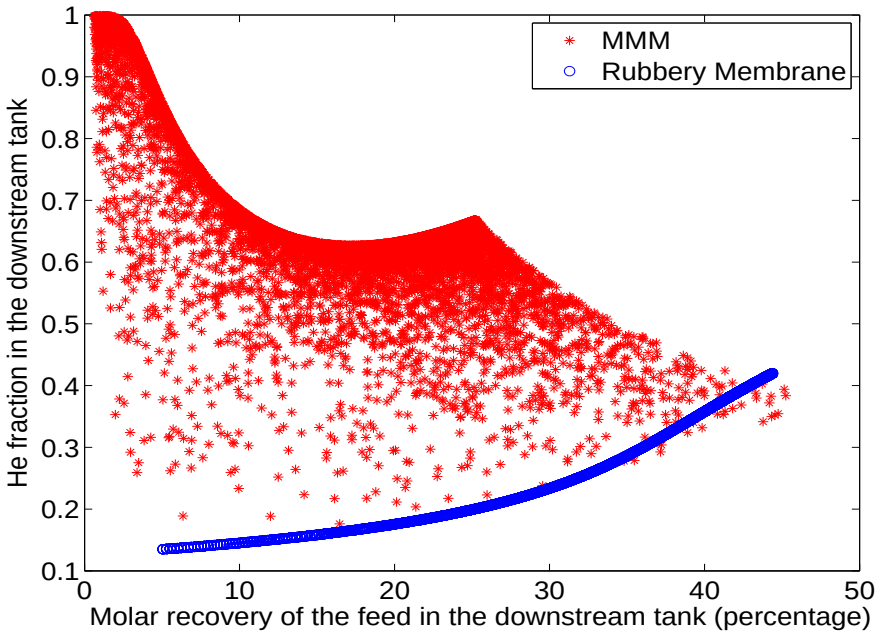

Figure 5.17: Comparison of He fraction and molar recovery of the feed in the downstream tank of cyclic processes using rubbery membranes (blue $\circ$) and using MMMs (red $*$).

The gas properties in the three tanks are compared in Figs. 5.17, 5.18 and 5.19. It can be noticed that in Fig. 5.17 considering the practical constraints, the cyclic process cannot reach the reverse selectivity in the case of unfilled rubbery membrane. In other words, the downstream tank is always enriched in CO_2. Nevertheless, in the case of using adsorptive fillers, rather pure He can be obtained with a stage cut of about 5%. If an extreme purity is not

necessary, a gas mixture with 75% He can be obtained with a stage cut of about 25%.

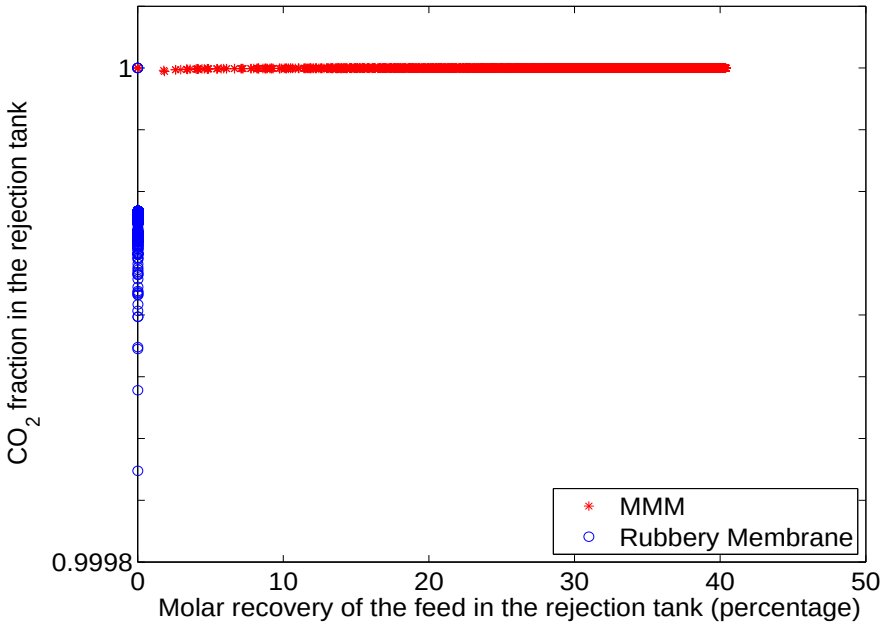

Figure 5.18: Comparison of CO_2 fraction and molar recovery of the feed in the rejection tank of cyclic processes using rubbery membranes (blue $\circ$) and using MMMs (red $*$).

Due to the important sorption coefficients, both membranes are enriched in CO_2. Thus quasi pure CO_2 is obtained in the rejection tank (Fig. 5.18). Nevertheless, the molar recovery of the feed in the rejection tank is extremely low in the case of unfilled rubbery membrane. In general, this quantity is neglected with respect to those in downstream and upstream tanks. By adding adsorptive fillers, the adsorption ability of the membrane is strongly increased, thus the molar recovery of the feed in the rejection tank can reach nearly 40%. At the same time, CO_2 purity is also increased.

In the upstream tank (Fig. 5.19), He mole fraction cannot exceed 0.6 in the case of unfilled rubbery membrane, thus the separation effect is not significant. However, the adsorptive fillers are able to enhance the He mole fraction up to 0.8. On the other hand, it can be noticed that as the adsorption ability of unfilled rubbery membrane is very low, the molar recovery of the feed in the upstream tank is limited in the range 50-100% while it is limited in the range 0-50% in the downstream tank. In the case of MMM, as the molar recovery of feed in the rejection tank becomes comparable to two other tanks, three

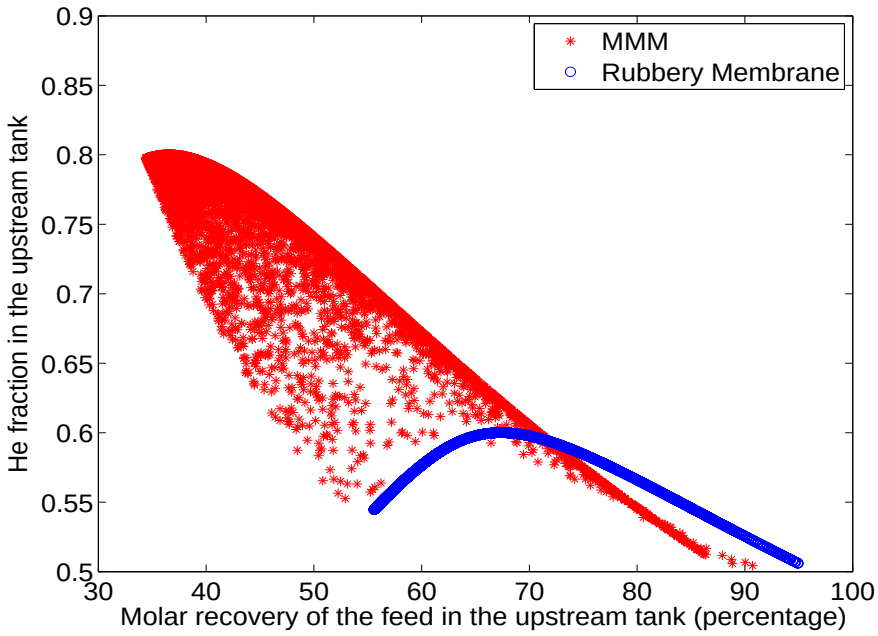

Figure 5.19: Comparison of He fraction and molar recovery of the feed in the upstream tank of cyclic processes using rubbery membranes (blue ∘) and using MMMs (red ∗).

useful products can be obtained and a larger range of molar recoveries of feed in upstream/downstream tanks can be obtained if necessary.

In conclusion, MMM usages in cyclic processes have been highlighted by simulation studies. It is also very important to notice that the simulated cyclic processes satisfy all practical constraints due to use of MMM. In other words, a pilot validation can be readily prepared.

5.2.8 Performance criteria for comparison

Figs. 5.17, 5.18 and 5.19 show that MMM allows us to increase the cyclic process separation efficiency, including purities in the three tanks and molar recoveries of feed in each tank. All these factors can be indeed obtained by a multiobjective optimization. However, the value of an objective function (purity or molar recovery of the feed) is in general higher for a single optimization compared to its value in the case of a multiobjective optimization. Consequently, the best enhancements in the three tanks cannot be obtained at the same time, and operating parameters (durations of each stage) should be precisely chosen in order to satisfy different needs. In our study, a general

optimization taking into account all quality factors is not performed. Similarly to Paul's cyclic process, the purity of the gas of interest and molar recovery in the downstream tank are considered as optimization objectives.

From the preliminary analysis, it can be qualitatively concluded that if the mole fraction of He in the downstream tank is considered as the only criterion (which is the criterion of Paul), the optimized operation conditions should be the following ones:

- The Free diffusion stage duration tends to zero in order to accumulate a quasi pure gas in the downstream side of the membrane module then to collect it.

- The Regeneration stage duration tends to infinity in order to perfectly regenerate the membrane.

On the other hand, the Feeding stage and the Reception stage durations are assumed to be as short as possible. It can be noticed that this qualitative conclusion is consistent with Paul's conclusion [Paul, 1971]. Nevertheless, as concluded in Section 5.1, these optimized conditions represent zero stage cut.

Similarly to the definitions of performance criteria in Section 5.1, two criteria are defined: separation factor and productivity. The diffusion coefficient of He is larger in our binary mixture. Thus the separation factor is defined as

$$\text{separation factor} = \frac{y_d}{1-y_d}\frac{1-y_f}{y_f} \tag{5.27}$$

where y_d is the mole fraction of He is the downstream tank and y_f the feed flux mole fraction of He. According to simulation studies in Section 5.1, the separation factor defined by Eq. (5.27) can be enhanced by the cyclic process with respect to conventional processes. It is important to notice that for the gas mixture $\{He,CO_2\}$, in steady-state, the separation factor defined by Eq. (5.27) is always lower than 1, since He, whose permeability is lower, is not accumulated preferentially in the downstream tank.

Another performance criterion, the productivity, is also defined preferentially with respect to He in the downstream tank. Its definition is the number of moles of He in the downstream tank n_d divided by the total time of operation Δt and by the surface area A of the membrane offered to transfer

$$\text{productivity (mol/m}^2\text{.s)} = \frac{n_d}{A\Delta t} \tag{5.28}$$

These two performance factors will be used in the following optimization study.

5.2.9 Comparison of steady-state operations and optimized short class processes based on MMM

In order to make a convincing comparison, both operations should be performed under the same simulation conditions. However, due to different operating ways, some consequences are unavoidable.

The steady-state operation corresponds to a classical single module in cross flow, with steady upstream pressure equal to the initial upstream pressure of the cyclic operation (10^5 Pa in Tab. 5.13) and a constant pressure ratio Ψ permeate/retentate equal to 0.01. The effective permeabilities $\mathcal{P}_m$ of each gas are calculated using Tab. 5.9 and the structural factor κ

$$\mathcal{P}_m = \kappa k_D \mathcal{D} \tag{5.29}$$

All other simulation conditions are exactly the same as described in Tabs. 5.4 and 5.13. Stage-cut is varied in order to evaluate process efficiency. It can be noticed again that in this comparison, the same thickness of 50μm is used for both operations. In a conventional steady-state operation, the membrane thickness is much lower in order to favor the production rate.

The cyclic operations are performed on two types of membranes as previously described: the homogeneous rubbery membrane and the corresponding MMM (Tab. 5.9). The practical constraints are respected (Tab. 5.13) in order to simulate a feasible process. Thus the durations in Tab. 5.14 are considered in optimization.

Denoting the duration of Free diffusion stage as x_1 and that of Regeneration stage as x_2, the optimization problem with respect to the separation factor and productivity is set as follows

$$\max_{x_1,x_2} \begin{pmatrix} \text{separation factor} \\ \text{productivity} \end{pmatrix}$$

submitted to

$$\begin{aligned} 1 \leq x_1 \leq 100s \\ 1 \leq x_2 \leq 200s \end{aligned}$$

To solve this multiobjective optimization problem of two objective functions and two variables, the genetic algorithm coded in FORTRAN (Section 4.3) is used.

The optimized results (10^{th} generation) of the cyclic process based on ordinary rubbery membrane and MMM are given in Fig. 5.20 with simulated cross flow processes at steady-state.

The following conclusions can be obtained from Fig. 5.20.

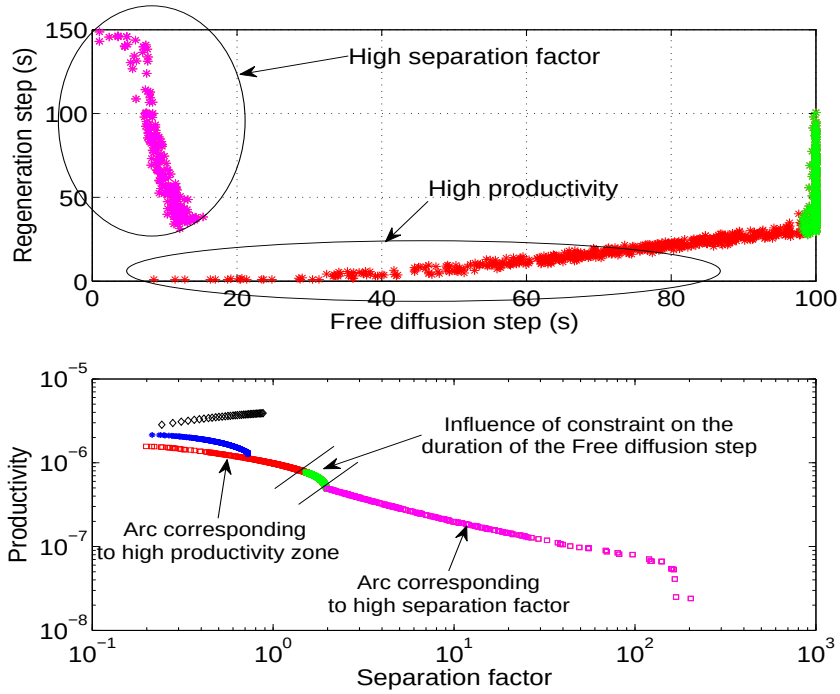

Figure 5.20: Top: Optimized durations of Free diffusion stage and Regeneration stage: results of 10^{th} generation of genetic algorithm. Bottom: Comparison of optimized separation performance (10^{th} generation of genetic algorithm) for steady steady (black $\diamond$) and cyclic operations using a rubbery membrane (blue $*$) and using an heterogeneous membrane (red, green and pink $\square$). ($\{He, CO_2\}$ separation, the reverse selectivity is presented by a separation factor lower than 1)

- A reverse selectivity is not observed in the case of a rubbery membrane since the time-lag of CO_2 in it is too short. This point is also predicted by simulations in Figs. 5.11 and 5.17. In other words, in order to achieve the cyclic process interests and satisfy the constraint valve opening frequency, the homogeneous membrane should be thicker than 300 μm. It can be noticed that this value is not usual in industry since it makes the productivity extremely low. Thus the short class cyclic process using the homogeneous membrane is not an efficient process in our simulation conditions: both separation and productivity are lower than for other processes.

- Using an heterogeneous membrane, the short class cyclic process clearly

offers a large range of performances in terms of productivity and separation factor with respect to conventional processes. A reverse and improved selectivity is observed in Fig. 5.20. At the expense of some productivity loss, the selectivity improvement is rather significant.

- The optimized durations of the Free diffusion stage and the Regeneration stage are illustrated in Fig. 5.20 (top). It can be first noticed that large productivities are obtained with low Regeneration stage durations, whereas large separation factors are achieved with low Free diffusion stage durations. Secondly, when the Free diffusion step duration takes it maximum value, this is a constraint for the variables of the optimization problem. In that case, the optimum couples (separation factor, productivity) form a constraint arc which marks the transition between the arcs corresponding respectively to high productivity and high separation factor. This constraint arc occurs for a separation factor around 1 to 2. Physically, it can be explained in following way: since the duration of Free diffusion stage is limited at 100 s, the productivity decreases when Regeneration stage duration becomes long. On the other hand, the membrane regeneration influences only the separation effect under transient-state. As a duration of 100 s is much larger than the time-lag of CO_2 (about 8 s), the influence of regeneration is minored. Consequently, on the Free diffusion stage constraint, the separation factor is nearly independent of the Regeneration stage duration.

5.2.10 {CO_2,N_2} reverse selective separation

For {CO_2,N_2} separation (or CO_2 capture application), the permeation process is in general selective with respect to CO_2 and the separation performance is represented by two factors: purity of CO_2 and its recovery ratio. The latter is defined as the ratio of recovered CO_2 over CO_2 in feed flow. Nevertheless, Favre et al. [2009] explained that a reverse selective membrane, i.e., N_2 selective membrane, would be of great interest for minimizing energy consumption. In the case where a moderate pressure ratio Ψ (permeate/retentate pressure ≈ 0.1) is applied, reverse selective membrane is the only choice in order to achieve the target performance: purity of 0.9 together with a recovery ratio of 0.9 for CO_2 capture. One theoretical possibility to achieve the reverse selectivity is to perform time-lag experiments since the diffusion coefficient of N_2 is larger than that of CO_2. Favre et al. [2009] indicate that the classical CO_2 selectivity will be obtained again when the same experiments are operated cyclically without complete regeneration of the membrane. Consequently, the reverse selectivity might be obtained by using a short class cyclic process composed consecutively of a high pressure stage and a regeneration

stage. However, according to the discussion in Section 5.1, in general, the exhaustion rate in upstream cannot exceed 0.1% in the case of a classical cyclic process based on a rubbery membrane. Thus the capture ratio target cannot be reached.

On the other hand, Bertelle et al. [2006] proposed and validated a design to incorporate active carbon in poly (dimethylsiloxane) (PDMS) up to 70 wt%. Since active carbon adsorbs largely CO_2 but slightly N_2, synthesized MMM possesses the potential to enlarge only significantly the time-lag of CO_2. As a result, a considerable reverse selectivity for $\{CO_2,N_2\}$ can be expected, as well as an important upstream exhaustion rate.

In this regard, a novel design cyclic process based on a PDMS with active carbon is simulated for $\{CO_2,N_2\}$ separation. Through a similar preliminary study, a MMM of 100 μm with 21.6 vol.% of active carbon is used at 283.15K to perform the separation. For sake of convenience, the adsorption effect on N_2 is neglected with respect to that of CO_2. Gas transport parameters are given in Tab. 5.15.

	C'_H $m^3(STP)/m^3$	b $(atm)^{-1}$	$k_D \times 10^3$ $m^3(STP)/m^3.atm$	$\mathcal{D} \times 10^{10}$ m^2/s
CO_2	46.43	2.1662	1.29	34
N_2	0	0	0.09	22

Table 5.15: Estimated mass transport parameters at 283.15K [Kikkinides et al., 1993, Merkel et al., 2000]. Poly(dimethylsiloxane) PDMS with 21.6 vol.% of active carbon.

All other simulation conditions are the same as described in Tabs. 5.12 and 5.13. As a result, the time-lag ratio $\frac{\theta_{CO_2}}{\theta_{N_2}} = 81.7$ at initial upstream and downstream pressures suggests a significant N_2 selective separation. The process is first simulated then optimized by a genetic algorithm with respect to the separation factor and the productivity based on N_2.

The optimized performances of cyclic processes based on pure PDMS and on PDMS with active carbon are shown in Fig. 5.21. First, the interests of using active carbon are highlighted again, a reverse selectivity is indeed obtained in the case of MMM but not for pure PDMS. Secondly, the influence of the constraint on the duration of the Free diffusion stage is again clearly observed in Fig. 5.21 so that the Pareto line between productivity and separation factor is composed of three arcs as in Fig. 5.20.

As regards the CO_2 capture application, the following strategy is applied in simulation:

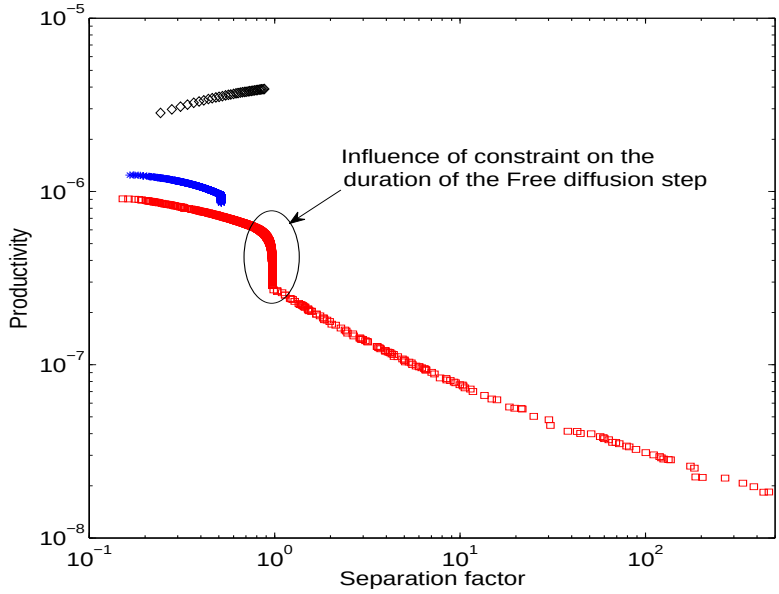

Figure 5.21: Comparison of optimized separation performance (10^{th} generation of genetic algorithm) for steady steady (black $\diamond$) and cyclic operations using pure PDMS (blue $*$) and using PDMS with active carbon (red $\square$). ($\{N_2$, $CO_2\}$ separation, the reverse selectivity is presented by a separation factor lower than 1)

- The feed composition is set to 10 vol.% fraction CO_2 (90 vol.% fraction N_2).
- Similarly to the previous study, 10 000 combinations of Free diffusion stage durations (1-100 s) and Regeneration stage durations (1-200 s) have been generated randomly according to a uniform distribution in their respective ranges in order to evaluate the cyclic process ability.
- The membrane thickness is fixed at 100 μm.
- All other simulation conditions are the same as described in Tabs. 5.4 and 5.13.

According to our simulation, CO_2 is preferentially accumulated in the membrane then released into the rejection tank. In Fig. 5.22, it can be noticed that CO_2 can be recovered at very high purity (larger than 0.99), nevertheless, its recovery ratio cannot exceed 65%. Thus the target performance is not reached in the case of cyclic processes based on PDMS with active carbon.

However, the extreme high purity still makes the cyclic process competitive with respect to classical processes. On the other hand, this result is obtained for a single stage membrane module, i.e., if the number of stages increases, the recovery ratio will be surely more important.

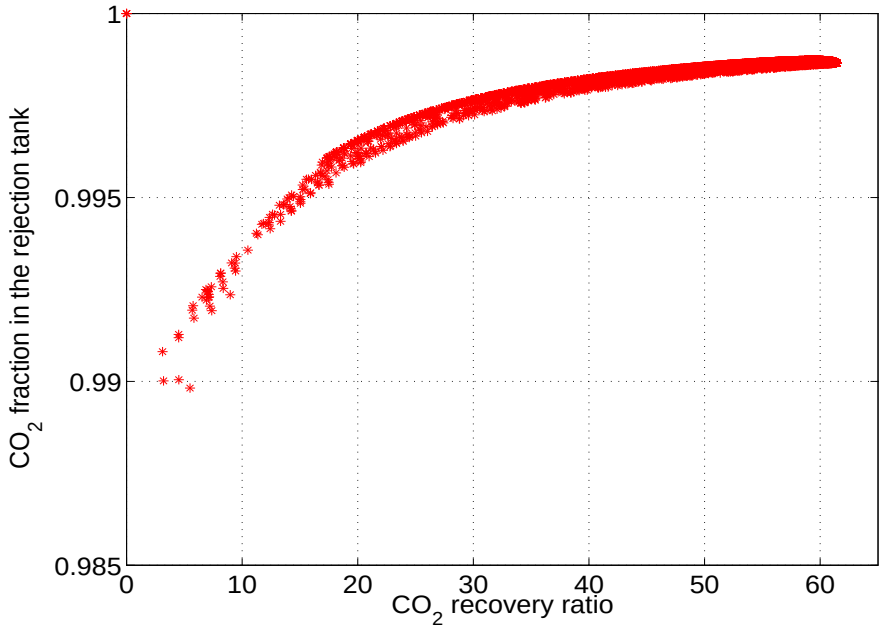

Figure 5.22: Separation performance of cyclic processes based on PDMS with active carbon for the recovery of carbon dioxide diluted in nitrogen (feed composition 10 vol.% fraction CO_2).

5.2.11 Discussion and Conclusion

In this case study, the classical short class process based on Paul's idea is renewed, not only configurations of operations, but also the membrane material. Therefore, two performance improvements mentioned in Chapter 2 have been combined. As shown in a previous case study (Section 5.1), the most important drawback of short class cyclic processes with respect to conventional operations is the low exhaustion rate of feed and low productivity. The use of MMMs offers great improvements to short class processes. It should be noticed that some MMM can efficiently improve the process selectivity whereas the MMM of our study is not in this case. This latter cannot bring any improvement for a conventional process since it provides the same permeselectivity as the ordinary homogeneous membrane. Nevertheless, based on a binary gas mixture

{He, CO_2} for a cyclic operation, it has been shown through a rigorous numerical approach that the exhaustion rate of feed can be significantly improved while the process is still extremely selective. Furthermore, a new design of cyclic processes is proposed, in which all valve practical constraints have been taken into account. The novel design makes use of a classical module layout (hollow fiber module) and no synchronous operations are needed. Moreover, three receiving tanks are proposed in order to adapt the particularity of using MMM. Therefore, an experimental validation should be easier to perform. Meanwhile, the novel design offers more operation possibilities and improves the global apparatus utilization rate, i.e., the products in all three tanks can be useful, instead of only one in Paul's design. According to the needs, highly purified products enriched in either He or CO_2 can be individually obtained in their proper tanks. Furthermore, the selectivity improvement is also obtained for {N_2, CO_2} separation.

It can be expected that with the technology development, the valve minimum opening or closing times can be reduced to smaller values. Consequently, the duration of Reception stage can be made shorter and other valve opening constraints can also be reduced. As a result, products with a better purity can be expected owing to the reduction of durations of corresponding steps.

It is indicated in Section 3 that a possible reason for little activity of cyclic processes is that membranes are typically promoted as simple passive devices, which serves as a selling argument with regard to PSA processes. The latter require multiple vessels and many valves which are often switched and need maintenance. Short class cyclic processes designed by Paul [1971] can no longer be considered as simple and will require a complex environment structure in some ways similar to a PSA process. However, the renewed design in this section should be more competitive since it reduces largely the process complexity. Furthermore, short class cyclic processes in particular the one based on heterogeneous membranes are able to provide a unique selectivity improvement with respect to conventional processes. This point is yet especially important and interesting for high purity standard gas production. Nevertheless, the investment capital and the operating cost, which are very important economics factors when assessing the feasibility of a process, have not yet been quantitatively enclosed in any investigation. This point should be included in a systematic study with all performance criteria in order to well situate the short class cyclic processes in the family of gas separation processes.

5.3 Novel cyclic process - long class process

As shown in previous case studies, in most cases, the huge productivity loss makes the short class process hardly competitive with respect to conventional membrane processes. Although the use of Mixed Matrix Membranes allows to improve the short class process performance, the regeneration stage takes an important part in one cycle (almost 90%). As explained in chapter 3, different from the short class processes, the transient behaviors occur in the system outside the membrane in the case of the long class processes. Consequently, long class processes are much less "time-lag depending". Therefore, the productivity loss is in general less important. What is more important is that the regeneration stage is not necessary long in the case of long class process. Thus a significant productivity improvement with respect to short class processes is expected. In this thesis, a long class process is designed then simulated in order to highlight its competitiveness with respect to conventional processes.

This case study will be based on three different binary gas mixtures where there are well defined interests: $\{O_2, CO_2\}$ (the one used in the method validation, Section 5.1.3), $\{O_2, N_2\}$ (air separation) and $\{CH_4, He\}$ (binary mixture used by Paul [1971] in the first cyclic process study). For sake of convenience, the transport model in rubbery membrane (Section 4.1.8) is used in all simulations. The credibility of the model will be later checked experimentally in Chapter 6. Their average transport parameters are found from the existing literature and given in Tabs. 5.5, 5.16 and 5.17.

$\alpha = 5.07$			
Gas	$\mathcal{P}\times 10^{15}$	$\mathcal{D}\times 10^{10}$	$k_D\times 10^{6}$
O_2	2.343	0.11	213
N_2	0.462	0.0282	164

Table 5.16: Mass transport parameters from Koros and Fleming [1993]. Polycarbonate with SBIPI (Spirobiindane polycarbonate) between bisphenol groups. (S.I. units)

5.3.1 Process description

The process design is given in Fig. 5.23. The valves C_1 and C_2 are optional, as well as the sidestream concerning operations. The structure of the module is the same as that in Fig. 4.18. The membrane is incorporated into a hollow fiber module. The internal volume of fibers is considered as upstream while the free volume between fibers and the module is considered as downstream. The upstream side possesses an inlet and an outlet. The downstream side is only

$\alpha = 2.96$			
Gas	$\mathcal{P}\times 10^{18}$	$\mathcal{D}\times 10^{10}$	$k_D\times 10^{8}$
He	8.596	3.07	2.8
CH_4	2.907	0.057	51

Table 5.17: Mass transport parameters from Polymer Handbook [Brandrup and Immergut, 1989]. Poly(ethylene), high density, 0.964 g.cm^{-3} HDPE. (S.I. units)

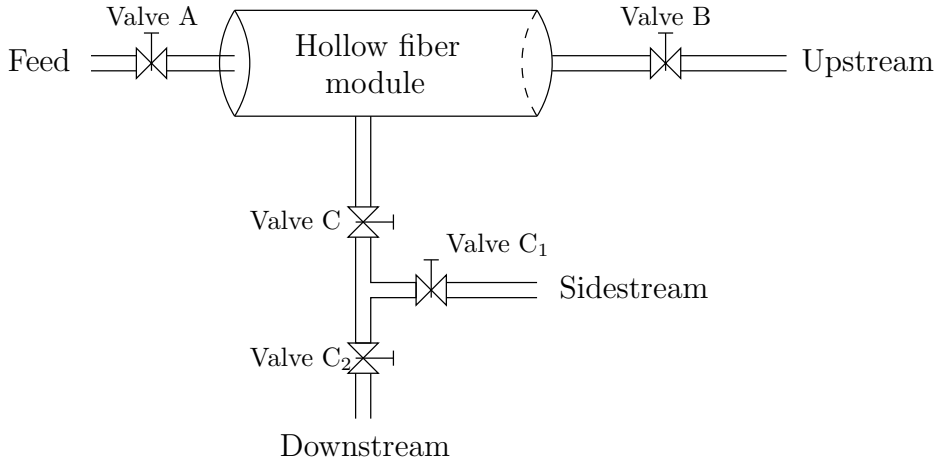

Figure 5.23: Novel long class cyclic process design, [Wang et al., 2011b]

connected to one outlet. All flow directions are controlled by corresponding valves.

Initially, all the module is emptied and all valves are switched off. Once the process is launched, the module will be fed to a given pressure by opening valve A. Similar to both previous case studies, this stage is named as Feed stage. Once the pressure set point is reached, valve A is closed then the diffusion occurs through the fibers. This stage is named as Free diffusion stage. Then, two options are available:

- Basic option. Valves C_1 (always closed) and C_2 (always open) are not in use. Consequently, the sidestream flow does not exist. After the Free diffusion stage, Valves B and C are opened in order to transport the gases in upstream and downstream to corresponding tanks. Due to the transport, the whole module is emptied. This stage is named as Transfer stage. After that, all valves are closed and the cycle is finished.
- Sidestream option. All valves are in use. After the Free diffusion stage, valves C and C_1 are opened, a sidestream flow is collected in the corre-

sponding tank. This stage is named as Sidestream stage, then both valves C and C_1 are closed again in order to resume the diffusion through the fibers, which is named as 2^{nd} free diffusion stage. After that, in Transfer stage, Valves B, C and C_2 are opened in order to transport the gases in upstream and downstream sides to corresponding tanks, due to the transport, the whole module is emptied and the membrane is regenerated. Then all valves are closed and the cycle is finished.

Similar to short class processes, the filling duration of the hollow fiber module is less than 0.2 second. Similar to both previous case studies, taking into account the realistic operating conditions [Feng et al., 2000], the feed stage duration is fixed to 1 second in the following studies.

On the other hand, the transfer stage is constrained by two things: the practical constraint of the valve opening duration and the required membrane regeneration duration. The transfer stage duration will be further discussed by means of a membrane regeneration study.

The described cyclic operations are summarized in Tab. 5.18.

Valve	A	B	C	**C_1**	**C_2**
Feed stage	o	-	-	-	-
Free diffusion stage	-	-	-	-	-
Sidestream stage	-	-	o	o	-
2^{nd} free diffusion stage	-	-	-	-	-
Transfer stage	-	o	o	-	o

Table 5.18: Cyclic operations of novel process design (Fig. 5.23). Optional stages are in bold. ("o" for open and "-" for closed.)

As a result, in the case of basic option, the feed gas is separated into two fluxes: upstream and downstream flux, which are almost the same as conventional processes (retentate and permeate). However, in the case of sidestream option, three fluxes can be obtained at outlet: upstream, downstream and sidestream fluxes.

5.3.2 Results and discussion

It can be noticed that the mathematical description of gas transports in the novel process is exactly the same as that in Section 5.1.2.

Since this novel process is classified as long class, the diffusion duration (stages between feed stage and transfer stage) is much longer than the time-

lags of respective gaseous components. Consequently, instead of diffusion coefficient ratio, the separation efficiency is determined by the permeability ratio like in the case of conventional processes.

5.3.2.1 Characteristics of outlet flows

As explained in process design, the novel process can generate two or three flux at outlet according to options. Thus the first question is to understand qualitatively the gas compositions in the respective fluxes. To do so, the "Free diffusion to pressure equilibrium" (Section 4.1.6) scenario is simulated based on {O_2, CO_2} (Tab. 5.5) and the simulation conditions are given in Tab. 5.19.

Temperature	297.15	K
Feed pressure	$1.013\ 10^5$	Pa
Upstream volume	0.0125	m^3
Downstream volume	0.125	m^3
Module length	1	m
Internal fiber diameter	$50\ 10^{-6}$	m
Internal membrane surface	1000	m^2
Membrane thickness	$1\ 10^{-6}$	m
O_2 fraction in feed	0.5	

Table 5.19: Simulation conditions for "Free diffusion to pressure equilibrium".

It is clearly observed in Fig. 5.24 (this kind of evolution curves are validated experimentally in Chapter 6) that due to the permeability difference, the CO_2 partial pressure decreases faster than that of O_2 in upstream. As a result, a gas enriched in O_2 whose permeability is lower is expected in upstream while CO_2 whose permeability is larger is preferentially accumulated in downstream. Mole fractions of each gas in upstream and downstream sides of membrane are shown in Fig 5.25. It can be noticed that a maximum mole fraction can be obtained in upstream for O_2 with a lower permeability while the mole fraction of CO_2 with a larger permeability in downstream is a strict decreasing function of time.

Furthermore, the maximum mole fraction of O_2 in upstream depends on the downstream/upstream volume ratio $\gamma = V_d/V_u$, Fig. 5.26 shows that this maximum mole fraction of O_2 becomes important as well as the necessary time to reach pressure equilibrium in the case of high volume ratio. The dependence of maximum mole fraction of O_2 on volume ratio γ is represented in Fig. 5.27. As a result, the novel process can be very selective in the case of high volume ratio although the permselectivity of {O_2,CO_2} is not spectacular ($\alpha = 5.6$).

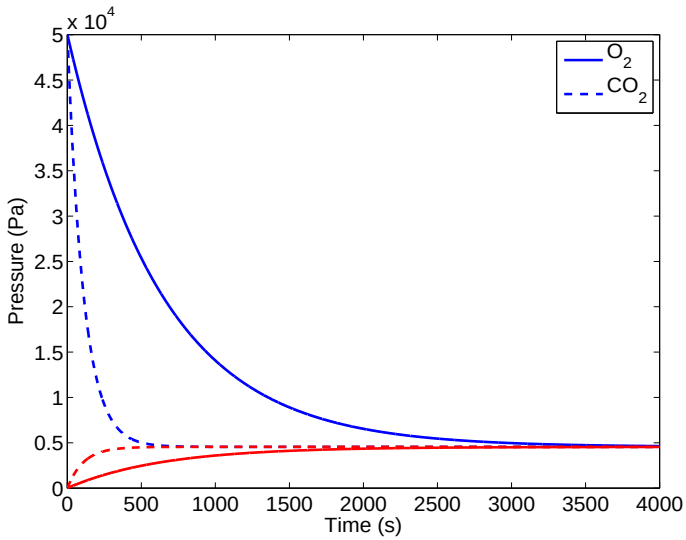

Figure 5.24: Simulated pressure evolutions of "free diffusion to pressure equilibrium" test for $\{O_2, CO_2\}$. Red lines for downstream evolution and blue lines for upstream evolution.

Consequently, the volume ratio γ should be considered as one of key issues of patent design.

In the case of sidestream option, it is logical that the upstream side will be enriched in slow gas and the sidestream flow enriched in rapid gas. As regards the downstream, the gas can be enriched in rapid gas, if the sidestream flux is low, most rapid gas goes across the membrane during the 2^{nd} free diffusion stage. Nevertheless, the downstream gas can also be enriched in slow gas, if the sidestream flux is important, most rapid gas goes into the sidestream. This characteristics leaves more degrees of freedom to the process and will be discussed later.

5.3.2.2 Membrane regeneration

In the case of short class processes, the regeneration stage is compulsory to ensure a good selectivity but should be minimized in order to optimize the productivity. As mentioned at the beginning of the section, this stage is rather long and cannot be much reduced in the case of short class processes due to the use of relative thick membranes, which is one key issue of productivity loss. In the case of long class processes, the time-lag is no more the key issue of separations. Thus the membrane thickness can be much thinner, so that the residual gas in membrane is much less than in a thick membrane. As a result, the regeneration duration can be expected to be short. The following

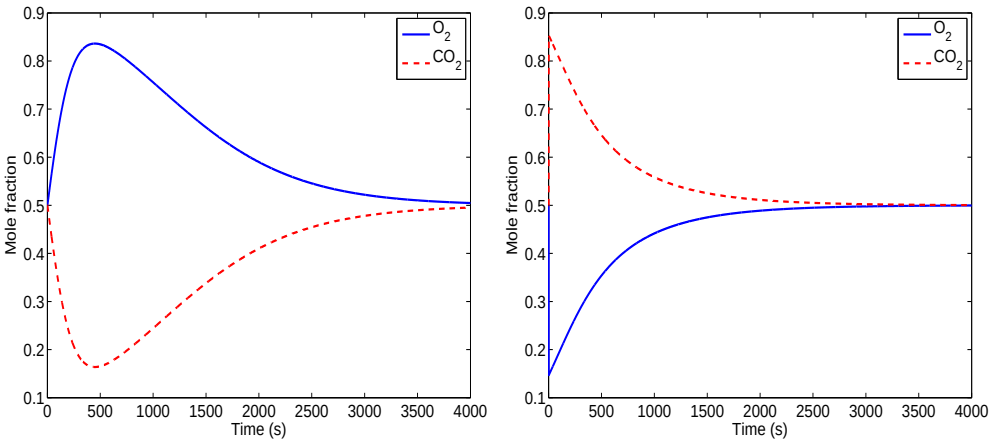

Figure 5.25: Simulated mole fraction evolutions of "free diffusion to pressure equilibrium" test for $\{O_2, CO_2\}$ according to simulation conditions of Tab. 5.19. Left: upstream. Right: downstream

tests have been performed in order to determine the adequate regeneration duration of long class processes.

The strategy is to perform several consecutive cycles from the start up cycle then to observe the difference between two consecutive cycles. The basic option is chosen here. The Free diffusion stage is fixed at 499 s in order to have the total high pressure duration (Feed stage + Free diffusion stage) equal to 500 s while the transfer stage duration is variable from 0.2 to 100 s. Other simulation conditions are given in Tab. 5.19. It can be noticed that 0.2 s corresponds to the magnitude of the time-lag ($\theta = \frac{L^2}{6\mathcal{D}}$) and 100 s $\gg$ the time-lag. Fig. 5.28 shows that for the tested duration values, the partial pressure evolutions are nearly independent on the Regeneration duration, a "pseudo steady-state" is established from the first cycle, i.e., no significant difference is observed between the first and the second cycles.

As a result, it can be concluded that the Transfer stage duration of novel process can be at least reduced to the order of magnitude of the time-lag without modifying separation efficiency. The latter is much less than 1 for all three gas pairs in our study. This value is even neglected with respect to the duration of the other stages. In other words, the short class process productivity loss due to long regeneration durations can be avoided in the case of the novel process. Nevertheless, the Transfer stage duration will be fixed at 1 second in the following studies according to the realistic constraints mentioned by Feng et al. [2000].

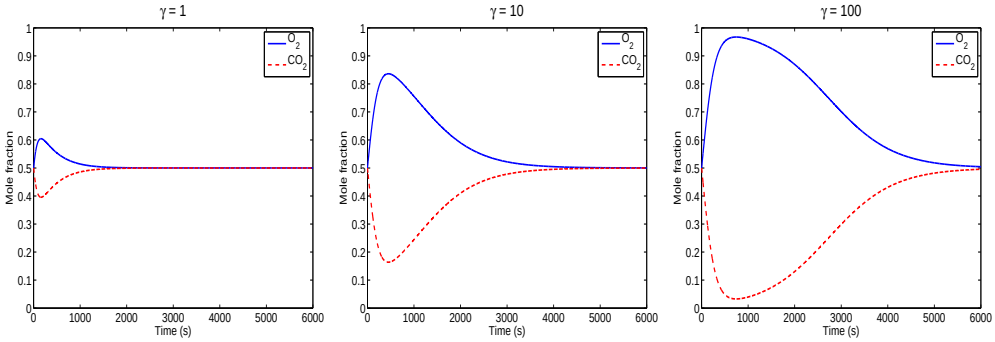

Figure 5.26: Simulated mole fraction evolutions of "free diffusion to pressure equilibrium" test for $\{O_2,\ CO_2\}$ with different volume ratios. Left: $\gamma = V_d/V_u = 1$. Middle: $\gamma = 10$. Right: $\gamma = 100$.

5.3.2.3 Comparison between basic and sidestream options

As indicated previously, the sidestream option makes the process provide three flux at outlet and the downstream flow composition varies in a large range. In order to better understand the performance of such process, the following investigations have been performed.

According to the process description, a novel cyclic process with sidestream option is characterized by 5 stage durations (Tab. 5.18). The Feed stage and the Transfer stage durations should be minimized according to our previous discussions, thus they are both fixed at 1 s in this study. As a result, the process with a given membrane module is characterized by 3 stage durations: Free diffusion stage, Sidestream stage and 2^{nd} free diffusion stage. Consequently, by considering any combinations of the 3 stage durations, the gas properties in three flux can be obtained in a simulation study. Therefore, 17 085 combinations have been generated randomly according to a uniform distribution by the generator mentioned in Section 4.3 in their respective ranges (Tab. 5.20) in order to evaluate the process ability. Other simulation conditions are also given in Tab. 5.20.

The simulated mole fractions in each flux are given in Fig. 5.29. The following conclusions can be obtained with respect to both basic and sidestream options:

- In upstream, O_2 whose permeability is lower always accumulates preferentially. Figs. 5.26 and 5.27 show that the maximum O_2 mole fraction in the case of basic option with volume ratio $\gamma = 10$ is 0.8363. However, in the case of sidestream with the same volume ratio, O_2 mole fraction in upstream can exceed 0.95 (Fig. 5.29 middle and bottom). If the slow gas

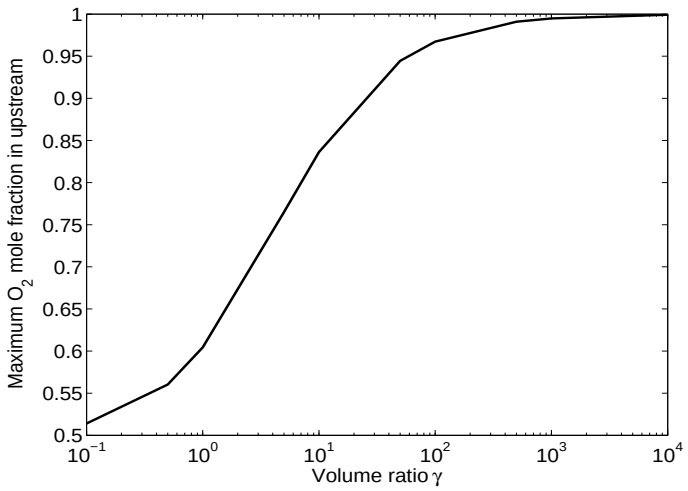

Figure 5.27: Maximum O_2 mole fraction in upstream of basic option in function of volume ratios $\gamma = V_d/V_u$.

is the desired product, the sidestream option can be used as a method to improve the process efficiency.

- In sidestream, CO_2 is always enriched. Its mole fractions range from 0.55 to 0.85, i.e, the sidestream flow is always enriched in the gas whose permeability is larger.

- In downstream, the O_2 mole fraction covers a large range from 0.2 to 0.8. It means that either O_2 or CO_2 can be enriched in downstream. It is also interesting to notice that the O_2 mole fraction of feed flow (0.5) is also included in this range.

- According to Tab. 5.20, the situation where the time of starting Sidestream stage is larger than the total diffusion duration is no excluded, i.e., the Sidestream stage will never occur in this case which is the situation of the basic option. In Fig.5.29 (bottom), the performance of the basic option (obtained by the previous way) is represented by points along the x-axis. Again, the maximum O_2 mole fraction in upstream with basic option (0.8363) is confirmed.

Consequently, it can be noticed that the sidestream option provides more degrees of freedom. Products enriched in larger permeability gas or lower permeability gas can be obtained in different places according to needs. An optimization investigation can be applied in one or some corresponding fluxes in order to improve process performances. Moreover, at the same volume ratio

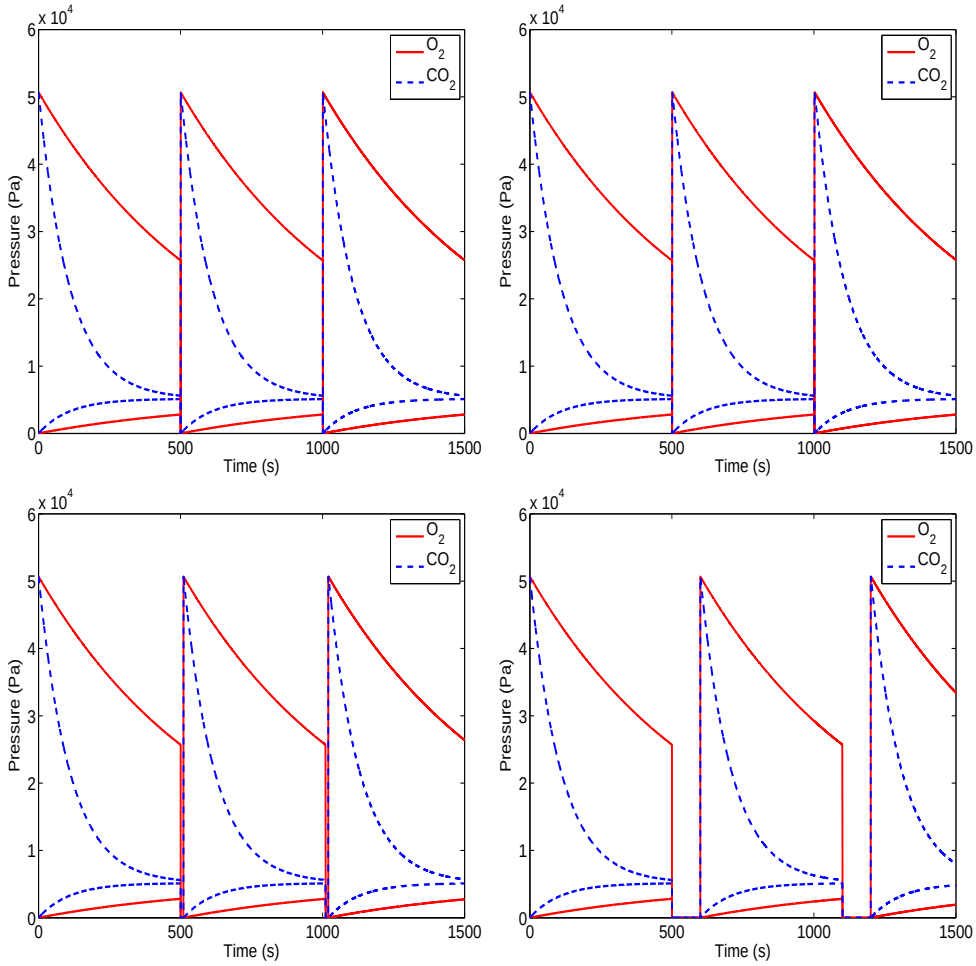

Figure 5.28: Partial pressure evolution of O_2 and CO_2 in upstream and downstream sides with different duration of transfer stage.: 200 ms (top left), 1 s (top right), 10 s (bottom left), 100 s (bottom right). Feed stage duration = 1 s, Free diffusion stage duration : 499 s.

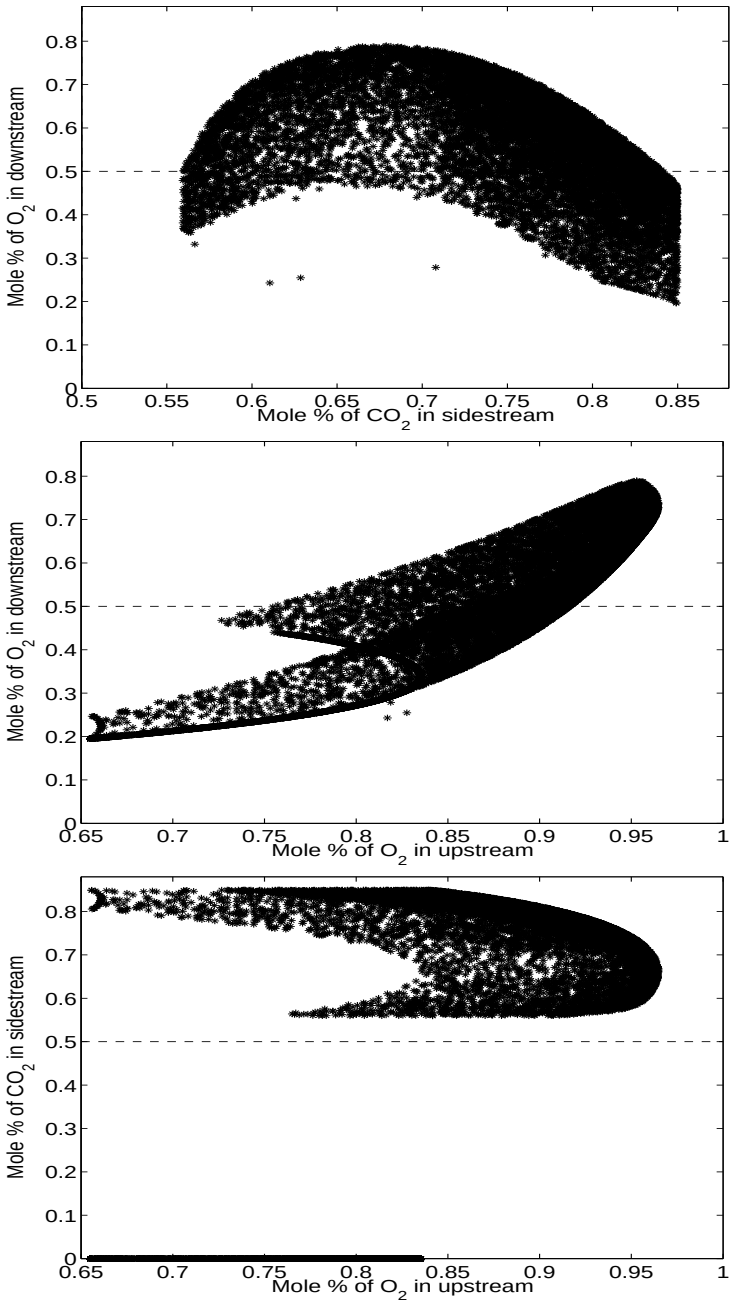

Figure 5.29: Relationship between mole fractions of O_2 in upstream, mole fraction of CO_2 in sidestream and mole fraction of O_2 in downstream. Initial mole fraction of O_2 or CO_2 is represented by dashed lines.

	O_2	CO_2
Diffusion coefficient	$7.9\ 10^{-12}$	$2.0\ 10^{-12}$
Sorption coefficient	$0.91\ 10^{-6}$	$20.9\ 10^{-6}$
Initial mole fraction	0.5	0.5
Membrane thickness	$1\ \mu$m	
Temperature	297.15	
Feed pressure	$1.013\ 10^5$	
Upstream volume	0.0125	
Downstream volume	0.125	
Total diffusion duration	[1 1200]	
Time of starting Sidestream stage	[1 800]	
Sidestream stage duration	[1 10]	
Number of random points	17 085	

Table 5.20: Simulation conditions (S.I. unites). "Total diffusion duration" = duration of Free diffusion stage + Sidestream stage (if exist) + 2^{nd} free diffusion (if exist)

γ, the sidestream option allows to provide a higher purity of the slow gas in upstream.

Similarly to the situation of the short class process based on MMM (Section 5.2), all these factors (purity and/or production ability in each flux) can be indeed maximized at the same time by a multiobjective optimization. However, the value of an objective function (purity or molar recovery of the feed) is in general higher for a single optimization compared to its value in the case of a multiobjective optimization. Consequently, the best enhancements in the three tanks cannot be obtained at the same time, the operating parameters (durations of each stage) should be precisely chosen in order to satisfy different needs.

Taking always the gas pair $\{O_2,\ CO_2\}$ as an example, if O_2 whose permeability is lower is the desired product whose productivity (defined as the number of moles of the desired gas that are collected in corresponding volume divided by the duration of one complete cycle and by the effective membrane surface) and purity (mole fraction) should be optimized, the following optimization problem is set classically as

$$\max_{x_1,x_2,x_3} \begin{pmatrix} O_2 \text{ mole fraction in upstream} \\ \text{Upstream productivity} \end{pmatrix}$$

submitted to:

$$x_1 \geq x_2 + x_3$$

with x_1 total duration of free diffusion, x_2 starting time of sidestream stage and x_3 duration of sidestream stage. This single constraint enforces the use of the sidestream option.

In order to solve this multiobjective optimization problem, the genetic algorithm mentioned in Section 4.3 is applied. The optimized results (10^{th} generation) in form of Pareto zone are given in Fig. 5.30. Similarly to Figs. 5.2, 5.3 and 5.5, a trade-off line with respect to two optimization criteria is given by the genetic algorithm. First, the O_2 mole fraction range determined by the optimization study is close to the conclusion from random combination study, even the optimized value 0.9650 is already represented in Fig. 5.29 (middle and bottom). Thus it can be concluded that the 17 085 random combinations represent well all possible scenarios of the novel process. Secondly, the maximum O_2 mole fraction (0.9650) is logically obtained at lowest productivity. Nevertheless, it should be noticed that the productivity definitions for both short and long class processes are the same. Productivity of short class processes defined in a similar way cannot exceed 10^{-6} mol/m^2.s (Figs. 5.2, 5.3, 5.5, 5.20 and 5.21) whereas in the case of novel processes, its value is in general 1 000 times more important. Consequently, it is highlighted that the long class process productivity loss is much less important with respect to short class processes.

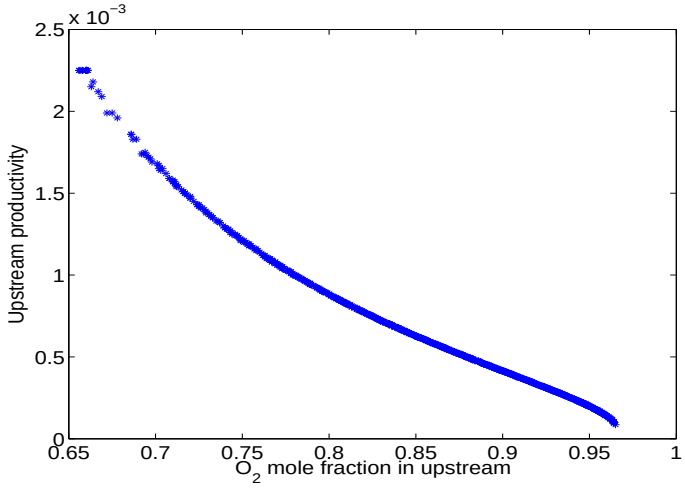

Figure 5.30: Pareto zone for the multiobjective genetic algorithm optimization (10^{th} generation) with respect to O_2 mole fraction in upstream and upstream productivity.

As the number of degrees of freedom of the process is important, the objective functions of optimization can be different. For example, two other criteria

can be proposed in comparison,

1. Mole fraction of desired gas.
2. Recovery ratio, defined by the desired gas mass in corresponding flux over its mass in feed flux.

By defining these two criteria, the novel process with sidestream option is optimized again by the genetic algorithm and compared to the same process with basic option in Fig. 5.31. This latter first confirms that the increase of the volume ratio γ allows to improve the process efficiency. Secondly, choosing sidestream option is an alternative for process optimization. By doing so, the performance at $\gamma = 100$ with basic option can be almost obtained at $\gamma = 10$ with sidestream option.

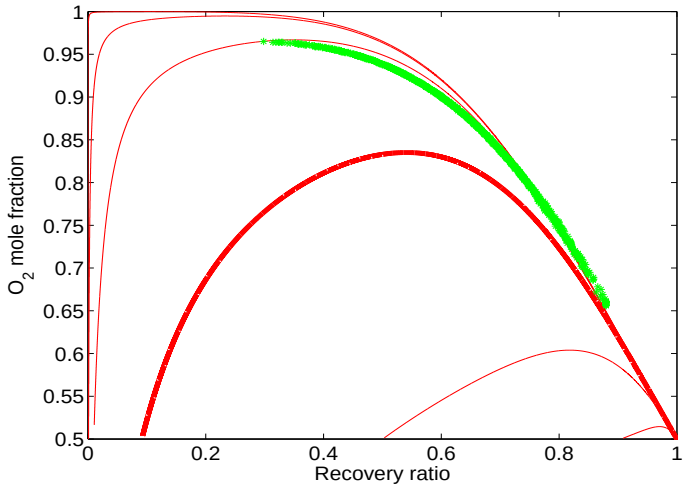

Figure 5.31: Comparison between novel processes using basic option with different volume ratios and optimized sidestream option with volume ratio $\gamma = 10$. Continued red lines: novel process using basic option with different volume ratios γ (0.1, 1, 10, 100, 1 000 and 10 000 from bottom to top respectively). Bold continued red line: $\gamma = 10$. Green stars: optimized novel process using sidestream option with $\gamma = 10$ with respect to O_2 mole fraction and recovery ratio in upstream.

In conclusion, besides increasing the volume ratio γ, the separation efficiency of the novel process can also be improved by choosing the sidestream option. In an example, the sidestream option can almost reach an equivalent of a basic option with 10 times of volume ratio γ. Furthermore, the sidestream option provides more degrees of freedom in operations which make the whole

process more flexible. Finally, the downstream in the case of the sidestream option can be enriched in either the slow or rapid gas according to the needs, which enlarges the application domains of the novel processes.

5.3.2.4 Comparison between the novel process and conventional steady-state operations

In a conventional steady-state membrane operation, one feed flux is introduced into the membrane module and two fluxes (retentate and permeate) are obtained at the outlet. As explained previously, the process with the basic option provides also two similar outlet fluxes: upstream and downstream fluxes. Thus a comparison between two processes can be reasonably performed. Nevertheless, due to the sidestream option, three outlet fluxes are generated by the novel process. A direct comparison seems difficult.

It is shown that the downstream flux of sidestream option can possess the same composition to the feed flux. If this flux is recycled (Fig. 5.32) in the process with the composition close to feed flux, the process generates globally only two outlet fluxes. According to the flux characteristics, a direct comparison between conventional operations and novel process can be readily carried out (Tab. 5.21).

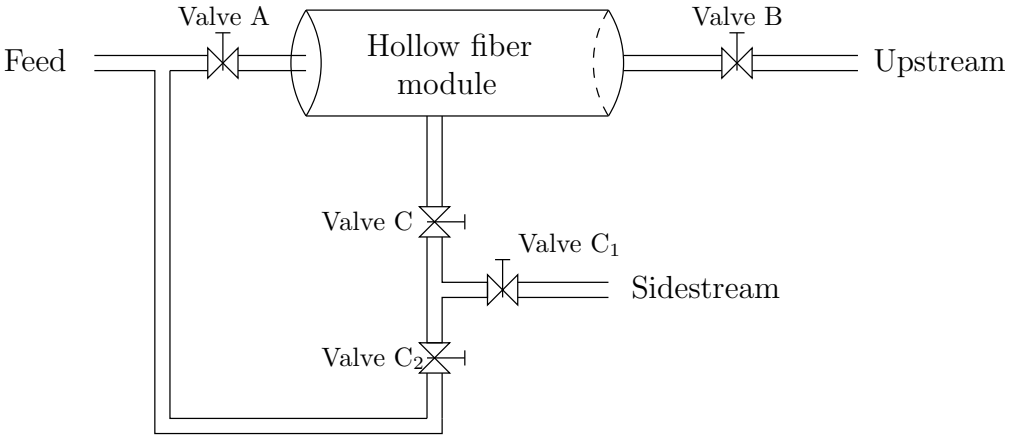

Figure 5.32: Novel process with sidestream option, the downstream flux representing similar composition to the feed is thus recycled.

Based always on the 17 085 random combinations of sidestream option, only the combinations which allow an downstream composition close to the feed are kept in comparison. In other words, the downstream O_2 mole fraction of selected combinations should be 50 % ± 1%.

In comparison, the conventional operations are based on conditions given

by Tab. 5.4 and the pressure ratio Ψ permeate/retentate is fixed to 0.01 for all simulations. Then two criteria: mole fraction and recovery ratio of desired gas, are used in comparison.

	O_2 (slow gas) enriched flux	CO_2 (rapid gas) enriched flux
Conventional operations	Retentate	Permeate
Basic option	Upstream	Downstream
Sidestream option	Upstream	Sidestream

Table 5.21: Flux in comparison for conventional operations and both options of novel process

Thus the comparison results in different ways between conventional processes and both options of novel processes are given in Figs. 5.33, 5.34 and 5.35. As explained in Chapter 2, the conventional processes are represented by two kinds of operations: the perfectly stirred models represent a simple but not efficient choice while the cross flow models represent a more sophisticated but efficient and a widely used choice in industry.

The following conclusions can be drawn:

- It should be noticed first that for all three types of comparison, points close to (1,1) (100% in mole fraction and 100% in recovery ratio) represent the best performance of a process while the poorest performances are close to (0,0) (0% in mole fraction and 0% in recovery ratio). Consequently, points from an efficient process should be concentrated close to (0,0) and far from (0,0).

- Fig. 5.33 shows that with the basic option, for the lower permeability gas enrichment (O_2 in this case) the novel process is not competitive with respect to conventional operations (especially the cross flow module) if the volume ratio γ is less than 10, in terms of both purity and recovery ratio. Nevertheless, if the volume ratio becomes important, the situation is inversed. The novel process becomes more efficient compared to conventional operations. Thus increasing the volume ratio γ is indeed an efficient way to improve the novel process. With regard to the sidestream option, the process efficiency improvement is also highlighted, at $\gamma = 10$, the novel process presents already a better efficiency with respect to conventional operations.

- With regard to the higher permeability gas enrichment (CO_2 in this case), Fig. 5.34 shows that the novel process performance can be improved by increasing the volume ratio γ. However, the sidestream option

is not cost effective, a high purity can only be obtained at very low recovery ratio and decreases rapidly with the recovery ratio. Therefore, the sidestream option is not recommended if both purity and recovery ratio are required for the rapid gas.

- Fig. 5.35 compares both rapid and slow gas purities in corresponding flux. First, the volume ratio increase is confirmed again as a process efficiency improvement in the case of the novel process. Secondly, the effect of the sidestream option is highlighted. In the case of novel processes with basic option and conventional operations, if one flux purity is optimized, the separation effect in another flux will not be significant. However, by using the sidestream option, both outlet fluxes present a very interesting high purity at the same time. Furthermore, this point is especially interesting for the separation of binary mixtures in which both gaseous components are useful. For the black star marked in Fig. 5.35, the recycle ratio defined by the downstream flux over the feed flux is 20.4 %. In general, the recycle ratio of points indicated in Fig. 5.35 is less than 30 %.

In conclusion, the novel process, especially with sidestream option, represents an efficient 'reverse' selectivity with respect to conventional processes: the separation effect of the lower permeability gas is more significant than that of the larger permeability gas. Similar simulations are also performed for gas pairs {He, CH_4} and {O_2,N_2}, comparisons with conventional processes are given in Figs. 5.36 and 5.37, similar conclusions can be obtained. It can be noticed that the membrane thickness is fixed to 0.1 μm for {He, CH_4} and 1 μm for {O_2,N_2} in order to obtain realistic stage durations.

5.3.3 Conclusion of novel processes

By applying cycle operations during much longer durations than the time-lag, a novel process is designed then novel within this thesis. As the novel process belongs to the family of long class processes, its productivity loss is in general much less important than that of short class processes. The upstream exhaustion rate (or the recovery ratio in downstream) can also be significant as shown in Figs. 5.34, 5.37 (middle) and 5.36 (middle). Consequently, two important classical drawbacks of short class processes are successfully avoided. On the other hand, with the novel process, valve operations are much easier to control with respect to short class processes. Moreover, the effective membrane used in the process can be made very thin to improve productivity.

Two options are given according to the operating complexity. Within the frame of basic option, the process performance can be readily improved by

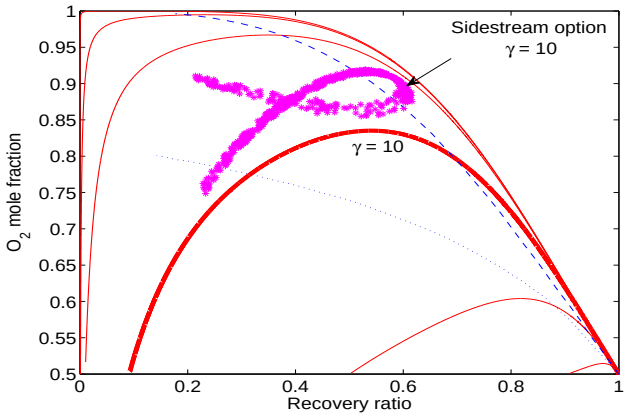

Figure 5.33: O_2 recovery ratio of O_2 enriched flux in function of O_2 mole fraction in the same flux (Tab. 5.21). Continued red lines: novel process using basic option with different volume ratios γ (0.1, 1, 10, 100, 1 000 and 10 000 from bottom to top respectively). Bold continued red line: $\gamma = 10$. Dashed blue line: conventional operations using cross flow modules. Dotted blue line: conventional operations using perfectly stirred modules. Green stars: novel process using sidestream option with $\gamma = 10$ and the downstream flux is recycled.

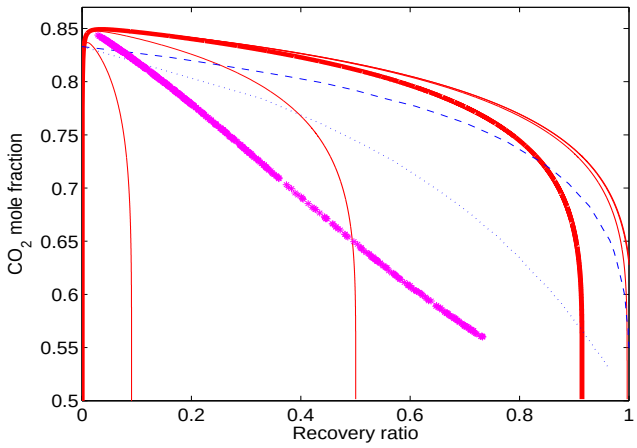

Figure 5.34: CO_2 recovery ratio of CO_2 enriched flux in function of CO_2 mole fraction in the same flux (Tab. 5.21). Continued red lines: novel process using basic option with different volume ratios γ (0.1, 1, 10, 100, 1 000 and 10 000 from bottom to top respectively). Bold continued red line: $\gamma = 10$. Dashed blue line: conventional operations using cross flow modules. Dotted blue line: conventional operations using perfectly stirred modules. Green stars: novel process using sidestream option with $\gamma = 10$ and the downstream flux is recycled.

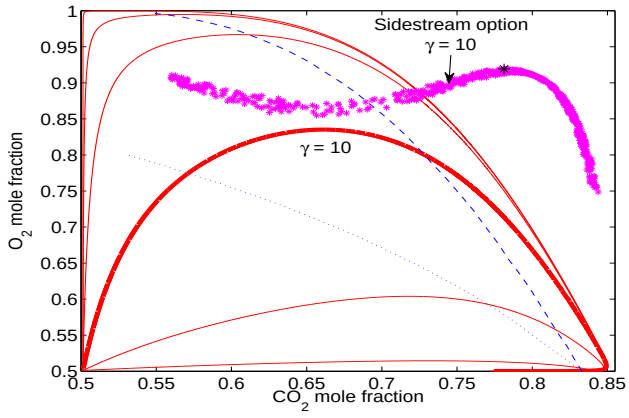

Figure 5.35: CO_2 mole fraction in CO_2 enriched flux in function of O_2 mole fraction in O_2 enriched flux (Tab. 5.21). Continued red lines: novel process using basic option with different volume ratios γ (0.1, 1, 10, 100, 1 000 and 10 000 from bottom to top respectively). Bold continued red line: $\gamma = 10$. Dashed blue line: conventional operations using cross flow modules. Dotted blue line: conventional operations using perfectly stirred modules. Green stars: novel process using sidestream option with $\gamma = 10$ and the downstream flux is recycled. Black star: example point representing a recycle ratio of 20.4 %.

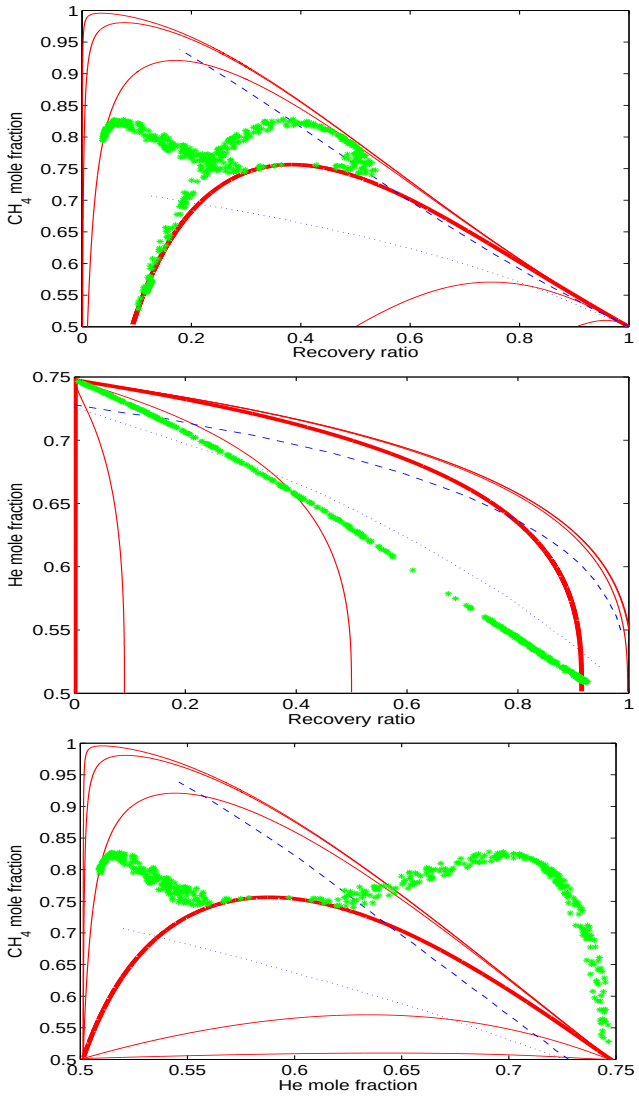

Figure 5.36: Comparison between conventional processes and novel processes with both basic and sidestream options. Top: CH_4 recovery ratio of CH_4 enriched flux in function of CH_4 mole fraction in the same flux. Middle: He recovery ratio of He enriched flux in function of He mole fraction in the same flux (Tab. 5.21). Bottom: He mole fraction in He enriched flux in function of CH_4 mole fraction in CH_4 enriched flux (Tab. 5.21). Continued red lines: novel process using basic option with different volume ratios γ (0.1, 1, 10, 100, 1 000 and 10 000 from bottom to top respectively). Bold continued red lines: $\gamma = 10$. Dashed blue lines: conventional operations using cross flow modules. Dotted blue line: conventional operations using perfectly stirred modules. Green stars: novel process using sidestream option with $\gamma = 10$ and the downstream flux is recycled.

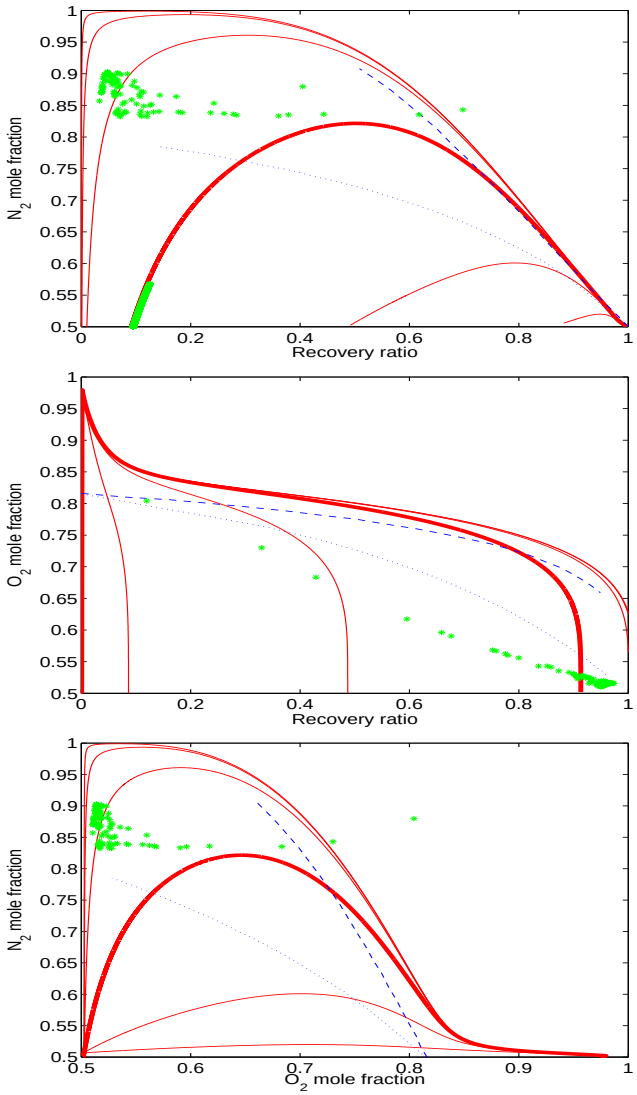

Figure 5.37: Comparison between conventional processes and novel processes with both basic and sidestream options. Top: N_2 recovery ratio of N_2 enriched flux in function of N_2 mole fraction in the same flux. Middle: O_2 recovery ratio of O_2 enriched flux in function of O_2 mole fraction in the same flux (Tab. 5.21). Bottom: O_2 mole fraction in O_2 enriched flux in function of N_2 mole fraction in N_2 enriched flux (Tab. 5.21). Continued red lines: novel process using basic option with different volume ratios γ (0.1, 1, 10, 100, 1 000 and 10 000 from bottom to top respectively). Bold continued red lines: $\gamma = 10$. Dashed blue lines: conventional operations using cross flow modules. Dotted blue line: conventional operations using perfectly stirred modules. Green stars: novel process using sidestream option with $\gamma = 10$ and the downstream flux is recycled.

increasing the downstream/upstream volume ratio γ. If this latter is larger than 100, the novel process becomes competitive with respect to conventional steady-state operations. Sidestream option is recommended as another method to improve the process efficiency in terms of selectivity. By adding the so called sidestream, the process possesses more degrees of freedom. First, a performance of basic option at $\gamma = 100$ can be obtained at $\gamma = 10$ if the sidestream option is adopted. Furthermore, any component of a binary gaseous mixture can be purified and collected with a high recovery ratio. Finally, by arranging stage durations in one cycle, the downstream flux can be transformed to be a recycle flux with the same composition as the feed flux. In that case, a spectacular separation is observed: two fluxes of high purity on different gaseous components are obtained at outlet of the process. To do so, the recycle ratio defined by recycle flux divided by feed flux is in general less than 30 %.

It can be noticed that the novel process is initially designed for gas separation using dense membranes. However, it is rather flexible and the idea can be readily extended. For example, the process is also theoretically applicable for liquid separation. Furthermore, porous membrane can also be another option for the novel process.

5.4 Conclusion of case studies

In this chapter, three cyclic processes are investigated by means of simulation and optimization studies. First, it should be noticed that the three processes are based on the same hollow fiber module, the differences between them are located in valve operations. Advantages and drawbacks of short class process based on Paul's idea using homogeneous membranes are first confirmed by our studies. As indicated in previous studies, on one hand, the process can indeed provide spectacular selectivity improvements. Nevertheless, on the other hand, the huge productivity loss and no upstream exhaustion make this kind of process difficult to be implemented largely in industry. The most probable application of short class processes based on homogeneous membranes might be limited to rare gas separations. Similarly to conventional processes, replacing homogeneous membrane by Mixed Matrix Membrane is also an interesting performance improving method for short class processes. By doing so, both productivity and upstream exhaustion ratio can be significantly increased. Consequently, the application domains of short class processes are thus enlarged. Finally, by abandoning Paul's idea, a novel cyclic process with significant upstream exhaustion is investigated as the last case study. This novel process belongs to long class and the process presents much less unavoidable drawbacks of cyclic processes. Even if its selectivity improvement is much

less significant compared to short class processes, the novel process provides more degrees of freedom in operations. Consequently, a properly designed novel process can be rather competitive with respect to existing membrane processes for gas separations in terms of both purity and recovery ratio.

Chapter 6

Experimental development of a cyclic process design

> It would be possible to describe everything scientifically, but it would make no sense; it would be without meaning, as if you described a Beethoven symphony as a variation of wave pressure.
>
> Albert Einstein

According to Section 5.3, one of the key issue of the novel process is the partial pressure evolution for a given gas during the 'free diffusion to pressure equilibrium' (Section 4). Valve opening conditions are all defined based on these evolution curves. In this chapter, pressure evolution curves are obtained by experiments in LRGP (Reaction and Process Research Laboratory in Nancy) then compared to simulation results. If the comparison is successful, the simulation can be validated and the novel process will be firmly supported. The validation is performed first for pure gas (nitrogen) with respect to pressure then for a given binary mixture (air) with respect to mole fraction of each component. Furthermore, it should be noticed that this validation design can be readily transformed to the novel process by simply adding gas tanks and properly programing valve opening durations.

6.1 Materials

6.1.1 Membrane module

Among glassy polymers, polyphenylene oxide (PPO, also mentioned in the literature as polyphenylene ether, PPE) possesses a glass transition temperature (T_g) ranging from 212 to 218 ℃. It has been reported to perform close to or higher than the Robeson's trade-off line [Albers et al., 1992]. In industry, the PPO membrane particularly deals with O_2/N_2 separation. It should be noticed that both gaseous components are not dangerous and their quantitative measurements are accurate and relatively easy in laboratory scale. Consequently, the commercial PPO module supplied by Parker Filtration and Separation B.V. (The Netherlands) is used in our experimental developments.

902 PPO fibers are disposed into a hollow fiber module, where the inside and outside diameters of each fiber are 370 and 520 μm respectively. The feed gas is introduced inside the fibers which is considered as upstream volume and the permeate is collected on the free volume between fibers and the module which is considered as downstream. The selective dense layers of the hollow fibers are located at the outside and the permeances of the gaseous components are calculated based on the outer surface area of hollow fibers [Pourafshari et al., 2006]. The permeation area is calculated as 0.3829 m^2. All experiments were performed at room temperature and considered as isothermal operations. The dimensional drawing of the module is given in Fig. 6.1.

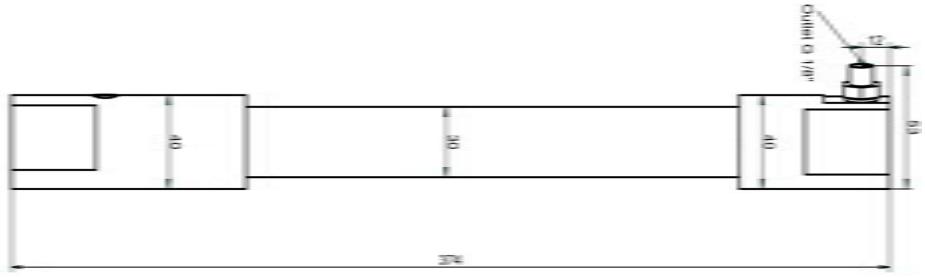

Figure 6.1: Dimensional drawing of the membrane module used in the experimental proof. PICCOLO 243, supplied by Parker Filtration and Separation B.V. (The Netherlands). The length is given in millimeter.

6.1.2 Accessories

4 pneumatic valves (VP 214 TT 6mm, supplied by FLOWLINK S.A., France) drived by compressed air are used in this experiment to control flow directions.

The upstream and downstream pressures are read from two highly precise pressure transmitters PR 33X 5/10 supplied by KELLER (Germany) Pressures are recorded automatically every 0.04 second. It should be noticed that the valves have 0.2 s delay of responses. Thus recorded values are systematically corrected.

A MGA 3000 multi-gas analyzer (ADC) is used in experiments in order to measure O_2 mole fraction in a binary gas mixture. The infrared analyzer can measure O_2 mole fraction in a mixture from 0 to 100 %. The resolution of the analyzer is 0.1% with an intrinsic accuracy of 1.0%.

6.1.3 Gas

2 gas flows have been used in experiments:

1. N_2, $\mathcal{P}_{N_2} = 5.49$ barrer [Jinjikhashvily et al., 2011], as the pure gas.
2. Compressed air, (considered as 19.5% O_2 and 80.5% N_2, O_2 mole fraction is measured by the multi-gas analyzer) $\mathcal{P}_{O_2} = 3.9\mathcal{P}_{N_2}$ [Pourafshari et al., 2006], as the mixed gas.

Since the PPO's transition temperature ranges from 212 to 218 ℃ [Albers et al., 1992], at room temperature, the PPO acts as a glassy polymer. The simple Dual Mode Model cannot describe correctly the competitive behaviors with important permeate pressures, numerous sophisticated models have been tested in order to provide a perfect description of the phenomena [Esekhile et al., 2011, Omole et al., 2010, Thundyil et al., 1999]. However, for sake of convenience, the basic transport model (Eq. (4.26), where the permeability $\mathcal{P}_k = k_{Dk}\mathcal{D}_k$ is thus constant) for rubbery membranes is still widely used in approximative studies and qualitatively good results have been obtained [Koros and Fleming, 1993] especially at a pressure not too high. In our experiments, the maximum upstream will be lower than 8 bar while that of downstream will not be larger than 5 bar. Consequently, the sorption curve should be probably quasi linear. As explained in Section 4.1.8, for all kinds of membranes in Polymer Handbook [Brandrup and Immergut, 1989], only basic transport model parameters are provided as transport data. Consequently, in our experimental proof, the permeability $\mathcal{P}$ of a given gas is considered as constant and this assumption will be further checked in our experiments.

6.2 Design of experiment pilot

The design of experiment is given in Figure 6.2. The membrane module is connected to four pneumatic valves: valves A and D to upstream, then valves B and C to downstream. Valve A is connected to the feed. Valves B and D are connected to the same vacuum pump. Then valve C controls the gas flux going to the gas analyzer. The upstream pressure transmitter (0-10 bar) is installed between the valve A and the module, while the downstream pressure transmitter (0-5 bar) is installed between the valve C and the module.

A receiving tank of about 200 ml with a tap at the outlet is placed between the valve C and the gas analyzer. The tank is initially emptied by vacuum pump. This system serves first as a gas collector which accumulates the gas from the downstream side of the module by means of pressure gradient. Secondly, its outlet flow is controlled manually by a tap in order to deliver a continuous flux at specific pressure and flow rate for the gas analyzer.

The instantaneous upstream/downstream pressure variations are monitored thanks to a computer. Thus for a pure gas test, the pressure profile can be obtained directly in the computer. However, for a gas mixture test, the corresponding mixture will be sent to the analyzer in order to measure the O_2 mole fraction.

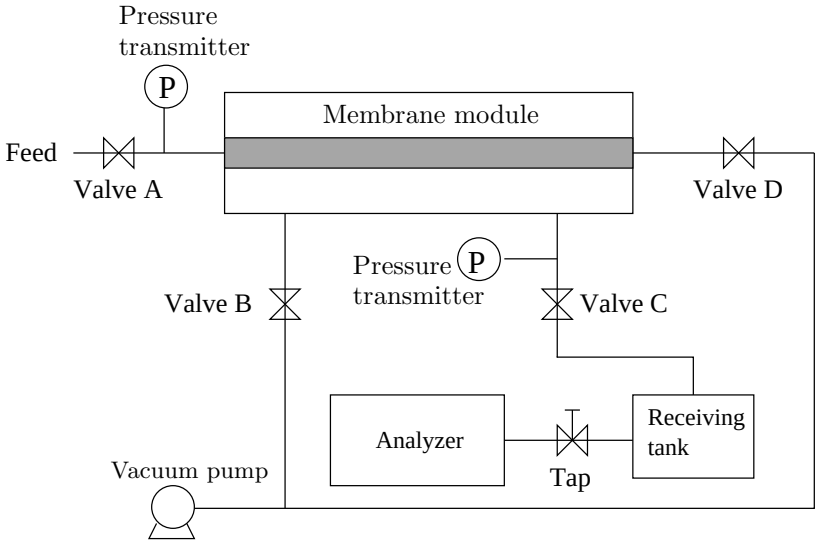

Figure 6.2: Experiment design

The whole system was assembled in the mechanical service of the LRGP then the experiments were performed in the laboratory of MSP (Membranes, Separation Processes) team.

6.3 Results and discussion

6.3.1 Verification of airtightness

The first step of experiments is the verification of airtightness. To do so, the whole system is initially at room pressure and all valves are closed. Then the upstream side is fed to a higher pressure by opening valve A. After several seconds, all valves are closed again, the pressure evolutions in upstream and downstream are recorded. This experiment is called "free diffusion to pressure equilibrium" test in Section 4.1.6. In Fig. 6.3, it can be noticed that when both upstream and downstream pressures go along the equilibrium, no obvious pressure loss is observed during more than 5 seconds. As a result, it can be concluded that the system airtightness is confirmed at least for a duration of about 5 seconds.

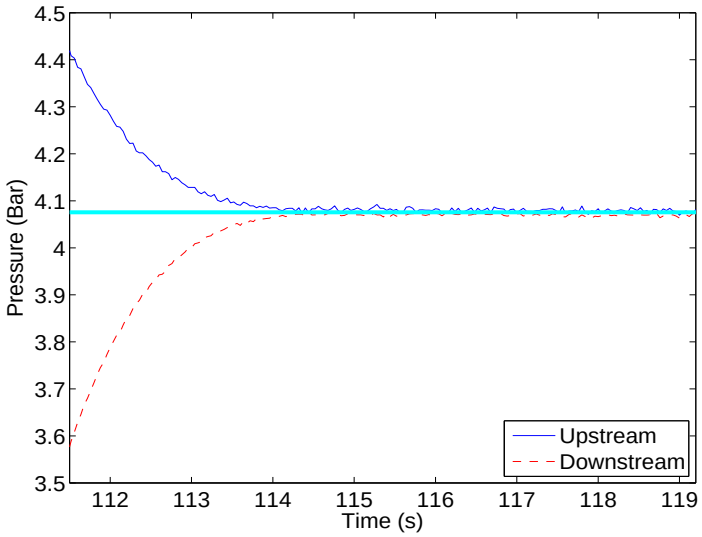

Figure 6.3: Airtightness verification, performed on 02/13/2011

6.3.2 Determination of volume ratio and effective membrane thickness

The volume ratio is a key parameter to correctly simulate pressure evolution in both upstream and downstream sides of the membrane module. The actual volume ratio should not only involve the respective volume in the module, but also take into account the dead volume in connecting tubes and other parts of the system. This latter can only be determined experimentally.

As explained previously, the whole membrane with its support material is about 25 μm. The effective fiber length is measured as 260 mm in LRGP. However, the effective selective thickness is much less [Pourafshari et al., 2006] and not communicated by the supplier. This latter is another key issue of simulation.

Consequently, first the approximative volume ratio and the effective membrane thickness have been determined by experiments, then an optimization method is applied in order to refine the solution.

Determination of approximative values

A similar experiment to "free diffusion to pressure equilibrium" test is performed. The upstream side of the module is first filled by feed gas (air or nitrogen) to a given pressure. Then all valves are closed and pressures in corresponding sides are recorded via pressure transmitters until reaching the pressure equilibrium between upstream and downstream sides. Assuming that the membrane is thin and all concerned gas is perfect, the residual gas in the membrane is then neglected with respect to the gas quantity in upstream and downstream. Since the system airtightness is confirmed, the mass conservation in the system can be written in following way for two time points A and B,

$$P_u^A V_u + P_d^A V_d = P_u^B V_u + P_d^B V_d \tag{6.1}$$

where P_u^k and P_d^k are the upstream and downstream pressures respectively (Fig. 6.4). Thus the volume ratio γ can be determined by

$$\gamma = \frac{V_d}{V_u} = \frac{P_u^B - P_u^A}{P_d^A - P_d^B} \tag{6.2}$$

In this way, the volume ratio γ was determined by 300 time couples using first compressed air then pure nitrogen. By doing so, the average volume ratio is estimated to 0.72. The latter will be used as the approximative value for exact volume ratio determination.

With regard to the effective membrane thickness, a similar "free diffusion to pressure equilibrium" test is simulated by considering the volume ratio as 0.72. The effective membrane thickness is roughly modified in simulation in order to make the necessary time to reach the pressure equilibrium close to the experimental values (about 5 seconds). By doing so, the approximative effective membrane thickness L is found as 0.1 μm. It can be noticed that the effective membrane is very thin, thus the assumption that the residual gas in it can be neglected with respect to gases in upstream and downstream is acceptable.

Parameter determination by optimization

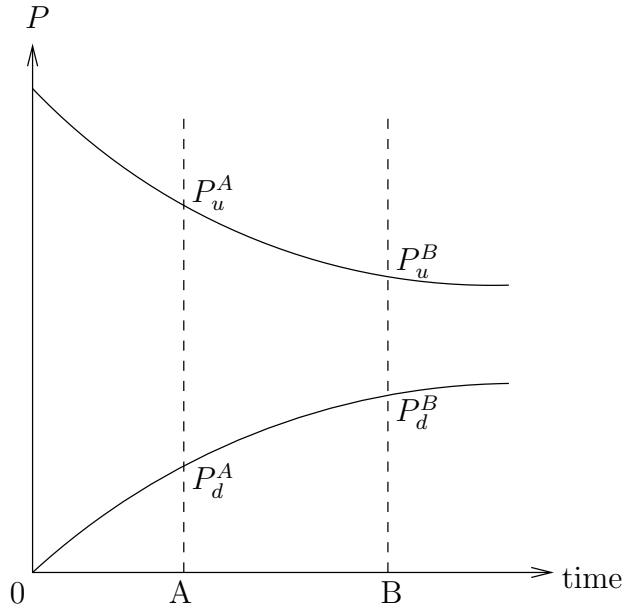

Figure 6.4: Method to determine the volume ratio

Based on the approximative values for the volume ratio and the effective membrane thickness, an optimization study was performed by using a second experiment. In order to reduce the influence of a second gas in modeling in the case of glassy polymers [Koros, 1980], pure nitrogen is used in this experiment.

The whole module with its accessories is first purged by nitrogen. Then the upstream side of the module is filled and maintained to a given pressure by feeding with pure nitrogen. The pressure evolution in downstream side is recorded until it reaches the upstream pressure. The downstream pressure evolutions for two consecutive cycles are given in Fig. 6.5, where the fixed upstream pressure curve is also mentioned. One notices that the experiment reproducibility is confirmed since two curves are almost superimposed.

Using the approximative values for the volume ratio and the effective membrane thickness, the previous experiment can be simulated by solving corresponding equations (Eq. (4.26) and its boundary conditions) then the theoretical downstream pressure evolution curve is obtained. The simulation is started close to but not at the experimental beginning point of each cycle in order to avoid the delay of valve opening. At a chosen starting point, the initial upstream pressure for simulation is obtained by averaging all experimental upstream pressures (which should be constant theoretically) while the initial downstream one is obtained by averaging the downstream pressures of two experiments at the start point.

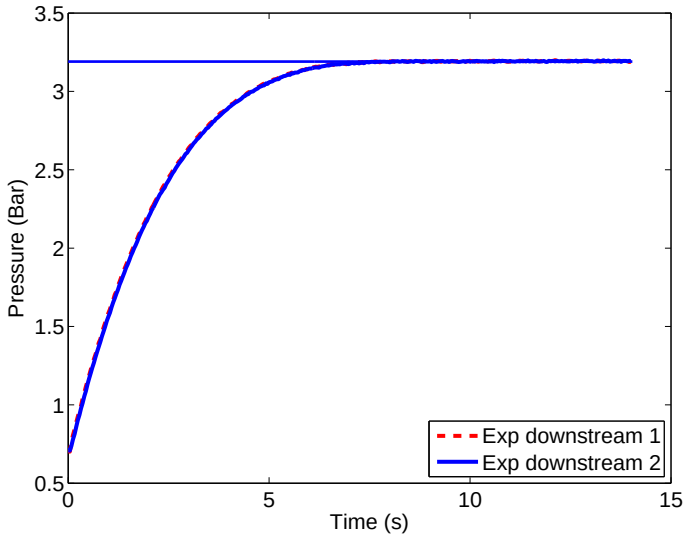

Figure 6.5: Experimental pressure evolutions in downstream by imposing a fixed upstream, performed on 02/13/2012

A relative error ψ for pressure P between experimental curves and the simulated one is defined as

$$\psi_P = \sum_{i=1}^{n} \frac{|\bar{P}_{exp} - P_{sim}|}{\bar{P}_{exp}} \tag{6.3}$$

where $\bar{P}_{exp}$ is the average pressure of two experiments at a given moment (Fig. 6.5), P_{sim} is the simulated pressure at the same moment and n is the total number of record points for one experimental curve. Consequently, with the optimized volume ratio γ and effective membrane thickness L, this relative error should be minimized. As a result, the optimization problem is set as follows

$$\min_{L,\gamma}(\tau)$$

with initial values

$$L \approx 0.1\ 10^{-6}\ \text{(m) and } \gamma \approx 0.72$$

Since this is an unconstrained non-linear optimization problem, Matlab code $fminsearch$ applying a Nelder-Mead simplex algorithm [Lagarias et al., 1998] is used here to perform the calculation. By means of the optimization, it is found that

$$L = 0.059\ 10^{-6}\ \text{(m) and } \gamma = 0.76$$

which are rather close to their approximative values. It can be noticed that during another experience in LRGP based on the same module, the effective membrane thickness is calculated as 0.05 μm by means of averaging several permeance measurements. This agreement allows to validate the determination work by optimization study. Furthermore, the 0.05 μm was determined by considering the N_2 permeability as 3.52 barrer, whereas in our study, this permeability is considered as 5.49 barrer. It should be noticed that many PPO variations are available commercially and their proper permeabilities are often confidential thus not communicated by the supplier. Consequently, if the same permeability was used, a better agreement could be expected between two methods. In following research, the permeability of 5.49 barrer will be kept and the effective membrane thickness is considered as 0.059 10^{-6} m.

Using the optimized values, the pressure evolution in downstream is simulated then compared to performed experimental results in Fig. 6.6. Although the simplified model with only two transport parameters $\mathcal{D}_D$ and k_D is used in simulation, a good agreement between simulation and experiments can be highlighted in the comparison figure.

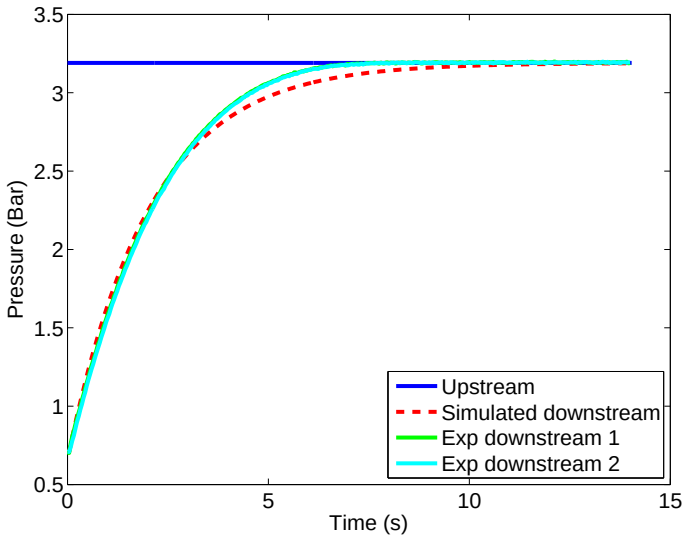

Figure 6.6: Simulated pressure evolution in downstream by imposing a fixed pressure at upstream with optimized volume ratio γ and effective membrane thickness L compared to experimental values, performed on 02/13/2012

In order to validate the optimization results, the same experiment was performed subsequently by applying another upstream pressure. Experimental results with simulated ones are given together in Fig. 6.7. Again, both

experimental and simulated curves are nearly superimposed. The optimization results are thus validated. Consequently, the determined volume ratio $\gamma = 0.76$ and effective membrane thickness $L = 0.059$ μm will be used in the following simulations as basic parameters.

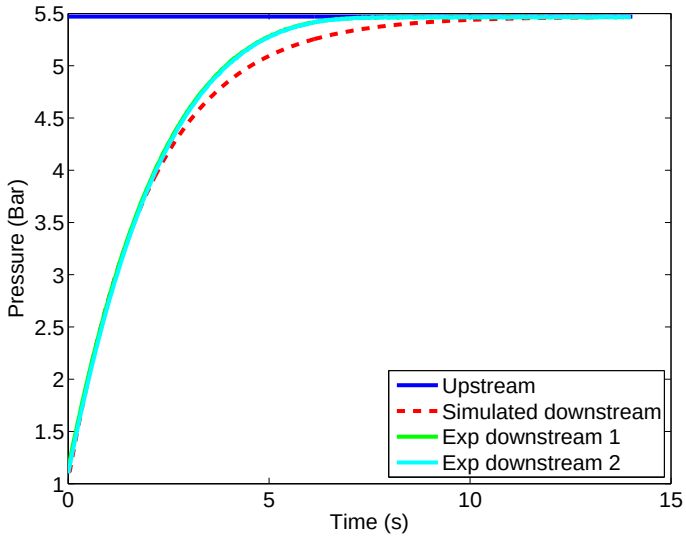

Figure 6.7: Validation of optimization results (volume ratio γ and effective membrane thickness L) compared to experiments performed on 02/20/2012

6.3.3 Pure gas permeation experiments (nitrogen)

For pure nitrogen permeation tests, the following operations are used: the whole system is first purged by nitrogen during 10 minutes. The same tests were repeated twice in two different days in order to verify the experiment reproducibility. Then the upstream side is filled by opening valve A to a high pressure. This stage lasts 1 second. After that, all valves are closed during 10 seconds in order to obtain a complete pressure evolution curve of "free diffusion to pressure equilibrium" tests. Then, valves B and D are opened at the same time in order to evacuate both sides of membrane to a low pressure by means of a vacuum pump. This stage lasts also 10 seconds. Consequently, one cycle contents 3 stages (feed stage, free diffusion stage and evacuation stage) and in total it lasts 21 seconds.

The results of a pure nitrogen permeation test is shown in Fig. 6.8, it is obviously observed that the experiment reproducibility is rather good, pressure curves obtained at different cycles are similar to each other. The "pseudo steady state" is established as soon as the first cycle as predicted by simulation in Fig. 5.28.

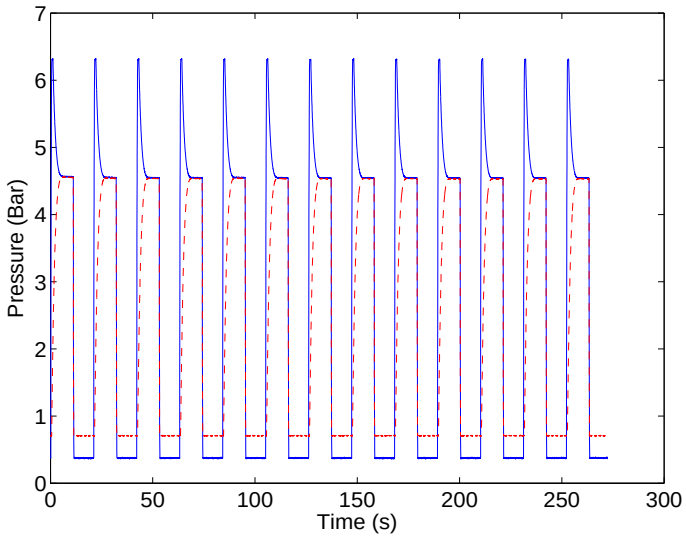

Figure 6.8: Consecutive experimental pressure evolutions of pure nitrogen in the case of a "free diffusion to pressure equilibrium" test (performed on 02/14/2012).(Continued blue lines for upstream pressure and dashed red lines for downstream pressure)

It can be noticed that during the feed stage and evacuation stage the mass balance is difficult to establish since the membrane module is connected to external environment. Thus the membrane module is not a conservative system, the simulation will be difficult and not accurate. Therefore, the simulation in comparison is not performed for complete cycles, but only for a part of the free diffusion stage which is the key issue of the novel process. By choosing a start and an end point, partial pressures of nitrogen are perfectly known. Moreover, during this stage, the membrane module is completely isolated by closing all valves and the permeation behavior is uniquely dominated by the diffusion phenomena.

Taking experimental upstream and downstream pressures at a given time in the free diffusion stage, successive pressure evolutions can be thus simulated until the pressure equilibrium. In Fig 6.9, experimental pressure evolutions of 2 consecutive cycles are compared to simulated results. First, pressure curves of 2 cycles are superimposed perfectly which confirms again the experiment reproducibility and the quick establishment of the "pseudo steady state". Secondly, in spite of slight difference to experimental results, the simple transport model where the permeability $\mathcal{P}$ is considered as constant is consistent with experimental results, at least qualitatively. Thus it can be concluded that for PPO membranes under relative low pressure (4-8 bar), the hole filling process (Langmuir adsorption) influence is not clearly observed in transport.

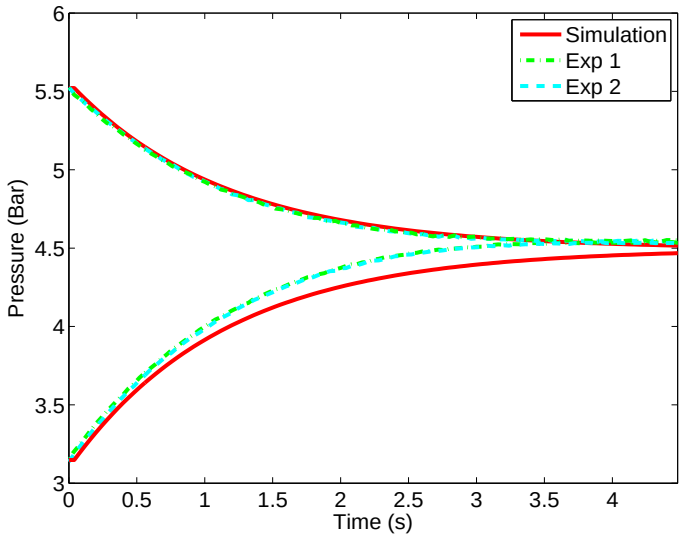

Figure 6.9: Comparison between two experimental pressure evolutions of nitrogen of the free diffusion stage of a "free diffusion to pressure equilibrium" test (performed on 02/14/2012) and simulated results.

The same experiment was performed again another day by modifying the feed pressure. The durations are 0.5, 10 and 5 second for feed stage, free diffusion stage and evacuation stage respectively. In Figs. 6.10 and 6.11, experimental and simulated curves are compared. Similarly to conclusions from Fig. 6.9, the experiment reproducibility is confirmed and the simulated results based on constant permeability $\mathcal{P}$ is qualitatively consistent with experimental data.

As explained previously, the slight deviation of the simulation can be explained first by the concentration dependence of permeability which is not taken into account in our simulations. Secondly, the difference between experiments and simulations can also be explained by the fact that all operations might not be strictly isothermal. It is well known that the gas permeability depends strongly on the temperature. During the feed stage, important high pressure flow enters in the membrane module. This procedure might not be isothermal if the feed pressure is important. Furthermore, for the evacuation stage, the pressure is reduced rapidly by the vacuum pump, which could also reduce the module temperature especially in the case of deep vacuum. Lastly, although the PPO membrane is known to show a stable permeation rate with time [Pourafshari et al., 2006], the declination of the permeability cannot be completely avoided after numerous tests.

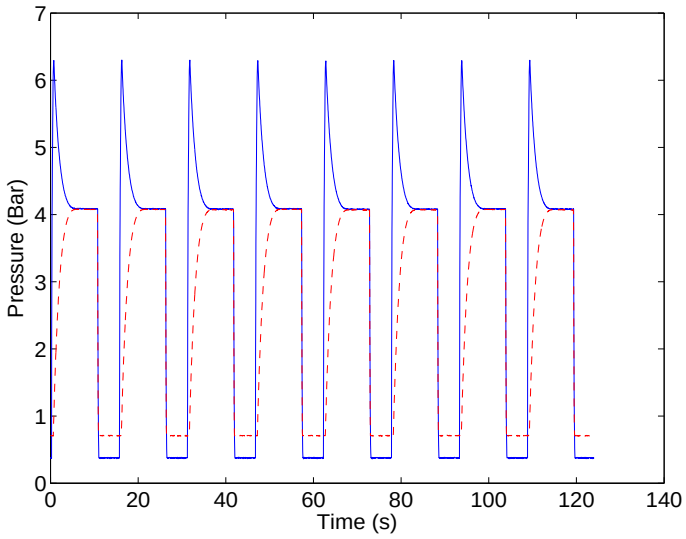

Figure 6.10: Consecutive experimental pressure evolutions of pure nitrogen in the case of a "free diffusion to pressure equilibrium" test (performed on 02/15/2012).(Continued blue lines for upstream pressure and dashed red lines for downstream pressure)

6.3.4 Mixed gas permeation experiments (air)

In the previous section, the pure gas permeation is validated by means of pressure measurements. The same apparatus is used for mixed gas permeation experiments in order to validate the mole fraction evolution in the module. As explained previously, the gas composition can be given by the multi-gas analyzer which is only sensitive to O_2 in the case of $\{O_2,N_2\}$ mixture.

For sake of simplicity, the upstream side is maintained at a high pressure by the feed. As a result, the upstream composition can be considered as constant in our experiments. The only unknown to measure in the experiment is the gas composition in downstream side or O_2 mole fraction in downstream. On the other hand, it should be noticed that the time to establish the pressure equilibrium in the case of a fixed upstream pressure is in general longer than that in the case of a "free diffusion to pressure equilibrium" which can be concluded by comparing Figs. 6.7 and 6.9. Thus the relative long duration allows an easier measurement.

Fig. 6.13 shows downstream pressure evolutions of the first two consecutive cycles in a case of 15 s of constant high pressure in upstream and 3 s of vacuum. First, the 0.2 s delay of response in valves is highlighted since the pressure increasing starts at 0.2 s instead of 0 s. Secondly, if the pressure equilibrium is defined by the relative difference between upstream and downstream pressures

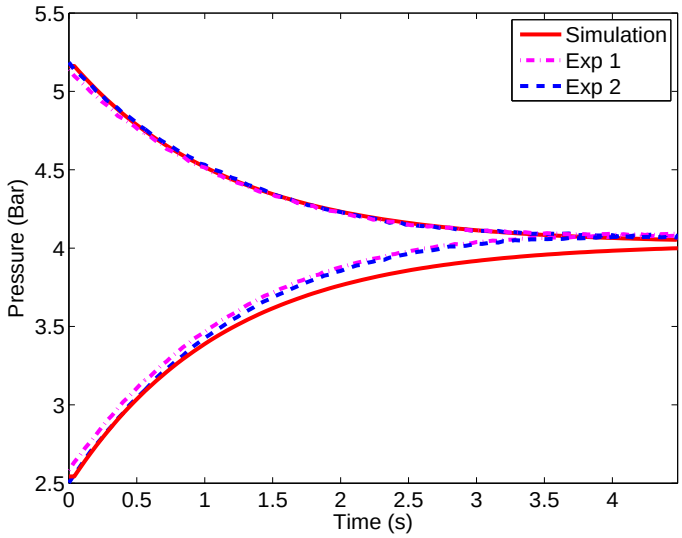

Figure 6.11: Comparison between two experimental pressure evolutions of nitrogen of the free diffusion stage of a "free diffusion to pressure equilibrium" test (performed on 02/15/2012) and simulated results.

is less than 0.1 %, the equilibrium is reached within less than 10 s. At pressure equilibrium, both upstream and downstream O_2 mole fractions should be equal to that in the feed (19.5%).

Consequently, the downstream composition measurements were performed in following way. The whole apparatus was first emptied by vacuum pump and all valves were initially closed. Then following cyclic operation was performed:

1. High pressure stage. Only valve A is opened in order to fill and maintain the upstream side of the module to the high pressure. Diffusion occurs through the membrane. The duration of this stage is variable.

2. Transfer stage. Only valve C is opened for a very short duration, in order to transfer some downstream gas into the receiving tank. This opening duration is set to 0.1 s due to the minimum opening duration of the pneumatic valve and the required minimum pressure for the gas analyzer. Downstream gas is thus transfered into the receiving tank due to the pressure gradient. Then the gas in it is continuously sent to the gas analyzer at the setpoint flow rate (between 100 and 1000 ml/min) and pressure (between 1 and 1.5 bar).

3. Vacuum stage. Only valves B and D are opened at the same time in order to completely empty both upstream and downstream sides of the

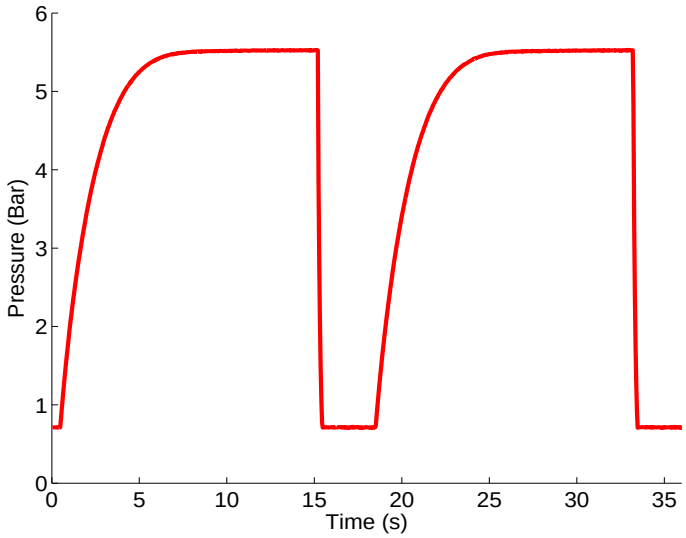

Figure 6.12: Experimental downstream pressure evolution in the case of a constant upstream pressure test (performed on 03/12/2012). The two first consecutive cycles are represented.

module. Then all valves are closed again and the next cycle is started. This stage is set to 5 s for all tests.

These operations are summarized in Tab. 6.1. Being given a duration of the high pressure stage, cycles are repeated. A gas mixture with a resulting composition is continuously accumulated in the downstream tank and then sent to the analyzer. Therefore, the mole fraction of O_2 at the end of a given high pressure stage is indicated by the gas analyzer. As shown previously, the experiment reproducibility is excellent. Performing such cycles to determine the downstream composition for a given duration of the high pressure stage is equivalent (Fig. 6.13) to consider a dynamic simulation where the concentration in the downstream side is considered at a time equal to the previously mentioned duration.

By setting different durations of the high pressure stage (Tab. 6.1), the evolution of the O_2 mole fraction in downstream side can be thus established experimentally and compared to the simulation results (Fig. 6.13).

It can be noticed in Fig. 6.13 that the first experimental point is obtained by setting the high pressure stage duration as 0.5 s. Tests for a shorter duration were also performed. Nevertheless, due to the low diffusion duration, the downstream pressure remains very low and the required pressure and flow rate for the gas analyzer cannot be stably reached at the outlet by regulating the tap. Furthermore, since the gas quantity in the downstream side is little,

Valve	A	B	C	D	Duration
High pressure stage	o	-	-	-	Variable from 0.5 to 10 s
Transfer stage	-	-	o	-	0.1 s
Vacuum stage	-	o	-	o	5 s

Table 6.1: Cyclic operations of experimental validation for a mixed gas. ("o" for open and "-" for closed.)

the residual gas due to the imperfect vacuum in the receiving tank cannot be neglected any more. Consequently, the measurement is not considered as accurate and not taken into account in comparison.

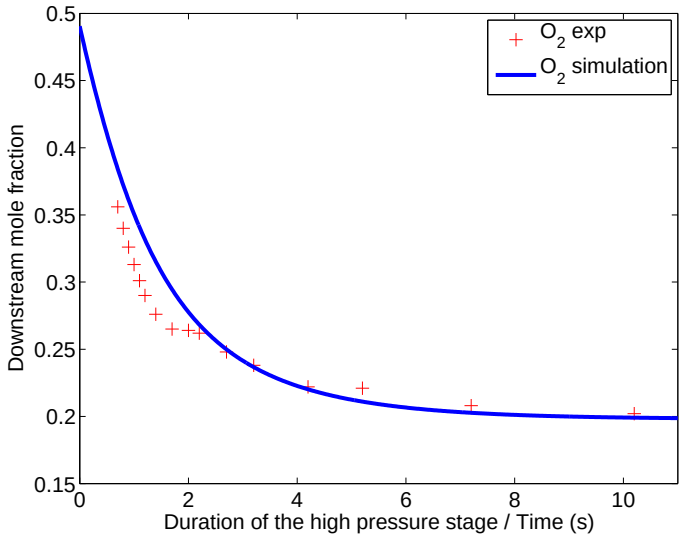

Figure 6.13: Comparison between experimental mole fraction evolution in downstream in the case of a fixed upstream pressure test (performed on 03/12/2012) and simulated results. "Duration of the high pressure stage" in the x-axis refers to experimental results and "Time" refers to simulation results.

Fig. 6.13 shows a reasonable agreement between the experimental O_2 mole fraction evolution in downstream and that obtained by simulations. Similarly to Eq. (6.3), an average relative error ψ_y for O_2 mole fraction y in downstream can be defined by

$$\psi_y = \frac{1}{n}\sum_{i=1}^{n}\frac{|y_{exp} - y_{sim}|}{y_{exp}} = 7.0\% \tag{6.4}$$

The same validation experiment is made again another day with a different

upstream pressure. The results are given in Fig. 6.14 and the average relative error is calculated as $\psi_y = 6.75\%$.

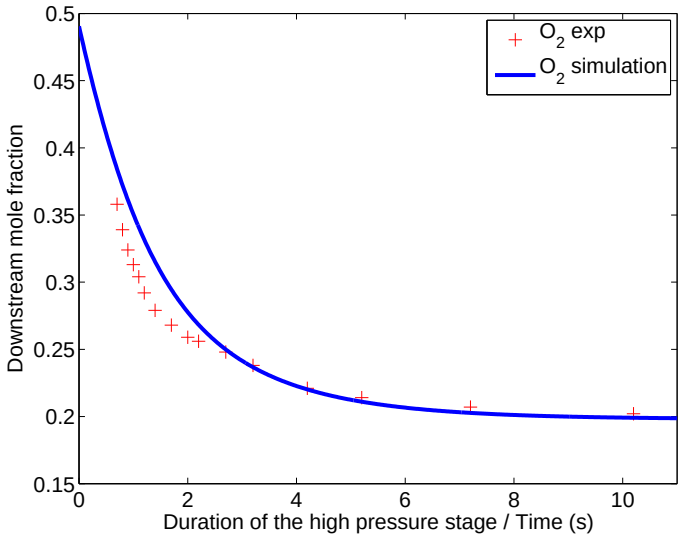

Figure 6.14: Comparison between experimental mole fraction evolution in downstream in the case of a fixed upstream pressure test (performed on 03/16/2012) and simulated results. "Duration of the high pressure stage" in the x-axis refers to experimental results and "Time" refers to simulation results.

Besides factors discussed in pure gas permeation experiments, it is important to notice that the mole fraction measurement is subject to introduce more errors with respect to a pressure measurement.

- The MGA 3000 multi-gas analyzer possesses an intrinsic accuracy of 1.0%, which cannot be neglected in our experiments.
- In simulations, the starting time of the high pressure stage is perfectly defined. Nevertheless, as explained previously, the control system represents in general 0.2 s of delay of response. Consequently, the exact starting time of the high pressure stage in experiments is somehow uncertain.
- In simulation, the initial downstream pressure is considered as null and the vacuum stage is supposed to empty perfectly the downstream after one cycle whereas those are not realistic. The residual gas in downstream can influence the permeate composition, in particular at a short diffusion time when the permeate quantity is low. This latter may explain the relative important gap between experiments and simulations at the beginning of the curve.

- The assumption of constant upstream composition can also be questioned. In reality, the upstream side would be slightly enriched in N_2 since O_2 whose permeability is larger leaves the upstream side more rapidly. As a result, the O_2 driving force of diffusion in reality would be less important than that in simulation. That may explain the general overestimation of O_2 mole fraction in downstream side.

Finally, as the experimental results and those obtained by simulation present reasonable relative errors of 7.0% and 6.75%, it can be concluded that the simulation can be validated in the case of a mixed gas permeation.

6.4 Conclusion of experimental developments

Within the frame of the thesis, an experimental validation of a long class cyclic process, the novel process (Section 5.3) in particular is performed. In these experimental developments, the characteristics of the commercial membrane module are first determined by means of experiments and optimization tools. The effective membrane thickness is consistent with results obtained by other experiments. Our simulated results are validated in the case of a pure gas permeation (N_2) with regard to the experimental pressure evolutions of the pure gas in both upstream and downstream sides of the modules. Then in the case of a mixed gas (air), a similar validation is performed with respect to the experimental O_2 mole fraction evolution in the downstream side of the module. All these experiments show that the used simple gas transport model is efficient and credible in such a simulation work. Thus the novel process which is designed according to this transport model is strongly supported.

Moreover, it can be noticed that the receiving tank operating at a manually fixed pressure and a fixed outlet flow rate used in experiments can be considered as the downstream receiving tank (Fig. 5.23). By adding a similar tank in the upstream side of the module, both upstream and downstream gases can thus be collected. Then, providing proper pumps for corresponding receiving tanks, a novel process with basic option in pilot size may be thus built. Furthermore, this pilot size process could also be completed by adding a sidestream system with its proper pump. By doing so, a more complete validation of novel process would be expected.

Chapter 7

Conclusion & perspectives

> Science is built up of facts, as a house is built of stones; but an accumulation of facts is no more a science than a heap of stones is a house.
>
> Henri Poincaré

As indicated in Chapter 2, the thesis study was conducted in three stages by means of both numerical simulations and experimental validations.

In the first stage, existing cyclic operations have been reviewed. By way of the review, all existing cyclic operations are in the first place classified into two classes: short class processes characterized by high pressure stage durations comparable to time-lags of treated gaseous components and long class processes characterized by a long high pressure stage with respect to the time-lags. More fundamentally, in short class processes, the transient behaviors occur in the selective layer of the membrane whereas in the case of the long class processes, the transient behaviors in the system outside the membrane are used. Then an important trade-off is obtained: a reasonable selectivity improvement is accompanied by a moderated productivity loss, while a great selectivity improvement goes with a significant productivity loss and so does the process complexity. Pros & cons of existing cyclic processes have been centralized and critically discussed.

Then, in a second stage, both classes have been investigated essentially in the way of simulation. The short class processes are studied in following steps:

- An inventory of interesting binary gas mixtures for short class processes using homogeneous membranes is performed via existing gas property

correlations. In the inventory, 66 gaseous components have been examined and the important advantage of short class processes is highlighted: selectivity improvement with respect to conventional steady-state processes. This is consistent with literature conclusions. Furthermore, by means of such a cyclic process, a so-called reverse selectivity is also predicted for some gas couples during the inventory.

- A review of gas transport modeling in polymers is performed. Among numerous models available in the literature, the Dual Mode Sorption theory [Vieth et al., 1976] is finally chosen as the transport model in process simulations. In general, by using the Partial Immobilization Model, the transport phenomena are described by Fick's second law with five transport parameters set for each gaseous component in a given polymer. According to a more general description, the PIM presents one limit behavior of the classical Dual Mode Sorption theory. Another limit behavior model (named as Dual Diffusion Model) is in particular investigated and compared to classical models during this stage. Consequently, the time-lag lower bound (provided by Dual Diffusion Model) which was not yet developed before us can also be considered as a simple but efficient model within the frame of Dual Mode Sorption theory.

- The first cyclic membrane gas separation process [Paul, 1971] is redesigned and then simulated by way of rigorous numerical simulations and optimizations. Based on some industrial interesting binary gas mixtures, the optimized simulation results are compared to conventional membrane gas separation processes under similar operating conditions in both separation factor and productivity. By doing so, the mentioned advantages of short class processes (selectivity improvement and reverse selectivity) have been confirmed while some unavoidable and important drawbacks are also indicated. As the productivity loss is too important and the exhaustion ratio in upstream is extremely low, short class processes might only be interesting for separation of specific gases.

- In order to reduce the unavoidable drawbacks of short class processes, the Mixed Matrix Membrane is introduced in such a process. Since the use of heterogeneous MMM can significantly increase gas time-lags with respect to the ordinary homogeneous membrane, the short class process performance can be thus improved. Therefore, a proper cyclic process design for MMM is proposed then simulated and optimized in this thesis. Important improvements with respect to homogeneous membrane have been pointed out and thus the short class processes become more competitive with respect to conventional processes by using MMM.

According to the review study, the long class processes have more degrees

of freedom with regard to their operation and their productivity may be comparable to steady-state operations. A novel design of long class process has been proposed and patented within this thesis. It is confirmed by means of simulations and optimizations that the patented process can be very competitive with regard to conventional processes, both in the purity and recovery ratio of the desired gas. Furthermore, either the slow or the rapid gas, or both of them can be accumulated preferentially in their proper receiving tank. Then the process efficiency can still be improved by either increasing the downstream/upstream volume ratio or adopting the sidestream option. Finally, in a different manner with respect to short class processes, the complexity of valve operations is much reduced and the productivity is in general 1 000 times that of a typical short class process. Therefore, the long class process, in particular the novel process proposed in this thesis, is strongly recommended in industry.

Last but not least, an experimental verification is performed in order to check the credibility of our simulation, in particular for the patented process. The building of the experimental setup was satisfactorily accomplished by using a commercial hollow fiber module in PolyPhenylene Oxide (PPO), four pneumatic valves and an infrared gas analyzer. The system airtightness and experiment reproducibility are first checked. For sake of convenience and consistency with regard to patented process investigation, the basic gas transport model for rubbery polymers is adopted in comparison. As a result, a reasonable agreement between simulations and experiments has been found first for pure nitrogen diffusion in term of its pressure and then for compressed air in terms of O_2 mole fraction. This fact confirms that the simulation results can be indeed used to give a credible gas transport phenomenon prediction in and through membranes. Furthermore, it provides a strong support to our patented process since the partial pressure/mole fraction evolution curve is the key issue of the patented process design. Lastly, it should be noticed that the apparatus used in validation can be readily transformed into a pilot of our patented process by adding some tanks and valves.

To our knowledge, although numerous advantages have been highlighted since 1971, cyclic membrane gas separation processes have not yet been implemented in industry. Therefore, future considerations, based on the results of present research should be directed towards first building a pilot setup of a complete cyclic process, for example the novel design based on Mixed Matrix Membrane and the patented process in order to check the feasibility of such processes. On the other hand, the focus can also be directed towards a cost-benefit analysis which is a key issue for industries but not at all discussed in this thesis. Such a study is able to assist in better understanding the position of cyclic operations with regard to conventional processes and attracting more attention from industry.

Bibliography

S. Adhikari and S. Fernando. Hydrogen membrane separation techniques. *Ind. Eng. Chem. Res.*, 45:875–881, 2006.

J. H. M. Albers, J. Smid, and A. P. M. Kusters. *Gas separation apparatus and also method for separating gases means of such an apparatus.* US Patent 5,129,920. 1992.

M. G. De Angelis, G. C. Sarti, and F. Doghieri. NELF model prediction of the infinite dilution gas solubility in glassy polymers. *J. Membr. Sci.*, 289: 106–122, 2007.

M. A. Aroon, A. F. Ismail, T. Matsuura, and M. M. Montazer-Rahmati. Performance studies of mixed matrix membranes for gas separation: A review. *Separation and Purification Technology*, 2:165–190, 2010.

R. A. Assink. Investigation of the dual mode sorption of ammonia in polystyrene by NMR. *J. Polym. Sci., Part B: Polym. Phys.*, 13:1665–1673, 1975.

R. W. Baker. Future directions of membrane gas separation technology. *Ind. Eng. Chem. Res.*, 41:1393–1411, 2002.

R. W. Baker. *Membrane Technology and Applications.* Wiley, Chichester, 2004.

R. W. Baker and K. Lokhandwala. Natural gas processing with membranes: An overview. *Ind. Eng. Chem. Res.*, 47:2109–2121, 2008.

R. M. Barrer. Nature of the diffusion process in rubber. *Nature*, 140:106–107, 1937.

R. M. Barrer. Permeation, diffusion and solution of gases in organic polymers. *Trans. Faraday Soc.*, 35:628, 1939.

R. M. Barrer. Diffusivities in glassy polymers for the dual mode sorption model. *J. Membr. Sci.*, 18:25–35, 1984.

R. M. Barrer, J. A. Barrie, and J. Slater. Sorption and diffusion in ethyl cellulose. Part I. history-dependence of sorption isotherms and permeation rates. *J. Polym. Sci., Part B: Polym. Phys.*, 23:315–329, 1957.

I. N. Beckman, A. B. Shelekhin, and V. V. Teplyakov. Separation of gas mixtures in unsteady-state conditions. *J. Membr. Sci.*, 55:283–297, 1991.

S. Bertelle, C. Vallière, D. Roizard, and E. Favre. Design, synthesis and characterization of mixed matrix material for CO_2 capture. *Desalination*, 200:456–458, 2006.

D. Bhatia and W. R. Vieth. The penetrant time-lag for the dual-sorption case with langmuir isotherms. *J. Membr. Sci.*, 6:351–357, 1980.

J. G. A. Bitter. *Transport mechanisms in membrane separation processes.* Plenum Press, New York, 1991.

J. Brandrup and E. H. Immergut. *Polymer Handbook Third Edition.* Wiley, New York, 1989.

J. Caro, M. Noack, P. Kolsch, and R. Schaefer. Zeolite membranes - state of their development and perpective. *Micropo. Mesopor. Mater.*, 38:3–24, 2000.

H. S. Carslaw and J. C. Jaeger. *Conduction of heat in solids.* Oxford University Press, London, 1959.

M. P. Chenar, M. Soltanieh, T. Matsuura, A. Tabe-Mohammadi, and C. Feng. Gas permeation properties of commercial polyphenylene oxide and Cardo-type polyimide hollow fiber membranes. *Separation and Purification Technology*, 51:359–366, 2006.

J. S. Chiou and D. R. Paul. Gas sorption and permeation in poly(ethyl methacrylate). *J. Membr. Sci.*, 45:167–189, 1989.

J. P. Corriou, C. Fonteix, and E. Favre. Optimization of a pulsed operation of gas separation by membrane. *AIChE J.*, 54:1224–1234, 2008.

M. M. Dal-Cin, A. Kumar, and L. Layton. Revisiting the experimental and theoretical upper bounds of light pure gas selectivity-permeability for polymeric membranes. *J. Membr. Sci.*, 323:299–308, 2008.

N. de Nevers. *Fluid Mechanics for Chemical Engineers.* McGraw-Hill, New York, 1991.

F. Doghieri and G. C. Sarti. Nonequilibrium lattice fluids: A predictive model for the solubility in glassy polymers. *Macromolecules*, 29:7885–7896, 1996.

F. Doghieri and G. C. Sarti. Predicting the low pressure solubility of gases and vapors in glassy polymers by the NELF model. *J. Membr. Sci.*, 147: 73–86, 1998.

F. Doghieri, D. Biavati, and G. C. Sarti. Solubility and diffusivity of ethanol in PTMSP: Effects of activity and of polymer aging. *Ind. Eng. Chem. Res.*, 35:2420–2430, 1996.

O. Esekhile, W. Qiu, and W. J. Koros. Permeation of butane isomers through 6FDA-DAM dense films. *J. Polym. Sci., Part B: Polym. Phys.*, 49:1605–1620, 2011.

E. Favre, D. Roizard, R. Bounaceur, and W. J. Koros. CO_2/N_2 reverse selective gas separation membranes: Technological opportunities and scientifc challenges. *Ind. Eng. Chem. Res.*, 48:3700–3701, 2009.

X. Feng, C. Y. Pan, and J. Ivory. Pressure swing permeation: Novel process for gas separation by membranes. *AIChE J.*, 46:724–733, 2000.

A. Fick. Ueber diffusion (on diffusion). *Annalen der Physik und Chemie von J. C. Pogendorff*, 94:59–86, 1855.

G. H. Fredrickson and E. Helfand. Dual-mode transport of penetrants in glassy polymers. *Macromolecules*, 18:2201–2207, 1985.

B. D. Freeman. Basis of permeability/permselectivity tradeoff relations in polymeric gas separation membranes. *Macromolecules*, 32:375–380, 1999.

B. D. Freeman and I. Pinnau. Gas and liquid separations using membranes: An overview. In *ACS Symposium Series*, Washington D.C., USA, 2004.

M. Galizia, M. G. De Angelis, E. Finkelshtein, Y. Yampolskii, and G. C. Sarti. Sorption and transport of hydrocarbons and alcohols in addition-type poly(trimethy silyl norbornene). I: Experimental data. *J. Membr. Sci.*, 385-386:141–153, 2011.

L. Garrido, M. Lopez-Gonzalez, E. Saiz, and E. Riande. Molecular basis of carbon dioxide transport in polycarbonate membranes. *J. Phys. Chem. B*, 112:4253–4260, 2008.

A. Higuchi and T. Nakagawa. Permselectivities through artificial membranes at a nonsteady state. *J. Appl. Polym. Sci.*, 37:2181–2190, 1989.

W. I. Higuchi. A new relationship for the dielectric properties of two phase mixtures. *J. Phys. Chem.*, 62:649–653, 1958.

W. I. Higuchi and T. Higuchi. Theoretical analysis of diffusional movement through heterogeneous barriers. *J. Am. Pharm. Assoc. Sci. Ed.*, 49:598–606, 1960.

J. R. Hildebrand. *Regular solutions*. Prentice Hall, 1962.

M. A. Islam and H. Buschatz. Gas permeation through a glassy polymer membrane: Chemical potential gradient or dual mobility mode? *Chem. Eng. Sci.*, 57:2089–2099, 2002.

G. Jinjikhashvily, L. Claassen, and R. Meir. CO_2 separation out of power station flue gases by asymmetric hollow fiber membranes, 2011.

D. R. Kemp and D. R. Paul. Gas sorption in polymer membranes containing adsorptive fillers. *J. Polym. Sci., Part B: Polym. Phys.*, 12:485–500, 1974.

V. R. E. Kesting. *Synthetic polymeric membranes. A structural perspective. 2nd Edition*. John Wiley and Sons, New York, 1985.

E. S. Kikkinides, R. T. Yang, and S. H. Cho. Concentration and recovery of CO_2 from flue gas by pressure swing adsorption. *Ind. Eng. Chem. Res.*, 32: 2714–2720, 1993.

W. J. Koros. Model for sorption of mixed gases in glassy polymers. *J. Polym. Sci., Part B: Polym. Phys.*, 18:981–992, 1980.

W. J. Koros and G. K. Fleming. Membrane-based gas separation. *J. Membr. Sci.*, 83:1–80, 1993.

W. J. Koros and W. Madden. Comments on "Gas permeation through a glassy polymer membrane: Chemical potential gradient or dual mobility model?" by M.A. Islam and H. Buschatz [Chemical Engineering Science 57 (2002) 2089–2099]. *Chem. Eng. Sci.*, 58:2461–2463, 2003.

W. J. Koros and D. R. Paul. Transient and steady-state permeation in poly(ethylene terephthlate) above and below the glass transition. *J. Polym. Sci., Part B: Polym. Phys.*, 16:2171–2187, 1978.

W. J. Koros, D. R. Paul, and A. A. Rocha. Carbon dioxide sorption and transport in polycarbonate. *J. Polym. Sci., Part B: Polym. Phys.*, 14:687–702, 1976.

W. J. Koros, A. H. Chan, and D. R. Paul. Sorption and transport of various gases in polycarbonate. *J. Membr. Sci.*, 2:165–190, 1977.

W. J. Koros, R. T. Chern, V. T. Stannett, and H. B. Hopfenberg. A model for permeation of mixed gases and vapors in glassy polymers. *J. Polym. Sci.*, 19:1513–1530, 1981.

D. W. Van Krevelen. *Properties of Polymers: Their Correlation with Chemical Structure; Their Numerical Estimation and Prediction from Additive Group Contributions*. Elsevier, Amsterdam, 1990.

J. C. Lagarias, J. A. Reeds, M. H. Wright, and P. E. Wright. Convergence properties of the Nelder-Mead simplex method in low dimensions. *SIAM Journal of Optimization*, 9:112–147, 1998.

M. A. LaPack and P. F. Dupuis. *Dynamic membrane separation process for improved selectivity*. U.S. Patent 5,354,474. 1994.

P. D. Lax and R. D. Richtmyer. Survey of the stability of linear finite difference equations. *Communications on Pure and Applied Mathematics*, 9:267–293, 1956.

D. R. Lloyd. Membrane materials science, an overview. In *ACS Symposium Series*, Washington D.C., USA, 1985.

P. Meares. The diffusion of gases through polyvinyl acetate. *J. Am. Chem. Soc.*, 76:3415–3422, 1954.

T. C. Merkel, V. I. Bondar, K. Nagai, B. D. Freeman, and I. Pinnau. Gas sorption, diffusion, and permeation in poly(dimethylsiloxane). *J. Polym. Sci., Part B: Polym. Phys.*, 38:415–434, 2000.

A. S. Michaels and H. J. Bixler. Solubility of gases in polyethylene. *Journal of Polymer Science*, 50:393–412, 1951.

M. Minelli, S. Campagnoli, M. G. De Angelis, F. Doghieri, and G. C. Sarti. Predictive model for the solubility of fluid mixtures in glassy polymers. *Macromolecules*, 12(44), 2011.

K. Nakanishi, H. Odani, M. Kurata, T. Masuda, and T. Higashimura. Sorption of alcohol vapors in a disubstituted polyacetylene. *Polym. J.*, 19(2):293–296, 1987.

S. M. Nemser. *Cyclic Membrane Separation Process*. U.S. Patent 6,887,300 B2. 2005.

S. M. Nemser and I. C. Roman. *Perfluoroxioxole membranes*. U.S Patent 5,051,114. 1991.

I. C. Omole, R. T. Adams, S. J. Miller, and W. J. Koros. Effects of CO_2 on a high performance hollow-fiber membrane for natural gas purification. *Ind. Eng. Chem. Res.*, 49:4887 – 4896, 2010.

K. G. Papadokostaki, A. Stavropoulou, M. Sanopoulou, and J. H. Petropoulos. An advanced model for composite planar three-layer matrix-controlled release devices. Part I. devices of uniform material properties and non-uniform solute load. *J. Membr. Sci.*, 312:193–206, 2008.

S. V. Patankar. *Numerical heat transfer and fluid flow.* Taylor & Francis, New York, 1980.

D. R. Paul. Effect of immobilizating adsorption on the diffusion time lag. *J. Polym. Sci., Part A-2*, 7:1811–1818, 1969.

D. R. Paul. Membrane separation of gases using steady cyclic operation. *Ind. Eng. Chem. Process Des. Dev.*, 10(3):375–379, 1971.

D. R. Paul and D. R. Kemp. The diffusion time lag in polymer membranes containing adsorptive fillers. *J. Polym. Sci.*, 41:79–93, 1973.

D. R. Paul and W. J. Koros. Effect of partially immobilizating sorption on permeability and the diffusion time lag. *J. Polym. Sci., Part B: Polym. Phys.*, 14:675–685, 1976.

J. H. Petropoulos. Quantitative analysis of gaseous diffusion in glassy polymers. *J. Polym. Sci., Part A-2*, 8:1797–1801, 1970.

M. Pourafshari, M. Soltanieh, T. Matsuura, A. Tabe-Mohammadi, and C. Feng. Gas permeation properties of commercial polyphenylene oxide and Cardo-type polyimide hollow fiber membranes. *Sep. Purif. Technol.*, 51:359–366, 2006.

W. H. Press, S. Teukolsky, W. Vetterling, and B. Flannery. *Numerical Recipes: The Art of Scientific Computing.* Cambridge University Press, third edition, 2007.

R. Rautenbach and R. Albrecht. *Membrane Processes.* John Wiley & Sons, Chichester, 1989.

M. T. Ravanchi, T. Kaghazchi, and A. Kargari. Application of membrane separation processes in petrochemical industry: a review. *Desalination*, 235:199–244, 2009.

L. M. Robeson. The upper bound revisited. *J. Membr. Sci.*, 320:390–400, 2008.

D. M. Ruthven, S. Farooq, and K. S. Knaebel. *Pressure Swing Adsorption.* VCH Publishers, Inc, 1993.

I. C. Sanchez and R. H. Lacombe. Statistical thermodynamics of polymer solutions. *Macromolecules*, 11(6):1145–1156, 1978.

E. S. Sanders and W. J. Koros. Sorption of CO_2, C_2H_4, N_2O and their binary mixtures in poly(methyl methacrylate). *J. Polym. Sci., Part B: Polym. Phys.*, 24:175–188, 1986.

G. C. Sarti and F. Doghieri. Predictions of the solubility of gases in glassy polymers based on the NELF model. *Chem. Eng. Sci.*, 53(19):3435–3447, 1998.

M. D. Sefcik and J. Schaefer. Solid-state ^{13}C NMR evidence for gas-polymer interactions in the carbon dioxide-poly(vinyl chloride) system. *J. Polym. Sci, Polym. Phys.*, 21:1055–1062, 1983.

T. K. Sherwood, R. L. Pigford, and C. R. Wilke. *Mass transfer.* McGraw Hill Chemical Engineering Series, 1975.

A. Singh and W. J. Koros. Significance of entropic selectivity for advanced gas separation membranes. *Ind. Eng. Chem. Res*, 35:1231–1234, 1996.

R. W. Spillman. Economics of gas separation membranes. *Chem. Eng. Prog*, 85:41–62, 1989.

J. Stewart. *Calculus: Early Transcendentals (Stewart's Calculus Series).* Brooks Cole, 2007.

B. J. Story and W. J. Koros. Comparison of three models for permeation of CO_2/CH_4 mixtures in poly(phenylene oxide). *J. Polym. Sci., Part B: Polym. Phys.*, 27:1927–1948, 1989.

M. J. Thundyil, Y. H. Jois, and W. J. Koros. Effect of permeate pressure on the mixed gas permeation of carbon dioxide and methane in a glassy polyimide. *J. Membr. Sci.*, 152:29 – 40, 1999.

J. A. Tshudy and C. Von Frankenberg. A model incorporating reversible immobilization for sorption and diffusion in glassy polymers. *J. Polym. Sci, Polym. Phys.*, 11:2027–2037, 1973.

A. K. Ueda, K. K. Haruna, and S. M. Inoue. *Process for separating gas.* U.S Patent 4,955,998. 1990.

H. K. Versteeg and W. Malalasekera. *An introduction to Computational Fluid Dynamics.* Pearson Education Limited, 1995.

W. R. Vieth. *Diffusion In and Through Polymers.* Hanser Publishers, Munich, 1991.

W. R. Vieth and K. J. Sladek. A model for diffusion in a glassy polymer. *J. Colloid Sci.*, 20:1014–1033, 1965.

W. R. Vieth, P. M. Tam, and A. S. Michaels. Dual sorption mechanisms in glassy polystyrene. *J. Colloid Interface Sci.*, 22:360–370, 1966.

W. R. Vieth, J. M. Howell, and J. H. Hsieh. Dual sorption theory. *J. Membr. Sci.*, 1:177–220, 1976.

D. Q. Vu, W. J. Koros, and S. J. Miller. High pressure CO_2 /CH_4 separation using carbon molecular sieve hollow fiber membranes. *Ind. Eng. Chem. Res.*, 35:1231–1234, 1996.

D. Q. Vu, W. J. Koros, and S. J. Miller. Mixed matrix membranes using carbon molecular sieves. I. Preparation and experimental results. *J. Membr. Sci.*, 211:311–334, 2003.

L. Wang, J. P. Corriou, C. Castel, and E. Favre. A critical review of cyclic transient membrane gas separation processes: State of the art, opportunities and limitations. *J. Membr. Sci.*, 383:170–188, 2011a.

L. Wang, J. P. Corriou, C. Castel, and E. Favre. *Procédé de séparation membranaire en régime discontinu.* France Patent: FR 11 60587. November 2011b.

L. Wang, J. P. Corriou, C. Castel, and E. Favre. Transport of gases in glassy polymers under transient conditions: Limit-behavior investigations of dual-mode sorption theory. *Ind. Eng. Chem. Res.*, 2012 (DOI: 10.1021/ie2027102).

L. Wang, J. P. Corriou, C. Castel, and E. Favre. Cyclic gas separation by mixed matrix membranes (MMM). *AIChE J.*, 2012 (Submitted).

Appendix A

Permeability at steady state

In order to determine the permeability at steady state for any fixed upstream/downstream pressures, the corresponding differential equations are solved with specified initial and boundary conditions.

A.1 Permeability of the Dual Diffusion Model

At steady state, the time dependent term becomes null in Eq. (4.18). Thus the gas behavior in the membrane is described as

$$\frac{\partial}{\partial x}\left(\mathcal{D}_i \frac{\partial C_i}{\partial x}\right) = 0 \qquad i = D, H \tag{A.1}$$

The upstream and downstream pressures are constant but not necessarily null. Thus the boundary conditions are

$$\begin{aligned} &C_D(0) = k_D P_u \quad \forall t \\ &C_H(0) = \frac{C_H^{'} b P_u}{1 + b P_u} \quad \forall t \\ &C_D(l) = k_D P_d \quad \forall t \\ &C_H(l) = \frac{C_H^{'} b P_d}{1 + b P_d} \quad \forall t \end{aligned} \tag{A.2}$$

At steady state, the gas flow rate through the membrane J_{DDM} is constant and written as

$$J_{\mathrm{DDM}} = -\left[\mathcal{D}_D \frac{\partial C_D}{\partial x} + \mathcal{D}_H \frac{\partial C_H}{\partial x}\right] \tag{A.3}$$

From Eqs. (A.1), it results that the gradients of concentration for both species are constant in the membrane. Thus the derivatives of concentration can be

calculated by the boundary conditions (A.2).

$$\begin{aligned} J_{\mathrm{DDM}} &= \frac{\mathcal{D}_D}{l}(k_D P_u - k_D P_d) + \frac{\mathcal{D}_H}{l}\left[\frac{C_H^{'} b P_u}{1+bP_u} - \frac{C_H^{'} b P_d}{1+bP_d}\right] \\ &= \mathcal{D}_D k_D \frac{P_u - P_d}{l} + \mathcal{D}_H \frac{C_H^{'} b (P_u - P_d)}{(1+bP_u)(1+bP_d) l} \end{aligned} \tag{A.4}$$

Using $F = \frac{D_H}{D_D}$ and $K = \frac{C_H^{'} b}{k_D}$,

$$J_{\mathrm{DDM}} = \mathcal{D}_D k_D \frac{P_u - P_d}{l}\left[1 + \frac{FK}{(1+bP_u)(1+bP_d)}\right] \tag{A.5}$$

Consequently, the permeability $\mathcal{P}_{\mathrm{DDM}}$ at steady state is given as

$$\mathcal{P}_{\mathrm{DDM}} = \frac{J_{\mathrm{DDM}}}{\Delta P / l} = \mathcal{D}_D k_D \left[1 + \frac{FK}{(1+bP_u)(1+bP_d)}\right] \tag{A.6}$$

A.2 Permeability of the Partial Immobilization Model

For the PIM, assuming the time dependent terms are null in Eq. (4.16), the gas behavior in the membrane at steady state is described as

$$\frac{\partial}{\partial x}\left[\mathcal{D}_D\left(1 + \frac{FK}{(1+aC_D)^2}\right)\frac{\partial C_D}{\partial x}\right] = 0 \tag{A.7}$$

where the Langmuir species C_H is eliminated by the Local Equilibrium. Assuming that the upstream and downstream pressures are constant but not null, the boundary conditions are

$$\begin{aligned} C_D(0) &= k_D P_u \quad \forall t \\ C_D(l) &= k_D P_d \quad \forall t \end{aligned} \tag{A.8}$$

By definition, the gas flow rate through the membrane J_{PIM} is constant and written as

$$J_{\mathrm{PIM}} = -\left[\mathcal{D}_D \frac{\partial C_D}{\partial x} + \mathcal{D}_H \frac{\partial C_H}{\partial x}\right] \tag{A.9}$$

As the Local Equilibrium is assumed in the membrane and $\mathcal{D}_H = F\mathcal{D}_D$, Eq. (A.9) can be rearranged as

$$J_{\mathrm{PIM}} = -\left[\mathcal{D}_D \frac{\partial C_D}{\partial x} + F\mathcal{D}_D \frac{\partial C_H}{\partial C_D}\frac{\partial C_D}{\partial x}\right] \tag{A.10}$$

where $\frac{\partial C_H}{\partial C_D}$ is given by the Local Equilibrium (Eq. (4.15)). Thus

$$J_{\text{PIM}} = -\underbrace{\mathcal{D}_D \left[\left(1 + \frac{FK}{(1+aC_D)^2}\right)\frac{\partial C_D}{\partial x}\right]}_{\text{Term 1}} \tag{A.11}$$

From Eq. (A.7), it results that the Term 1 of Eq. (A.11) is constant and is denoted as β

$$\begin{aligned} &\beta = \mathcal{D}_D \left(1 + \frac{FK}{(1+aC_D)^2}\right)\frac{\partial C_D}{\partial x} \\ &\Rightarrow \left[1 + \frac{FK}{(1+aC_D)^2}\right] dC_D = \frac{\beta}{\mathcal{D}_D} dx \\ &\Rightarrow \int_{C_D(0)}^{C_D(l)} \left[1 + \frac{FK}{(1+aC_D)^2}\right] dC_D = \int_0^l \frac{\beta}{\mathcal{D}_D} dx \end{aligned} \tag{A.12}$$

The constant β can be obtained by solving Eq. (A.12) and using (A.8)

$$\beta = -\mathcal{D}_D k_D \frac{P_u - P_d}{l}\left[1 + \frac{FK}{(1+bP_u)(1+bP_d)}\right] \tag{A.13}$$

Thus

$$J_{\text{PIM}} = -\beta = \mathcal{D}_D k_D \frac{P_u - P_d}{l}\left[1 + \frac{FK}{(1+bP_u)(1+bP_d)}\right] \tag{A.14}$$

Consequently, the steady state permeability $\mathcal{P}_{\text{PIM}}$ can be deduced as

$$\mathcal{P}_{\text{PIM}} = \frac{J_{\text{PIM}}}{\Delta P/l} = \mathcal{D}_D k_D \left[1 + \frac{FK}{(1+bP_u)(1+bP_d)}\right] \tag{A.15}$$

Since Eqs. (A.6) and (A.15) are equivalent, it can be concluded that the PIM and the DDM predict the same permeability at steady state for any pressure fixed on upstream and downstream.

It can be noticed that, in the conditions of the time-lag method measurement, $P_d = 0$, so that Eqs. (A.6) and (A.15) are reduced to Eq. (4.20). As a result, the measured transport parameters from the time-lag method measurement can be used in both PIM and DDM.

Appendix B

Time lag of the Dual Diffusion Model

Barrer [1939] proposed an analytical solution of the time-lag. This procedure is adapted here in order to determine the time-lag of the DDM. Barrer studied a rubbery polymer membrane in which the gas concentration is noted C. Therefore, the gas behavior can be described by Fick's law

$$\frac{\partial C}{\partial t} = \mathcal{D}\frac{\partial^2 C}{\partial x^2} \tag{B.1}$$

submitted to

$$\begin{array}{ll} C(x,0) = 0 & \forall x \\ C(l,t) = C_0 & \forall t \\ C(0,t) = 0 & \forall t \end{array} \tag{B.2}$$

where C_0 is constant. Thus Eq. (B.1) is solved analytically as a Fourier series by separation of time and space variables as

$$C(x,t) = \frac{C_0}{l}x + \frac{2}{\pi}\sum_{1}^{\infty}\frac{C_0 \mathrm{Cos}\ n\pi}{n}\mathrm{Sin}\ \frac{n\pi x}{l}e^{-\frac{\mathcal{D}n^2\pi^2 t}{l^2}} \tag{B.3}$$

Assuming that the gas flows through the membrane into a volume V, the gas concentration C^g in this volume corresponding to the accumulation line of permeate in Fig. 4.1 is given by

$$V\frac{dC^g}{dt} = \mathcal{D}\left(\frac{\partial C}{\partial x}\right)_{x=0} A \tag{B.4}$$

$\left(\frac{\partial C}{\partial x}\right)_{x=0}$ can be found using Eq. (B.3). Then Barrer gave an analytical expression of $C^g(t)$ by integrating Eq. (B.4) between 0 to t, yielding the

following expression of $C^g(t)$

$$C^g(t) = \frac{\mathcal{D}C_0 t}{lV/A} + \frac{2l}{\pi^2 V/A}\sum_1^\infty \left(\frac{C_0 \text{Cos } n\pi}{n^2}\right)\left(1 - e^{-\frac{\mathcal{D}n^2\pi^2 t}{l^2}}\right) \tag{B.5}$$

When $t \to \infty$, Eq. (B.5) tends towards the straight line corresponding to the steady-state portion of Eq. (4.1). Then the time-lag value $\theta = l^2/6\mathcal{D}$ is obtained at the intercept of this straight line and the time axis.

The DDM can be considered as a linear combination of two independent gas diffusion behaviors in a rubbery polymer. Thus the total gas concentration C_t^g in a volume V is given by

$$C_t^g = C_D^g + C_H^g \tag{B.6}$$

Barrer's solution is used here to describe C_D^g and C_H^g of the DDM corresponding to the concentration of Henry population and the concentration of Langmuir population respectively. Thus,

$$C_t^g(t) = \frac{(\mathcal{D}_D C_{D0} + \mathcal{D}_H C_{H0})t}{lV/A} + \frac{2l}{\pi^2 V/A}\left[\sum_1^\infty \left(\frac{C_{D0}\text{Cos } n\pi}{n^2}\right)\left(1 - e^{-\frac{\mathcal{D}_D n^2\pi^2 t}{l^2}}\right)\right.$$
$$\left. + \sum_1^\infty \left(\frac{C_{H0}\text{Cos } n\pi}{n^2}\right)\left(1 - e^{-\frac{\mathcal{D}_H n^2\pi^2 t}{l^2}}\right)\right] \tag{B.7}$$

where $\mathcal{D}_H = F\mathcal{D}_D$.

When $t \to \infty$, Eq. (B.7) tends towards the straight line

$$C_t^g(t) = \frac{(\mathcal{D}_D C_{D0} + \mathcal{D}_H C_{H0})}{lV/A}t + \frac{2l}{\pi^2 V/A}\left[\sum_1^\infty \left(\frac{C_{D0}\text{Cos } n\pi}{n^2}\right) + \sum_1^\infty \left(\frac{C_{H0}\text{Cos } n\pi}{n^2}\right)\right]$$
$$= \frac{\mathcal{D}_D(C_{D0} + FC_{H0})}{lV/A}t + \frac{2l(C_{D0} + C_{H0})}{\pi^2 V/A}\left[\sum_1^\infty \left(\frac{\text{Cos } n\pi}{n^2}\right)\right]$$
$$= \frac{\mathcal{D}_D(C_{D0} + FC_{H0})}{lV/A}t - \frac{l(C_{D0} + C_{H0})}{6V/A} \tag{B.8}$$

since $\sum_1^\infty \left(\frac{\text{Cos } n\pi}{n^2}\right) = -\frac{\pi^2}{12}$. Thus the time-lag θ defined in Eq. (4.1) is given by the intercept of the line and the time axis,

$$\theta = \frac{l^2}{6\mathcal{D}_D}\frac{C_{D0} + C_{H0}}{C_{D0} + FC_{H0}} \tag{B.9}$$

using $C_{D0} = k_D P_u$ and $C_{H0} = \frac{C_H^{'} b P_u}{1 + b P_u}$, Eq. (B.9) finally yields

$$\theta = \frac{l^2}{6\mathcal{D}_D} \frac{1 + K + b P_u}{1 + FK + b P_u} \tag{B.10}$$

Appendix C

Fiber filling time estimations

The hollow fiber module can be considered as a system of multitubes. The hydrodynamics of the fiber filling problem is studied in order to determine whether the Feed step can be considered as instantaneous. This problem is described in Fig. C.1: a capillary fiber of volume V is initially in vacuum ($P_2^0 = 0$) is connected to a gas reserve at constant pressure (P_1). The connection is controlled by a valve, at $t = 0$, the valve is open and the tube filling starts. The study aims to determine the necessary time t_f to have $P_2 \geq 99.9\% P_1$.

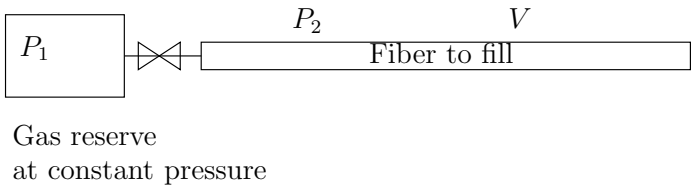

Figure C.1: Schema of the fiber filling problem

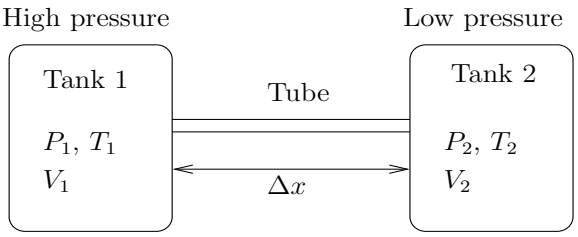

Figure C.2: The tank filling problem investigated by de Nevers [1991]

de Nevers [1991] studies the gas behavior at high velocity (larger than 61m/s at the neck point). Particularly, the gas behavior at high velocity with friction resistance during an isothermal filling to a tank (Fig. C.2). The mass

flow rate at the neck point is given as

$$\dot{m} = \frac{dm}{dt} = \left[\frac{(P_1^2 - P_2^2)D^5 M(\pi/4)^2}{4flRT_K}\right]^{1/2} \tag{C.1}$$

where m the gas mass, P_1 pressure of the Tank 1, P_2 pressure in the Tube and in Tank 2, D tube diameter, M gas molecular weight, l tube length, R gas constant, T_K temperature and f a dimensionless coefficient determined by $f = 0.0024/D^{1/3}$. Consequently, the mass flow rate at the neck point can be estimated by Eq. (C.1), then the necessary filling time can be determined knowing the volume of the Tank 2.

de Nevers [1991] assumes that the friction resistance is located only in the tube, thus the mass flow rate decreases with the tube length. An analogy is made between our tube filling problem and the problem of de Nevers [1991]. The fiber to fill in Fig. C.1 is virtually cut into two parts, corresponding to the tube and the Tank 2 in Fig. C.2 respectively. The estimation is performed by overestimating the fiber filling duration: according to Eq. (C.1), the mass flow rate decreases with the fiber length, thus the minimum flow rate is used as constant in every point in the fiber in our overestimation. However, the volume to fill is still the totality of the fiber internal volume. Thus the fiber filling time will be overestimated.

According to this analogy, P_1 is the constant setpoint pressure, P_2 the internal fiber pressure varying with time, V internal fiber volume, D fiber diameter and M mole mass of the gas.

The estimation proceeds in the following way,

$$\frac{dm}{dP_2} = \frac{dm}{dt}\frac{dt}{dP_2} = \frac{\dfrac{dm}{dt}}{\dfrac{dP_2}{dt}} \tag{C.2}$$

then $\dfrac{dm}{dP_2}$ can be determined by the perfect gas law,

$$m = \frac{VMP_2}{RT_K} \Rightarrow \frac{dm}{dP_2} = \frac{VM}{RT_K} \tag{C.3}$$

By combining Eqs. (C.1), (C.2) and (C.3)

$$\frac{dP_2}{dt} = \dot{m}\frac{VM}{RT_K} \Longrightarrow dt = \frac{RT_K}{\dot{m}VM}dP_2 \tag{C.4}$$

thus

$$\left[\frac{4flRT_K}{(P_1^2 - P_2^2)D^5 M(\pi/4)^2}\right]^{1/2} \frac{RT_K}{VM}dP_2 = dt \tag{C.5}$$

Thus the filling time to a given pressure P_2 can be estimated by integrating Eq. (C.5).

$$\int_0^{P_2} \left[\frac{4flRT_K}{(P_1^2 - P_2^2)D^5 M(\pi/4)^2} \right]^{1/2} \frac{RT_K}{VM} dP_2 = \int_0^{t_f} dt \tag{C.6}$$

Numerical applications give an estimated fiber filling duration of 0.213 s to reach $P_2 = 99.9\%P_1$. It is important to notice that this duration is an overestimated value, the real fiber filling time would be shorter. Consequently, the Feed step should be long enough with respect to 0.213 s in order to ensure a perfect filling.

Appendix D

Solution algorithm of Partial Immobilization Model

D.1 Grid-point definition

As explained in section 4.2.2, the hollow fiber module is modeled by the Partial Immobilization Model with boundary and initial conditions. In this thesis, The finite volume method is used as the essential solution algorithm for this problem.

The finite volume method starts, as always, with the discretization of the flow domain and of the relevant transport equations [Versteeg and Malalasekera, 1995]. As the considered geometry is cylindric (Fig. D.1), a uniform mesh is used where e is the est face and w is the west face. For any given mesh, e is not certain to be the middle point of PE segment and w is not the middle point of WP. The point P is in the middle of WE, thus in the middle of control volume. Consequently, by defining ΔR_w as the distance PW and ΔR_e as the distance EP, following relationships can be obtained:

$$\begin{aligned} \Delta R_w(i) &= \frac{\Delta R(i-1) + \Delta R(i)}{2} \\ \Delta R_e(i) &= \frac{\Delta R(i) + \Delta R(i+1)}{2} \end{aligned} \tag{D.1}$$

The subscript i from 1 to N is defined in Fig. D.2. For a given thickness L, $N-2$ complete volumes and 2 half-volumes are considered in following way

(Fig. D.3):

$$\begin{aligned}
&i = 1 \Leftrightarrow r = R_i \\
&i = N \Leftrightarrow r = R_e \\
&R_{i+1} - R_i = \Delta R = \frac{L}{N-1} \qquad \forall \quad 2 \leq i \leq N-2 \quad \text{(uniform meshing)} \\
&R_2 - R_1 = \frac{L}{2(N-1)} \\
&R_N - R_{N-1} = \frac{L}{2(N-1)}
\end{aligned} \tag{D.2}$$

Thus the control volume P (Fig. D.1) is given by

$$V_P(i) = \pi(R_e(i)^2 - R_w(i)^2)l_t \tag{D.3}$$

with l_t length of fiber. Internal and external surfaces of one fiber is then defined respectively as

$$\begin{aligned}
&\Delta S_w(i) = 2\pi r_w(i) l_t \\
&\Delta S_e(i) = 2\pi r_e(i) l_t
\end{aligned} \tag{D.4}$$

D.2 Discretization

As explain in Chapter 4, the goal of our study is to seek to solve a non-linear (linear in some cases) unsteady one-dimensional diffusion equation (Eq. 4.26). Since time is a one-way coordinate, the solution will be obtained by marching in time from a given initial concentration profile. Thus, in a typical "time step" the task is: given the control volume values of concentration C at time t, find the values of C at time $t + \Delta t$. The known values of concentration C at the grid points will be denoted by C_P^n, C_E^n and C_W^n, and the unknown values at time $t + \Delta t$ by C_P^{n+1}, C_E^{n+1} and C_W^{n+1}.

D.2.1 $N-2$ complete control volumes

Each of the $N-2$ complete control volumes has two neighbors, thus the discretization equation is now derived by integrating Eq. (4.26) over the control

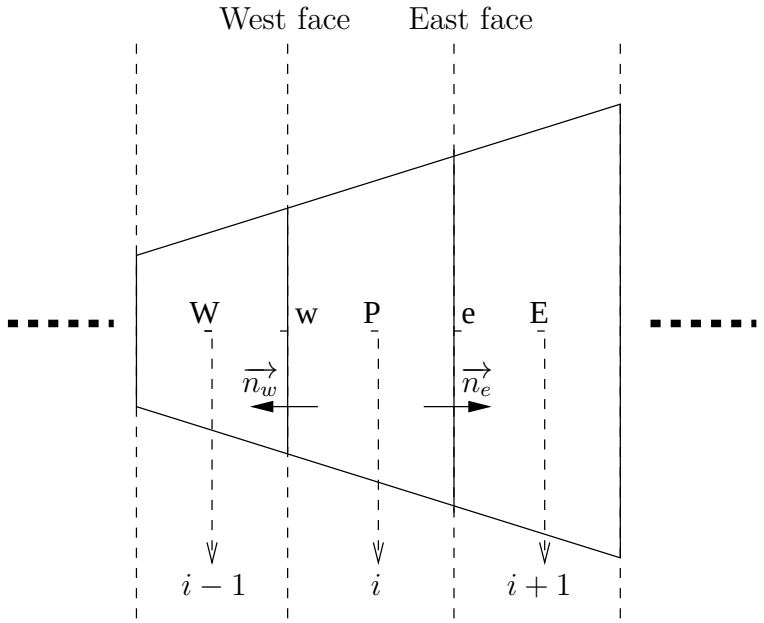

Figure D.1: Complete control volume P for the one-dimensional situation with its neighbors W and E.

volume shown in Fig. D.1 and over the time interval from t to $t + \Delta t$.

$$\underbrace{\int_V \int_t^{t+\Delta t} \left[1 + \frac{K_i}{(1 + \sum_{k=1}^{n} a_k C_{Dk})^2} \right] \frac{\partial C_{Di}}{\partial t} \mathrm{d}t\mathrm{d}V}_{\text{term 1}} = \underbrace{\int_V \int_t^{t+\Delta t} \frac{1}{r} \frac{\partial}{\partial r} \left[r \mathcal{D}_{Di} \left(1 + \frac{F_i K_i}{(1 + \sum_{k=1}^{n} a_k C_{Dk})^2} \right) \frac{\partial C_{Di}}{\partial r} \right] \mathrm{d}t\mathrm{d}V}_{\text{term 2}} \tag{D.5}$$

For convenience, C is used instead of C_D in following formula. Moreover, for the same reason, the subscript is only used if the corresponding symbol is NOT reserved to the component i. Then in the case of an implicit schema

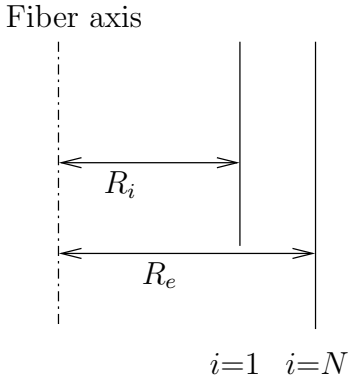

Figure D.2: Axial cut of fiber with internal and external radius.

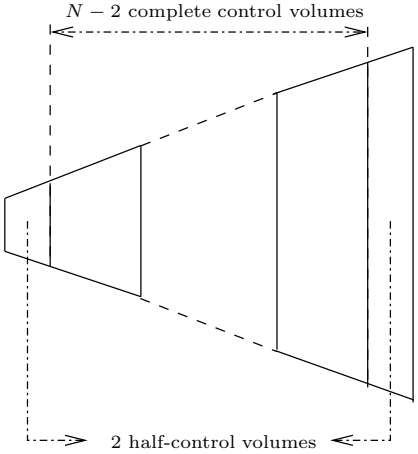

Figure D.3: Distribution of control volumes in fiber.

[Patankar, 1980], the term 1 is approximated to

$$\left[1+\frac{K}{(1+\sum_{k=1}^{n}a_kC_{Pk})^2}\right]\left.\frac{\partial C}{\partial t}\right|_P V_P = \left[1+\frac{K}{(1+\sum_{k=1}^{n}a_kC_{Pk}^{n+1})^2}\right]\frac{C_P^{n+1}-C_P^n}{\Delta t}V_P \tag{D.6}$$

According to divergence theorem (a special case of the more general Stokes' theorem [Stewart, 2007]), the outward flux of a vector field through a closed surface $\overrightarrow{S}$ is equal to the volume integral V of the divergence of the region

inside the surface,

$$\int_V F \mathrm{d}V = \int_S F \mathrm{d}\overrightarrow{S} \tag{D.7}$$

thus the term 2 becomes

$$\begin{aligned}
&\int_S \mathcal{D}_D \left(1 + \frac{FK}{(1 + \sum_{k=1}^{n} a_k C_k)^2} \right) \frac{\partial C}{\partial r} S d\overrightarrow{n} \\
&= \mathcal{D}_D \left[\left(1 + \frac{FK}{(1 + \sum_{k=1}^{n} a_k C_k)^2} \right) \frac{\partial C}{\partial r} \right]_e \Delta S_e - \mathcal{D}_D \left[\left(1 + \frac{FK}{(1 + \sum_{k=1}^{n} a_k C_k)^2} \right) \frac{\partial C}{\partial r} \right]_w \Delta S_w \\
&= \mathcal{D}_D \left(1 + \frac{FK}{(1 + \sum_{k=1}^{n} a_k C_{ek}^{n+1})^2} \right) \frac{C_E^{n+1} - C_P^{n+1}}{\Delta R_e} \Delta S_e \\
&- \mathcal{D}_D \left(1 + \frac{FK}{(1 + \sum_{k=1}^{n} a_k C_{wk}^{n+1})^2} \right) \frac{C_P^{n+1} - C_W^{n+1}}{\Delta R_w} \Delta S_w
\end{aligned} \tag{D.8}$$

Consequently, the implicit schema is given by

$$\begin{aligned}
&\left[1 + \frac{K}{(1 + \sum_{k=1}^{n} a_k C_{Pk}^{n+1})^2} \right] \frac{C_P^{n+1} - C_P^n}{\Delta t} V_P = \mathcal{D}_D \left(1 + \frac{FK}{(1 + \sum_{k=1}^{n} a_k C_{ek}^{n+1})^2} \right) \frac{C_E^{n+1} - C_P^{n+1}}{\Delta R_e} \Delta S_e \\
&- \mathcal{D}_D \left(1 + \frac{FK}{(1 + \sum_{k=1}^{n} a_k C_{wk}^{n+1})^2} \right) \frac{C_P^{n+1} - C_W^{n+1}}{\Delta R_w} \Delta S_w
\end{aligned} \tag{D.9}$$

where C_e^{n+1} et C_w^{n+1} are determined by a linear interpolation:

$$\begin{aligned} C_e^{n+1} &= \frac{C_P^{n+1} + C_E^{n+1}}{2} \\ C_w^{n+1} &= \frac{C_P^{n+1} + C_W^{n+1}}{2} \end{aligned} \tag{D.10}$$

In order to solve this problem, Eq. (D.9) should be rewritten in a linear canonic form proposed by Patankar [1980]:

$$a_P C_P^{n+1} = a_E C_E^{n+1} + a_W C_W^{n+1} + b \tag{D.11}$$

where a_P, a_E and a_W are coefficients to determine. Thus Eq. (D.9) should be linearized first. By combining Eqs. (D.9) and (D.10), a function $f(C_P^{n+1}, C_W^{n+1}, C_E^{n+1}) = 0$ is obtained and can be written in form of a first order Taylor series approximation in a neighborhood of (C_P^n, C_W^n, C_E^n),

$$\begin{aligned} &f(C_P^{n+1}, C_W^{n+1}, C_E^{n+1}) \\ &= f(C_P^n, C_W^n, C_E^n) + \frac{\partial f}{\partial C_P}\Big|_n (C_P^{n+1} - C_P^n) + \frac{\partial f}{\partial C_E}\Big|_n (C_E^{n+1} - C_E^n) + \frac{\partial f}{\partial C_W}\Big|_n (C_W^{n+1} - C_W^n) \end{aligned} \tag{D.12}$$

then, coefficients in Eq. (D.11) are given by

$$\begin{aligned} a_E &= -\frac{\partial f}{\partial C_E}\Big|_n \\ a_W &= -\frac{\partial f}{\partial C_W}\Big|_n \\ a_P &= \frac{\partial f}{\partial C_P}\Big|_n \\ b &= -f(C_P^n, C_W^n, C_E^n) + \frac{\partial f}{\partial C_P}\Big|_n C_P^n + \frac{\partial f}{\partial C_E}\Big|_n C_E^n + \frac{\partial f}{\partial C_W}\Big|_n C_W^n \end{aligned} \tag{D.13}$$

these partial derivatives $\frac{\partial f}{\partial C_P}$, $\frac{\partial f}{\partial C_E}$ and $\frac{\partial f}{\partial C_W}$ are calculated analytically as

$$\frac{\partial f}{\partial C_P} = \left[1 + \frac{K}{(1+\sum_{k=1}^{n} a_k C_{Pk}^{n+1})^2}\right]\frac{V_P}{\Delta t}$$
$$+\mathcal{D}_D\frac{\Delta S_e}{\Delta R_e}\left[1 + \frac{FK}{(1+\sum_{k=1}^{n} a_k C_{ek}^{n+1})^2}\right] + \mathcal{D}_D\frac{\Delta S_w}{\Delta R_w}\left[1 + \frac{FK}{(1+\sum_{k=1}^{n} a_k C_{wk}^{n+1})^2}\right]$$
$$+\mathcal{D}_D FKa\frac{\Delta S_e}{\Delta R_e}\frac{C_E^n - C_P^n}{(1+\sum_{k=1}^{n} a_k C_{ek}^{n+1})^3} - \mathcal{D}_D FKa\frac{\Delta S_w}{\Delta R_w}\frac{C_P^n - C_W^n}{(1+\sum_{k=1}^{n} a_k C_{wk}^{n+1})^3} \tag{D.14}$$

$$\frac{\partial f}{\partial C_E} = \mathcal{D}_D FKa\frac{\Delta S_e}{\Delta R_e}\frac{C_E^n - C_P^n}{(1+\sum_{k=1}^{n} a_k C_{ek}^{n+1})^3} - \mathcal{D}_D\frac{\Delta S_e}{\Delta R_e}\left[1 + \frac{FK}{(1+\sum_{k=1}^{n} a_k C_{ek}^{n+1})^2}\right] \tag{D.15}$$

$$\frac{\partial f}{\partial C_W} = \mathcal{D}_D FKa\frac{\Delta S_w}{\Delta R_w}\frac{C_W^n - C_P^n}{(1+\sum_{k=1}^{n} a_k C_{wk}^{n+1})^3} - \mathcal{D}_D\frac{\Delta S_w}{\Delta R_w}\left[1 + \frac{FK}{(1+\sum_{k=1}^{n} a_k C_{wk}^{n+1})^2}\right] \tag{D.16}$$

It can be noticed that in expression of partial derivatives, the symbols C_e and C_w are still used in order to simplify the script length. According to Patankar [1980], the determined coefficients have to satisfy following conditions,

$$\begin{aligned} a_P &= a_E + a_W - S_P\Delta r + a_P^0 \\ b &= S_C\Delta r + a_P^0 C_P^0 \end{aligned} \tag{D.17}$$

where S_C and S_P are referred to source terms. Consequently, following coefficients are obtained,

$$a_E = -\mathcal{D}_D F K a \frac{\Delta S_e}{\Delta R_e} \frac{C_E^n - C_P^n}{(1 + \sum_{k=1}^{n} a_k C_{ek}^{n+1})^3} + \mathcal{D}_D \frac{\Delta S_e}{\Delta R_e} \left[1 + \frac{FK}{(1 + \sum_{k=1}^{n} a_k C_{ek}^{n+1})^2} \right] \tag{D.18}$$

$$a_W = -\mathcal{D}_D F K a \frac{\Delta S_w}{\Delta R_w} \frac{C_W^n - C_P^n}{(1 + \sum_{k=1}^{n} a_k C_{wk}^{n+1})^3} + \mathcal{D}_D \frac{\Delta S_w}{\Delta R_w} \left[1 + \frac{FK}{(1 + \sum_{k=1}^{n} a_k C_{wk}^{n+1})^2} \right] \tag{D.19}$$

$$\begin{aligned} a_P^0 &= \left[1 + \frac{K}{(1 + \sum_{k=1}^{n} a_k C_{Pk}^{n+1})^2} \right] \frac{V_P}{\Delta t} + 2\mathcal{D}_D F K a \frac{\Delta S_e}{\Delta R_e} \frac{C_E^n - C_P^n}{(1 + \sum_{k=1}^{n} a_k C_{ek}^{n+1})^3} \\ &- 2\mathcal{D}_D F K a \frac{\Delta S_w}{\Delta R_w} \frac{C_P^n - C_W^n}{(1 + \sum_{k=1}^{n} a_k C_{wk}^{n+1})^3} \\ S_P &= 0 \\ S_C &= 0 \end{aligned} \tag{D.20}$$

It can be noticed that for the $N-2$ complete control volumes, both source terms are null since only diffusion occurs here.

D.2.2 2 half-control volumes

The first (number 1) and the last (number N) control volumes are two half-control volumes and in contact with outside of the membrane. By imposing different operating conditions (pressure conditions at outside of the membrane), two situations for both half-control volumes should be first distinguished:

- Fixed pressure.

- Variable pressure.

The fixed pressure case corresponds to the feed stage when the upstream pressure is maintained at a high pressure or the regeneration stage when the upstream and downstream are emptied by vacuuming. The variable upstream pressure corresponds to the free diffusion stage when both upstream and downstream pressures evaluate with diffusion through the membrane.

The half-control volume situated on the internal membrane side is first discussed (Fig. D.4). According to Fig. D.3, this half-control volume is on contract with the upstream side and numbered as 1. If the upstream pressure is fixed at P_u^0, the concentration C (referred to ordinary dissolution, but the subscript D is removed for convenience) is constant on the interfacial surface,

$$C_1^{n+1} = k_D P_u^0 \tag{D.21}$$

According to Eqs. (D.11) and (D.17), corresponding parameters can be determined as

$$\begin{aligned} a_P^0 &= 0 \\ S_P &= -\frac{1}{\Delta r} \\ S_c &= \frac{k_D P_u}{\Delta r} \\ a_E &= 0 \\ a_W &= 0 \end{aligned} \tag{D.22}$$

It can be noticed that in the case fixed upstream pressure, the source terms are not null since the upstream is fed.

If the upstream pressure is variable, the perfect gas law is used to describe pressure evolution in upstream side. In a differential form, the perfect gas law is given by,

$$\frac{dP_u^0}{dt} = \underbrace{\frac{dn^{out}}{dt}}_{\text{term 1}} \frac{RT}{V_u} \tag{D.23}$$

The term 1 corresponds to the molar flow rate leaving the upstream side (or entering the membrane). This term can be given by Fick's first law as

$$\begin{aligned}\frac{dn^{out}}{dt} &= -\mathcal{D}_D \left[\left(1 + \frac{FK}{(1+\sum_{k=1}^{n} a_k C_{Pk})^2} \right) \frac{\partial C}{\partial r} \right]_P \Delta S_e \\ &\approx \mathcal{D}_D \left(1 + \frac{FK}{(1+\sum_{k=1}^{n} a_k C_{Pk})^2} \right) \frac{C_e - C_P}{\frac{\Delta R_e}{2}} \Delta S_e\end{aligned} \tag{D.24}$$

with

$$C_P = k_D P_u \tag{D.25}$$

Consequently, Eq. (D.23) can be discretized as

$$\underbrace{\frac{P_u^{n+1} - P_u^n}{\Delta t}}_{=\frac{C_P^{n+1} - C_P^n}{k_D \Delta t}} = \left[\mathcal{D}_D \left(1 + \frac{FK}{(1+\sum_{k=1}^{n} a_k C_{Pk}^{n+1})^2} \right) \frac{C_e^{n+1} - C_P^{n+1}}{\frac{\Delta R_e}{2}} \Delta S_e \right] \frac{RT}{V_u} \tag{D.26}$$

If $C_e = \dfrac{C_P + C_E}{2}$ is admitted, Eq. (D.26) is rewritten as

$$\frac{C_P^{n+1} - C_P^n}{k_D \Delta t} = \mathcal{D}_D \left(1 + \frac{FK}{(1+\sum_{k=1}^{n} a_k C_{Pk}^{n+1})^2} \right) \left[\frac{\frac{C_P^{n+1} + C_E^{n+1}}{2} - C_P^{n+1}}{\frac{\Delta R_e}{2}} \right] \Delta S_e \frac{RT}{V_u} \tag{D.27}$$

Eq. (D.27) can be written as one equation of $g(C_P^{n+1}, C_W^{n+1}, C_E^{n+1})$, the same linearization strategy for function f is applied here for function g in order to obtain the coefficients in Eq. (D.11).

$$\begin{aligned}&g(C_P^{n+1}, C_W^{n+1}, C_E^{n+1}) \\ &= g(C_P^n, C_W^n, C_E^n) + \frac{\partial g}{\partial C_P}\Big|_n (C_P^{n+1} - C_P^n) + \frac{\partial g}{\partial C_E}\Big|_n (C_E^{n+1} - C_E^n) + \frac{\partial g}{\partial C_W}\Big|_n (C_W^{n+1} - C_W^n)\end{aligned}$$

(D.28)

where the partial derivatives are

$$\begin{aligned}
&\frac{\partial g}{\partial C_P}\Big|_n = \frac{1}{k_D \Delta t} + \mathcal{D}_D \frac{\Delta S_e}{\Delta R_e}\left[1 + \frac{FK}{(1+\sum_{k=1}^{n} a_k C_{Pk}^{n+1})^2}\right]\frac{RT}{V_u} \\
&+2\mathcal{D}_D \frac{\Delta S_e}{\Delta R_e}\frac{RT}{V_u}\frac{aFK(C_E^n - C_P^n)}{(1+\sum_{k=1}^{n} a_k C_{Pk}^{n+1})^3} \\
&\frac{\partial g}{\partial C_E}\Big|_n = -\mathcal{D}_D \frac{\Delta S_e}{\Delta R_e}\left[1 + \frac{FK}{(1+\sum_{k=1}^{n} a_k C_{Pk}^{n+1})^2}\right]\frac{RT}{V_u} \\
&\frac{\partial g}{\partial C_W}\Big|_n = 0
\end{aligned} \tag{D.29}$$

Thus coefficients of Eq. (D.11) can be determined as,

$$\begin{aligned}
a_P^0 &= \frac{1}{k_D \Delta t} + 2\mathcal{D}_D \frac{\Delta S_e}{\Delta R_e}\frac{RT}{V_u}\frac{aFK(C_E^n - C_P^n)}{(1+\sum_{k=1}^{n} a_k C_{Pk}^{n+1})^3} \\
a_E &= \mathcal{D}_D \frac{\Delta S_e}{\Delta R_e}\left[1 + \frac{FK}{(1+\sum_{k=1}^{n} a_k C_{Pk}^{n+1})^2}\right]\frac{RT}{V_u} \\
a_W &= 0 \\
S_P &= 0 \\
S_C &= 0
\end{aligned} \tag{D.30}$$

As regards the last half-volume situated on the external membrane side, the coefficients for Eqs. (D.11) and (D.17) are determined by a similar way to the first half-control volume. According to Fig. D.3, this half-control volume is on contract with downstream side and numbered as N. If the downstream

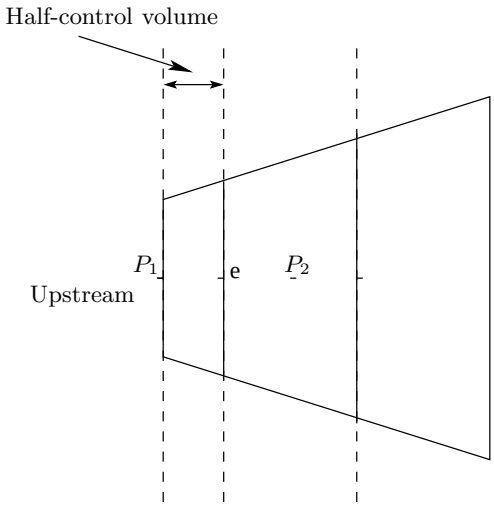

Figure D.4: Half-control volume situated on the internal membrane side.

pressure is fixed at P_d^0, following coefficients are determined

$$\begin{aligned} a_P^0 &= 0 \\ S_P &= -\frac{1}{\Delta r} \\ S_c &= \frac{k_D P_d^0}{\Delta r} \end{aligned} \tag{D.31}$$

In the case that the downstream pressure P_d is not constant, following coefficients are determined

$$\begin{aligned} a_P^0 &= \frac{1}{k_D \Delta t} + 2\mathcal{D}_D \frac{\Delta S_w}{\Delta r_w} \frac{RT}{V_d} \frac{aFK(C_P^n - C_W^n)}{(1 + \sum_{k=1}^{n} a_k C_{Pk}^{n+1})^3} \\ a_W &= \mathcal{D}_D \frac{\Delta S_w}{\Delta r_w} \left[1 + \frac{FK}{(1 + \sum_{k=1}^{n} a_k C_{Pk}^{n+1})^2} \right] \frac{RT}{V_d} \\ a_E &= 0 \\ S_P &= 0 \\ S_c &= 0 \end{aligned} \tag{D.32}$$

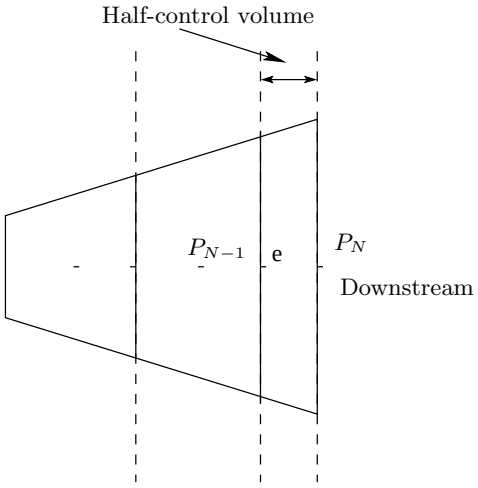

Figure D.5: Half-control volume situated on the external membrane side.

As a result, the discretization process has yielded one equation for each of the (half-)control volume at time t. Different methods have been proposed by Patankar [1980], Versteeg and Malalasekera [1995] to solve such a system. In this thesis, the iterative method suggested by Patankar [1980] is applied. It should be noticed that due to use of linearizing operation, an underrelaxation strategy is used [Patankar, 1980]. At the same time, in order to ensure the convergence, a rather small time step is used. Consequently, in the case of high non-linear situation, the solving time is very long.

Appendix E

Résumé en français

> Connais ton ennemi et connais-toi toi-même; eussiez-vous cent guerres à soutenir, cent fois vous serez victorieux. Si tu ignores ton ennemi et que tu te connais toi-même, tes chances de perdre et de gagner seront égales. Si tu ignores à la fois ton ennemi et toi-même, tu ne compteras tes combats que par tes défaites.
>
> L'art de la guerre, Sun Tzu

Cette thèse s'appuient sur trois publications en anglais:

(I) Cyclic Gas Separation by Mixed Matrix Membranes (MMM). L. Wang, J.P. Corriou, C. Castel, E. Favre. *AIChE Journal*, (soumis en 2012)

(II) Transport of Gases in Glassy Polymers under Transient Conditions: Limit Behavior Investigations of Dual Mode Sorption Theory. L. Wang, J.P. Corriou, C. Castel, E. Favre. *Industrial & Engineering Chemistry Research*, (accepté en 2012)

(III) A critical review of cyclic transient membrane gas separation processes: State of the art, opportunities and limitations. L. Wang, J.P. Corriou, C. Castel, E. Favre. *Journal of Membrane Science*, 383(2011), 170-188

Ces trois publications correspondent essentiellement aux chapitres 3, 4 et une partie importante du chapitre 5. Une quatrième publication anglaise en

préparation complétera le chapitre 5. En plus, vu l'originalité de ces travaux, nous souhaitons amplifier une diffusion de ces résultats à l'aide de la langue anglaise. Tout ceci explique la raison pour laquelle ce manuscrit est rédigé principalement en anglais. Par contre, dans le cadre d'une thèse française rédigée en anglais, un résumé étendu en langue française est toujours requis. Dans ce chapitre, le contenu de la thèse est condensé en environ 40 pages en français.

Avant d'entamer cet unique chapitre en français, je tiens à avertir les lecteurs que, dans ce résumé étendu, j'ai conservé les termes anglais d'usage courant dans le domaine des membranes et les symboles (plus ou moins anglais aussi) listés dans la partie Nomenclature afin de maintenir la cohérence avec le texte principal. Par exemple, P_f représente la pression d'alimentation même si l'index $_f$ ne représente rien en français dans cette circonstance, ainsi que A pour la surface, L pour l'épaisseur, PIM pour modèle d'immobilisation partielle (Partial Immobilization Model) etc.... D'autre part, nous lirons ainsi, 'time-lag' au lieu d'un étrange 'retard temporel' et 'stage cut' pour 'taux de prélèvement', ainsi que 'dual mode' à la place de 'double mode', etc....

Introduction

Cette thèse réalisée au sein du LRGP (Laboratoire Réactions et Génie des Procédés, Nancy) est consacrée à d'abord passer en revue les procédés membranaires pour la séparation gazeuse en fonctionnement cyclique, puis définir un procédé compétitif face à un procédé membranaire conventionnel, et à la fin effectuer une démonstration expérimentale.

Perméation gazeuse: étude bibliographique

Dans ces deux premiers chapitres, le contexte du développement de la perméation gazeuse est d'abord expliqué. Selon cette explication, le plan de thèse est ainsi défini. Une étude bibliographique est donnée dans le chapitre 2 afin de fournir les notions basiques d'un tel procédé et ouvrir les discussions. La perméation gazeuse est un procédé de séparation qui repose sur la différence de vitesse de perméation à travers une membrane des composants gazeux d'un mélange. Un courant d'alimentation, délivré à haute pression, est amené au contact de la membrane. La fraction la plus perméable de cette alimentation va traverser préférentiellement la membrane sous l'effet d'une différence de pression partielle des composants gazeux (figure E.1)

La fraction de gaz perméée, nommée *perméat*, est enrichie en gaz les plus perméables (ceux qui ont la vitesse de perméation la plus élevée). La fraction

de gaz non perméée, désignée par le terme *rétentat*, est concentrée en espèces les moins perméables (vitesse de perméation la plus faible). L'efficacité de séparation d'un tel procédé est conditionnée par:

- La nature des gaz constituant le mélange.
- Trois paramètres pour chaque flux (alimentation, rétentat et perméat): débit molaire Q, fraction molaire X or Y et pression P.
- Les matériaux membranaires utilisés.
- L'hydrodynamique à l'intérieur des modules membranes et les conditions d'opération, telles que le rapport des pressions aval et amont $\Psi = \frac{P_d}{P_u}$ et le stage cut $\zeta = \frac{Q_d}{Q_f}$.

Par comparaison avec les autres procédés de séparation gazeuse en concurrence, les procédés membranaires possèdent les propriétés suivantes:

- Les procédés membranaires ne font pas intervenir un changement de phase.
- L'opération d'un procédé membranaire se fait en général en régime permanent.
- Les procédés membranaires ne sont pas rentables pour obtenir un produit de haute pureté, étant donné que la force motrice (le gradient des pressions) est relativement faible par rapport aux technologies comme la cryogénie. [Spillman, 1989].
- La membrane est aisée à moduler, un procédé membranaire peut ainsi élargir sa production facilement. Dans le cas d'une petite ou moyenne production, le procédé membranaire est plus compétitif en terme d'économie. [Spillman, 1989].
- Les procédés membranaires sont respectueux de l'environnement [Spillman, 1989]. Ils ne requièrent pas d'agent de transfert de masse pour la séparation et ne génèrent pas de déchets (vapeurs, solvants et particules solides).

Koros and Fleming [1993] décrivent un procédé membranaire de séparation gazeuse performant avec trois critères: productivité, sélectivité et stabilité de la membrane.

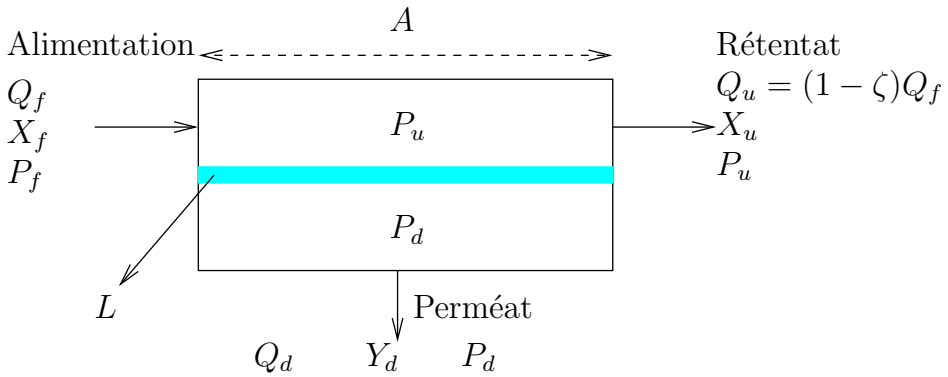

Figure E.1: Schéma d'un procédé membranaire conventionnel pour la séparation gazeuse

- La productivité dépend du débit de perméation déterminé par la perméabilité du matériau, l'épaisseur effective de la membrane et le taux de remplissage du module (surface effective sur l'unité du volume de module). Un haut débit de perméation peut être obtenu en utilisant des membranes fines et un module optimisé pour avoir une grande surface d'échange.

- La sélectivité dépend non seulement du matériau de la membrane, mais aussi des conditions de fonctionnement du procédé complet (comme le rapport des pressions Ψ et le stage cut ζ). En règle générale, l'optimum de productivité ne peut être obtenu avec l'optimum de sélectivité. Ce compromis est souvent présenté sous forme d'une zone de Pareto [Robeson, 2008].

- Enfin, la stabilité de la membrane mesure la durée pendant laquelle la perméabilité et la sélectivité d'une membrane peuvent être maintenues. Dans les traitements des gaz condensables, des membranes avec forte résistance chimique, thermique et mécanique sont indispensables.

Dans le cadre de cette étude, uniquement les gaz peu corrosifs sont considérés, ainsi la stabilité de la membrane n'est pas développée en détail. La productivité et la sélectivité sont prises en compte comme deux facteurs clés d'un procédé membranaire de séparation gazeuse.

En fonction des matériaux utilisés et de la façon dont ils sont mis en oeuvre, les opérations de perméation gazeuse vont se dérouler selon différents mécanismes (figure E.2). En ce qui concerne les membranes poreuses, les mécanismes "Knudsen diffusion" ou "Molecular sieving" ou une combinaison des deux sont applicables selon les tailles de pores. Les membranes denses (non poreuses)

sont dans la plupart des cas en polymère et le mécanisme solution-diffusion est de loin le plus appliqué [Koros and Fleming, 1993]. En règle générale, les membranes denses sont utilisées comme une couche sélective, alors que les membranes poreuses sont insérées dans le module pour supporter la couche sélective. Dans cette thèse, seul le mécanisme solution-diffusion est considéré et discuté en détail, particulièrement dans le chapitre 4.

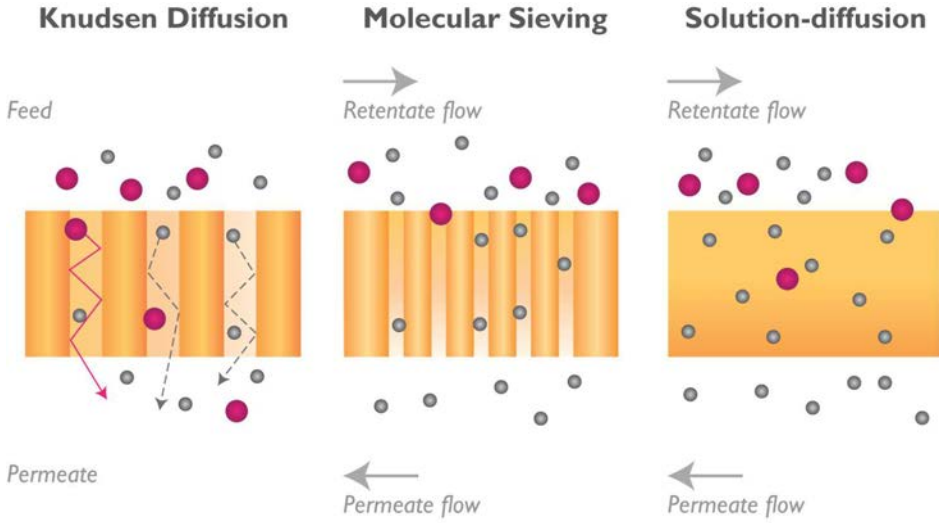

Figure E.2: Représentation schématique des mécanismes de transport des gaz dans la membrane, selon [Koros and Fleming, 1993]

L'étude du mécanisme solution-diffusion a été d'abord effectuée par Barrer [1937]. En outre, les équations fondamentales de diffusion ont été proposées par Fick [1855], qui a imaginé l'analogie entre le transfert de chaleur et celui de masse.

Selon le mécanisme solution-diffusion, la perméation gazeuse se décompose en trois étapes (figure E.3):

1. Dissolution des gaz dans le polymère d'un côté du film (de la même manière que les gaz se dissolvent dans un liquide). A la surface membrane-gaz, la concentration C d'un gaz dans la membrane s'exprime selon la loi d'Henry dans les cas simples:

$$C = k_D P_u \tag{E.1}$$

avec k_D coefficient de sorption (ou solubilité) et P pression partielle du gaz.

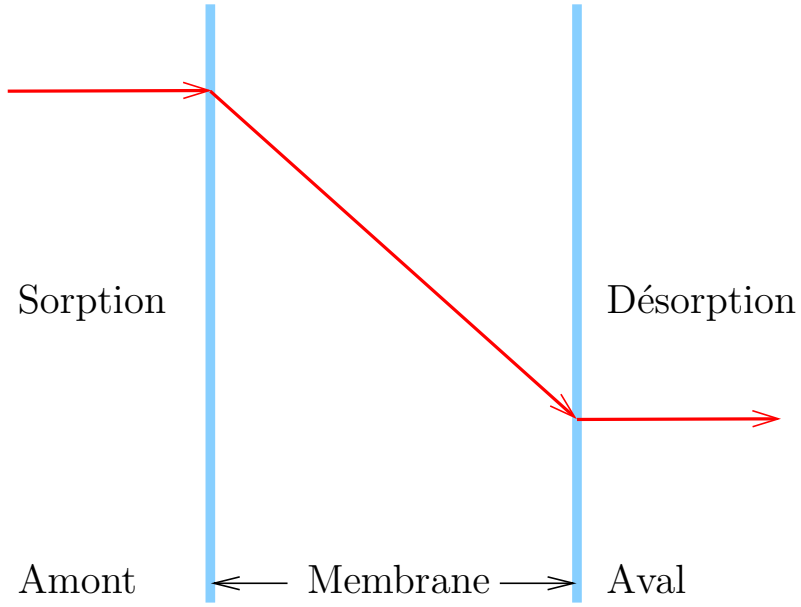

Figure E.3: Diagramme du mécanisme solution-diffusion

2. Diffusion des gaz à travers le film polymère avec le gradient de concentration comme force motrice. En régime isotherme, la perméance J est décrite par la première loi de Fick:

$$J = -\mathcal{D}\nabla C \tag{E.2}$$

où ∇C est le gradient de concentration et $\mathcal{D}$ le coefficient de diffusion (ou la diffusivité). Le signe moins signifie que la diffusion a lieu spontanément dans le sens de la concentration forte vers la concentration basse.

3. Désorption des gaz du côté aval du film:

$$C = k_D P_d \tag{E.3}$$

Dans le cas d'un polymère caoutchoutique isotherme immergé à faible pressions, la diffusivité $\mathcal{D}$ est quasi constante. Par conséquent, la variation de concentration C dans une membrane plane isotrope et homogène est décrite par la deuxième loi de Fick en coordonnées cartésiennes:

$$\frac{\partial C}{\partial t} = \mathcal{D}\frac{\partial^2 C}{\partial x^2} \tag{E.4}$$

En régime permanent, le terme t n'intervient pas. L'équation (E.4) peut être résolue aisément en posant les équations (E.1) et (E.3) comme conditions aux

limites. Nous obtenons l'expression de la perméance J:

$$J = \mathcal{D}k_D\frac{\Delta P}{L} \tag{E.5}$$

avec L épaisseur effective de la membrane, ΔP différence de pression entre l'amont et l'aval. Comme la perméabilité $\mathcal{P}$ d'un gaz est définie par $\frac{J}{\Delta P/L}$, dans ce cas simple, nous obtenons:

$$\mathcal{P} = k_D\mathcal{D} \tag{E.6}$$

En outre, le rapport des deux perméabilités (i, j et $\mathcal{P}_i > \mathcal{P}_j$) est défini comme la permsélectivité α:

$$\alpha = \frac{\mathcal{P}_i}{\mathcal{P}_j} = \frac{J_i}{J_j} = \frac{\mathcal{D}_i k_{Di}}{\mathcal{D}_j k_{Dj}} \tag{E.7}$$

Si le rapport de diffusivités est noté par $\alpha_{\mathcal{D}}$ et le rapport de solubilités par α_{k_D}, la permsélectivité peut être exprimée par le produit des deux rapports:

$$\alpha = \alpha_{\mathcal{D}}\alpha_{k_D} \tag{E.8}$$

Dans le cas des polymères vitreux, la situation est plus complexe, les équations (E.1) et l'équation (E.3) ne sont plus valables. Une théorie dite "Dual Mode Sorption theory" décrit assez bien la nouvelle situation selon un mécanisme binaire (figure 2.6):

- La loi d'Henry, pour la dissolution ordinaire C_D.
- La loi de Langmuir qui décrit l'adsorption dans les micro-vides C_H.

Il en résulte que la sorption (et la désorption) d'un corps pur est décrite par:

$$C = C_D + C_H = k_D P + \frac{C_H' bP}{1 + bP} \tag{E.9}$$

Le chapitre 4 est consacré à développer en détail cette théorie.

La formation des membranes et les modules membranaires ainsi que les applications actuelles des procédés membranaires dans l'industrie sont développés dans le chapitre 2.

Revue des procédés cycliques: étude bibliographique

Nous avons évoqué dans le chapitre 2 que les procédés membranaires de séparation gazeuse fonctionnent principalement en régime permanent. Autrement

dit, la membrane est immergée à pression constante en amont et en aval, ainsi la production et la sélectivité sont indépendantes du temps. Toutefois, Paul [1971] a proposé un nouveau fonctionnement du procédé membranaire, en imposant des pressions variables en amont et en aval d'une manière cyclique. Selon son analyse théorique, des intérêts exclusifs ont été démontrés. Après cette initiative, l'idée du fonctionnement cyclique a été reprise par plusieurs chercheurs et les intérêts ont été également confirmés. Dans le cadre de cette thèse, une revue critique des procédés cycliques a été effectuée. D'après cette revue, les procédés cycliques existants sont classés en deux catégories. En outre, les avantages et les inconvénients de chaque catégorie sont récapitulés.

Comme expliqué auparavant, seul le mécanisme solution-diffusion sera discuté dans cette thèse. En outre, la permsélectivité définie par l'équation (E.7) est bien adaptée au cas où les membranes sont caoutchoutiques. Dans le cas des membranes vitreuses, cette relation est également largement utilisée comme une approximation qualitative [Bitter, 1991]. Avec peu d'exceptions, la solubilité k_D est favorisée dans le cas de molécules gazeuses de taille importante . En revanche, la diffusivité est défavorisée dans la même circonstance [Corriou et al., 2008]. Par conséquent, les deux rapports $\frac{\mathcal{D}_i}{\mathcal{D}_j}$ et $\frac{k_{Di}}{k_{Dj}}$ dans l'expression de la permsélectivité (équation (E.7)) reposent sur deux comportements en sens opposé, il en résulte une limitation de la permsélectivité α.

Supposons deux gaz avec les propriétés suivantes:

$$\begin{aligned} &\mathcal{D}_1 = 2\mathcal{D}_2 \\ &k_{D1} = 0.5k_{D2} \\ &\Rightarrow \mathcal{P}_1 = \mathcal{P}_2 \end{aligned} \tag{E.10}$$

comme leurs perméabilités sont égales, ce couple gazeux n'est pas séparable par un procédé membranaire classique en régime permanent. Par contre, la situation change dans l'exercice suivant: en supposant qu'une membrane vierge est mise en contact avec ses volumes amont et aval initialement vides, l'amont est rapidement chargé à une haute pression P_u puis l'évolution de la pression (ou nombre de mole de gaz) aval en fonction du temps est enregistrée (figure E.11).

Le but est de maintenir l'augmentation de la pression aval négligeable devant la pression amont P_u afin d'obtenir une courbe comme celle présentée à la figure E.11, qui est manifestement divisée en une partie non linéaire correspondant à un régime transitoire et une autre partie linéaire correspondant au régime permanent. Cette expérience est largement utilisée afin de déterminer la perméabilité du gaz considéré (et le a diffusivité $\mathcal{D}$ et la solubilité k_D si une membrane caoutchoutique est appliquée). En utilisant uniquement la partie

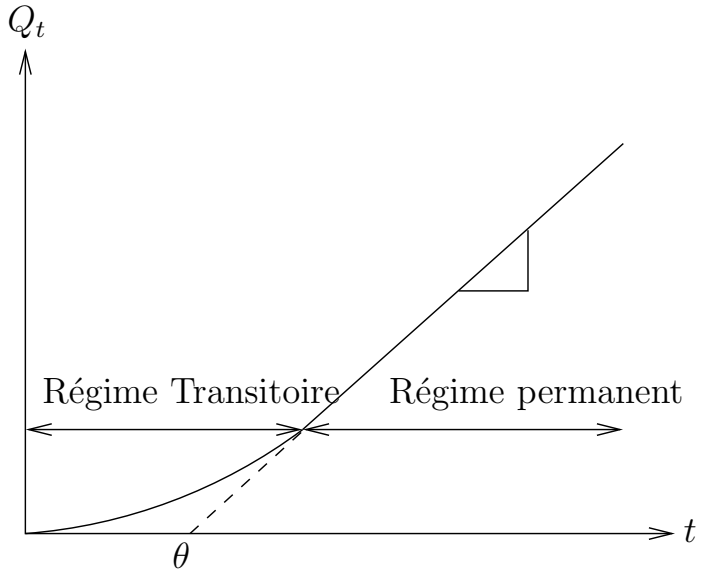

Figure E.4: Courbe qualitative de l'évolution du nombre de moles de gaz en aval Q_t en fonction du temps t

linéaire, la perméabilité peut être obtenue par

$$\mathcal{P} = \frac{\text{pente}}{(P_u - P_d)A/L} \tag{E.11}$$

avec L épaisseur de la membrane et A surface de la membrane.

En simulant cette expérience avec le couple de gaz virtuels, la figure E.5 montre qu'après une durée suffisamment longue, les débits de perméation des deux gaz deviennent égaux à cause de l'égalité de leurs perméabilités. Par contre, avant d'atteindre ce régime, ces deux gaz présentent deux débits de perméation très différents. Cette différence permet une séparation significative.

Ces deux régimes consécutifs sont visualisés à la fois dans les figures E.4 et E.5. La frontière des deux régimes est représentée dans la figure E.4 par un paramètre dit 'time-lag' θ qui est défini par la valeur du temps de l'intersection entre l'extrapolation de la partie linéaire et l'abscisse t. Dans une configuration simple, la valeur de θ peut être obtenue en résolvant l'équation (E.4) avec les conditions aux limites adéquates. Une solution analytique est disponible selon Barrer [1939] (Appendix B):

$$\theta_k = \frac{L^2}{6\mathcal{D}_k} \tag{E.12}$$

il en résulte que le time-lag d'un gaz k est indépendant de sa solubilité k_{Dk}. Ceci montre qu'un mélange gazeux comportant différentes diffusivités $\mathcal{D}$ est

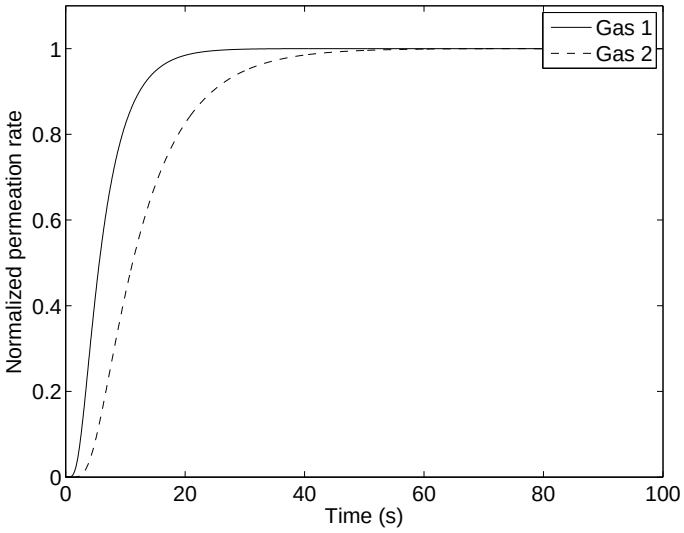

Figure E.5: Débits de perméation lors d'une expérience de time-lag avec $\mathcal{D}_1 = 2\mathcal{D}_2$ et $\mathcal{P}_1 = \mathcal{P}_2$.

séparable pendant une durée comparable à celle du time-lag même si leurs perméabilités sont égales. Autrement dit, l'effet de la solubilité qui est souvent un effet négatif dans le cas d'un fort rapport de diffusivités $\frac{\mathcal{D}_1}{\mathcal{D}_2} \gg 1$ est minimisé pendant cette durée.

Paul [1971] a conçu un procédé membranaire fonctionnant en régime cyclique (figure E.6) afin de profiter de cette séparation en fonctionnement transitoire: une membrane plane sépare un réservoir initialement vide en deux parties. La partie amont est alimentée par une source de pression cyclique. Les vannes 1-3 et 2-4 s'ouvrent de façon synchrone. Quand la chambre amont de séparation est à haute pression, le réservoir aval 1 reçoit le gaz diffusé. Symétriquement pour le réservoir aval 2. A la fin de chaque cycle, l'amont de la chambre est vidé par l'ouverture de la vanne 2. On obtiendra deux réservoirs remplis de gaz à la fin de l'opération. Le gaz désiré se trouve dans le réservoir lié à la vanne 3 (réservoir aval 1).

Paul [1971] réalise une étude théorique de ce procédé moyennant des hypothèses simplificatrices [Carslaw and Jaeger, 1959]. Le fonctionnement du procédé est optimisé du point de vue de la sélectivité et Paul [1971] montre une sélectivité importante du procédé cyclique par rapport à une sélectivité nulle en régime permanent pour le couple de gaz virtuels précédent. Pour atteindre cette sélectivité optimale, la durée de la haute pression d'un cycle doit être du même ordre de grandeur que le time-lag du composé gazeux avec

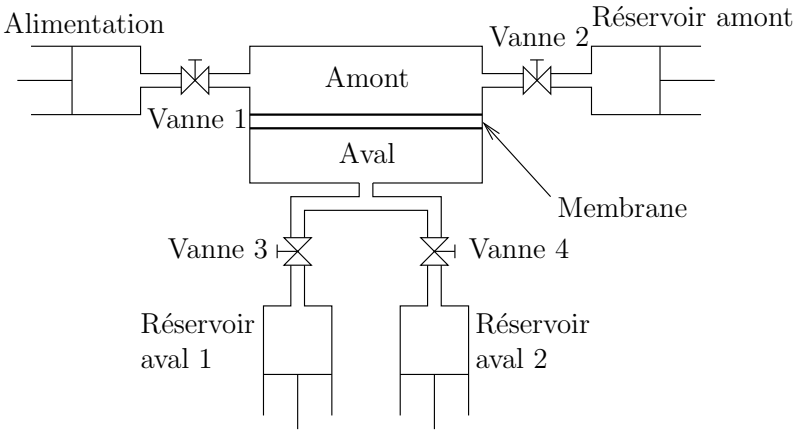

Figure E.6: Schéma du procédé de Paul [1971]

la diffusivité moins importante. En plus, le procédé de Paul est également caractérisé par le fait que la durée de la haute pression ne peut dépasser 10% de la durée totale d'un cycle dans le cas de la sélectivité optimale.

Cette idée de fonctionnement cyclique possède plusieurs points communs avec le procédé d'adsorption, notamment l'adsorption modulée en pression: Pressure Swing Adsorption (PSA). D'abord, la notion du cycle est similaire. Deuxièmement, une étape longue de régénération (basse pression) est indispensable pour assurer le fonctionnement. Par conséquent, comme dans le PSA, plusieurs vannes rapides sont nécessaires dans le procédé cyclique membranaire. Ceci rend le procédé beaucoup plus compliqué et entraîne une forte exigence de maintenance. C'est probablement la raison pour laquelle le procédé cyclique membranaire a été rarement poursuivi malgré l'initiative de Paul.

D'autre part, malgré l'intérêt montré par Paul [1971], son étude reste à un niveau de description qualitative avec de nombreux problèmes réels à résoudre. Par contre, toujours dans le cadre d'un fonctionnement cyclique, certains chercheurs ont tenté d'appliquer une durée de haute pression plus longue et de beaucoup réduire la durée de régénération. Ceci donne une autre vision du procédé cyclique qui n'a rien à voir avec le time-lag. Par conséquent, les procédés cycliques sont classés en deux catégories dans notre étude (tableau E.1): classe courte et classe longue.

A notre connaissance, l'étude de Paul a été poursuivie par un nombre très limité de chercheurs. Le tableau E.2 fournit un récapitulatif des procédés cycliques existants de classe courte mais aussi de classe longue.

	Classe courte (Procédé de Paul)	Classe longue
Durée d'étape	$\approx$ time-lag	$\gg$ time-lag
Etape de régénération	Nécessairement longue	Pas nécessairement longue

Table E.1: Classification des procédés cycliques

Chercheurs	Classe	Année	Investigation	Mélange
Paul [1971]	Courte	1971	Simulation	{CH_4 , He}
Higuchi and Nakagawa [1989]	Courte	1989	Simulation	{O_2 , N_2}
Beckman et al. [1991]	Courte	1991	Simulation & Expériences	{He , CO_2}
LaPack and Dupuis [1994]	Courte	1994	Expérience	Gaz organiques
Corriou et al. [2008]	Courte	2008	Simulation	{H_2 , CO_2}
Ueda et al. [1990]	Longue	1990	Expérience	{O_2 , N_2}
Feng et al. [2000]	Longue	2000	Simulation & Expérience	{H_2 , N_2}
Nemser [2005]	Longue	2005	Expérience	{Air , COV}

Table E.2: Récapitulatif des recherches sur le procédé cyclique membranaire.

Inventaire pour les procédés cycliques de classe courte

Paul [1971] montre que le procédé cyclique permet de contourner le compromis de sélectivité d'une membrane en minorant l'effet de solubilité. Par contre, cela ne s'applique pas à tous les mélanges gazeux. Une condition nécessaire pour le procédé cyclique est qu'un gaz diffuse plus rapidement que l'autre en régime transitoire. Cela peut se traduire par un facteur de diffusion $\alpha_{\mathcal{D}}$ (rapport de diffusivités) significativement supérieur à la permsélectivité α. Pour cette raison, un inventaire des gaz usuels est réalisé afin de déterminer les couples de gaz réels intéressants dans le cadre d'un procédé cyclique.

Actuellement, plusieurs corrélations sont disponibles pour calculer la limite supérieure (meilleures performances théoriques) des paramètres du gaz ($\mathcal{P}$, k_D et $\mathcal{D}$) à partir des données physiques des gaz concernés. En utilisant le mécanisme solution-diffusion, une bonne cohérence avec la réalité a été démontrée dans divers articles [Freeman, 1999, Robeson, 2008]. A l'aide de ces corrélations, il est possible d'estimer le rapport de diffusivités $\alpha_{\mathcal{D}}$ et la permsélectivité α. Dans notre inventaire, 66 gaz [Sherwood et al., 1975] ont été pris en compte à la fois pour un polymère dans son état caoutchoutique et son état vitreux. Ceci donne 2145 combinaisons de paires de gaz possibles.

Par convention, la permsélectivité est supérieure à 1. Les résultats sont classés en trois catégories selon le rapport $\frac{\alpha_{\mathcal{D}}}{\alpha}$:

- Domaine I. Lorsque $\frac{\alpha_{\mathcal{D}}}{\alpha} \gg 1$, le procédé cyclique permet d'avoir une meilleure sélectivité que le procédé fonctionnant en régime permanent.
- Domaine II. Lorsque $\frac{\alpha_{\mathcal{D}}}{\alpha} \ll 1$, le gaz rapide en régime permanent devient le gaz lent en régime transitoire. Le procédé cyclique fournit une sélectivité inversée par rapport au procédé fonctionnant en régime permanent.
- Domaine III. Lorsque $\frac{\alpha_{\mathcal{D}}}{\alpha} \approx 1$, du point de vue de la sélectivité, les procédés cyclique et en régime permanent ne diffèrent pas beaucoup. Vu la diminution de productivité et la complexité du procédé cyclique, l'intérêt du procédé cyclique est réduit dans ce cas.

A travers cet inventaire, nous constatons que le procédé cyclique ne montre pas uniquement une meilleure sélectivité potentielle, mais aussi un autre intérêt 'exclusif': la sélectivité inversée. Par contre, il faut noter que la limite supérieure calculée est une valeur théorique. Il se peut que les membranes existantes n'atteignent pas la limite supérieure et un tri dans la banque des données des membranes existantes est nécessaire. Il faut également noter que ce rapport n'est pas le critère unique et les frontières des domaines ne sont définies que arbitrairement. Supposant que ces trois domaines sont séparés arbitrairement selon la figure E.7, nous obtenons un récapitulatif des intérêts du procédé cyclique sur les 66 gaz considérés dans le tableau E.3. En conclusion, dans le cas d'un polymère caoutchoutique, le procédé cyclique de classe courte fournit a plupart du temps une sélectivité inversée alors que la tendance d'une sélectivité améliorée est plus attendue pour un polymère de type vitreux. Néanmoins, pour environ 20% de cas, notre inventaire n'est pas en mesure de fournir une conclusion 'définitive' car leurs rapports calculés se trouvent dans le domaine III.

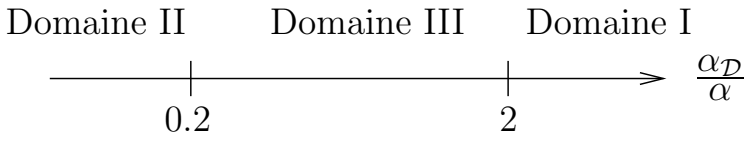

Figure E.7: Distribution des domaines définis en inventaire

Comparaison entre la classe courte et la classe longue

Nous avons évoqué que l'idée du procédé cyclique de classe courte utilise la différence des débits de perméations en régime transitoire dans la membrane.

Type de polymère	Domaine		
	I	II	III
Caoutchoutique	5.4%	73.8%	20.8%
Vitreux	31.4%	50.7%	17.9%

Table E.3: Récapitulatif de l'inventaire des 66 gaz considérés, 2145 combinaisons possibles

Plus généralement, pour un procédé membranaire, le débit de perméation peut s'écrire sous la forme suivante:

$$\dot{n}_k = f(\mathcal{P}_k, \Delta P_k, L, A) \tag{E.13}$$

Lors d'un fonctionnement en régime permanent, tous les paramètres sont fixés en production normale. En revanche, dans le cas du procédé cyclique de classe longue, ces quatre paramètres deviennent variables en fonction du temps. Ceci permet d'augmenter la liberté de l'opération sur le procédé lui-même afin de mieux adapter un procédé à une production spécifiée. Par conséquent, le régime 'transitoire' de classe courte se produit à l'intérieur de la membrane cependant que pour un procédé cyclique de classe longue, un régime 'transitoire' est observé à l'extérieur de la membrane.

Les procédés cités dans le tableau E.2 sont tous développés en détail dans le chapitre 3. Des discussions concernent certains points critiques. Nous constatons que l'étude sur les procédés cycliques de classe courte est assez complète d'un point de vue théorique et de l'optimisation. Ce genre de procédé permet de fournir des améliorations en sélectivité spectaculaires, mais en payant énormément en productivité. D'autre part, nous avons montré théoriquement que l'épuisement du flux d'alimentation d'un tel procédé est très faible.

Autrement dit, contrairement aux procédés en régime permanent, ceux de classe courte génèrent un rétentat qui a une composition très proche de celle du flux d'alimentation. Donc ce genre de procédé ne permet pas de séparer un mélange mais simplement d'extraire une très faible partie à une pureté élevée. Par conséquent, les procédés cycliques de classe courte ont du mal à être compétitifs en grande production face aux procédés en régime permanent. En revanche, il se peut qu'une application soit possible dans le domaine d'extraction de gaz de haute valeur ajoutée.

En ce qui concerne les procédés cycliques de classe longue, leurs améliorations en sélectivité sont moins importantes que celles de classe courte, alors que leurs pertes en productivité sont également moins considérables. Dans la littérature, les études sur les procédés cycliques de classe longue sont encore moins nombreuses. En plus, la plupart d'entre elles sont qualitatives et ont

été rarement optimisées. Néanmoins, des intérêts exclusifs ont été montrés par Feng et al. [2000], Nemser [2005], Ueda et al. [1990] mais de nombreux problèmes restent à résoudre.

Dans cette thèse, les procédés cycliques de classe courte sont d'abord étudiés et améliorés plus en détail en imposant des conditions opératoires réalisables. Un exemple de classe longue est donné par la suite, des intérêts remarquables ont été démontrés d'abord théoriquement puis par des expériences réalisées au sein du LRGP.

Modélisation du transport et optimisation

L'étude sur les procédés cycliques est réalisée essentiellement par simulation. Ainsi, un modèle de transport au sein de la membrane doit être d'abord sélectionné en satisfaisant les deux critères: simplicité et efficacité. Nous avons évoqué dans le chapitre 2 que les membranes utilisées dans nos études sont pratiquement toutes en polymère, pour lesquelles le mécanisme solution-diffusion est bien adapté. En revanche, nous avons également évoqué que le cas le plus simple du mécanisme solution-diffusion qui résulte en une loi de Fick linéaire (l'équation (E.4)) ne permet pas de décrire quantitativement le phénomène dans le cas d'une membrane vitreuse. Pour corriger l'écart avec la réalité, de nombreux chercheurs [Koros et al., 1976, Paul, 1969, Vieth et al., 1966, 1976] ont proposé la théorie "Dual Mode Sorption". Dans le chapitre 4, cette théorie a été révisée sous un angle critique et un comportement aux limites non exploité a été mis en évidence.

Modèles classiques de la théorie Dual Mode Sorption

Comme expliqué auparavant, la sorption d'un corps pur peut être décrite par l'équation (E.9). Ceci a été extrapolé en mélange binaire par Koros [1980]. Pour un mélange $\{A, B\}$, un terme compétitif intervient dans la sorption du gaz A:

$$C_A = C_{DA} + C_{HA} = k_{DA} P_A + \frac{C'_{HA} b_A P_A}{1 + b_A P_A + b_B P_B} \tag{E.14}$$

Koros [1980], Sanders and Koros [1986] montrent que l'équation (E.14) présente une erreur de 2% dans leur démonstration expérimentale, en plus, les paramètres utilisés dans l'équation (E.14) sont les mêmes que ceux utilisés pour décrire la sorption d'un corps pur. Ainsi, la théorie Dual Mode Sorption est élargie dans la description du transport des mélanges.

En ce qui concerne la deuxième partie du mécanisme solution-diffusion, la situation est plus compliquée. Durant le développement de la théorie, deux hypothèses ont été considérées:

- Immobilisation partielle. Les molécules obéissant à la loi de Langmuir sont considérées posséder une mobilité réduite (diffusivité $\mathcal{D}_H$) par rapport aux molécules obéissant à la loi de Henry (diffusivité $\mathcal{D}_D$) dans la direction de perméation. Au début du développement de la théorie et dans certains cas spéciaux, la mobilité des molécules de type Langmuir est considérée comme nulle.
- Equilibre local. Un équilibre local existe entre deux types de molécules au sein de la membrane. Cet équilibre s'établit instantanément et selon la loi suivante:

$$C_H = \frac{\frac{C_H^{'} b}{k_D} C_D}{1 + \frac{b}{k_D} C_D} \tag{E.15}$$

La théorie Dual Mode Sorption avec ces deux hypothèses aboutit à un modèle dit PIM (Partial Immobilization Model). Le transport au sein de la membrane est décrit ainsi par une loi de Fick non linéaire:

$$\left[1 + \frac{K}{(1 + aC_D)^2}\right] \frac{\partial C_D}{\partial t} = \frac{\partial}{\partial r}\left[\mathcal{D}_D \left(1 + \frac{FK}{(1 + aC_D)^2}\right) \frac{\partial C_D}{\partial r}\right] \tag{E.16}$$

où $K = \frac{C_H^{'} b}{k_D}$ et $a = \frac{b}{k_D}$. C_H est substituée par C_D à l'aide de l'équilibre local (équation (E.15)). Le paramètre F représente le rapport des mobilités $\frac{\mathcal{D}_H}{\mathcal{D}_D}$ entre deux types de molécules. Il est en général inférieur à 1.

La pertinence de l'équation (E.16) a été montrée expérimentalement par Koros and Paul [1978], Koros et al. [1976], Vieth et al. [1976]. L'équation (E.16) a été appliquée à un mélange gazeux en faisant intervenir les termes compétitifs:

$$\left[1 + \frac{K_k}{(1 + \sum_{i=1}^{n} a_i C_i)^2}\right] \frac{\partial C_k}{\partial t} = \frac{1}{r}\frac{\partial}{\partial r}\left[r\mathcal{D}_k \left(1 + \frac{F_k K_k}{(1 + \sum_{i=1}^{n} a_i C_i)^2}\right) \frac{\partial C_k}{\partial r}\right] \tag{E.17}$$

Cette équation (E.17) est considérée comme l'équation générale PIM de modélisation dans cette thèse et est résolue à l'aide des outils numériques, notamment la méthode des volumes finis (Annexe D) dans la simulation.

Afin d'améliorer la performance de la membrane, un type de membrane hétérogène (Mixed Matrix Membrane) est largement utilisé dans l'industrie [Aroon et al., 2010]. Ce genre de membrane comporte une phase continue en polymère et une phase dispersée en particules inorganiques. Si la phase continue est un polymère caoutchoutique, Paul [1969], Paul and Kemp [1973] montrent que le mécanisme du transport de gaz dans ce milieu hétérogène est similaire à celui dans une membrane vitreuse: le gaz est dissout dans le polymère caoutchoutique selon la loi de Henry alors qu'il peut aussi être capté par les particules inorganiques selon la loi de Langmuir. En revanche, ces dernières ne sont pas du tout mobiles. Ceci se traduit mathématiquement par $F = 0$. Une relation similaire à l'équilibre local (équation (E.15)) permet de relier ces deux types de molécules dans ce milieu hétérogène.

Selon Paul [1969], le comportement gazeux dans ce milieu hétérogène est similaire à l'équation (E.16):

$$\left[1 + \frac{K\dfrac{v_d}{v_p}}{(1 + \dfrac{a}{v_p}C_D)^2}\right]\frac{\partial C_D}{\partial t} = \mathcal{D}_m\frac{\partial^2 C_D}{\partial r^2} \tag{E.18}$$

avec $\mathcal{D}_m$ diffusivité effective due à l'ajout de phase dispersée. v_p et v_d sont les fractions volumiques de phase continue et de phase dispersée respectivement. L'équation (E.18) a été validée par Kemp and Paul [1974], Paul [1969], Paul and Kemp [1973] et est utilisée dans cette thèse pour une simulation d'un procédé cyclique basé sur une membrane hétérogène.

Comportement aux limites du modèle PIM

Dans le modèle classique PIM, l'équilibre local est considéré comme instantané dans la membrane. Dans un cas plus général, cette relation entre deux types de molécules peut être décrite par une réaction chimique réversible [Tshudy and Frankenberg, 1973]. Pour des raisons de simplicité, chaque site d'adsorption de type Langmuir est supposé pouvoir immobiliser une seule molécule gazeuse:

$$\text{site } (C_H' - C_H) + \text{molécule dissoute } (C_D) \underset{k_r}{\overset{k_f}{\rightleftharpoons}} \text{complexe } (C_H)$$

Ainsi les bilans locaux sur chaque type de molécule sont donnés par:

$$\begin{aligned}\frac{\partial C_D}{\partial t} &= \frac{\partial}{\partial r}(D_D\frac{\partial C_D}{\partial r}) - \left[k_f C_D(C_H' - C_H) - k_r C_H\right]\\ \frac{\partial C_H}{\partial t} &= \frac{\partial}{\partial r}(D_D\frac{\partial C_H}{\partial r}) + \left[k_f C_D(C_H' - C_H) - k_r C_H\right]\end{aligned} \tag{E.19}$$

avec k_f et k_r constantes cinétiques des réactions correspondantes. Par conséquent, deux comportements aux limites peuvent être considérés selon les équations (E.19),

- Dans un cas d'échange rapide, k_f et k_r tendent vers infini, l'équilibre local (l'équation (E.15)) s'établit ainsi instantanément. Autrement dit, l'hypothèse de l'équilibre local est admise. Ce premier comportement aux limites correspond au modèle classique PIM.
- Dans un cas d'échange lent, k_f et k_r tendent vers zéro. Les deux types de molécules s'approchent du régime permanent avec leur propre vitesse. L'équation (E.19) est réduite à:

$$\begin{aligned} \frac{\partial C_D}{\partial t} &= \frac{\partial}{\partial r}\left(\mathcal{D}_D \frac{\partial C_D}{\partial x}\right) \\ \frac{\partial C_H}{\partial t} &= \frac{\partial}{\partial r}\left(\mathcal{D}_H \frac{\partial C_H}{\partial x}\right) \end{aligned} \tag{E.20}$$

Ce deuxième comportement aux limites de la théorie Dual Mode Sorption est noté par Dual Diffusion Model (DDM) dans cette thèse. Au lieu d'une équation aux dérivées partielles non-linéaire (l'équation (E.17)), le transport dans la membrane est décrit par une combinaison des deux équations aux dérivées partielles linéaires. Selon nos connaissances, ce deuxième comportement au limite n'a pas été exploité auparavant et sera discuté en détail en comparant avec le PIM dans cette thèse.

Comparaison entre les comportements aux limites

Nous notons d'abord que seuls les comportements des corps purs sont comparés dans cette étude.

Perméabilité théorique en régime permanent

Dans un premier temps, nous étudions la perméabilité en régime permanent qui est une caractéristique du régime permanent du transport dans la membrane.

Nous avons montré dans le chapitre 2 que la perméabilité théorique $\mathcal{P}$ d'un gaz peut être déterminée en fournissant les conditions aux limites nécessaires à l'équation aux dérivées partielles. Pour le modèle le plus simple, la perméabilité est constante $\mathcal{P} = k_D\mathcal{D}$. Cependant, en résolvant l'équation (E.16) soumise aux mêmes conditions aux limites, la perméabilité dans le cas du PIM est donnée par:

$$\mathcal{P} = k_D\mathcal{D}_D\left[1 + \frac{FK}{1 + bP_u}\right] \tag{E.21}$$

La perméabilité dans le cas du DDM peut être obtenue de manière similaire (Annexe A). En faisant ce calcul, nous constatons que les deux comportements aux limites fournissent exactement la même expression analytique de perméabilité. En plus, cette similitude peut être déployée dans un cas plus général: pour une membrane immergée aux pressions fixées en amont et en aval, les PIM et DDM prédisent exactement la même perméabilité en régime permanent (Annexe A) selon la théorie Dual Mode Sorption. En outre, en sommant les deux équations (E.19), les termes de 'réaction" sont éliminés indépendamment de la vitesse d'échange entre les deux types de molécules. Ceci explique la raison pour laquelle la même perméabilité est déterminée par les deux comportements aux limites. Par conséquent, la perméabilité dans le cadre de la théorie Dual Mode Sorption est toujours la même pour une vitesse d'échange quelconque.

Time-lag théorique

Dans la suite de l'étude, nous nous intéressons à la détermination du time-lag, qui est une caractéristique du régime transitoire du transport dans la membrane. Paul and Koros [1976] ont résolu analytiquement l'équation aux dérivées partielles du PIM et fourni une expression analytique du time-lag:

$$\theta = \frac{l^2}{6\mathcal{D}_D} \frac{1 + K(f_0 + FKf_1 + (FK)^2 f_2) + FKf_3 + (FK)^2 f_4}{\left(1 + \frac{FK}{1+y}\right)^3} \tag{E.22}$$

avec

$$\begin{aligned}
f_0 &= \frac{6}{y^3}\left(\frac{y^2}{2} + y - (1+y)\ln(1+y)\right) \\
f_1 &= \frac{6}{y^3}\left(\frac{y}{2} + \frac{3y}{2(1+y)} - \frac{\ln(1+y)}{1+y}\right) \\
f_2 &= \frac{6}{y^3}\left(\frac{1}{6} - \frac{1}{2(1+y)} + \frac{1}{2(1+y)^2} - \frac{1}{6(1+y)^3}\right) \\
f_3 &= \frac{6}{y^3}\left(-\frac{3}{2}y + \frac{y}{2(1+y)} + (1+y)\ln(1+y)\right) \\
f_4 &= \frac{6}{y^3}\left(\frac{1}{2} - \frac{1}{2(1+y)^2} - \frac{\ln(1+y)}{1+y}\right) \\
y &= bP_u
\end{aligned} \tag{E.23}$$

Le time-lag est également déterminé par le DDM en Annexe B:

$$\theta = \frac{l^2}{6\mathcal{D}_D} \frac{1 + K + bP_u}{1 + FK + bP_u} \tag{E.24}$$

Contrairement à la perméabilité en régime permanent, ces deux modèles prédisent des time-lags différents dans les mêmes conditions. Il est important de noter que les paramètres dans les équations (E.22) et (E.24) ont trait aux mêmes définitions et fournissent les mêmes valeurs et qu'ils peuvent être déterminés expérimentalement de la même manière. En revanche, il est aussi important de noter que deux prédictions sont cohérentes dans le cas limite:

$$\begin{aligned} \lim_{P_u \to 0} \theta &= \frac{l^2}{6\mathcal{D}_D} \frac{1+K}{1+FK} \\ \lim_{P_u \to +\infty} \theta &= \frac{l^2}{6\mathcal{D}_D} \end{aligned} \tag{E.25}$$

Ceci suggère que les deux prédictions permettent de borner une zone fermée de prédiction de time-lag comme illustré dans la figure E.8. En règle générale, le PIM fournit la borne supérieure alors que la borne inférieure est prédite par le DDM. On pourrait en déduire que dans le cas des valeurs intermédiaires de constantes d'échange k_f et k_d, la prédiction du time-lag se trouverait entre ces deux bornes.

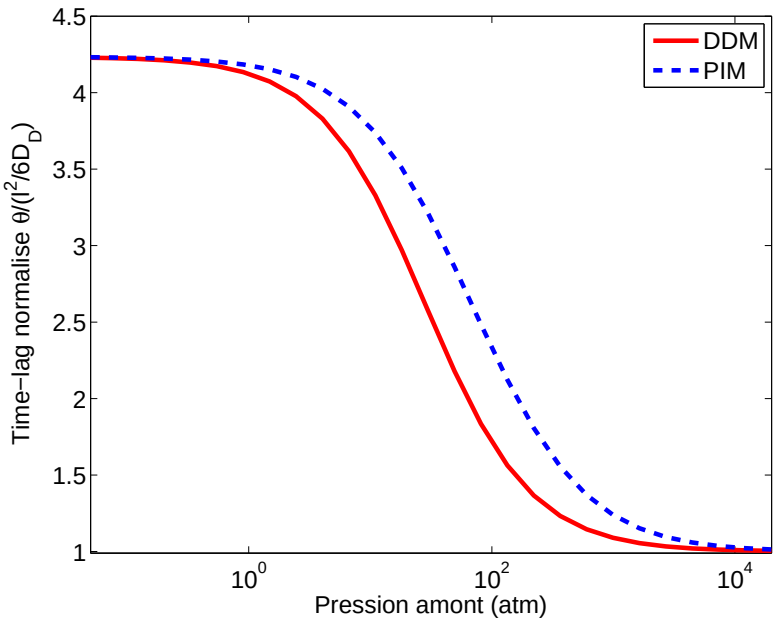

Figure E.8: Prédiction du time-lag selon le DDM et le PIM avec $K = 5$ et $b = 0.05$ atm^{-1}. (DDM = Dual Diffusion Model, PIM = Partial Immobilization Model

Comparaison avec les valeurs de time-lags déterminées expérimentalement

Nous avons mis en évidence que la différence entre les deux comportements aux limites apparaÃ®t pendant le régime transitoire, notamment par la valeur du time-lag. Dans le cadre de cette thèse, les deux prédictions du time-lag fournies par le DDM et le PIM sont comparées aux données expérimentales. Ce genre de mesures de time-lag a été largement effectué dans les années 1970, notamment par les équipes de Paul et de Koros. En prenant les paramètres déterminés expérimentalement par les auteurs, le time-lag peut être déterminé théoriquement par le DDM, le PIM et le IM (Immobilization Model). Ce dernier a été proposé au début du développement de la théorie Dual Mode Sorption mais remplacé plus tard par le PIM. Dans ce modèle IM, le rapport de mobilité F est considéré comme nul cependant que l'équilibre local est toujours pris en compte.

Dans nos comparaisons, trois matériaux sont étudiés: PET, polycarbonate et PEMA dans leur état vitreux. Les figures 4.11, 4.12 et 4.13 illustrent cette comparaison, nous constatons que dans tous les cas, la borne inférieure prédite par le DDM représente la meilleure approche des données expérimentales. Afin de quantifier le pouvoir de prédiction de chaque modèle, une erreur relative e est définie pour chaque matériau testé,

$$e = \frac{|\theta_{exp} - \theta_i|}{\theta_{exp}} \qquad i = \text{DDM, PIM et IM} \tag{E.26}$$

Selon le tableau E.4, pour les trois matériaux testés, la prédiction fournie par le DDM donne le meilleur accord avec les données expérimentales. L'erreur relative du DDM est en général inférieure à 11%. D'autre part, le tableau E.4 confirme la qualité de prédiction du PIM par rapport à son prédécesseur: IM.

Cependant, il est très important de noter que la détermination du time-lag risque d'introduire des erreurs importantes. Premièrement, la perméation dans la membrane dépend de l'histoire de son utilisation. Deuxièmement, la procédure de la formation de la membrane, la durée de chaque mesure, la façon et la durée de régénération de la membrane sont tous des éléments importants qui induisent par conséquence des erreurs expérimentales que l'on constate dans les figures de comparaison. En outre, l'épaisseur effective de la membrane L n'est pas strictement constante lors de l'application d'une pression forte. En plus, l'influence de l'épaisseur est amplifiée dans le calcul du time-lag par une expression de L^2.

Enfin, nous notons que la théorie Dual Mode Sorption est simple et efficace, mais elle ne représente pas toute la réalité. Des exceptions ont été mentionnées par Doghieri and Sarti [1996], Galizia et al. [2011], Minelli et al. [2011],

Matériaux	e_{DDM}	e_{PIM}	e_{IM}
PET	8.43%	11.46%	33.46%
Polycarbonate	10.42%	17.08%	50.03%
PEMA	3.79%	-	5.77%

Table E.4: Erreur relative moyenne e pour les trois types de matériaux : PET, Polycarbonate et PEMA

Nakanishi et al. [1987]. Malgré tout, cette théorie reste un outil puissant d'un point de vue de l'ingénieur et a souvent été utilisée avec succès [Koros et al., 1976, Vieth et al., 1976]. Dans cette thèse, la théorie est complétée à l'aide de l'analyse sur l'autre comportement aux limites (DDM). L'étude théorique de cette thèse est basée sur l'équation générale du PIM (l'équation (E.17)) en fournissant les conditions aux limites adéquates. La résolution de cette équation aux dérivées partielles dans un cas général est fournie en Annexe D. Malgré tout, les paramètres de transport sont disponibles dans la littérature uniquement sous forme de deux paramètres moyens k_D et $\mathcal{D}$ comme une approximation [Brandrup and Immergut, 1989]. Par conséquent, le modèle simple avec les k_D et $\mathcal{D}$ moyens est utilisé principalement dans notre simulation (Sections 5.1 and 5.3). Comme une membrane hétérogène a été étudiée en détail par Paul [1969], tous les paramètres de Dual Mode Sorption sont disponibles pour le couple gaz-membrane, le procédé correspondant est ainsi simulé en utilisant le modèle complet.

Modélisation et optimisation

Selon le modèle de la théorie Dual Mode Sorption, un procédé membranaire peut être ainsi simulé. Dans cette étude, le module à fibres creuses (Hollow fiber module) est exclusivement utilisé comme séparateur membranaire. Ainsi les coordonnées cylindriques en 1D sont utilisées dans la simulation. Tout le volume à l'intérieur des fibres est considéré comme le volume amont alors que le volume à l'extérieur des fibres est considéré comme le volume aval. Chaque volume est considéré comme homogène et le remplissage ou la vidange dans un volume donné est instantané.

Les gaz dans la membrane obéissent à la loi de Fick exploitée précédemment, et ceux dans les volumes amont et aval sont considérés comme des gaz parfaits.

Dans la modélisation, les hypothèses suivantes sont prises:

- La membrane est uniforme et son support ne représente aucune résistance aux transferts de masse.

- Toutes les opérations sont isothermes.
- La plastification de la membrane est négligée.
- Les paramètres de transport (k_D, $\mathcal{D}$, etc) sont considérés comme constants.
- Les couplages de flux sont négligés.

La résolution du problème est programmé en FORTRAN en appliquant la méthode des volumes finis pour les équations aux dérivées partielles.

Ensuite, la performance du procédé est optimisée en définissant un ou plusieurs critères d'optimisation tout en respectant une ou plusieurs consignes d'opération. Ceci forme un problème d'optimisation multicritère:

$$\max_{x_i, i=1..k} \begin{pmatrix} \text{Critère 1} \\ .... \\ \text{Critère n} \end{pmatrix}$$

soumis aux contraintes:

$$g_j(\boldsymbol{x}) \leq 0 \qquad j = 1, m$$

Afin de résoudre ce problème, l'algorithme génétique programmé également en FORTRAN est appliqué. Grâce à cet outil d'optimisation quasi-globale, une performance optimale est obtenue pour chaque conception du procédé. A l'aide d'une comparaison systématique avec les meilleures performances d'un procédé en régime permanent, nous arrivons à identifier les avantages et les inconvénients du procédé étudié.

Etude de cas

Classe courte avec membranes caoutchoutiques

Dans un premier temps, un procédé cyclique basé sur l'idée de Paul est étudié. La conception du procédé et le fonctionnement sont similaires au procédé de Paul (figure E.9), mais trois différences importantes sont mises en évidence:

- Un module à fibres creuses est utilisé dans notre étude au lieu d'une membrane plane étudiée par Paul. La surface spécifique peut alors atteindre 1000 m^2/m^3. La longueur d'une fibre est fixée à 1 m et le diamètre interne de la fibre est 50 μm.

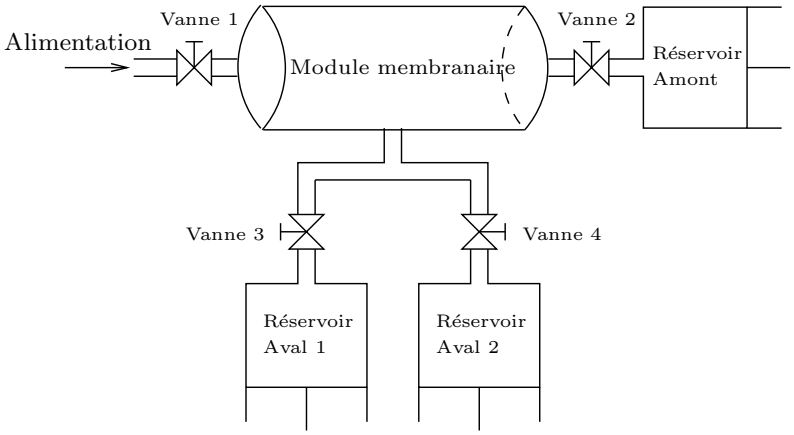

Figure E.9: Schéma du procédé étudié dans cette thèse

- Au lieu d'imposer les pressions totales et les compositions du gaz en amont et en aval, l'épuisement en amont et l'accumulation en aval de chaque composé gazeux sont pris en compte. Ainsi, une rétro-diffusion pourrait avoir lieu si un gradient de pression l'autorisait.

- Les opérations de vannes ne sont pas forcément synchrones. Les durées d'ouverture de chaque vanne seront notées par x_1, x_2, x_3 et x_4 respectivement. Le meilleur fonctionnement sera déterminé à l'aide d'une étude d'optimisation.

Dans l'étude de Paul, un seul critère est pris en compte: la sélectivité. Par conséquent, un produit ultra pur est obtenu avec une productivité nulle. Ceci n'offre aucun intérêt dans la réalité. Au contraire, dans notre étude, la performance d'un tel procédé est définie par deux critères: le facteur de séparation et la productivité. En supposant que le composé gazeux 1 est le produit désiré, le facteur de séparation est défini par:

$$\text{facteur de séparation} = \frac{y_1^{d,\mathcal{L}}}{1-y_1^{d,\mathcal{L}}}\frac{1-y_1^f}{y_1^f} \tag{E.27}$$

où $y_1^{d,\mathcal{L}}$ est la fraction molaire du composé 1 dans le réservoir aval 1 (figure E.9) où le produit désiré est enrichi selon Paul [1971], et y_1^f la fraction molaire du même composé dans le flux d'alimentation. La productivité est définie par le nombre de moles du composé désiré collecté dans le réservoir aval 1 divisé par la durée totale d'opération et la surface effective de la membrane:

$$\text{productivité (mol/m}^2\text{.s)} = \frac{n_1^{d,\mathcal{L}}}{A\Delta t} \tag{E.28}$$

Dans notre étude, un mélange binaire équimolaire est considéré. L'objectif est alors d'obtenir un flux enrichi en composé gazeux désiré à la fois avec une forte productivité et un haut facteur de séparation.

Par conséquent, le problème d'optimisation est posé par rapport au facteur de séparation et à la productivité.

$$\max_{x_1,x_2,x_3} \begin{pmatrix} \text{facteur de séparation} \\ \text{productivité} \end{pmatrix}$$

soumis aux contraintes

$$\begin{gathered} x_1 + x_2 = x_3 + x_4 \\ x_i \geq 1 \qquad i = 1..4 \\ x_1 + x_2 \leq 100 \end{gathered}$$

La première contrainte a pour but d'assurer l'intégralité du cycle. La deuxième représente une contrainte pratique: dans l'industrie, la fréquence d'ouverture de vanne ne dépasse pas 1 fois par seconde en règle générale [Feng et al., 2000]. La troisième représente une durée maximale d'un cycle qui est fixée arbitrairement.

Dans le chapitre 3, nous avons mis en évidence que le time-lag du composé avec une faible diffusivité joue un rôle très important dans les durées de chaque étape du procédé de Paul. Paul [1971] propose d'estimer la durée totale τ d'un cycle par:

$$\tau = U \frac{L^2}{6\mathcal{D}_k} \tag{E.29}$$

avec L épaisseur de la membrane et U facteur proposé par Paul qui dépend de la fraction de la haute pression dans un cycle. Selon Paul [1971], dans le cas où l'étape de la haute pression occupe 10% d'un cycle, la séparation optimale est observée pour $U = 3$. Bien que moins d'hypothèses simplificatrices soient prises dans notre étude, l'équation (E.29) est utilisée dans notre étude comme une approximation. Par conséquent, l'épaisseur de la membrane L est judicieusement choisie à l'aide de l'équation (E.29) pour que la durée totale d'un cycle τ soit comprise dans l'intervalle [1, 100]s.

Les conditions de simulation sont récapitulées dans le tableau E.5. La performance optimale d'un procédé cyclique est systématiquement comparée à celle d'un procédé classique en régime permanent. Ce dernier fonctionne à un rapport de pression perméat/rétentat $\Psi = 0.01$ et en courants croisés (figure 4.16). Tous les autres paramètres du fonctionnement se trouvent dans le tableau E.5. Les critères de performance sont définis d'une manière similaire

Surface d'échange	10^3	m^2
Température	297.15	K
Haute pression	1.013 10^5	Pa
Pression initiale en amont	0	Pa
Volume amont/aval	0.0125	m^3
Volume du réservoir aval 1	0.0125	m^3
Volume du réservoir aval 2	0.0125	m^3

Table E.5: Conditions de simulation d'un procédé de classe courte

à ceux du procédé cyclique. Leur stage cut ζ (taux de prélèvement) varie afin d'obtenir une courbe de performance.

A titre d'exemple, un mélange binaire équimolaire {He,N_2} est séparé en simulation par le procédé cyclique et un procédé en régime permanent. Selon le tableau E.6, ce mélange possède une permsélectivité $\alpha = 1.03$ très proche de 1, qui suggère que la séparation est difficile dans le cas d'un procédé en régime permanent. En revanche, $\alpha_{\mathcal{D}} = 4.82$ montre qu'une sélectivité améliorée est attendue dans le cas d'un procédé cyclique. Par conséquent, le facteur de séparation et la productivité sont définis par rapport au gaz rapide en régime transitoire: He.

Usage: récupération d'Helium $\alpha = 1.03$			
Gas	$\mathcal{P}\times 10^{15}$	$\mathcal{D}\times 10^{10}$	$k_D\times 10^6$
He	175	41	0.424
N_2	170	8.5	2.0

Table E.6: Paramètres de transport issus de Polymer Handbook [Brandrup and Immergut, 1989]. Poly(oxydimethylsilylene) avec 10% additif Scantocel CS, vulcanisé en silicone caoutchoutique. (Unités S.I.)

La figure E.10 montre que comme prévu, le procédé en régime permanent ne permet pas vraiment de séparer le mélange car le facteur de séparation se trouve proche de 1. Par contre, si le procédé cyclique de classe courte est appliqué sur le même mélange binaire et la même membrane, une séparation est observée avec un facteur de séparation important (entre 1 et 1000). L'intérêt du procédé cyclique indiqué par Paul [1971] est mis en évidence. En revanche, il faut noter que cette amélioration du facteur de séparation n'est obtenue qu'en baissant la productivité. Grossièrement, en multipliant le facteur de séparation par 100, la productivité est réduite à 1/50.

En outre, ces productivités sont calculées par une membrane de 300 μm à la fois pour le procédé cyclique et le procédé en régime permanent. Dans le

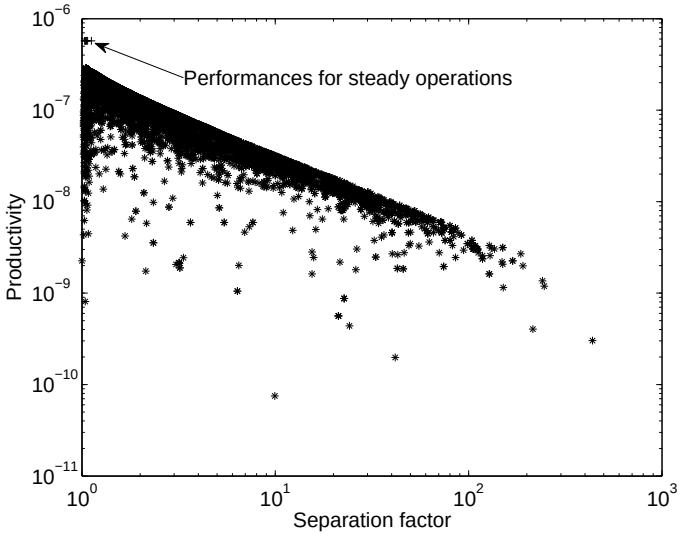

Figure E.10: Comparaison de performances d'un procédé en régime permanent (+) et un procédé cyclique de classe courte (*), avec un mélange équimolaire {He,N_2}. Conditions de simulation dans le tableau E.5 et paramètres de transport dans le tableau E.6 pour une membrane de 300 μm.

cas du procédé cyclique, cette grande épaisseur a pour but d'assurer une ouverture de vannes réalisable. Comme le procédé en régime permanent ne fait pas intervenir l'ouverture fréquente des vannes et que la productivité est inversement propositionnelle à l'épaisseur active, dans les applications actuelles, l'épaisseur active de la membrane est en fait beaucoup plus petite (de l'ordre de 1 μm ou encore moins) que cette valeur afin d'obtenir une bonne productivité. C'est ainsi que l'écart entre les deux types de fonctionnement du point de vue de la productivité sera encore beaucoup plus important en réalité. Ceci confirme que la perte de productivité du procédé cyclique limite fortement l'implantation d'un tel procédé dans l'industrie.

D'une manière similaire, les procédés cycliques basés sur trois autres mélanges binaires ({He,Ar}, {H_2,C_3H_8} et {$^{235}UF_6$,$^{238}UF_6$}) ont été simulés, optimisés puis comparés aux procédés en régime permanent. Des conclusions similaires sont obtenues.

En outre, une étude théorique sur l'épuisement maximal d'un procédé cyclique de classe courte a été réalisée dans cette thèse. Si un taux d'épuisement Θ_k du composé k est défini par le rapport du nombre de moles ayant quitté le volume amont dn_k^{out} à la fin d'un cycle sur le nombre de mole initiales dans

le volume amont,

$$\Theta_k = \frac{\int_0^{t\text{end}} \left(\frac{dn_k^{\text{out}}}{dt} \right) dt}{n_k^0} \tag{E.30}$$

La valeur de Θ_k ne dépasse pas 0.1 % dans un cas où l'épuisement est fortement favorisé. Ceci suggère que le procédé cyclique de classe courte ne permet pas de "séparer" le flux d'alimentation, mais simplement d'"extraire" une faible partie à une haute pureté. Autrement dit, nous confirmons que le rétentat possède une composition très proche de celle dans le flux d'alimentation. L'hypothèse de départ proposée par Paul [1971] n'est pas absurde.

En conclusion, le seul mais exclusif intérêt du procédé cyclique est l'amélioration en sélectivité par rapport au procédé en régime permanent. Un facteur de séparation spectaculaire peut être obtenu avec le procédé cyclique de classe courte cependant que cet effet est toujours accompagné d'une forte chute en productivité et d'un faible taux d'épuisement en amont. En général, la productivité d'un procédé cyclique ne dépasse pas 10^{-6} mol.m^{-2}.s^{-1}. Bien que l'utilisation d'un module à fibres creuses permette d'avoir une surface d'échange importante, il est encore très difficile d'atteindre une production usuelle de 100 mol.s^{-1} dans l'industrie [Baker, 2002]. Pour atteindre à cet objectif, la surface de la membrane doit être supérieure à 10^8 m^2 selon nos simulations. Toutefois, ce type de procédé peut être intéressant pour une extraction d'un gaz rare qui fait intervenir régulièrement du recyclage lorsque la valeur ajoutée du produit final est élevée.

Classe courte avec membranes hétérogènes

Paul [1969] montre que l'ajout des adsorbants dans une membrane caoutchoutique permet d'augmenter significativement le time-lag du composé gazeux fortement adsorbé. Cependant, l'augmentation du time-lag du composé gazeux faiblement adsorbé est peu importante. Dans le chapitre 5, nous avons évoqué que l'efficacité d'un procédé cyclique de classe courte est favorisée par une grande différence des time-lag entre les composés gazeux à séparer. Ainsi, une étude du procédé cyclique est effectué en considérant une membrane hétérogène.

Nous avons choisi le couple {CO_2,He} dans cette étude. A travers une membrane RTV-602 Silicone Rubber avec 21.6 vol.% de zéolite, Paul and Kemp [1973] indiquent que l'augmentation du time-lag de CO_2 est clairement observée alors que l'effet de zéolite n'est pas significatif pour He. Par conséquent, le transport de CO_2 dans cette membrane hétérogène est décrit par l'équation (E.18) bien que celui de He soit considéré comme dans

une membrane caoutchoutique homogène (équation (E.17) avec $K = 0$ et $F = 0$). Les paramètres de transport sont donnés dans le tableau E.7.

	$C_H^{'}$ $\text{cm}^3(\text{STP})/\text{cm}^3$	b $(\text{cmHg})^{-1}$	$k_D \times 10^3$ $\text{cm}^3(\text{STP})/\text{cm}^3.\text{cmHg}$	$\mathcal{D} \times 10^9$ m^2/s
CO_2	102.6	0.0928	14.5	2.14
He	-	-	0.582	7.86

Table E.7: Paramètres de transport dans le RTV-602 Silicone Rubber avec 21.6 vol.% de zéolite selon Paul and Kemp [1973].

D'après une étude préliminaire, nous avons découvert que la quantité résiduelle du gaz fortement adsorbé reste très importante dans la membrane. Par conséquent, le procédé pour une membrane hétérogène n'est pas le même que celui utilisé pour les membranes caoutchoutiques. Ce nouveau procédé est d'abord plus réalisable et en plus permet de récupérer le gaz resté dans la membrane pendant l'étape de régénération (figure E.11).

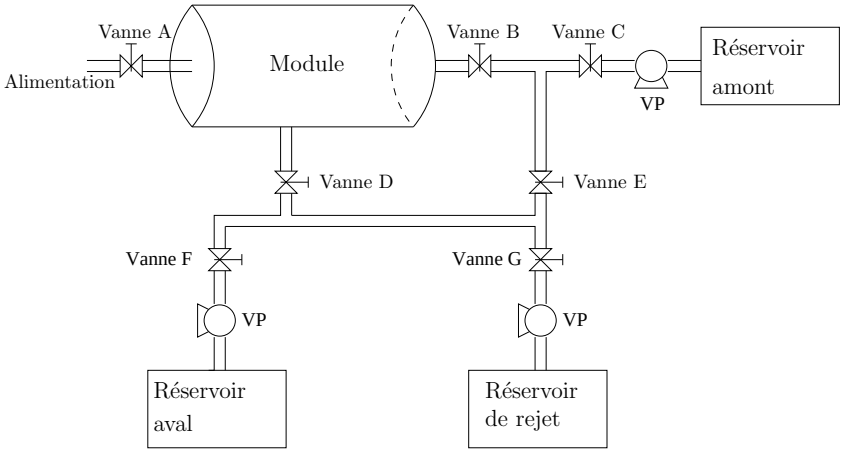

Figure E.11: Schéma du procédé cyclique dédié aux membranes hétérogènes, VP = pompe à vide.

L'opération cyclique de ce procédé est décrite dans le tableau E.8. Selon le tableau E.7 et nos inventaires sur le procédé cyclique de classe courte, une sélectivité inversée serait observée. Ainsi à la fin de chaque cycle, le flux d'alimentation est séparé en trois parties: de manière semblable au procédé de Paul, un mélange enrichi en He est obtenu dans le réservoir aval. Selon nos études préliminaires, le réservoir amont recueille un mélange également enrichi en He alors qu'une très haute pureté est observée dans le réservoir de rejet où le gaz résiduel dans la membrane est essentiellement collecté.

Valve	A	B	C	D	E	F	G
Alimentation	o	-	-	-	-	-	-
Perméation libre	-	-	-	-	-	-	-
Réception	-	o	o	o	-	o	-
Régénération	-	o	-	o	o	-	o

Table E.8: Opérations cycliques du procédé de figure E.11. ('o' pour ouvert et '-' pour fermé)

Nombre de modules	1	
Longueur du module	1	m
Surface spécifique	10^3	m^2/m^2
Température	303.15	K
Composition dans le courant d'alimentation	1:1	
Pression totale haute en amont	10^5	Pa
Epaisseur de la membrane	$50\ 10^{-6}$	m
Pression aval initiale	0	Pa
Volume amont/aval dans le module	0.0125	m^3
Volume du réservoir amont	1	m^3
Volume du réservoir aval	1	m^3
Volume du réservoir de rejet	1	m^3

Table E.9: Conditions de simulation pour le procédé utilisant le MMM.

Comme dans le procédé cyclique utilisant des membranes caoutchoutiques, deux critères de performances sont pris en compte dans nos études: le facteur de séparation (l'équation (E.27)) et la productivité (l'équation (E.28)). Pour des raisons de simplicité, ces critères de performance sont uniquement définis par rapport à He dans le réservoir aval afin de faciliter une comparaison avec le procédé cyclique utilisant des membranes caoutchoutiques et le procédé en régime permanent. En revanche, les critères de performance peuvent être tout à fait définis par rapport à un autre gaz dans un autre réservoir selon les besoins.

En outre, en tenant compte des contraintes d'opération sur les vannes et l'étude préliminaire, les durées de chaque étape sont définies dans le tableau E.10, où les durées de l'étapes d'alimentation et de la réception prennent leurs valeurs sur la contrainte minimale d'ouverture de vannes. Par conséquent, si les quatre durées sont fournies, un procédé peut être défini. Un problème d'optimisation est ainsi posé par

$$\max_{x_1,x_2} \begin{pmatrix} \text{facteur de séparation} \\ \text{productivité} \end{pmatrix}$$

soumis aux contraintes

$$1 \leq x_1 \leq 100s$$
$$1 \leq x_2 \leq 200s$$

Etape	Symbole	Durée
Alimentation		1 s
Perméation libre	x_1	1-100 s
Réception		1 s
Régénération	x_2	1-200 s

Table E.10: Intervalle des durées de chaque étape dans l'étude du procédé cyclique dédié aux membranes hétérogènes.

Les résultats d'optimisation sont présentés dans la figure E.12, les conclusions suivantes sont obtenues:

- En prenant en compte les contraintes d'opération, la sélectivité inversée n'est pas obtenue dans le cas d'un procédé cyclique utilisant une membrane homogène. Ceci peut être expliqué par le fait que la contrainte d'opération (1 s) est trop importante par rapport au time-lag de CO_2 (gaz lent en régime transitoire) dans la membrane homogène.
- L'intérêt du procédé cyclique de classe courte est conservé en utilisant la membrane hétérogène même si les contraintes d'opérations sont toutes prises en compte. La sélectivité inversée est clairement observée car l'ajout d'adsorbant augmente significativement le time-lag de CO_2. Dans ce cas, la contrainte d'opération (1 s) devient inférieure au time-lag augmenté par l'ajout d'adsorbant, l'intérêt du procédé cyclique de classe courte est ainsi observé.
- Malgré une sélectivité bien intéressante dans le cas d'un procédé cyclique, notamment avec la membrane hétérogène, une perte de productivité n'est pas évitable. Grossièrement, pour gagner un ordre de grandeur de sélectivité, il faut payer de même en productivité.

En outre, une étude pour une séparation du couple $\{N_2,CO_2\}$ à travers une autre membrane hétérogène a été réalisée comme un deuxième exemple avec l'intérêt industriel. Des conclusions similaires ont été obtenues, l'intérêt d'utiliser une membrane hétérogène a été mis en évidence.

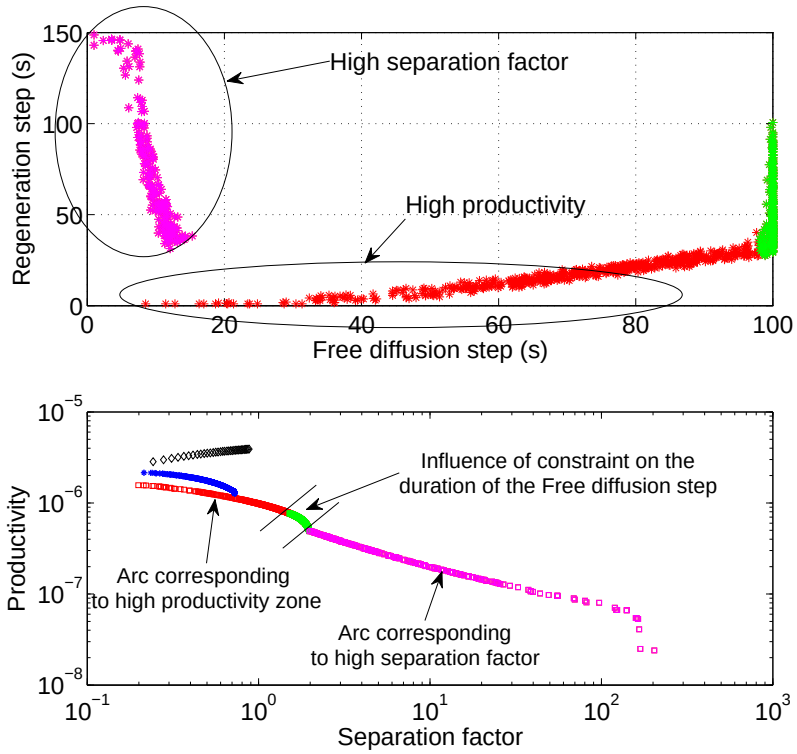

Figure E.12: Haut: durées optimisées de perméation libre et de régénération. Bas: Comparaison des performances entre trois procédés: procédés en régime permanent ($\diamond$ noirs), procédés cycliques utilisant des membranes caoutchoutiques ($*$ bleus) et utilisant des membranes hétérogènes ($\square$ rouges, verts et roses)(Séparation de {He, CO_2}, la sélectivité inversée est présentée par un facteur de séparation inférieur à 1)

Classe longue

Après avoir révisé les études existantes et étudié numériquement plusieurs cas dans le cadre du procédé cyclique de classe courte, nous constatons que la perte en productivité de ce genre de procédé limite fortement son implantation dans l'industrie malgré l'intérêt bien observé. Cette perte peut être expliqué essentiellement par deux aspects:

- La proportion de la haute pression dans un cycle est très faible, surtout en cas d'un haut facteur de séparation. L'étape de la basse pression (régénération) est indispensable mais ne produit rien.

- L'utilisation des membranes épaisses est incontournable afin de satisfaire les contraintes d'opération réelle dans le cas du procédé cyclique de classe courte. L'augmentation de l'épaisseur fait diminuer significativement la productivité.

Nous avons évoqué dans le chapitre 3 qu'un autre fonctionnement du procédé cyclique, appelé classe longue, a été très peu exploité dans la littérature. Ce type de procédé cyclique fournit une amélioration en sélectivité moins importante mais la perte en productivité est en général plus faible.

Dans le cadre de cette thèse, une nouvelle conception du procédé cyclique de classe longue a été proposée, puis enregistrée dans un brevet français [Wang et al., 2011b]. Ce procédé est schématisé dans la figure E.13. Initialement, tout le module est sous vide et toutes les vannes sont fermées. Lorsque le procédé est démarré, le module est alimenté à une haute pression par ouverture de la vanne A. Cette étape est appelée étape d'alimentation. Dès que la consigne de pression est atteinte dans le compartiment amont, la vanne A est fermée et la perméation libre a lieu à travers les fibres. Cette étape est appelée étape de perméation libre. Après cette étape, deux options sont disponibles (tableau E.11):

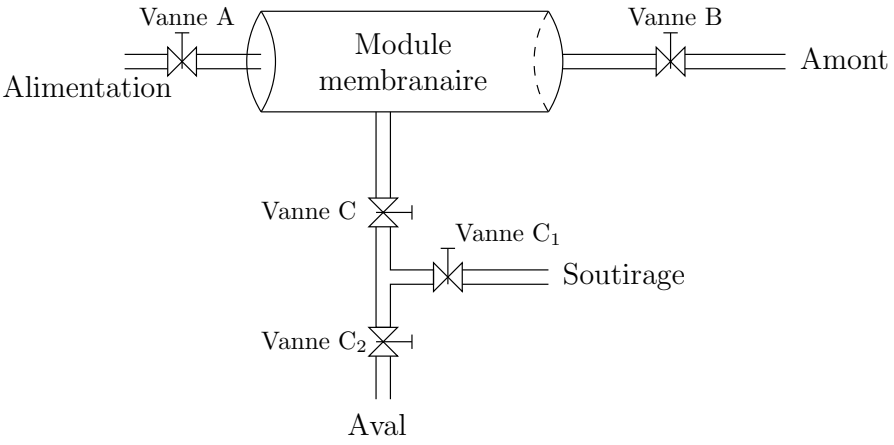

Figure E.13: Schéma d'une proposition du procédé cyclique de classe longue [Wang et al., 2011b]

- Option basique. Les vannes C_1 (tout le temps fermée) et C_2 (tout le temps ouverte) ne sont pas en service. Par conséquent, le soutirage n'existe pas. Après l'étape de perméation libre, les vannes B et C sont ouvertes afin de transférer les gaz amont et aval dans les réservoirs correspondants. A cause de ce transfert, le module entier est vidé et la membrane est régénérée. Cette étape est appelée étape de transfert. Après ceci, toutes les vannes sont fermées et le cycle est terminé.

Vanne	A	B	C	$\mathbf{C_1}$	$\mathbf{C_2}$
Alimentation	o	-	-	-	-
Perméation libre	-	-	-	-	-
Soutirage	-	-	o	o	-
2^{nde} perméation libre	-	-	-	-	-
Transfert	-	o	o	-	o

Table E.11: Opérations cycliques du nouveau procédé cyclique de classe longue. Les étapes optionnelles sont marquées en gras. ("o" pour ouvert et "-" pour fermé, version française de tableau 5.18)

- Option soutirage. Toutes les vannes sont en service. Après l'étape de perméation, les vannes C et C_1 sont ouvertes, un soutirage est effectué. Cette étape est appelée étape de soutirage. Ensuite, les vannes C et C_1 sont fermées de nouveau afin de reprendre la perméation libre. Cette étape est appelé étape de 2^{nde} perméation libre. Ensuite, dans l'étape de transfert, les vannes B, C et C_2 sont ouvertes afin de transférer les gaz dans leurs propres réservoirs. A cause de ce transfert, le module entier est vidé et la membrane est régénérée. Après ceci, toutes les vannes sont fermées et le cycle est terminé.

Comme ce nouveau procédé est classé en classe longue, la durée de la haute pression dans un cycle n'est pas du tout limitée par le time-lag. Ainsi, la membrane peut être très fine afin de favoriser le débit de perméation. D'autre part, selon nos simulations, dans le cas du nouveau procédé, la durée de régénération est très courte voire négligeable devant la durée de la haute pression dans le cas de membranes fines (figure 5.28). Par conséquent, une perte de productivité fortement réduite est attendue. En outre, selon notre simulation, le rapport des volumes aval/amont γ du module joue un rôle très important dans la séparation, un grand rapport permettant une séparation plus efficace.

Selon le fonctionnement, un procédé en régime permanent génère deux flux à la sortie: le rétentat et le perméat. Avec l'option basique du procédé cyclique considéré, deux flux similaires sont obtenus. Par contre, si l'option soutirage est prise, trois flux seront obtenus à l'issue de l'opération: flux amont, aval et de soutirage.

Par conséquent, dans un premier temps, nous avons réalisé une série de simulations afin de comprendre l'enrichissement des flux pour chaque procédé (le procédé en régime permanent et deux options du nouveau procédé cyclique de classe longue). Nous notons que le flux amont de l'option soutirage peut être enrichi en gaz rapide ou en gaz lent selon l'opération. Avec les résultats montrés dans le tableau E.12, nous effectuons les comparaisons de manière

suivante: si l'option soutirage est prise, les durées de chaque étape sont ajustées afin que le flux amont possède la composition du flux d'alimentation. Dans ce cas, ce flux peut être recyclé et le procédé avec l'option soutirage ne génère que deux flux à la sortie: le flux soutirage et le flux aval.

	O_2 (gaz lent) enrichi en	CO_2 (gaz rapide) enrichi en
Régime permanent	Rétentat	Perméat
Option basique	Amont	Aval
Option soutirage	Amont	Soutirage

Table E.12: Comparaison de l'enrichissement des flux pour les procédés en régime permanent et deux options du nouveau procédé cyclique de classe longue

La performance d'un procédé est définie par deux critères:

- Fraction molaire du composé désiré.
- Taux de récupération, défini par le rapport de la quantité du composé gazeux désiré récupérée sur la quantité introduite dans le module pendant un cycle.

Dans la comparaison, le procédé en régime permanent fonctionne soit à courants croisés, soit comme un système parfaitement agité, avec un rapport de pressions perméat/rétentat égal à 0.01.

Les résultats sont présentés dans les figures E.14 et E.15. Nous pouvons en déduire que,

- Pour les deux figures, les points proches de (1,1) (100% en fraction molaire et 100% en taux de récupération) représentent la meilleure performance d'un procédé.
- En augmentant le rapport de volumes aval/amont γ, la performance du procédé cyclique de classe longue peut être significativement améliorée. Lorsque ce rapport devient supérieur à 100 avec l'option basique, l'efficacité de séparation est compétitive face à un procédé en régime permanent à courants croisés.
- L'utilisation du soutirage permet clairement d'améliorer la séparation. Avec un rapport de volumes $\gamma = 10$, si le flux aval est recyclé grâce aux opérations optimisées des vannes, les deux critères peuvent être améliorés simultanément (figure E.14). Des performances meilleures qu'un procédé

en régime permanent sont mises en évidence. En outre, la figure E.15 montre que avec un taux de recyclage 20.4%, le procédé cyclique de longue classe permet de générer deux flux très purs à la sortie du procédé. Ceci est en général impossible dans une séparation membranaire.

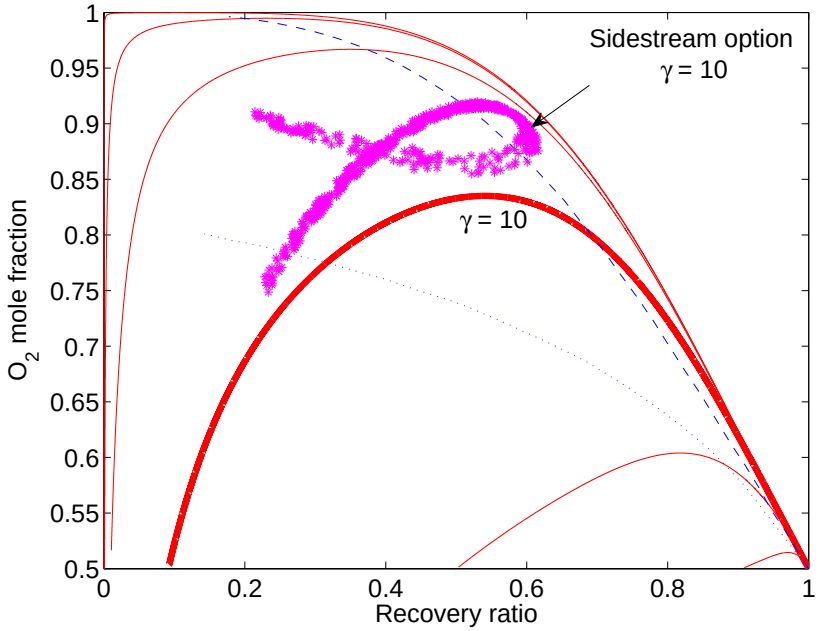

Figure E.14: Taux de récupération de O_2 dans les flux enrichis en O_2 en fonction des fractions molaires de O_2 (tableau E.12). Courbes rouges continues: nouveau procédé cyclique avec l'option basique en utilisant différents rapports de volumes γ (0.1, 1, 10, 100, 1 000 and 10 000 de bas en haut respectivement). Courbe rouge continue en gras: $\gamma = 10$. Courbe bleue discontinue: procédé en régime permanent à courants croisés. Courbe bleue pointillée: procédé en régime permanent parfaitement agité. Etoiles vertes: nouveau procédé cyclique avec l'option soutirage $\gamma = 10$ et le flux aval est recyclé.

D'une manière similaire, les études du nouveau procédé cyclique de classe longue ont été réalisées sur d'autres couples gazeux comme $\{N_2,O_2\}$ et $\{He,CH_4\}$. Les avantages du nouveau procédé ont été confirmés.

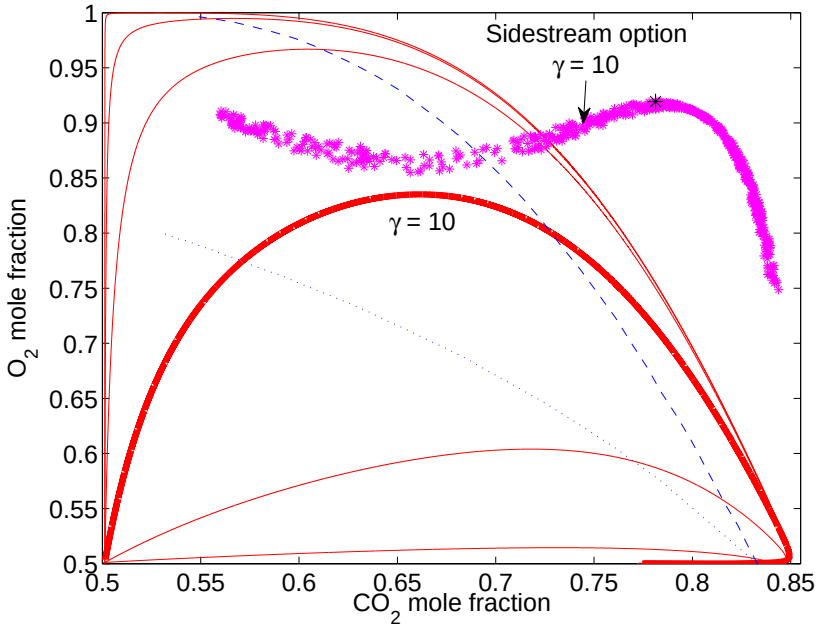

Figure E.15: Fraction molaire de CO_2 dans le flux enrichi en CO_2 en fonction de la fraction molaire de O_2 dans le flux enrichi en O_2 (tableau E.12). Courbes rouges continues: le nouveau procédé cyclique avec l'option basique en utilisant différents rapports de volumes γ (0.1, 1, 10, 100, 1 000 and 10 000 de bas en haut respectivement). Courbe rouge continue en gras: $\gamma = 10$. Courbe bleue discontinue: procédé en régime permanent à courants croisés. Courbe bleue pointillée: procédé en régime permanent parfaitement agité. Etoiles vertes: nouveau procédé cyclique avec l'option soutirage $\gamma = 10$ et flux aval recyclé. Etoile noire: un exemple avec un taux de recyclage de 20.4 %.

Développement expérimental

Dans le cadre de cette thèse, un développement expérimental a été réalisé afin de fournir un support au nouveau procédé cyclique de classe longue. Pour ce faire, un module à fibres creuses de polyphénylène oxide (PPO) a été acheté chez Parker Filtration and Separation B.V. (The Netherlands).

L'air comprimé et l'azote pur sont utilisés dans l'expérience comme un mélange binaire et un corps pur respectivement. L'installation expérimentale (figure E.16) a été assemblée au sein du LRGP. Les quatre vannes pilotables permettent de contrÃ´ler les directions de flux. Une pompe à vide permet de vider le module en entier. Les pressions amont/aval sont suivies par deux capteurs de pression. La composition dans le volume aval peut être détectée par un détecteur infrarouge qui est sensible à O_2 dans le cas d'un mélange binaire $\{O_2,N_2\}$.

Grâce à la pompe à vide, toute l'installation est initialement sous vide et tous les vannes sont fermées. L'expérience commence par l'ouverture de la vanne A afin d'alimenter le volume amont à une haute pression. Le but de l'expérience est de tracer l'évolution de pression amont/aval pour un corps pur une fois que le volume amont est chargé à une haute pression. Cette expérience consiste en une deuxième étape (Perméation libre) du nouveau procédé cyclique de classe longue évoqué dans le chapitre 5. L'expérience est répétée pour le mélange binaire (l'air comprimé), l'évolution de fraction molaire est ainsi tracée puis comparée avec celle obtenue par la simulation. Si la courbe générée par notre simulation est cohérente avec celle obtenue expérimentalement, la validation du procédé peut être acquise. Nous avons procédé de la manière suivante:

- Vérification de l'étanchéité du système. Toute l'installation est chargée à une pression supérieure à 1 bar. Si la pression est maintenue pendant une certaine durée avec toutes les vannes fermées, l'étanchéité sera vérifiée pour la durée considérée.
- Détermination du rapport des volumes aval/amont et de l'épaisseur effective de la membrane. Comme évoqué dans le chapitre 5, ce rapport de volumes est important pour tracer l'évolution de la pression ou de la fraction molaire. D'autre part, l'épaisseur effective de la membrane est un autre facteur clé de la simulation. Cependant, ces deux paramètres ne sont pas communiqués par le fabricant.

  Le rapport des volumes est d'abord calculé approximativement à l'aide d'un bilan global dans le système en négligeant la quantité résiduelle dans la membrane. Ensuite, une expérience suivie d'une optimisation a été effectuée afin d'affiner les valeurs du rapport des volumes et de

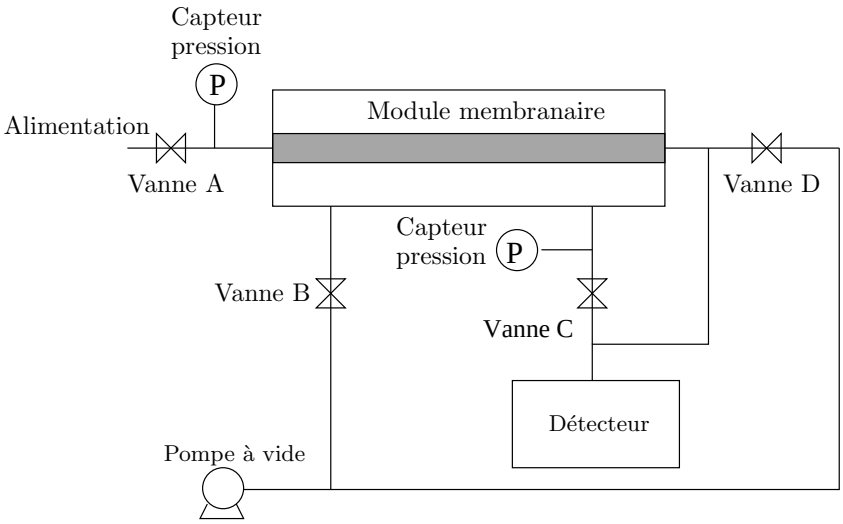

Figure E.16: Installation expérimentale

l'épaisseur de la membrane. En utilisant l'épaisseur déterminée approximativement, nous essayons de mettre en accord les résultats de simulation et ceux obtenus expérimentalement en faisant varier l'épaisseur de la membrane. Une épaisseur approximative de la membrane est ainsi obtenue. Ensuite, l'écart entre les courbes expérimentale et théorique est minimisé en faisant varier l'épaisseur de la membrane et le rapport des volumes avec leurs valeurs initiales déterminées auparavant. Grâce à cette optimisation, nous avons pu déterminer que le rapport des volumes est de 0.76 et l'épaisseur effective de la membrane est de 0.059 μm. Cette dernière est cohérente par rapport à une autre expérience réalisée au sein du LRGP sur le même module.

- Expérience avec un corps pur (l'azote). Pour un corps pur, il est possible de suivre la variation de sa pression en amont et en aval à l'aide des deux capteurs de pression. Cette mesure est en ligne et très précise. D'autre part, la reproductibilité d'expériences est excellente. Dans la figure E.17, les deux courbes expérimentales se superposent quasiment. Les résultats de simulation sont très voisins des courbes expérimentales, ceci permet de valider notre simulation d'abord pour un corps pur.

- Expérience avec un mélange binaire (l'air comprimé). Pour un mélange binaire, le compartiment amont est tout le temps alimenté par une source d'air comprimé, sa composition est ainsi considérée comme constante. La fraction molaire d'O_2 dans le volume aval est enregistrée. La figure E.18 montre un accord acceptable entre les expériences et la simulation. Une

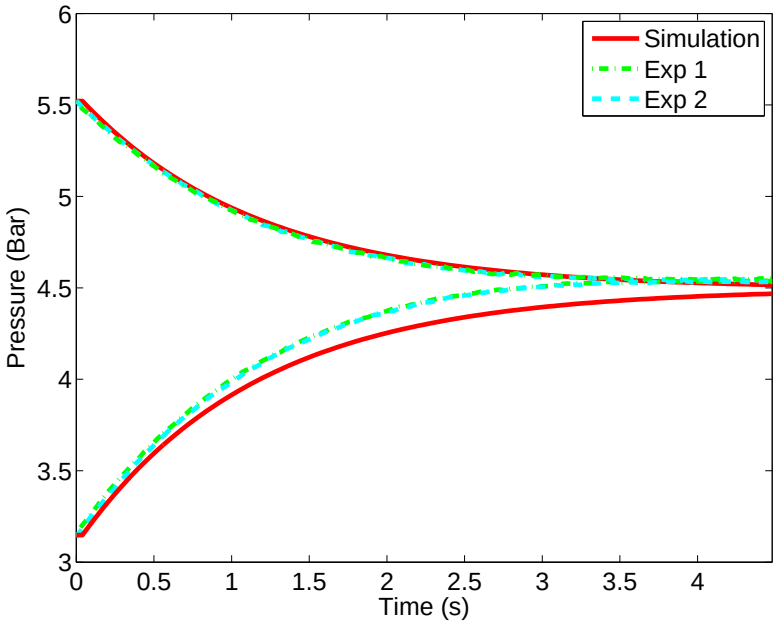

Figure E.17: Comparaison entre deux courbes expérimentale d'évolution de la pression d'azote et celle obtenue par simulation.

erreur relative moyenne ψ_y pour la fraction molaire d'O_2 y est calculée

$$\psi_y = \frac{1}{n}\sum_{i=1}^{n}\frac{|y_{exp} - y_{sim}|}{y_{exp}} = 7.0\% \tag{E.31}$$

Cette erreur faible permet de validation nos simulations.

Conclusion

Dans le cadre de cette thèse, une étude systématique sur les procédés membranaires pour les séparations gazeuses en mode cyclique a été réalisée. Dans un premier temps, l'état de l'art des procédés membranaires est révisé suivi par une revue particulièrement focalisée sur les procédés membranaires cycliques. A travers cette revue, nous avons pu définir les avantages et les inconvénients d'un tel procédé cyclique par rapport à un fonctionnement en régime permanent. En plus, les procédés cycliques existants ont été classés en deux catégories à l'aide d'un critère bien défini. Les procédés selon l'idée de Paul sont classés comme courts alors que les autres types de procédé cyclique sont considérés comme de classe longue.

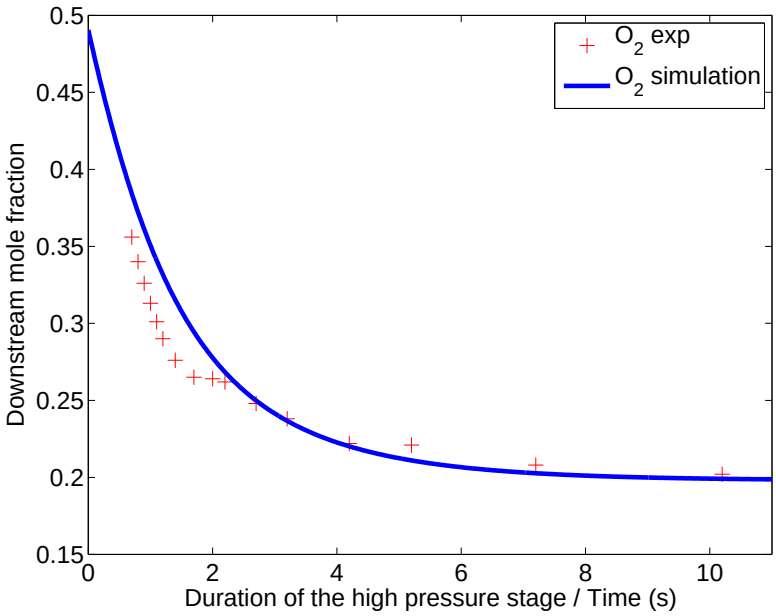

Figure E.18: Comparaison des évolutions de la fraction molaire d'O_2 expérimentale et obtenue par simulation.

Deuxièmement, le mécanisme du transfert au sein de membranes est étudié dans le cadre d'une théorie appelée Dual Mode Sorption. Un nouveau comportement aux limites de cette théorie non découvert a été exploité dans cette thèse et l'intérêt d'utiliser ce comportement a été mis en évidence. En utilisant la théorie Dual Mode Sorption et des conditions opératoires réalisables, nous avons réalisé trois types d'études de cas: deux procédés de classe courte avec différents matériaux et un nouveau procédé cyclique de classe longue. Les avantages et les inconvénients de chacun sont mis en évidence grâce à une comparaison systématique avec des procédés en régime permanent.

Enfin, une validation expérimentale a été mise en oeuvre au sein du LRGP afin de fournir un support pour cette étude théorique. Le bon accord constaté entre la simulation et les résultats expérimentaux permet de valider d'abord nos simulations mais aussi l'idée du nouveau procédé cyclique de classe longue.

UNIVERSITÉ DE LORRAINE

AUTORISATION DE SOUTENANCE
DU DOCTORAT DE L'UNIVERSITE DE LORRAINE

o0o

VU LES RAPPORTS ETABLIS PAR :

Monsieur SANCHEZ José, Directeur de Recherche CNRS, Institut Européen des Membranes, Montpellier,

Monsieur MEYER Xuan Mi, Professeur, Campus INP-ENSIACET Toulouse.

Le Président de l'Université de Lorraine, autorise :

Monsieur WANG Lei

à soutenir devant un jury de l'UNIVERSITE DE LORRAINE, une thèse intitulée :

"Cyclic membrane gas separation processes"

en vue de l'obtention du titre de :

DOCTEUR DE L'UNIVERSITE DE LORRAINE

Intitulé du doctorat : **"Génie des Procédés et des Produits"**

Fait à Vandoeuvre, le **22 juin 2012**

Le Président de l'Université de Lorraine,

Pierre MUTZENHARDT

Université de Lorraine

UNIVERSITÉ DE LORRAINE
34 COURS LÉOPOLD - CS 25233
54052 NANCY CEDEX
TÉL : 03 54 50 54 00
CONTACT@UNIV-LORRAINE.FR
WWW.UNIV-LORRAINE.FR

Abstract

This study deals with a systematic investigation of the performance of cyclic membrane gas separation processes. First, a state of the art of membrane separation processes, including material challenges and mass transfer modeling issues is proposed. In a second step, a review of the different theoretical and experimental studies performed on cyclic processes is reported. With respect to the length of the high pressure stage and its fraction in one cycle, these operations are classified into short and long classes. Based on this classification, a systematic analysis of the potential interest of short class compared to steady-state operation performances has been achieved by means of numerical simulation and optimization. In order to improve the performance, the use of MMM in such a process has been further discussed.

In parallel with the short class study, a design of novel long class has been proposed. Spectacular advantages with respect to classical membrane-based processes have been highlighted by means of our simulation and optimization studies. Finally, an experimental verification has been performed in order to provide a solid support to this novel process.

Keywords: gas, membrane, separation, cyclic operation, time-lag, dual mode, transient state

Résumé

Ce travail traite une investigation systématique des performances du procédé membranaire cyclique par séparation gazeuse. Premièrement, l'état de l'art du procédé membranaire cyclique, les problèmes techniques et la modélisation du transfert à travers la membrane ont été exposés. Deuxièmement, les études théoriques et expérimentales existantes sur le procédé cyclique sont passées en revue. Selon la durée de pression haute et sa fraction dans un cycle, ce genre d'opération est divisé en deux classes: classes courte et longue. D'après cette classification, une analyse systématique de l'intérêt potentiel de la classe courte par rapport aux performances d'une opération en régime permanent a été accomplie par des simulations et optimisations numériques. Par ailleurs, afin d'améliorer la performance, l'usage du MMM dans un tel procédé a été discuté.

En parallèle à l'étude sur la classe courte, une nouvelle conception du procédé cyclique de classe longue a été proposée. Les avantages spectaculaires par rapport aux procédés membranaires classiques ont été mis en évidence à l'aide de nos simulations et optimisations. Finalement, une validation expérimentale a été effectuée afin de fournir un support solide à cette nouvelle conception.

Mots-clés: gaz, membrane, séparation, opération cyclique, time-lag, dual mode, régime transitoire